

**GOLD EXPLORATION NORTHEAST OF NGUNDU HALT,  
NORTHERN MARGINAL ZONE OF THE LIMPOPO BELT,  
ZIMBABWE**

A thesis submitted in fulfilment of the  
requirements for the degree of

**MASTER OF SCIENCE**

of

**RHODES UNIVERSITY**

by

**ROBERT ZULU SIMANGO**

February 2003

## **ABSTRACT**

Gold exploration was conducted in northern margin, granulite-facies rocks of the Limpopo Belt. Methods used in the prospecting include drainage, soil and rock geochemistry, geophysical surveys, geological mapping, trenching and diamond drilling. These techniques successfully led to the discovery of two medium size, mesothermal gold deposits (Grid 2s and Grid 4).

Objectives of this study were to (a) document the exploration methodology used; (b) describe the regional geology; (c) establish a mineral deposit model; (d) outline the methods and results of various exploration techniques; (e) outline follow-up procedures and evaluation of anomalies; and (f) discuss results of the exploration exercise and conclusions.

The granulite-facies terrain comprises charno-enderbites, mafic and felsic to intermediate meta-volcanic rocks and meta-sediments. Renco Mine situated immediately east of the study area, was selected as the ore deposit model for the exploration program. Gold mineralization occurs in shear and thrust zones within an enderbite.

The gold deposits are structurally controlled by a first-order, sinistral transcrustal Mauch Shear Zone, which is parallel to a regional east-northeast penetrative foliation. The deposits are in dilation zones where the Mauch Shear (a) is intersected by a dextral east-west shear (Grid 2s), or (b) has a sinistral splay (Grid 4 and Renco). Close to these deposits, the Mauch Shear is in contact with a "greenstone belt", which is a possible source of crustal metamorphic ore fluids and gold.

The Grid 2s deposit contains fine-grained, disseminated free gold, and small amounts of pyrrhotite, pyrite and chalcopyrite in quartz veins within third-order shears in K-feldspar granite. K-feldspar, sericitic, silicic, sulphidation and carbonate alteration characterizes the deposit, which has a proposed mantle-degassing model. The Grid 4 deposit is magmatic porphyry-type, with Cu-Mo and Au in third- and fourth-order shears respectively. Mineralization comprises disseminated to semi-massive pyrrhotite, pyrite, chalcopyrite, sphalerite, bismuth, molybdenite and gold. Wall rock alteration includes biotitic, chloritic, silicic, sulphidation and carbonate.

In Grid 2s, Grid 4 and Renco deposits, the alteration mineral assemblages are in three facies, which are granulite, amphibolite and greenschist. In the three deposits, the mineralization occurs with the amphibolite-facies, indicating post-peak, retrograde metamorphic conditions.

## CONTENTS

	<b>Page</b>
ABSTRACT .....	ii
LIST OF ILLUSTRATIONS .....	vi
LIST OF APPENDICES .....	xi
PREFACE .....	xii
<b>CHAPTER 1 - INTRODUCTION .....</b>	<b>1</b>
1.1 Study Area – Location, licensing, selection criteria .....	1
1.2 Exploration methods .....	3
1.3 Objectives of the study .....	3
<b>CHAPTER 2 - REGIONAL GEOLOGY - THE LIMPOPO BELT .....</b>	<b>4</b>
2.1 Introduction .....	4
2.2 The Zimbabwe Craton .....	6
2.3 The Kaapvaal Craton .....	8
2.4 The Central Zone .....	9
2.5 The Southern Marginal Zone .....	13
2.6 The Northern Marginal Zone .....	14
2.7 Gold Mineralization and hydrothermal alteration in the Limpopo Belt .....	28
<b>CHAPTER 3 - LOCAL GEOLOGY – TOKWE E.P.O. 847 .....</b>	<b>32</b>
3.1 Introduction .....	32
3.2 Metamorphosed greenstone belts (Supracrustal Assemblage) .....	33
3.3 Charno-enderbites (Plutonic Assemblage) .....	40
3.4 Leuco-mylonites and proto-mylonites .....	44
3.5 Migmatites and leucogneiss (leucosome) .....	46
3.6 Potash feldspar granite .....	48
3.7 Quartz veins, feldspar porphyry and pegmatites .....	49
3.8 Picritic rocks, olivine pyroxenite and dolerite .....	52
3.9 Geochemistry (XRF Analyses) .....	53
3.10 Metamorphism .....	57
3.11 Structural geology .....	59
<b>CHAPTER 4 – GEOPHYSICAL SURVEYS .....</b>	<b>63</b>
4.1 Introduction – magnetic and radiometric methods .....	63
4.2 Airborne Surveys .....	67
4.3 Aeromagnetic data .....	68
4.4 Radiometric data .....	72
4.5 Conclusions .....	77
<b>CHAPTER 5 - DRAINAGE GEOCHEMISTRY .....</b>	<b>79</b>
5.1 Introduction .....	79
5.2 Orientation drainage sampling .....	80
5.3 First-pass drainage sampling .....	85
5.4 Second-pass drainage sampling .....	87

## CONTENTS (continued)

<b>CHAPTER 6 - SOIL GEOCHEMISTRY</b>	<b>92</b>
6.1 Introduction	92
6.2 Orientation soil sampling	92
6.3 Grid soil sampling	96
6.4 Grid 4 – soil geochemistry	101
6.5 Grid 2s – soil geochemistry	104
6.6 Grid 1s – soil geochemistry	106
6.7 Grid 6 – soil geochemistry	108
<b>CHAPTER 7 – GRID MAPPING, ROCK SAMPLING AND TRENCHING</b>	<b>109</b>
7.1 Introduction	109
7.2 Grid 4	112
Geology	112
Rock sampling	113
Trenching	115
Structural controls on gold mineralization	116
7.3 Grid 2s	119
Geology	119
Rock sampling	120
Trenching	121
Structural controls on gold mineralization	122
7.4 Conclusions	124
<b>CHAPTER 8 - DIAMOND DRILLING</b>	<b>127</b>
8.1 Introduction	127
8.2 Method	127
8.3 Grid 4	131
East Anomaly	131
West Anomaly	138
Mineralized zones and ore resource estimation	141
Wall rock alteration	141
8.4 Grid 2s	144
Cross-section 10 800E	145
Cross-section 10 000E	148
Longitudinal section 8025N	149
Mineralized zones and ore resource estimation	151
Wall rock alteration	152
8.5 Models for the gold deposits	154
Preferred genetic model for Grid 4 deposit	160
Preferred genetic model for Grid 2s deposit	161
<b>CHAPTER 9 – SUMMARY AND CONCLUSIONS</b>	<b>163</b>
9.1 Geology and metamorphism	163
9.2 Structure	164
9.3 Geophysical surveys	164
9.4 Drainage geochemistry	166
9.5 Soil geochemistry	166
9.6 Grid mapping and rock sampling	168
9.7 Trenching	169
9.8 Diamond drilling	171
9.8.1 Diamond drilling – Grid 2s	172
9.8.2 Ore resource estimation – Grid 2s	172
9.8.3 Wall rock alteration – Grid 2s	173
9.8.4 Diamond drilling – Grid 4	174

**CONTENTS (continued)**

9.8.5	Ore resource estimation – Grid 4	174
9.8.6	Wall rock alteration – Grid 4	175
9.9	Ore deposit model for the Northern Marginal Zone – Limpopo Belt	175
Appendices		179
References		185

## ILLUSTRATIONS

<u>FIGURE No.</u>	<u>TITLE</u>	<u>TYPE</u>
1.1	Location Map of Tokwe E.P.O.	Plan
2.1	Location of Limpopo Belt	Plan
2.2	Geological Map of the Limpopo Belt and adjacent cratons	Plan
2.3	Crustal profile across the Limpopo Belt	Section
2.4	Schematic geological evolution of the Northern Marginal Zone	Sketch
3.0	Geological Map of Tokwe E.P.O	Plan
3.1	Modal compositions of meta-andesites	QAPF $\Delta$
3.2	Modal compositions of rhyolites	QAPF $\Delta$
3.3	Modal compositions of charnockites	QAPF $\Delta$
3.4	Modal compositions of magnetite-charnockites	QAPF $\Delta$
3.5	Modal compositions of enderbites	QAPF $\Delta$
3.6	Modal compositions of potassic granites	QAPF $\Delta$
3.7	XRF Analyses	Table
3.8	Sample Symbols for XRF Analyses	Legend
3.9	Major elements geochemistry	Harker diagram
3.10	Major elements geochemistry – K <sub>2</sub> O-Na <sub>2</sub> O-CaO	Trivariate diag.
3.11	Total Alkalis versus Silica – plutonic rocks	TAS diagram
3.12	Total Alkalis versus Silica – volcanic rocks	TAS diagram
3.13	Classification of terrigenous sandstones	Ratio diagram
3.14	Trace element abundance versus atomic number - plutonic rocks	"Spider" diag.
3.15	Transition metal concentrations versus atomic number – plutonic rocks	"Spider" diag.
3.16	Rb-(Y+Nb) Geotectonic discrimination diagram – plutonic rocks	Variation diag.
3.17	Nb-Y Geotectonic discrimination diagram – plutonic rocks	Variation diag.
3.18	Trace element abundance versus atomic number – Meta-basites and enderbite	"Spider" diag.
3.19	Transition metal concentrations versus atomic number – meta-basites and enderbite	"Spider" diag.
3.20	TiO <sub>2</sub> -Zr/(P <sub>2</sub> O <sub>5</sub> ×10000) Discrimination diagram for Basalts	Variation diag.

<b>FIGURE No.</b>	<b>TITLE</b>	<b>TYPE</b>
3.21	MnO-TiO <sub>2</sub> -P <sub>2</sub> O <sub>5</sub> Geotectonic discrimination diagram for basalts and basaltic andesites	Variation diag.
3.22	Trace element abundance versus atomic number – meta-sediments	“Spider” diag.
3.23	Transition metal concentrations versus atomic number – meta-sediments	“Spider” diag.
3.24	(Ce/Y) <sub>N</sub> -Y <sub>N</sub> ratio diagram – REE fractionation with changing REE content	Ratio diagram
3.25	(La/Y) <sub>N</sub> -Y <sub>N</sub> ratio diagram - REE fractionation with changing REE content	Ratio diagram
4.1	Total field aeromagnetic map	Plan
4.2	Radiometric map – Potassium channel	Plan
4.3	Radiometric map – Thorium channel	Plan
4.4	Radiometric map – Uranium channel	Plan
4.5	Radiometric map – Th/K ratios	Plan
4.6	Geophysical interpretation map	Plan
4a	Magnetic susceptibilities of some lithologies	Table
4b	Statistics of radiometric data	Table
5.1	Orientation drainage sampling – Sample location	Plan
5.2	Classification of trap sites	Sketch
5.3	Orientation drainage samples – size fraction Au values	Bar graphs
5.4	Orientation drainage samples – size fraction total Au values	Pie chart
5.5	Orientation drainage samples – size fraction total Au values	Bar graphs
5.6	First-pass drainage sampling, -75µm size fraction	Plan
5.7	First-pass drainage samples – Gold values	Histogram
5.8	First-pass drainage samples – Gold values - Log-probability plot	Graph
5.9	Second-pass drainage sampling – Sample positions	Plan
5.10	Second-pass drainage sampling – Panned concentrates – Gold values	Plan
5.11	Second-pass drainage samples – Panned concentrates – Gold values	Histogram
5.12	Second-pass drainage samples – Panned	

<u>FIGURE No.</u>	<u>TITLE</u>	<u>TYPE</u>
	concentrates – Gold values – Log probability plot	Graph
5.13	Poor reproducibility of gold values in HMC samples from Area 2s	Table
5(a)	Gold grains from Grid 2s showing roundness	Plate
5(b)	Gold grains from Grid 2s with irregular shapes	Plate
6.1	Orientation soil sampling – Pit positions	Plan
6.2	Orientation soil sampling - Pit 9755E/7975N – Au values	Section
6.3	Orientation soil sampling - Pit 9755E/8000N – Au values	Section
6.4	Orientation soil sampling - Pit 9755E/8025N – Au values	Section
6.5	Orientation soil sampling - Pit 9755E/8050N – Au values	Section
6.6	Orientation soil sampling - Pit 9755E/8075N – Au values	Section
6.7	Orientation soil sampling - Pit 9755E/8100N – Au values	Section
6.8	Orientation soil sampling - Pit 9755E/8125N – Au values	Section
6.9	Orientation soil sampling - Pit 9755E/8150N – Au values	Section
6.10	Orientation soil samples – Au values versus soil horizon	Table
6.11	Orientation soil samples – Au values versus size fraction	Table
6.12	Orientation soil samples – Total Au values versus soil horizon	Bar graphs
6.13	Orientation soil samples – Total Au values versus size fraction	Bar graphs
6.14	Soil geochemical map – Grid 4 – Gold values	Plan
6.15	Soil geochemical map – Grid 4 – Gold and Copper values – Interpretation	Plan
6.16	Soil geochemical map – Grid 4 – Copper values	Plan
6.17	Grid 4 soil samples – Gold values	Histogram
6.18	Grid 4 soil samples – Gold values – Log-probability plot	Graph
6.19	Grid 4 soil samples – Copper values	Histogram
6.20	Grid 4 soil samples – Copper values – Log-probability plot	Graph
6.21	Soil geochemical map – Grid 2s – Gold values	Plan
6.22	Soil geochemical map – Grid 2s – Gold values and interpretation	Plan
6.23	Grid 2s soil samples – Gold values	Histogram

<u>FIGURE No.</u>	<u>TITLE</u>	<u>TYPE</u>
6.24	Grid 2s soil samples – Gold values – Log-probability plot	Graph
6.25	Soil geochemical map – Grid 1s – Gold values	Plan
6.26	Soil geochemical map – Grid 1s – Copper values	Plan
6.27	Grid 1s soil samples – Gold values	Histogram
6.28	Grid 1s soil samples – Gold values – Log-probability plot	Graph
6.29	Grid 1s soil samples – Copper values	Histogram
6.30	Grid 1s soil samples – Copper values – Log-probability plot	Graph
7.1	Grid 4 – Geology and Rock sampling	Plan
7.2	Grid 4 – Feldspar porphyry veins/dykes - Gold values – Log-probability plot	Graph
7.3	Grid 4 – Feldspar porphyry veins/dykes – Gold values	Histogram
7.4	Grid 4 – Quartz veins in charnockite – Gold values - Log-probability plot	Graph
7.5	Grid 4 – Quartz veins in charnockite – Gold values	Histogram
7.6	Grid 4 – Quartz veins in “Cu Shear” – Copper values - Log-probability plot	Graph
7.7	Grid 4 – Trenching and drilling	Plan
7.8	Grid 4 – Trench samples – Feldspar porphyry and leuco-mylonite – Gold values – Log-probability plot	Graph
7.9	Grid 4 – Trench samples – Feldspar porphyry and leuco-mylonite – Gold values	Histogram
7.10	Grid 4 – Trench samples – Feldspar porphyry and leuco-mylonite – Cu values – Log-probability plot	Graph
7.11	Grid 4 – Trench samples – Feldspar porphyry and leuco-mylonite – Cu values	Histogram
7.12	Grid 4 – Structural setting of mineralized zones	Sketch
7.13	Grid 2s - Geology and Rock sampling	Plan
7.14	Grid 2s - Rock samples – Gold values – Log-probability plot	Graph
7.15	Grid 2s - Rock samples – Gold values	Histogram
7.16	Grid 2s – Trenching and drilling	Plan
7.17	Grid 2s - Trench samples – Gold values – Log-probability plot	Graph

<u>FIGURE No.</u>	<u>TITLE</u>	<u>TYPE</u>
7.18	Grid 2s - Trench samples – Gold values	Histogram
7.19	Grid 2s – Structural setting of mineralized zones	Sketch
7.20	Development of dilation	Sketch
8.1	Grid 4 – Drill hole C4D3	Section
8.2	Grid 4 – Drill hole C4D5	Section
8.3	Grid 4 – Drill hole C4D12	Section
8.4	Grid 4 – Drill hole C4D13	Section
8.5	Grid 4 – Drill hole C4D14	Section
8.6	Grid 4 – Drill hole C4D6	Section
8.7	Grid 4 – Drill hole C4D7	Section
8.8	Grid 4 – Drill hole C4D9	Section
8.9	Grid 2s – Drill holes C2D1 – C2D5, Line 10800E	Section
8.10	Grid 2s – Drill holes C2D6 – C2D10, Line 10000E	Section
8.11	Grid 2s – Drill holes C2D19 + C2D20, Line 8025N	Section
8.12	Grid 4 – Drill hole mineralized intersections	Table
8.13	Grid 2s – Drill hole mineralized intersections	Table
8.14	Schematic crustal profile at the time of gold mineralization	Section
8.15	Grid 4 deposit – Preferred Model	3D Sketch
8.16	Grid 2s deposit – Preferred Model	3D Sketch

## APPENDICES

	<b>Page</b>
APPENDIX A Mineral assemblages of rock types-----	179
APPENDIX B Fire Assay + AAS method-----	180
APPENDIX C Aqua Regia + ICP-MS method-----	182
APPENDIX D Grid 4 – Drill core mineral assemblages-----	183
APPENDIX E Grid 2s – Drill core mineral assemblages-----	184

### **ACKNOWLEDGEMENTS**

I would like to thank the management of Rio Tinto Zimbabwe, particularly Kevin Fox, for permission to use geochemical and airborne geophysical data sets acquired during the course of exploration in the study area. I also express my gratitude to the draughtsman, Moven Musonza for Auto CAD production of numerous illustrations.

I thank my supervisor, Professor J. M. Moore, for guidance and comments in the field, laboratory, and in compilation of text.

I also thank my field crew for conducting proper procedures in surveys, sampling and sample preparation.

## CHAPTER 1

### INTRODUCTION

#### 1.1 Study Area

This study is based on gold exploration conducted northeast of Ngundu Halt, in the Northern Marginal Zone (NMZ) of the Limpopo Belt, Zimbabwe. The Limpopo Belt, which comprises high-grade (granulite facies) metamorphic rocks, is situated between the Zimbabwe Craton in the north and the Kaapvaal Craton in the south. The study area is to the immediate southwest of Renco Gold Mine, owned and operated by Rio Tinto Zimbabwe (Pvt.) Limited. To date, Renco Mine is the sole gold producer in the NMZ, and the second largest producer in Zimbabwe. Renco Mine has an average grade of 5.5 g/t Au and an annual production of 1.5 t Au. The NMZ has not been thoroughly explored for gold, since it was believed to be devoid of greenstone belts, which are the traditional hosts to gold deposits.

#### Physical Location

Figure 1.1 shows the location of the study area. The area is situated between Renco Mine and Ngundu Halt in the southeast lowveld in Zimbabwe. Ngundu Halt is 100 km south of the city of Masvingo, along the tarmac road between Harare and the border town of Beitbridge. The tarmac road between Ngundu Halt and Chiredzi approximately marks the southern boundary of the area. A network of gravel roads and tracks is present inside the area. At the centre of the study area, the approximate coordinates are 30° 59' 00" E and 20° 42' 53" S. The area lies in UTM Zone 36, with eastings between 270 000 E and 308 000 E. The northings are between 7 696 000 N and 7 718 000 N. The size of the study area is 40 715 ha.

#### Licence and duration

Rio Tinto Zinc Plc, London and Rio Tinto Zimbabwe (Pvt.) Limited jointly funded the exploration work in the study area. The exploration was carried out under Exclusive Prospecting Order (E.P.O.) No. 847, named TOKWE. The licence was valid for a total duration of 6 years, from January 1994 to December 1999. The writer was the Project Geologist for the E.P.O. This study was commenced towards the end of the exploration work.

#### Area selection criteria

The study area (Tokwe E.P.O. 847) was selected for gold exploration because of its proximity to a known gold deposit, which is Renco. In the northeast, Tokwe E.P.O. shares

a common boundary with Renco Mining Lease. With respect to the regional northeast structural trend, the study area is along strike from Renco.

A regional, first-order structural "break", known as the Mauch Shear Zone, extends along and beyond the E.P.O. In the Renco Mining Lease, the shear zone is locally known as the Mtirikwi Shear Zone. The Renco deposit is located in a second-order shear/thrust system, which is essentially a splay, most likely from the nearby Mauch Shear Zone. Renco Mine is located in a deformation zone 2 km north of the Mauch Shear Zone. The structural setting can be compared to mineralization in the Canadian Shield, Yilgarn Block (Australia) and the Zimbabwe Craton (Hodgson, 1989; Groves *et al.*, 1989; Campbell & Pitfield, 1994). All the giant deposits occur in deformation zones within a few kilometres, mostly <5 km, of the first-order shear zones/faults (Hodgson, 1989).

It was anticipated that similar shear-hosted, mesothermal gold mineralization could be found on Tokwe E.P.O., where the Mauch Shear Zone has interfering structures such as splays, flexures, offsets or intersecting shears. Tokwe E.P.O. was selected because it had good mineral potential.

## **1.2 Exploration Methods**

Tokwe E.P.O. was prospected using a large-scale exploration program, which entailed a logical sequence of operations. The area was explored using several methods such as (a) image interpretation (aerial photographs, Spot images and Landsat TM images); (b) regional geological mapping; (c) airborne geophysical surveys (magnetics and radiometrics); (d) drainage sampling; (e) soil sampling; (f) trenching, detailed grid mapping and rock sampling; and (g) diamond drilling. The exploration program resulted in the discovery of two medium size gold deposits, provisionally known as Grid 2s and Grid 4.

The initial methods (a)-(d) were broad-scale reconnaissance stages that helped to delimit smaller areas for detailed study in subsequent stages. At the end of the reconnaissance stages, available information was evaluated and used to select smaller areas with the best mineral potential. The process of eliminating unfavourable areas and increasing detailed study of the favourable areas continued in successive steps up to the final stage of proving a deposit by drilling. The ultimate objective of the technical exploration program was the selection of drill sites, since drilling is by far the largest portion of the prospecting budget.

### 4.3 Objectives of the study

The objectives of this study were to:

- (a) document the exploration methodology used to explore for gold mineralization in Tokwe E.P.O.;
- (b) describe the regional geology of the area;
- (c) establish a mineral deposit model to be used in the exploration program;
- (d) outline the methods and the results of various exploration techniques employed, which included geophysics, drainage geochemistry, soil geochemistry, rock geochemistry, trenching, and diamond drilling;
- (e) outline follow-up procedures and evaluation of anomalous target areas, and
- (a) discuss the results of the exploration exercise and decisions arrived at.

## CHAPTER 2

### REGIONAL GEOLOGY - THE LIMPOPO BELT

**2.0** Literature review was carried out on previous work conducted on the Limpopo Belt. Most of the work has been published in journals, Zimbabwe and South Africa Geological Survey reports, and the Geological Society of South Africa. Unpublished Ph D. theses were also used.

The study area is situated in the Northern Marginal Zone of the Limpopo Belt. The literature review was carried out to broaden knowledge and understanding of the geological setting of the entire Limpopo Belt.

#### **2.1** Introduction

The Limpopo Belt is an extensive east–north–east trending tract of high grade metamorphic rocks that lies between the Zimbabwean (Rhodesian) and Kaapvaal cratons (Stagman, 1978). The Limpopo Belt is a zone of complexly deformed Archaean gneisses and meta-sediments of high metamorphic grade, which lie between lower metamorphic grade granites and greenstones of the Zimbabwean (Rhodesian) and Kaapvaal cratons (Coward *et al.*, 1976). The Limpopo Belt is a tectonic province with a complex history of multiple tectono-metamorphic events stretching in time from over 3.0 Ga to around 2.0 Ga (Berger *et al.*, 1995). Gan and van Reenen (1995) define the Limpopo Belt as an Archaean granulite facies metamorphic terrain, which resulted from the collision of the Kaapvaal and Zimbabwe cratons during the Limpopo orogeny. Figure 2.1 shows the location of the Limpopo Belt in southern Africa.

Rollinson & Blenkinsop (1995) describe the Limpopo Belt as a zone of granulite facies Archaean crust, 700 km in length and 250 km in width, located between two Archaean cratons: the Kaapvaal craton to the south and the Zimbabwe craton to the north. The Limpopo Belt emerges from beneath a relatively undisturbed sequence of Umkondo (Proterozoic) and Karoo cover in the Sabi Valley, and continues across the southern portion of Zimbabwe into Botswana where it apparently terminates beneath the Kalahari sands (Stagman, 1978). In South Africa, part of the Southern Marginal Zone of the Limpopo Belt is also beneath post–Archaean cover sequences.

The Limpopo Belt comprises three distinct tectonic units: Northern and Southern Marginal Zones and a Central Zone, each separated from the other and from the cratons by tectonic contacts. The ages of these units are still uncertain, but are thought to vary

between 3200 and 2600 Ma (Rollinson & Blenkinsop, 1995). The Central Zone (CZ), with north-trending structures, lies between the northern (NMZ) and the southern (SMZ) marginal zones that have east-north-east trends (Stagman, 1978). The three zones have contrasting structural trends and patterns as well as lithology (Berger *et al.*, 1995). The CZ is characterized by an at least 3.1 Ga old granulite grade supracrustal succession, the Beit Bridge Group, and older tonalitic gneisses (Sand River Gneisses). The late Archaean history of the CZ involves the intrusion of the Bulai Granitoid Suite at 2.57 Ga, comprising charnockites, enderbites and tonalitic to granodioritic rocks. Seventy percent of the SMZ rocks are charno-enderbite gneisses and their amphibolite facies equivalents. Supracrustal rocks, including ultramafic to mafic meta-volcanics, quartz-magnetite lithologies, quartzites and meta-pelites, constitute the remainder. Zircons from an enderbite sample yielded an age of  $2715 \pm 5$  Ma. The Matok intrusion is a late intrusive body, which includes charnockites as well as granitoids, for which zircon ages of 2664 and 2671 Ma were determined. The NMZ is comparable to the SMZ, but is even more dominated by charno-enderbitic gneisses and their lower grade equivalents, and contains fewer supracrustal rocks. Existing age determinations on the NMZ rocks range from 2.9 to 2.6 Ga. In contrast to the CZ, both NMZ and SMZ have been interpreted as high-grade metamorphic equivalents of the respective adjacent cratons.

The three zones of the Limpopo Belt are separated from each other by major strike-slip shear zones (Berger *et al.*, 1995). The Contacts are the sinistral Palala Shear Zone on the CZ-SMZ transition, and the 2.0 Ga dextral Tuli-Sabi-Triangle Shear Zone on the NMZ-CZ boundary. The contacts between the Limpopo Belt and the adjacent cratons are defined by two thrust-sense shear zones. The Umlali Thrust Zone is at the Zimbabwe Craton-NMZ transition (Mkweli *et al.*, 1995), and the Hout River Thrust Zone marks the Kaapvaal Craton-SMZ boundary (Gan & van Reenen, 1995). Figure 2.2 shows the three zones of the Limpopo Belt, the shear zones and the thrust zones.

The Tuli-Sabi-Triangle Shear Zone strikes ENE, sub-parallel to the Limpopo Belt margins and dips to the SE (Mason, 1973). The shear zone is up to 50 km wide. Horizontal to sub-horizontal mineral lineations and mylonitic textures dominate, but small areas with down-dip lineations are common (Coward *et al.*, 1973). In total, the Tuli-Sabi-Triangle Shear Zone has accommodated strike-slip movement of the order of hundreds of kilometres and some of this movement has been dated at 2000 Ma.

The Palala Shear Zone strikes roughly parallel to the Tuli–Sabi–Triangle Shear Zone and dips to the NW. The shear zone is up to 10 km wide and has horizontal to sub-horizontal mineral lineations and mylonitic textures (Mc Court & Vearncombe, 1987).

The boundary of the NMZ with the Zimbabwe Craton (Umlali Thrust Zone) appears to be marked by a series of southerly dipping thrust faults, along which, partly sheared, ENE-trending elongate bodies of porphyritic granite (Razi Suite) have intruded (Robertson, 1973). These thrust faults are not very well developed and are only exposed as intermittent outcrops along strike. The Razi porphyritic granite intrusions are found throughout the NMZ, but are most common at the northern boundary of the NMZ, adjacent to the Zimbabwe Craton (Berger & Rollinson, 1997). The Razi-type granites have been dated at ages between 2690 Ma (Pb–Pb) and 2583 Ma (Rb–Sr).

The boundary of the SMZ with the Kaapvaal Craton is marked by the northerly dipping Hout River Shear System, thrusting along which is reported as being coeval with the intrusion of the Matok porphyritic granite at around 2670 Ma (van Reenen *et al.*, 1988). The Hout River Thrust Zone comprises a system of frontal and lateral ramps, which include large proportions of oblique and strike-slip movement (Rollinson & Blenkinsop, 1995).

Figure 2.3 shows the probable crustal profile across the Limpopo Belt (after Roering *et al.*, 1992). The cross-section shows the three zones of the Limpopo Belt, the adjacent cratons, the major shear zones and the thrust zones. Gan & van Reenen (1995) proposed that the NMZ was thrust northwards onto the Zimbabwe Craton and the SMZ southwards onto the Kaapvaal Craton during the Limpopo orogeny (2700–2650 Ma).

The tectonic evolution of the Limpopo Belt is still subject to debate. Several models have been proposed and some of them include: (a) collision of the Kaapvaal and Zimbabwe Cratons during the Limpopo Orogeny c. 2700–2650 Ma (Roering *et al.*, 1992); (b) emplacement of the Central Zone onto a single Zimbabwe–Kaapvaal plate during a northeast–southwest collision event ~2700 Ma ago (Mc Court & Vearncombe, 1987); (c) terrain accretion (Rollinson 1993); and (d) isostatic uplift of an anomalously thick continental crust (Ridley 1992). All these models leave major questions unresolved.

## **2.0 The Zimbabwe Craton**

The Zimbabwe Craton (ZC) comprises granite–greenstone terrains ranging in age from 3.5 Ga to 2.6 Ga (Berger *et al.*, 1995). The oldest of these is the Tokwe Segment in the southern part of the ZC, which includes the 3.5 Ga Tokwe River and Shabani Gneisses of

Sebakwian age. Greenstone belt remnants (Sebakwian) are tightly infolded within the gneisses. This Tokwe Segment is believed to be the basement to the late Archaean greenstone successions (Bulawayan Group) with ages ranging from 2.9 Ga to 2.6 Ga. The greenstone belts have a characteristic sequence from ultramafic and mafic volcanic, to felsic volcanic, and sedimentary rocks. These have been classified into three groups named (from the oldest to the youngest) Sebakwian, Bulawayan and Shamvaian. Sebakwian Group greenstones near Shurugwe have been dated at 3.2 Ga (Moorbath *et al.*, 1976). Shamvaian Group rocks have been dated at between 2.7 Ga and 2.6 Ga (Hawkesworth *et al.*, 1975). Three suites of mid- to late-Archaean granitoids have been distinguished as (a) Chingezi Suite (2.9–2.8 Ga), (b) Sesombi Suite (2.65–2.6 Ga) and, (c) Chilimanzi Granite Suite (2.6 Ga). The emplacement of the widespread Chilimanzi Granite Suite was quasi-contemporaneous with the thrust tectonism between the NMZ and the Zimbabwe Craton (Berger *et al.*, 1995).

In the cratonic rocks (greenstone belts and granites) immediately north of the Limpopo Belt, greenschist facies of metamorphism prevails, although Limpopo structural effects may be discerned in the form of a strong ENE trend (Stagman, 1978). Towards the Zimbabwe Craton–Limpopo Belt contact, a transitional region, the Craton Margin, has greenstone belt rocks which have been tightly folded, deformed and aligned to the tectonic trend of the Limpopo Belt (Robertson, 1974). At the craton margin, the greenstones were converted into amphibolites known as schist belts, such as the Buchwa Schist Belt and Mweza Schist Belt. The ENE-trending shear deformation affected all the cratonic rocks for a distance of up to 60 km north of the Limpopo Belt (Mason, 1973). The craton margin has a weak to moderate foliation that dips steeply SE, with occasional down-dip lineations. The schist belts, such as the Mweza in Zimbabwe and the Tati in Botswana, have been thinned and stretched parallel to the Limpopo Belt and subjected to increased grades of metamorphism. In some cases, the transitions from greenschist facies to granulite facies metamorphism can be mapped along individual lithological units. ENE-striking basic dyke swarms are as common in this area as they are on the Limpopo Belt itself. The granulite zone, which lies south of the Umlali Thrust Zone and the orthopyroxene isograd, consists of a similar granite–greenstone terrain, now represented by highly deformed and attenuated granulite facies gneisses which vary from charno-enderbitic, through mafic to ultramafic, and contain meta-sediments as well.

In the southern parts of the Zimbabwe Craton, the curvature of greenstone belts (see Figure 2.2) suggests that at some time, the whole of the Zimbabwe Craton was displaced to the SW, relative to the Kaapvaal Craton, along the Limpopo Belt.

The greenstone belts and the granites/gneisses are truncated by the approximately north–south striking Great Dyke and its satellites. The Great Dyke has been dated between 2560 Ma and 2580 Ma, and the Zimbabwe Craton must therefore, have been rigid by that time (Armitage 1993). The Great Dyke is younger than the Limpopo Belt since it overprints the NMZ and is not affected by any of the Limpopo related deformation.

Porphyritic granite of the Kyle sub-province intruded the Craton Margin (Robertson, 1974). The porphyritic granite is coeval and similar to the Razi-type granite, which intruded the Umlali Thrust Zone and the NMZ. In the Kyle sub-province, the porphyritic granite forms discontinuous exposures along the strike of the schist belts.

### 2.3 The Kaapvaal Craton

The kaapvaal Craton is geologically similar to the Zimbabwe Craton, with the oldest rocks in both cratons having ages of c. 3.5 Ga. In the area immediately to the south of the Limpopo Belt, the Kaapvaal Craton has been deformed in a similar manner to the way the Zimbabwe Craton has been immediately to the north of the belt. ENE–trending shear zones persist as far south as the so–called “Murchison Line” (see Figure 2.1) 60 km south the belt. The Sutherland Greenstone Belt has been sheared parallel to the Limpopo Belt and subjected to increased grades of metamorphism in the same way as the Mweza and Tati greenstone belts to the north. ENE–trending basic dykes are common along the craton margin.

The north easterly–trending Sutherland Greenstone Belt, which is located at the north eastern extremity of the Kaapvaal Craton immediately south of the Limpopo Belt, comprises ultramafic, mafic and rarely felsic schists, with subordinate banded iron-formations, quartzites and pelitic schists (Gan & Van Reenen, 1995). The northern part of the greenstone belt is composed mainly of tremolite–actinolite schist, amphibolite and banded iron-formation, while the southern part consists mainly of amphibolite, banded iron-formation, tremolite–actinolite schist and quartz–sericite schist. One of the important characteristics of the Sutherland Greenstone Belt is that it has relatively undeformed low–grade rocks in the southern part, which are juxtaposed against strongly foliated amphibolites, and kyanite–and garnet–bearing schists in the northern part. The typical mineral assemblage of mafic schists in the greenstone belt is hornblende + plagioclase + quartz + sphene + ilmenite. The metamorphic grade increases from lower amphibolite facies in the south to middle amphibolite facies in the north. This is also indicated by the

appearance of kyanite and anthophyllite in pelitic rocks towards the north. The occurrence of kyanite is spatially restricted to the footwall of the Hout River Thrust Zone, which separates the Sutherland Belt from the Limpopo Belt. The presence of kyanite, which is being replaced by sillimanite, resulted from the overthrusting of the granulite terrain of the SMZ onto the adjacent greenstone belt.

#### 2.4 The Central Zone

The Central Zone (CZ) comprises moderately to highly metamorphosed and intensely folded rocks of sedimentary, volcanic and intrusive origin, with characteristic N-S trending foliations (Armitage, 1993). The rocks are dominantly metamorphosed supracrustal, passive continental margin type lithologies, infolded with high metamorphic grade gneisses (Sand River Gneiss). The high-grade supracrustal rocks of the Beitbridge Complex (Group) consist of meta-quartzite, meta-pelite, magnetite quartzite and quartzofeldspathic gneisses with minor intercalations of marble, calcareous meta-pelites and amphibolite. These rocks have been interpreted as a sedimentary cratonic shelf sequence (Jaekel *et al.*, 1997). The rocks display early (pre-3000 Ma) N-S trending deformation features not observed in the marginal zones or in the adjacent cratons. The structures record a poly-phase tectonic evolution and cannot be correlated across the bounding shear zones with those in the SMZ and NMZ (Watkeys *et al.*, 1983). The CZ lithologies are not related to those of either adjacent craton. The lithologies, structural trends and isotopic signatures are different (Mc Court & Veamcombe, 1987).

The CZ is situated in southern Zimbabwe and northern parts of South Africa. In Zimbabwe, rocks of the CZ are classified into formations of the Beitbridge Group, ancient gneiss inliers of the basement Macuville Group, Bulai Gneiss intrusions and Ultramafic Complexes (Stagman, 1978). The Beitbridge Group is sub-divided into the Diti Formation in the north, overlain by an infolded sequence known as the Nulli Formation in the south. The Nulli Formation is equivalent, in part, to the Messina Subgroup of South Africa. The rocks of the Macuville Group are banded, migmatitic and often nebulitic grey rocks, of dioritic, tonalitic, granodioritic or enderbitic composition and characteristically contain little or no garnet.

The Diti Formation, which occupies the greater part of the of CZ in Zimbabwe, consists predominantly of banded garnetiferous biotite gneisses which may contain up to 70% of these minerals, but more usually have significant quantities of perthite, microcline, plagioclase and quartz. Also present are occasional lenses composed garnet and biotite, with barrel-shaped corundum crystals and intergrown sillimanite. Thin horizons of

massive quartzite, magnetite quartzite, dolomitic marble and calc-silicate rocks are intercalated throughout the succession. A layered anorthosite suite dated at  $3221 \pm 48$  Ma (Broderick, 1979) intrudes the Diti Formation rocks. Near the top of the Diti Formation, is an orange-brown weathered gametiferous biotite-feldspar paragneiss of granitic aspect, known as the Singelele Gneiss (Stagman, 1978). Jaeckel *et al.* (1997) describe the Singelele Gneiss as a heterogeneous granodioritic to quartz monzonitic rock. Also towards the top of the formation are grunerite-bearing magnetite quartzites with associated biotite-cordierite gneiss.

In the Messina area of the Beitbridge Complex (Group), the Singelele Gneiss locally cuts the layering of the supracrustal lithologies, contains xenoliths of paragneiss and also cuts the Messina Layered Intrusion (Watkeys *et al.*, 1983). The Singelele Gneiss has yielded protolith ages between 2.58 and 2.55 Ga (Jaeckel *et al.*, 1997) and has suffered poly-phase high-strain ductile deformation. This poly-phase deformation (also in the Sand River Gneiss) must have therefore, occurred later than 2.55 Ga.

The Nulli Formation, which overlies the Diti Formation, forms a prominent range of hills and consists of massive and granular sillimanite-bearing quartzites and beds of diopside-bearing calc-silicate rocks. Both lithologies are truncated by sills and dykes of mafic composition now granulite and amphibolite.

Two major types of syntectonic Ultramafic Complexes have intruded the Beitbridge Group (Stagman, 1978). Meta-pyroxenite and serpentinite form interbands and pods associated with magnetite quartzite horizons and occur as large oval plugs in fold closures. Layered meta-anorthosite complexes ( $3221 \pm 48$  Ma) occur east of Beitbridge, trending northwards from South Africa, across the Limpopo River. They comprise sheets up to 400m thick of banded, mesocratic and medium-grained, anorthite-hornblende granulites. There are rare inclusions containing large crystals of kornepine in association with corundum, sillimanite, sapphirine, cordierite and gedrite. In the Messina area, the supracrustal assemblage is intruded by rocks of the Messina Layered Intrusion (Jaeckel *et al.*, 1997). The intrusion is a magmatic complex in granulite facies principally consisting of anorthositic and leucogabbroic gneisses.

The Bulai Gneiss occurs northwest and southwest of Beit Bridge. It is syn-tectonic and is considered to have formed by anatexis from gneisses of the Macuville Group (Stagman, 1978). Its composition varies from grey tonalite to porphyroblastic granodiorite and is surrounded by a chamockitic halo. In South Africa, the Bulai Gneiss, also known as the

Bulai Batholith, occurs NW of Messina and comprises enderbitic, charno-enderbitic, tonalitic, granodioritic and granitic gneisses (Jaeckel *et al.*, 1997). It is considered to represent a composite plutonic body, which was emplaced into an already deformed and metamorphosed basement under high- grade metamorphic conditions on account of the recognition of relict magmatic orthopyroxene. The Bulai Gneiss truncates the Singelele Gneiss and has been dated at 2450 Ma. It has also experienced a c. 2.0 Ga metamorphic event that affected the CZ of the Limpopo Belt.

The north–easterly–trending Sand River Gneiss occurs south–east of the town of Messina. The Sand River Gneiss comprises migmatitic and layered grey granitoid gneisses, which have been previously considered to be the oldest (3.8 Ga) rocks in the Limpopo Belt (Jaeckel *et al.*, 1997). The gneisses are tonalitic, trondhejmitic, quartz dioritic and granodioritic, locally orthopyroxene–bearing, and are cut by mafic dykes and a variety of granitoid bodies. Supracrustal rocks of the Beitbridge Complex (Group) are infolded and tectonically interleaved with the Sand River Gneiss and are intruded by the Alldays Gneiss. The gneisses display evidence for poly-phase deformation and have been considered to represent a basement to adjacent and infolded granulite facies meta-sediments. The age of 3.8 Ga (Barton *et al.*, 1983), for the Sand River Gneiss, was determined using the Rb–Sr whole–rock method and U–Pb on zircons. Rocks from the same locality have recently been dated and yielded Nd mean crustal residence ages of 3.2–3.0 Ga. Retief *et al.* (1990) obtained ages of 3.29–3.2 Ga and also found a clear zircon phase, occurring as overgrowth and discrete grains, with an age of 2.05 Ga. Jaeckel *et al.* (1997) obtained protolith ages between 3.2 Ga and 2.6 Ga for the Sand River Gneiss. These recently determined ages provide evidence against the Sand River Gneiss constituting an early Archaean basement to the Beitbridge supracrustal sequence. The Sand River Gneiss contains several amothosite xenoliths which probably belong to the Messina Layered Intrusion and which now occur as tectonic lenses or boudins. Therefore, the Messina Layered Intrusion predates both the Sand River Gneiss and the Alldays Gneiss. The 2.0 Ga age represents a major high-grade metamorphic event in the Central Zone of the Limpopo Belt, and in the Triangle Shear Zone at the CZ–NMZ boundary.

The tectonic history of the CZ is complex and is thought to have commenced with the folding and metamorphism of the Macuville Group, prior to the deposition of the Beitbridge cover sequence in which it is possible to distinguish four major deformational events (Stagman, 1978). The first event led to the production of recumbent isoclinal folds with easterly axes and was accompanied by a metamorphic phase, of kyanite–granulite

grade, during which the ultramafic complexes were emplaced. A long quiescence period was followed by a phase that produced upright isoclinal folds about northeasterly to north–northeasterly axes. Metamorphism of sillimanite–granulite granulite grade progressed locally to anatexis of the basement and intrusion of the Bulai Gneiss. Subsequently, the intensity of metamorphism declined through the final phase of folding which resulted in north–west–trending, upright cylindrical folds that gave rise to the open dome and basin structures of the present topography.

Granulite–facies pelitic gneisses of the Beitbridge Complex contain abundant spherical, multifaceted zircons, which reflect new zircon growth near or at the peak of metamorphism (Jaeckel *et al.*, 1997). The multifaceted zircons provide ages with a mean at  $2026.5 \pm 6.3$  Ma, which is interpreted as reflecting a high P–T event ( $>10$  kbar,  $825^\circ \pm 25^\circ\text{C}$ ). Granitic melt patches in the meta-pelites, as well as in the Sand River Gneiss and anatectic granites, are probably related to rapid near–isothermal decompression to below 3–5 kbar and  $600^\circ - 700^\circ\text{C}$ , shortly after the peak of metamorphism. These rocks contain new magmatic zircons, which yielded a mean age of  $2005.6 \pm 4.4$  Ma and probably reflect a crustal melting event as a result of rehydration of the granulitic assemblage. The zircons do not have an indication of poly-metamorphism in the CZ. The zircon data supports earlier suggestions for only one, single granulite–facies event in the Central Zone (Watkeys, 1984), and this could have occurred *c.* 2027 Ma. Since most of the deformation seen in the gneisses of the Messina area must have occurred later than 2.55 Ga, it is likely that the “Limpopo Orogeny”, at least in the Central Zone, is not an Archaean event, but occurred in the early Proterozoic (Jaeckel *et al.*, 1997). Rapid uplift and cooling to below  $500^\circ\text{C}$  in the rocks of the Central Zone is recorded by Rb–Sr whole-rock and mineral ages of *c.* 1960 to just over 2000 Ma (Barton *et al.*, 1983). The CZ reflects similar features as other high-grade terrains in the world, namely that crustal thickening and granulite metamorphism was followed almost immediately by rapid uplift and cooling. Thus, the “Limpopo Orogeny” must have occurred about 2.0 Ga, at least for the Central Zone.

Since the Central Zone has contrasting geological features (lithology and structure), when compared to the adjacent marginal zones and cratons, it is a distinct terrain. It was either (a) wedged in sideways as a block from the NE between the NMZ and SMZ (Treloar *et al.*, 1992), or (b) transported as a giant nappe (Mc Court & Vearncombe, 1987), or (c) exotic thrust sheet (Mc Court & Vearncombe, 1992), or (d) a “pop-up” structure related to collision of the Kaapvaal and Zimbabwe cratons (De Wit *et al.*, 1992).

## 2.5 The Southern Marginal Zone

Rocks of the Southern Marginal Zone (SMZ) have similar geochemical characteristics to those of the Kaapvaal Craton and have been regarded as their metamorphosed equivalents. The SMZ is also, characterized by a northwesterly dipping, pervasive, ENE-trending foliation. NNW and NNE striking fractures are common and are often filled with dolerite dykes. The sinistral and northerly-dipping Palala Shear Zone marks the boundary between the SMZ and the Central Zone.

Seventy percent of the SMZ consists of charno-enderbitic gneisses (Baviaan Kloof Formation) and their amphibolite equivalents (Berger *et al.*, 1995). Supracrustal rocks (Bandelierkop Formation), including ultramafic to mafic meta-volcanics, quartz-magnetite lithologies, quartzites and meta-pelites, constitute the remainder. The supracrustal lithologies are highly attenuated and tectonically dismembered (Gan & van Reenen, 1995). Zircons from an enderbite sample yielded an age of  $2715 \pm 5$  Ma (Retief *et al.*, 1990). The Matok Intrusive at the SMZ–Kaapvaal Craton boundary, comprises charno-enderbites and granitoids. Zircons from the intrusive have yielded ages between 2664 and 2671 Ma (Retief *et al.*, 1990).

The SMZ has been sub-divided into a granulite zone in the north and a rehydrated granulite zone in the south, separated by a retrograde ortho-amphibole isograd. Granulite facies prograde metamorphism occurred during the Limpopo orogeny, under conditions of 800°C and 9 kbar (van Reenen, 1986), and is characterized by the mineral assemblage: -

- (a) quartz + plagioclase + hypersthene + biotite  $\pm$  garnet  $\pm$  cordierite  $\pm$  sillimanite, in meta-pelitic granulite;
- (b) olivine + spinel + enstatite + parasitic hornblende, in ultramafic granulite; and
- (c) hypersthene + augite + plagioclase + hornblende, in mafic granulite.

A late alteration (rehydration) event established a retrograde ortho-amphibole isograd, which is defined in pelitic granulite, by the replacement of cordierite by gedrite and kyanite, and of hypersthene by anthophyllite (van Reenen, 1986), at temperatures of 600°-620°C and pressure of 6 kbar. Rehydration, was considered to have been caused by carbon dioxide-rich fluids, derived either from the dehydration of underthrust greenstone sequences, or from a deep-seated mantle source during the Limpopo orogeny, when the SMZ was thrust onto the Kaapvaal Craton.

## 2.6 The Northern Marginal Zone

The Northern Marginal Zone (NMZ) is 450 km long, WSW–ENE striking, and has a maximum width of 70 km. To the east, the mid-Proterozoic, southern Mozambique Belt cuts the NMZ, while the westward continuation is partly obscured by Karoo basalts. The NMZ can be sub-divided into three zones: (a) Northern Marginal Zone (*sensu stricto*) in the north, (b) Transition Zone, and (c) Triangle Shear Zone in the south (Kamber & Biino, 1995). The Northern Marginal Zone *sensu stricto* is a granulite facies zone comprising charno-enderbites, porphyritic granites and supracrustal rocks. The study area is situated in this NMZ (*sensu stricto*).

A reverse-sense shear zone (Umlali Thrust Zone) forms the boundary between the NMZ and the Zimbabwe Craton. The thrust zone is ENE-trending and comprises a series of southerly dipping thrust faults. The thrust zone has intermittent exposures along strike (Mkweli *et al.*, 1995). The apparent absence of the shear zone in places is due to syn-late tectonic intrusion of Razi granites into the shear zone. These granites, which are commonly porphyroclastic, can be found as mylonites, protomylonites and undeformed intrusions in the shear zone, and therefore intruded the shear zone throughout the deformation (Rollinson & Blenkinsop, 1995). The ortho-pyroxene (hypersthene)–in isograd occurs at or within a few kilometres of the hanging-wall boundary of the thrust zone. Hypersthene is characteristic of all the rock types in the NMZ, from ultramafic to quartzo-feldspathic gneisses. Diopside is usually subordinate to hypersthene (Robertson, 1974).

The dextral Tuli–Sabi–Triangle Shear Zone marks the boundary between the NMZ and the Central Zone. The Triangle Shear Zone has pervasive gentle dipping and plunging fabrics. The outcrop width of the shear zone is 30–50 km. The shear zone is dominated by protomylonites and mylonites derived from the NMZ lithologies, such as garnetiferous felsic gneisses and porphyroclastic granites. Also, quartzitic rocks, calc-silicate rocks and pelites have been recognized in the shear zone, suggesting that the Central Zone lithologies were also entrained in the Triangle Shear Zone.

The NMZ (*sensu stricto*) has some similarities with a granite–greenstone terrain at granulite facies (Rollinson & Blenkinsop, 1995). It is juxtaposed with the greenschist/amphibolite-facies granite–greenstone terrain of the Zimbabwe Craton. The NMZ and Zimbabwe Craton have very similar crustal thicknesses (Stuart & Zengeni, 1987), implying that the NMZ represents a zone of crustal thickening relative to the

Zimbabwe Craton. The majority of the rock types in the NMZ are magmatic in origin and crustal thickening is believed to have occurred through a combination of magmatic and tectonic processes. Two main groups of lithologies occur in the NMZ. A "Plutonic Assemblage" is dominant and intrudes a volumetrically minor "Supracrustal Assemblage" (Rollinson & Blenkinsop, 1995).

#### The Plutonic Assemblage

The Plutonic Assemblage dominates the NMZ. In places of less intense deformation, supracrustal rocks are truncated and dismembered by intrusion of Plutonic Assemblage rocks. Satellite images and field observations indicate individual plutons with rounded outlines. Individual plutons have diameters of a few kilometres and may be diapirs. Some bodies have a massive appearance implying that they have not been significantly deformed since their emplacement. The major plutonic bodies are granitic, tonalitic and trondhejmitic in composition, and these are cut by veins and larger bodies of a white, garnet–mesoperthite granite.

Ridley (1992) proposed that some of the granulites of the Plutonic Assemblage are magmatic granulites, which crystallized directly from a dry magma at depth in the crust. This would suggest that the granitic, tonalitic and trondhejmitic plutonic bodies are more strictly charnockites and enderbites. The charnockites and enderbites are primary magmatic granulites. Three lines of evidence may be used to support this hypothesis: (a) mineralogical studies have shown biotite–quartz symplectites pseudomorphing orthopyroxene in the NMZ granulites. This may be interpreted as a product of the reaction: *orthopyroxene + melt* → *biotite + quartz*; during the cooling of a magma, emplaced at depth in the crust. Experimental studies indicate temperatures of between 800° and 850°C for this reaction. The lack of association between biotite and K-feldspar indicates that comparable, subsolidus reaction involving K-feldspar and water was not responsible for the production of biotite. Thus, the orthopyroxene is a magmatic phase and not a product of later granulite–facies metamorphism.

Further mineralogical evidence is in the observation, in granitic composition rocks, of mesoperthite feldspars and garnets sieved with quartz, which are interpreted as magmatic (Rollinson & Blenkinsop, 1995); (b) another argument in favour of dry, granulite facies magmas emanates from the presence of mafic xenoliths in the felsic rocks. Some of the xenoliths preserved in homogeneous felsic granulites are amphibolitic in mineralogy, but have a dehydrated rim up to 1 cm wide, containing pyroxenes. It is argued that the dehydration was caused by the dry felsic magma, emplaced around the

amphibole inclusion, and (c) the felsic granulites are even-grained, with igneous textures. If they were tonalites, subjected to later granulite facies metamorphism, then they are remarkably undeformed. The textures argue for their emplacement as dry, high temperature melts. Pressures calculated from garnet–orthopyroxene–equilibria suggest that they were emplaced directly into the lower crust at pressures of 8–9 kbar (Rollinson & Blenkinsop, 1995).

The quartzo–feldspathic gneisses range in composition, from charnockitic to enderbite where hypersthene–bearing, and from adamellite to potassium–rich granite where hypersthene–free (Robertson, 1974). The charno–enderbites are dark to pale brown and have a greasy appearance. They are rich in blue quartz and honey-brown, cryptically twinned, high–temperature perthites. The charno–enderbites are hypersthene–bearing, oversaturated, leucocratic to mesocratic rocks, which occur in the zone of granulite metamorphism (Odell, 1975). The rock is a charnockite (*sensu stricto*) if the potash feldspar is the dominant feldspar. When plagioclase is the dominant feldspar, the rock is an enderbite (s.s.)

XRF analyses on a charnockite yielded similar chemistry to adamellites in the (Rhodesian) Zimbabwe Craton (Odell, 1975), suggesting that the two terrains may be related.

#### Later Porphyritic Granites; the Razi Suite

A suite of K-rich, porphyritic granites, known as the Razi Suite (Robertson, 1974), intrudes the NMZ–Zimbabwe Craton transition in the area SW of the Buchwa Greenstone Belt, and extends along strike for approximately 100 km. The granites form a continuous ENE–trending body, which approximates to the ortho–pyroxene isograd (Odell, 1975). The porphyritic granites are also found throughout the NMZ and in the Triangle Shear Zone. In places they appear to be locally derived by partial melting. The granites are generally weakly deformed and in places, they were emplaced synchronously with the thrusting of the NMZ onto the Zimbabwe Craton. The porphyritic granites are most common in the zone between the low-pressure granitic gneisses of the craton and the granulite felsic gneisses of the NMZ. The Samba–Rongwe is a prominent (17 km long) porphyritic granite body within the NMZ (Odell, 1975). Their mineralogy is variable, implying that they crystallized under a range of water pressure conditions. On the craton margin, the Razi granites contain biotite and hornblende and are dominated by white feldspars in hand specimen. In the NMZ, biotite and hornblende overgrow ortho–pyroxene,

and in handspecimen, the rocks are darker with honey-brown feldspars and blue-grey quartz, typical of felsic igneous rocks at granulite facies (Rollinson & Blenkinsop, 1995).

The granite is coarse-grained and contains abundant, large potash feldspar megacrysts. The megacrysts, which are grey to brown, may be round, ovoid or, more commonly, rectangular in shape, range from 10 to 50 mm across and display a preferred orientation near the contact, where a foliation has developed. The interior of the granite is massive with the megacrysts being disorderly and containing specks and patches of biotite and other mafic material. The megacrysts are often so numerous that their volume exceeds that of the groundmass, which is very rich in mafic material (Robertson, 1974). Leucocratic xenoliths, of the surrounding charno-enderbites, are common in the porphyritic granite. The xenoliths, with sharp contacts and are truncated by the granite, which is clearly intrusive.

#### The Supracrustal Assemblage

In the NMZ, supracrustal lithologies occupy approximately 10% of the exposed area. The major rock types are meta-basites (mafic granulites and amphibolites) and magnetite quartzites/banded iron-formation. They form narrow bands up to a few hundred metres wide and several kilometres long (Odell, 1975) and are easily identified on satellite images of the area. Other sedimentary rocks are pelites, quartzites and calc-silicate rocks, but these are rare. Ultramafic layered complexes are intimately associated with, and possibly intrusive into the meta-sediments and meta-basites. They are best preserved in the central part of the NMZ, south of the Buchwa Greenstone Belt, and comprise serpentinites and meta-pyroxenites with chromite layers. Some layered complexes contain a metagabbro–anorthosite association (Robertson, 1974).

The meta-basites comprise only about 5% of the NMZ area (Odell, 1975). They occur infolded with charno-enderbites throughout the area, but are mainly concentrated in two major zones, where they are often associated with magnetite-quartz granulites and depict the structure. The two dominant linear zones are situated (a) in the south, with tight folding, swarm of dolerite dykes and small pods of ultramafics, and (b) in the north, with more open folds. The meta-basites have a generalized assemblage: pyroxene + plagioclase ± hornblende ± biotite. There are two types of mafic granulite (a) plagioclase–pyroxene granulites, and (b) plagioclase–amphibole–pyroxene granulites. Evidence of later retrogressive metamorphism is shown by small amounts of pale green amphibole on the edges of orthopyroxene grains.

A geochemical study (Rollinson & Lowry, 1992) showed that the meta-basites are olivine tholeiites with flat REE patterns and geochemically resemble basaltic lavas found in the greenstone belts of the Zimbabwe Craton. The meta-basites are typical Archaean tholeiites and their association with banded iron-formation suggests that they could be greenstone belt remnants. They are the oldest recognizable part of the NMZ. The mafic granulites are the most abundant of the greenstone belt remnants and their structural setting depicts the mobile belt folding (Robertson, 1974).

Magnetite–quartz granulites form long, narrow bands, some being garnetiferous, closely associated with mafic granulites. They occur in three types: (a) siliceous type, which is grey and glassy in appearance, (b) iron-rich, which is brown with hydrated iron oxides on weathered surfaces, and (c) garnetiferous, which is grey, coarse-grained with garnet crystals. Two varieties of calc-silicate rocks occur: (a) white, medium-grained gneisses with a sugary texture and blotched with green amphibole, and (b) with ochre-coloured weathered skin, beneath which is a grey, fine-grained, fresh rock. Grey, banded, quartz–cordierite–garnet–sillimanite paragneisses are sometimes encountered, with layers of cordierite–garnet–sillimanite–biotite assemblage, interspaced with layers of quartz–plagioclase and quartz–microcline. The paragneisses are probably metamorphosed pelites (Odell, 1975).

#### Metamorphic Petrology

Rocks of the NMZ (*sensu stricto*) have been metamorphosed to granulite facies, with calculated peak metamorphic conditions varying along the belt from  $5 \pm 1$  kbar,  $825^\circ \pm 50^\circ\text{C}$  in the west, to  $8.4 \pm 1$  kbar,  $850^\circ \pm 50^\circ\text{C}$  in the east, indicating differential uplift (Rollinson & Blenkinsop, 1995). There is a zone of variable metamorphism, comprising both granulite and amphibolite facies rocks (Transition Zone) approximately 25 km wide north of, and associated with, the Triangle Shear Zone. The metamorphic history of the NMZ is complex, as suggested by mafic granulites of the supracrustal assemblage. The mafic granulites contain the mineral assemblage orthopyroxene–clinopyroxene–plagioclase–parasitic hornblende. Replacing the hornblende are coronas of a quartz–magnetite–orthopyroxene symplectite. These textures are interpreted as an equilibrium pyroxene–hornblende–plagioclase granulite–facies assemblage in which the hornblende was dehydrated in a subsequent metamorphic event (Rollinson & Blenkinsop, 1995). Probable meta-sediments, containing the granulite–facies assemblage: quartz–plagioclase–clinopyroxene–magnetite, show coronas of euhedral garnet intergrown with quartz on the magnetite and clinopyroxene. Therefore, these rocks have also experienced two granulite facies events.

In contrast, relatively undeformed members of the plutonic assemblage show a very simple metamorphic history. Biotite–quartz symplectites pseudomorphing orthopyroxene, interpreted by Ridley (1992) as indicative of a magmatic charnockite origin, represent the final stage of a single granulite facies crystallization. Unlike the pelites, there is no evidence for a later dehydration. Rocks of both assemblages are retrogressed in places. The retrogression is associated with heterogeneously developed late deformation (Ridley 1992), P–T conditions of which are poorly constrained, but are *c.* 4 kbar, 600°C.

Hypersthene, garnet, diopside, scapolite and cordierite characterize the granulite terrain (Odell, 1975). Also, the feldspars have a honey-brown and greasy appearance. Potash feldspar has distinct, very fine-scale cross-hatch twinning (micropertthite), or is occasionally untwinned. Some sodic feldspars are also untwinned and contain antiperthitic patches of untwinned potash feldspar. Such minerals and their textures are characteristic of intermediate pressure, orthopyroxene-plagioclase granulite sub-facies. The occurrence of olive-green, granulite facies hornblende, in some assemblages, indicates an overlap with the hornblende–orthopyroxene–plagioclase granulite sub-facies. Evidence is seen in thin section, of (a) dehydration of hornblende to pyroxene, and (b) hydration of pyroxene to hornblende.

#### Geochronology

The age of the granulite facies metamorphism of the NMZ is constrained by a 13–point Rb–Sr whole rock errorchron to  $2880 \pm 47$  Ma (Rollinson & Blenkinsop, 1995). This may also be the emplacement age of the Plutonic Assemblage. Zones of shearing, retrogression and associated metasomatism were tentatively dated at 2590 Ma.

The syn- to late-tectonic Razi Granite Suite is an important time marker in the evolution of the NMZ. The granite was emplaced into the Umlali Thrust Zone and appears to be synchronous with thrusting. The porphyritic granite indicates a close association between granite emplacement, and the shearing, metasomatism and retrogression of the NMZ granulites (Rollinson & Blenkinsop, 1995). Recent zircon geochronology on a late tectonic microgranite dyke truncating a member of the Razi Granite Suite has constrained the age of these granites to  $2627 \pm 7$  Ma (Mkweli 1995). The age of this microgranite dyke also constrains the timing of the thrusting of the NMZ onto the Zimbabwe Craton to before 2627 Ma. This age is within error of an Rb–Sr errorchron of  $2583 \pm 52$  Ma obtained on porphyritic Razi Granites and retrogressed rocks in the NMZ. These results also suggest that the Razi Granites and the thrusting are of the same age (within error)

as the  $2570 \pm 70$  Ma (Rb–Sr errorchron) Chilimanzi Suite granites in the Zimbabwe Craton. At present, it is not clear whether the wide time interval, between the emplacement/granulite facies metamorphism of the granitic and tonalitic gneisses at c. 2800 Ma, and granite emplacement/thrusting/retrogression at 2600 Ma, represents a period of continuous or episodic crustal growth.

#### Geochemistry and origins of the plutonic assemblage

On the Ab–An–Or classification diagram (after O'Connor, 1965) for felsic igneous rocks, rocks of the granulite facies Plutonic Assemblage of the NMZ plot as tonalites, trondhejmites, granodiorites and granites (Rollinson & Blenkinsop, 1995). Enderbites plot, by definition, in the fields of tonalite and trondhejmite, whereas charnockites lie in the fields of granodiorite and granite (Berger & Rollinson, 1997). Retrogressed samples plot principally as granites, as expected from their observed K–enrichment. The majority of these charno–enderbites plot as granites and tonalites (also including diorites). Trondhejmites are not common, indicating that the NMZ Plutonic Assemblage is less sodic than other Archaean tonalite–trondhejmite–granodiorite (TTG) suites. In addition to their Na–poor character, the enderbites and charnockites of the NMZ are peraluminous.

Rocks of the Plutonic Assemblage have compositional variations from dioritic to granitic ( $\text{SiO}_2$  contents 50–78 wt %). On Harker diagrams, the major element oxides  $\text{TiO}_2$ ,  $\text{Al}_2\text{O}_3$ , FeO,  $\text{Fe}_2\text{O}_3$ , CaO, MgO, MnO and  $\text{P}_2\text{O}_5$  all show strong negative correlations with  $\text{SiO}_2$  (Rollinson & Blenkinsop, 1995; Berger *et al.*, 1995). On a ternary diagram of  $\text{K}_2\text{O}$ ,  $\text{Na}_2\text{O}$  and CaO, the trend for the less evolved lithologies is characterized by a general increase in  $\text{K}_2\text{O}$  and  $\text{Na}_2\text{O}$ , whereas the more differentiated rocks show increasing  $\text{K}_2\text{O}$  (Berger *et al.*, 1995). In enderbites, charnockites, retrogressed charnockites and Razi Granites, the pattern of high Rb, Ba, Th, U and K, and low Nb, Ti, Y and Tb is apparent (Berger & Rollinson, 1997). The trace element character of the suite is typified by highly fractionated rare earth elements (REE), and chondrite normalized multi-element plots indicate that the suite has positive Th and negative Nb, Sr, P and Ti anomalies (Rollinson & Blenkinsop, 1995). Depletion in Rb was noted in some samples, but is not universal. Within the Plutonic Assemblage, dioritic rocks ( $\text{SiO}_2 = 48\text{--}63$  wt %) have moderately fractionated REE patterns  $(\text{Ce}/\text{Yb})_N = 2.4$  to 10, with negative Eu anomalies, which show increasing steepness with increasing light REE content. The porphyritic Razi Granites ( $\text{SiO}_2 = 66\text{--}72$  %) have trace element patterns similar to those of charno–enderbites.

The most striking features of the geochemistry of the granulite facies Plutonic Assemblage are the highly fractionated REE, the Nb depletion and the Th enrichment.

The Nb depletion is usually associated with crust-forming processes and is thought to arise from the retention of Nb in a Ti-bearing species during partial melting. The extreme REE fractionation is indicative of residual garnet (or hornblende) in equilibrium with the felsic melt (Rollinson & Blenkinsop, 1995).

The tonalite-granite magmas of the NMZ were most probably derived from a mafic source, either by partial melting or by fractional crystallization. The dominance of tonalitic and granitic members over dioritic mafic rock types suggests an origin by partial melting of a mafic source.

#### Structural Geology of the NMZ

The predominant structural feature throughout the NMZ is a persistent ENE foliation, approximately parallel to the margins of the Limpopo Belt. As this invariably dips south, isoclinal folding is strongly suggested (Stagman, 1978). The foliation generally dips SSE, but between the upper reaches of Bangala Dam (Renco Mine area) and Samba-Rongwe porphyritic granite, dips are variable in direction and amount (Odell, 1975). This zone of variable dip directions and amounts is locally known as the Mauch Shear Zone (in the study area), or Mtirikwi Shear Zone (Renco Mine area). Coward *et al.* (1976) separated two major deformation phases for the NMZ. A gneissic fabric in the charno-enderbites, represents the earliest phase (F1). The F1 has a relatively constant ENE-WSW trend and steep southerly dips. The second phase of deformation (F2), formed broad anastomosing zones, up to 1 km wide, in the centres of which narrow mylonitic zones were developed. The fabric also has an ENE-WSW trend, but has moderate to steep (N or S) dips. These zones enclose up to 5 km wide lenses massive and homogeneous charno-enderbites (Odell, 1975). Narrow straightened zones of intense shearing occur separated by large, relatively unsheared areas. Plastic deformation led to extreme attenuation, boudinaging and refolding of fold limbs. Later deformation about north-westerly axes sporadically produced asymmetric domes and basins. Major dextral shearing, characterized in several areas by flaser gneisses, is almost always associated with reduction in metamorphic grade. The latest deformation activity was brittle fracture, related to the intrusion of the Great Dyke, which produced a conjugate set of faults often filled with mafic dykes (Stagman, 1978).

#### The northern margin of the NMZ

The Umlali Thrust Zone consists of several mylonitic high strain zones typically a few tens of metres wide, which are separated by protomylonites (Rollinson & Blenkinsop, 1995). The total width of the thrust zone amounts to several kilometres. In the mylonite

zones, the foliation dips at 30°- 40° southeast and a strong mineral stretching lineation is always within approximately 10° of the down-dip direction of the foliation. A reverse shear sense is clearly indicated by several excellent shear sense indicators, including  $\sigma$  and  $\delta$  porphyroclast tails, and rolling structures. The latest stage of this reverse shearing occurred under greenschist facies conditions as indicated by syn-tectonic growth of chlorite and epidote.

Various estimates of displacement (about the Umlali Thrust Zone) have been mentioned by a number of authors. James (1975) estimated a throw of 25 km and a heave of 27 km, using integration of strain trajectories, in an area southeast of Masvingo. Ridley (1992) estimated vertical displacements of 5–20 km and net displacements of 10– 40 km from the metamorphic contrast across the shear zone around Renco Mine. Estimates by Rollinson & Blenkinsop (1995), using integration of strain trajectories from an area southwest of Buchwa (~100 km southwest of Renco), indicate a maximum of a few kilometres of displacement.

The fabrics in the mylonites and protomylonites are truncated by a system of shear zones that are typically one to a few metres wide, occurring in vertical to sub-vertical orientations and striking either to the NNE or NW. The shear zones with NNE trends and sub-horizontal lineations are invariably sinistral, and those with NW trends and sub-horizontal lineations are dextral. These shear zones are concentrated in the northern part of the NMZ, but are common throughout the NMZ.

#### *The Northern Marginal Zone*

The Plutonic and Supracrustal Assemblages of the NMZ have a moderately developed foliation with sub-vertical dips to the southeast or, rarely northwest. The foliation is common throughout the NMZ, but there are bodies of charnockite/enderbite that are massive and only foliated near their margins. Down-dip linear fabrics are rare. Meta-basic rocks and meta-sediments occur in narrow bands that define isoclinal folds, with wavelengths of several hundreds of metres. Fold axes plunge gently to the northeast or southwest. Also identified are eye-shaped structures, with plunges of fold axes only changing by a few tens of degrees from one end of the structures to another: these structures are therefore periclinal and not sheath folds as reported by previous workers (Rollinson & Blenkinsop, 1995).

All the structures in the NMZ are compatible with a bulk strain consisting of NNW–SSE horizontal shortening and vertical extension. The reverse sense shear zone, at the

Zimbabwe Craton–NMZ boundary, also indicates a NNW–SSE shortening direction. Coward *et al.* (1976) and Ridley (1992) distinguished two phases of deformation in the NMZ on the basis that later fabrics are associated with granulite retrogression to amphibolite facies. Since fabrics belonging to both phases of deformation are parallel and have the same strain geometry, Rollinson & Blenkinsop, (1995) interpreted all these structures as part of a single progressive deformation.

#### The southern margin of the NMZ

On approaching the southern limit of the NMZ, the steeply–dipping foliations are replaced by foliations that dip gently to the southeast and carry horizontal to sub-horizontal mineral stretching lineations. The frequency of these foliations increases over a zone of approximately 25 km wide, until the foliations become pervasive in the southernmost part of this zone. This area with both steep and gentle dipping foliations is known as the Transition Zone (Rollinson & Blenkinsop, 1995). The lineations in the Transition Zone may be divided into those that (a) plunge steeply to the SE and associated with steeply dipping foliations, and (b) are sub-horizontal and associated with gently dipping foliations.

The northern boundary of the Triangle Shear Zone is where the gently dipping and plunging fabrics in the Transition Zone become pervasive. The outcrop width of the Triangle Shear Zone is 30–50 km. The Triangle Shear Zone is composed of protomylonites and mylonites that dip gently to the southeast. The mylonites carry strong sub-horizontal mineral stretching lineations, and have consistent dextral shear sense indicators, including  $\sigma$  and  $\delta$  porphyroclast tails and rolling structures. Syn-kinematic garnets from the Triangle Shear Zone yielded two Sm-Nd whole-rock dates of *c.* 2000 Ma. Deformation under granulite facies at this age, has been suggested in the Triangle Shear Zone, and such a proposal raises major problems for the chronology of the Limpopo Belt.

#### Evolution of the granulites in the NMZ

Using evidence on relative age relation, nature of PT evolution and deformation, it may be concluded that none of the current models can correctly explain the evolution of the NMZ. The evolution of the NMZ is complex and includes 4 metamorphic stages, 2 major plutonic episodes and at least 3 deformation events (Kamber & Biino, 1995). The oldest rocks, mafic granulites, record all the four stages of metamorphic mineral growth. The first two stages predate deposition of sediments and the intrusion of voluminous enderbites and chamockites between 2.72 and 2.62 Ga. Abundant reaction textures, preserved in mafic granulites, meta-sediments, metamorphosed chamockite and

enderbite, allow for the qualitative reconstruction of the PT evolution. Prograde heating occurred in the sillimanite stability field. Temperatures between 800°C and 850°C, at pressures as low as 0.4–0.5 Gpa, are indicated by various mineral assemblages. The thermal peak was followed by an increase in pressure to a maximum of 0.85 Gpa. The NMZ granulites were finally exhumed in a separate event along upper greenschist-facies thrusts, in response to a transpressive orogeny affecting the units further south at 2.0 Ga (Kamber & Biino, 1995). All Archaean rocks in the NMZ underwent granulite facies metamorphism and varying degrees of retrogression. Kamber & Biino (1995) identified 4 metamorphic mineral blastesis (growth of a metamorphic mineral) events, which they used as relative time markers, representing the 4 metamorphic stages.

- (a) The pre-intrusive units are characterized by an association of meta-ironstones, meta-pelites, quartzites, calc-silicate rocks and meta-basites, and subordinate ultramafics. The majority of them represent remnants of greenstone belts. Their protolith ages are not known, but a minimum of 2.72 Ga is indicated, given by the oldest enderbite intrusion. Xenoliths of meta-basites and meta-sediments in later intrusions sometimes show a pre-intrusive metamorphic fabric defined by banding of pyroxene, hornblende and plagioclase. This high-grade event is *Stage 1*, which is followed by a retrograde *Stage 2*.
- (b) Chamo-enderbitic plutons intruded the NMZ (*sensu stricto*) from 2.72 to 2.62 Ga (see Figure 2.6). Macroscopically, these intrusives are slightly and randomly deformed. Where deformation is least developed, the rounded shape of individual plutons can be seen, as well as magmatic fabrics.
- (c) Between 2.62 and 2.58 Ga, porphyritic granites and subordinate chamo-enderbitic intruded the NMZ. These bodies intruded as concordant sheets preferentially along the contact of the craton and the NMZ during a major phase of NNW-SSE compression. The coeval low P granulite facies metamorphic event affected all lithologies, except the very latest intrusions, and is designated metamorphic *Stage 3*.
- (d) After the peak of metamorphism, intrusion of granitic melts stopped, and the regional structures were transected by a conjugate set of dextral, ESE-trending and sinistral, NNW-striking shears, which also occur throughout the southern part of the Zimbabwe Craton. These shears pre-date the 2.46 Ga intrusion of the Great Dyke system.

- (e) A retrograde, upper greenschist facies metamorphic event, *Stage 4*, occurred at ~1.9 Ga. Mineralogical changes, turning high-grade rocks into typical upper greenschist facies assemblages, only occurred where H<sub>2</sub>O-rich fluids were available, mainly in decimetre to metre wide reverse shear zones. The reverse shear zones are sub-parallel to the compressional structures developed during stage 3. This event has also affected the craton, since K-Ar and Rb-Sr biotite ages are reset.

The high-pressure granulites of the NMZ, some of which are supracrustal, overlie a normal thickness of continental crust. A model for the origin of the granulites must explain the burial of the supracrustal rocks and the processes of crustal thickening and uplift (Rollinson & Blenkinsop, 1995). The dominant rock types in the NMZ are magmatic (tonalitic to granitic) and some of them still retain their diapiric form. It is believed therefore, that the addition of tonalite–granite magmas to the crust by underplating caused crustal thickening. Magmatic crustal thickening is known to occur when the crust is underplated by either basaltic or tonalitic magmas. The principal source of thermal energy for metamorphism is supplied by the magmas.

The mechanisms of uplift are isostasy (with erosion), extension (tectonic denudation), or compression (Rollinson & Blenkinsop, 1995). The timing of uplift may be synchronous with crustal thickening or may post-date it and be a separate tectonic event. There is evidence for a single progressive compressional deformation involving NNW–SSE shortening of the NMZ and reverse-sense shear at the NMZ–craton boundary in the late Achaean. This deformation was syn- to closely post-magmatic. There is no evidence for extensional structures and therefore, the uplift of the NMZ granulites must have been driven by compression. An isostatic component of uplift was likely during the protracted event. Major dextral strike-slip movement of the Triangle Shear Zone occurred at c. 2.0 Ga and therefore, may not be related to the origin of the NMZ. The mechanism of incorporating supracrustal rocks into the lower crust could be due to magmatic crustal thickening. Extensive diapiric magmatism would be accompanied by subsidence around the margins of the plutons, where supracrustal rocks can be brought to lower crustal levels. The clearest evidence for plutonism (intrusive contacts and circular igneous bodies) is found in areas of supracrustal rocks, such as Manjirenji Dam (Rollinson & Blenkinsop, 1995). These areas have the greatest density contrast between magma and intruded rocks.

The oldest rocks observed in the NMZ are lavas and sediments. This early crust was thickened by voluminous tonalite–granite magmatism. Geochemical evidence indicates

that the tonalite–granite magmas were derived by partial melting of a mafic source (Rollinson & Blenkinsop, 1995). Sm–Nd data suggests that the formation of the charno–enderbites involved a major component of crustal reworking. Remelting of enderbites resulted in the formation of the Razi–Suite charnockites and granites (Berger *et al.*, 1995). The extreme depletion of heavy REE indicates a garnet–bearing, possibly eclogitic residue (Rollinson & Blenkinsop, 1995). The volume of magmas and their mafic parentage suggest that they are mantle-derived, and represent addition of new material to the continental crust.

### Structural History

The study by Kamber & Biino (1995) found evidence for 4 separate deformation events (see Figure 2.4). The oldest deformation is only recorded by pre-intrusive mafic xenoliths. The remaining three episodes are the syn-stage 3 NNW–SSE compression, the post-metamorphic peak horizontal displacement in a conjugate set of shears, and SSE over NNW thrusting during metamorphic stage 4 in a set of low T reverse shear zones, sub-parallel to the old compressional fabric. The only cm-wide horizontal shears may have disrupted the original stage 3 structure to some degree. However, the other two deformations are the major features influencing granulite evolution, because they are responsible for the relative vertical movements, and are discussed below:

*Stage 3* deformation was responsible for the prevalent SSW–NNE trending, moderately steep shears, associated with NNW–SSE horizontal shortening and vertical extension. Strain was concentrated along the NMZ–craton boundary, the North Limpopo Thrust Zone (Umlali), which also indicates a NNW–SSE shortening direction. Thrusting of the entire NMZ over the craton can therefore, at least partially, be seen as a result of stage 3 deformation.

*Stage 4* deformation was responsible for the final exhumation of the NMZ (*sensu stricto*) at ~2.0 Ga, along a set of SSW–NNE–trending, moderately SE dipping, several metre wide, low T thrusts. The NMZ (*sensu stricto*) granulites were only finally exhumed in a separate, ~2.0 Ga tectono–metamorphic event.

### The NMZ in the context of Limpopo Belt models

The bulk of proposed tectonic models for the Limpopo Belt evolve around the concept of a late Archaean continental collision (e.g. Treloar *et al.*, 1992) and hence aim to explain *Stage 3* evolution (Kamber & Biino, 1995). The validity of these models has recently been questioned, based on the discovery of a 2.0 Ga tectono–metamorphic event, which affected large parts of the Limpopo Belt and is a *Stage 4* event. The most recent studies

in the NMZ and CZ show that, at present, no model correctly describes the evolution of the Limpopo Belt.

Current models for the origin and structure of the Limpopo Belt fall into two main groups (Rollinson & Blenkinsop, 1995). One category of models emphasizes the symmetry of the Belt and the uniformity of 2.7 Ga structures and metamorphism (e.g. Roering *et al.*, 1992). The second group of models regards the Limpopo Belt as an asymmetric structure and emphasizes the differences in geological history between the separate zones of the Belt (e.g. De Wit *et al.*, 1992). Central to the symmetrical models for the Limpopo Belt, is the argument that the NMZ is a mirror image of the SMZ, a zone of similar granulite facies rocks. However, there are important differences between the two marginal zones:

- (a) In the NMZ, the dominant lithologies are plutonic rocks, many of which crystallized at depth in the crust and are magmatic granulites. Supracrustal rocks are rare. The dominant lithologies in the SMZ are supracrustal rocks. Granulite facies plutonic rocks are less abundant and are only preserved as magmatic granulites in the Matok Pluton (Rollinson & Blenkinsop, 1995). The SMZ has two different kinds of charno-enderbites, a magmatic and a metamorphic type, whereas the NMZ charno-enderbite suite is of magmatic origin only (Berger *et al.*, 1995).
- (b) The P-T path for meta-pelites of the SMZ shows a three-stage metamorphic/uplift history. Isothermal decompression was followed by isobaric cooling; the present exposure of the granulites requires a further stage of uplift. In contrast, the P-T path for the NMZ is not well documented, but published versions differ from that of the SMZ, implying a difference in the metamorphic history between the marginal zones (Rollinson & Blenkinsop, 1995).
- (c) The NMZ has a magmatic age and crystallization age of 2.88 Ga and was uplifted at 2.6 Ga. The SMZ has a protolith age of 2.9–3.0 Ga and a metamorphic age of 2.67 Ga.
- (d) The NMZ has a simple and homogeneous structure of NE-trending, steeply dipping foliation with down-dip lineations, and sub-horizontal fold axes parallel to the foliation trend. The SMZ has variable foliation trends and large-scale sheath folds. The contacts between the two marginal zones and their respective cratons are different from each other. At the SMZ–Kaapvaal Craton contact, the Hout River Shear Zone comprises a system of frontal and lateral ramps, which include large proportions of

oblique and strike-slip movement. The Umlali Shear (Thrust) Zone, at the NMZ–Zimbabwe Craton contact, is relatively linear and has consistent dip-slip movement. The contacts between the marginal zones and the Central Zone are different. The SMZ–CZ contact is the sinistral Palala Shear Zone, which is 10–12 km wide and dips at  $>65^\circ$  to the northwest (Mc Court & Vearncombe, 1987). At the NMZ–CZ contact is the dextral Triangle Shear Zone, which is 30–50 km wide (true thickness 17–20 km) and dips at  $30^\circ$ – $40^\circ$  to the southeast.

The differences in (a)–(d) are not consistent with a symmetrical model for the large-scale structure of the Limpopo Belt and the two marginal zones are not mirror images of each other. Therefore, the model of Roering *et al.* (1992) cannot be accepted, where they proposed uplift of both marginal zones and the Central Zone as a symmetric and synchronous process of isothermal decompression creating a regional 'pop-up' (Roliinson & Blenkinsop, 1995).

## 2.7 **Gold mineralization and hydrothermal alteration in the Limpopo Belt**

In the Limpopo Belt, known gold deposits occur in the marginal zones only. In the Northern Marginal Zone, Renco Mine is the only known gold deposit at present, and is the second largest producer in Zimbabwe. The Southern Marginal Zone has several gold deposits, such as Klein Kemp, Overscot, Doornhoek, Bontfontein, Louis Moore, Osprey, White Reefs, Bochum and Harlequin (Gan and van Reenen, 1995).

Renco Mine is situated 2 km north of the Mauch (Mirikwi) Shear Zone and 5 km south of the North Limpopo Thrust Zone. The gold deposit occurs in an enderbite, which has been dated at 2.57 Ga (U–Pb zircon age) by Blenkinsop and Frei (1996). The mineralization is in a system of mylonite zones, which are categorized into (a) "shallow reefs" and (b) "steep reefs". The shallow reefs are a series (up to 4 reefs) of lodes, which are anastomosing, north-northeast- to east-northeast-trending, and gently dipping ( $25^\circ$ ) to the southeast. In the southern and central parts of the mine, the strike-slip movement along the shallow reefs is sinistral. A thrust sense of movement occurs in the north, where the shallow reefs become sub-parallel to the regional east-northeast trend. The steep reefs are sub-vertical and gentle easterly raking ( $20^\circ$ – $30^\circ$ ) lodes, which are in Riedel shears that developed contemporaneously with the shallow reef mylonites. A north up and south down sense of movement is indicated on the steep reefs. The kinematics and orientation of the mineralized shear zones are consistent with a lateral and frontal thrust zone geometry, which formed during the Late Archaean thrusting of the northern marginal zone onto the Zimbabwe craton (Kisters *et al.*, 1998). The lateral ramp with sinistral

strike-slip movement in the south and central parts of the mine, possibly represents a second-order splay of the Mauch Shear Zone, or a splay within the northern marginal thrust zone system. The main control of the gold mineralization is an effective structural focussing of fluids into preferably narrow shear zones (i.e. the reef structures) by lowering the volume or surface area of rock interacting with the fluid (Kisters *et al.*, 1998). The narrower the shear zones (i.e. the higher the strain concentration and strain partitioning) the more likely high fluid-to-rock ratios will be accomplished.

In the Renco deposit, pyrrhotite is the major ore mineral ( $\geq 80\%$  volume of sulphides), with lesser pyrite and chalcopyrite. The accessory ore minerals are sphalerite, molybdenite, cubanite, gold, magnetite, ilmenite, rutile-leucoxene, bismuth and gold-bismuth alloys. Magnetite is commonly partly replaced by sulphides including pyrrhotite and chalcopyrite, and to a lesser extent, pyrite. Sulphides occur finely disseminated, as fracture infillings, in mylonitic foliations of the reefs, or as massive ores. "Breccia" ore comprises sub-angular to rounded wall-rock fragments set within a massive sulphide matrix. The deformation that produced the high-temperature mylonites and mineralization occurred at temperatures approximately  $600^\circ\text{C}$  (garnet-biotite thermometry) under mid-amphibolite conditions, slightly post-dating regional peak metamorphic conditions (Kisters *et al.*, 1998). The late Archaean timing of deformation and mineralization is substantiated by the dating of syn-kinematic pegmatites yielding ages of  $2553 \pm 114$  Ma (Rb-Sr) and Pb-Pb ages of  $2532 \pm 35$  Ma of the high-grade skarn-type alteration in the reefs.

Three distinct hydrothermal alteration assemblages can be distinguished within and adjacent to the Renco reefs (Kisters *et al.*, 1998). The assemblages, which indicate different P-T conditions during varying stages of fluid infiltration and alteration, are classified according to overprinting relationships from early (high grade) to late (low grade).

(a) *Granulite-facies mineral assemblages*

Reef parallel stringers or lenticular pods (up to 10 cm wide) have calcite + garnet (grossular) + clinopyroxene (hedenbergite) + plagioclase + scapolite (meionite) + orthite + quartz mineral paragenesis ("skarn-type"). The presence of meionite-rich scapolite indicates high-formation temperatures of approximately  $800^\circ\text{C}$  (Kisters *et al.*, 1998). Local preservation of recrystallized orthopyroxene in and adjacent to the reef structures also indicates that initial shearing in the auriferous reefs occurred under high-grade, granulite-facies metamorphic conditions. However, sulphide mineralization is only subordinately associated with the granulite-facies mineral paragenesis.

(b) *Amphibolite-facies mineral assemblages*

In the reef structures, a garnet + biotite + quartz ± carbonate (siderite) alteration assemblage dominates the macrolithons, whereas a quartz + feldspar + biotite + hornblende assemblage occurs in ductile shear bands. The abundance of alteration minerals in the lithons range from 2 to 25% garnet, 5 to 30% biotite, 5 to 30% quartz, and commonly <5% carbonate. Sulphides vary from 5 to 80 volume percent of the lithons. The garnet has abundant inclusions of opaque minerals (pyrrhotite, chalcopyrite and ilmenite) and biotite is intimately intergrown with the sulphides, indicating a close genetic relationship between sulphide mineralization and the garnet-biotite-quartz alteration (Kisters *et al.*, 1998). Biotite commonly defines a reef parallel foliation and garnet is locally rotated. In the mylonite bands that envelope the macrolithons, orthopyroxene may be present as relics, but is commonly replaced by foliation parallel biotite and subordinate hornblende. Feldspar in the wall rocks is, except for rounded porphyroclasts, commonly pervasively recrystallized.

(c) *Greenschist-facies mineral assemblages*

Greenschist-facies retrogression affected large parts of the Renco reefs and wall rocks. Feldspars have undergone sericitization, carbonatization, saussuritization, and/or chloritization, and biotite may be partially affected by chloritization. Orthopyroxene is commonly replaced by serpentine along cleavage planes. The greenschist-facies retrogression is well developed in the proximity of late, brittle faults where high-grade metamorphic wall rock and reef assemblages have been completely replaced by a calcite + chlorite + sericite + quartz + clinozoisite + epidote + prehnite + laumontite + albite paragenesis. Pyrite and chalcopyrite are the main opaque minerals associated with this alteration. A network of calcite veinlets, rimmed by chlorite-sericite-quartz ± laumontite ± prehnite ± clinozoisite, cut the reef structures at high and low angles. The alteration zone may be up to 50m wide on either side of the faults.

In the Southern Marginal Zone, most of the gold deposits are located within the rehydrated granulite zone (Gan and van Reenen, 1995). These deposits include Klein Kemp, Overscot, Bontfontein, White Reefs, Louis Moore, Osprey and Doornhoek. The Osprey deposit occurs in metamorphosed banded iron-formation and is hosted in a ductile shear zone that forms part of the Hout River Shear (Thrust) Zone. Gold mineralization at Louis Moore and Doornhoek is located in shear zones and occurs as

sulphide-quartz veins in mafic, ultramafic and pelitic rocks. A few gold deposits, such as Harlequin and Bochum, are located in shear zones in the granulite zone of the SMZ, where they are associated with quartz-feldspathic rocks.

There are similarities in the mineralization at Renco in the northern marginal zone, and that described by van Gan and van Reenen (1995) from deposits in the southern marginal zone (SMZ). Both occur in granulite-facies rocks, and in both cases, the mineralization is associated with retrogression in the host shear zones. In the SMZ deposits, the mineralization occurred at temperatures of 600-620° C and pressure of 6 kbar, and is associated with the Hout River Shear Zone and thrusting of the SMZ onto the Kaapvaal craton. Rehydration was considered to be a result of CO<sub>2</sub>-rich fluids derived from a deep-seated mantle source during the thrusting (Gan and van Reenen, 1995). The known gold mineralization in both marginal zones can be used as a model for the exploration program in the study area (Tokwe E.P.O.).

**CHAPTER 3**  
**LOCAL GEOLOGY**  
**TOKWE EPO 847**

**3.1 Introduction**

The author carried out geological mapping on the study area (Tokwe EPO 847). The objectives of the exercise were to study (a) the geological history of the area, and (b) structures, structural patterns and their relationships, and implications for gold mineralization in Area 2s and Area 4. The geology was also to be utilized to interpret geochemical and geophysical data sets.

The study area is located in the Northern Marginal Zone (NMZ) *sensu stricto*, described in Chapter 2. The rocks in the area have been metamorphosed to granulite facies, and some have undergone retrograde metamorphism to upper greenschist and lower amphibolite-facies. The metamorphic rocks in the study area may be categorized into two main groups: (a) metamorphosed greenstone belts (Supracrustal Assemblage), and (b) charno-enderbites (Plutonic Assemblage). The geological setting of these groups has been described in Chapter 2. The Plutonic Assemblage is dominant and intrudes a volumetrically minor Supracrustal Assemblage (approximately 10 % of area). Intense shearing of the charno-enderbites produced leuco-mylonites and proto-mylonites. In places, migmatites were developed from supracrustal rocks (meta-basalts) close to or in contact with the mylonite zones. Quartz veins intrude both groups of rocks throughout the area. In Area 4, mineralized feldspar porphyry dykes intrude a shear zone at the contact of silicified meta-basalt and meta-andesite. Post-deformation intrusives include dolerite dykes, olivine pyroxenite dykes and picritic rocks.

The mapping was carried out with the aid of 1:50 000 aerial photographs, orthophoto maps, an aeromagnetic map, TM Landsat Imagery, SPOT maps and topocadastral maps. Ground traverses were conducted across strike and a GPS instrument was used for accurate location. The geology was plotted on a 1:50 000 topocadastral map.

Representative rock specimens were obtained from various rock types and used to make thin sections, polished sections and for XRF analyses. The specimens were obtained from outcrops and drill core. Petrography was used to determine the names used for the rock types. Appendices A, D and E show the mineral assemblages of the rock types. Figure 3.0 shows the geology of the study area. Rock sample locations are shown on Figure 3.0 and drill hole sections.

### 3.2 Metamorphosed Greenstone Belts (Supracrustal Assemblage)

The metamorphosed greenstone belts comprise the oldest rocks in the study area (Rollinson & Blenkinsop, 1995). In places where deformation is least intense, supracrustal rocks are truncated and dismembered by intrusion of Plutonic Assemblage rocks. The supracrustal lithologies include ultramafic rocks (lherzolite), mafic meta-volcanic rocks (mafic granulite, silicified mafic granulite and amphibolite), intermediate meta-volcanic rocks (meta-andesite), acid meta-volcanic rocks (meta-rhyolite), and meta-sediments (garnet-biotite gneiss), meta-quartzite, calc-silicate rocks, and banded chert and tuff). The rocks of the supracrustal assemblage form narrow bands up to a few hundred metres wide and several kilometres long. They occur infolded with charno-enderbites, and form the major fold structures. High magnetic signatures on the aeromagnetic map characterize the metamorphosed greenstone belts.

#### Lherzolite

Lherzolite occurrence is very rare in the area and was observed only on one exposure east of the Tokwe River. The ultramafic rock appears to be intercalated with the meta-basalts.

The lherzolite, represented by specimen RS 18, is pale green and fine- to medium-grained. In thin section, the rock is composed of olivine, serpentine, clinopyroxene, orthopyroxene and magnetite. The crystals are aligned parallel to the regional foliation. The olivine is being altered to serpentine and magnetite. The lherzolite is a peridotite (olivine > 40 %) with both clinopyroxene and orthopyroxene. Since it occurs with meta-basalts, the lherzolite could be a relict peridotitic komatiite.

#### Meta-basalts

The meta-basalts are the most common supracrustal rocks in the area. They occur as (a) basaltic granulite, (b) basaltic amphibolite and (c) silicified basaltic granulite. All these lithologies have a strong foliation.

- (a) The basaltic granulite is represented by specimens RS 10, RS 22, RS 28, RS 29, RS 56, RS 72, RS 76, RS 77, and RS 82. The rock is generally dark green and fine- to medium-grained. The typical assemblage is:-  
orthopyroxene + clinopyroxene + plagioclase ± hornblende ± biotite ± magnetite ± ilmenite.

Compositional banding, made up of alternating orthopyroxene-rich and clinopyroxene-rich layers, is present in some of the basaltic granulites, such as RS 56. In most specimens, hornblende is replacing clinopyroxene ± orthopyroxene, in a late-stage event. The amphibole indicates a retrograde metamorphic event (Kamber & Biino, 1995). In RS 10, RS 56 and RS 72, ilmenite is present and associated with the amphibole. In RS 22 and RS 56, biotite occurs as a late-phase mineral that overgrows the amphibole. Magnetite, where present, is a late-phase accessory mineral that cuts biotite.

Some specimens with pyrite mineralization, such as RS 56, have apatite ± sphene as additional accessory minerals. The apatite is closely associated with biotite. In places, chlorite replaces pyroxenes. Small grains of tourmaline are present in RS 56. The tourmaline crystals are green, and have hexagonal basal-sections. The pyrite is late-phase as it cuts biotite. The mineralized basaltic granulites have secondary quartz in interstices and late veins. The veins crosscut pyroxenes and feldspars. The quartz in the veins commonly forms glomero-porphyroblasts and is cut by the sulphides and red biotite (such as in RS 28 and RS 29). RS 28 and RS 29 have intense biotite alteration. In RS 28, which has semi-massive sulphides (pyrrhotite, pyrite and chalcopyrite), orthopyroxene crystals wrap around quartz grains, forming reaction rims between the quartz and sulphides.

- (b) Specimen RS 8 represents basaltic amphibolite. The rock is schistose, dark green to black, and medium- to coarse-grained. The rock is composed of hornblende (~ 80% of rock), clinopyroxene and plagioclase feldspar. Magnetite, sphene and apatite are accessory minerals. Calcite forms reaction rims around magnetite grains, between the magnetite and hornblende. Clinopyroxene is being replaced by hornblende. The hornblende is a product of a retrograde metamorphic event. Some of the plagioclase grains are being altered to sericite. Orthopyroxene is absent, therefore the rock is not a granulite. Quartz occurs with plagioclase in late-stage veins.
- (c) Specimens RS 23, RS 30 and RS 83 represent silicified basaltic granulite. The typical assemblage is:- orthopyroxene ± clinopyroxene + plagioclase + hornblende + quartz ± biotite ± magnetite. In RS 23, the plagioclase grains are lozenge-shaped due to shearing. In all of three specimens, hornblende is replacing pyroxene. Plagioclase is being altered to sericite. Magnetite, biotite, apatite, zircon and chlorite are accessory minerals. Specimen RS 83 has symplectic garnet rims around pyroxenes and opaque minerals. Quartz is abundant and is a late-phase mineral that cuts pyroxenes and plagioclase. The quartz occurs in (a) the groundmass, as small grains surrounding larger

grains of feldspar, and (b) discontinuous veins, forming ribbons. The veins cut across the interstitial quartz in (a), and the earlier-phase minerals (pyroxenes and plagioclase). Biotite is a late-phase mineral that overgrows hornblende. The magnetite is also a late-phase mineral that cuts biotite and hornblende.

The three specimens were obtained from sulphide-bearing silicified basaltic granulites that contain several late-phase minerals. The sulphides are late-phase minerals that cut pyroxenes and plagioclase. The sulphides are not restricted to the quartz veins, but also occur in the basalt itself. In RS 23, a late-stage calcite vein cuts across the foliation. In RS 30, an Fe-rich carbonate (ankerite) is abundant and closely associated with the sulphides. Chlorite is also associated with the sulphides. Other alteration minerals in RS 30 are serpentine, colourless amphiboles and hornblende.

The original rock represented by the three specimens was a basalt, with pyroxene and plagioclase as the main constituent minerals. The rock was later metamorphosed and silicified to the present state. It now resembles a rock of andesitic (intermediate) composition (TAS plot, Figure 3.12).

#### Meta-andesites

Meta-andesites were mapped in the metamorphosed greenstone belts of Area 4 and Ngundu Block. Specimens RS 15, RS 32, RS 43, RS 59 and RS 81 were obtained from the meta-andesites. The rocks are grey, medium-grained and sheared. The typical assemblage is:- clinopyroxene ± orthopyroxene + plagioclase ± microperthite + quartz ± biotite. In RS 43, clinopyroxene and orthopyroxene are concentrated in separate bands that are parallel to foliation. In RS 43, chlorite replaces clinopyroxene. In RS 32, orthopyroxene is being altered to epidote (zoisite) and chlorite (retrograde alteration).

In RS 81, plagioclase occurs in the groundmass and as porphyroblasts. The porphyroblasts are lensoid (due to shearing) and aligned parallel to the foliation. Some of the plagioclase grains are being altered to sericite. Antiperthite also occurs in the groundmass and as lensoid porphyroblasts aligned parallel to the foliation. Antiperthite is also present in RS 43. RS 81 and RS 43 also have microperthite in the groundmass and as porphyroblasts. The amount of the potash feldspar is less than that of plagioclase. Quartz occurs as early- and late-phases, and is usually the most abundant mineral. Ribbon quartz forms veins that cut across the pyroxenes, feldspars and the primary quartz. Late-stage pegmatite veins are also present in RS 43. Accessory minerals are

biotite (in RS 15, RS 32 and RS 59), apatite (in RS 15, RS 59 and RS 81), magnetite (in RS 15, RS 59 and RS 81), and sphene (in RS 43, RS 59 and RS 81).

Specimens RS 32, RS 43, RS 59 and RS 81 are sulphide-bearing. The sulphides are associated with quartz veining, biotite and pyroxenes. The biotite is a late-phase mineral that overgrows pyroxenes, feldspars, quartz and sulphides. The sulphides cut pyroxenes, feldspars and quartz. In RS 43, the sulphides are anhedral and constitute approximately 3% of the rock. Magnetite is a late-phase mineral that cuts biotite. In RS 32, late-phase calcite veins cut across the quartz veins and early-phase minerals. In RS 43, calcite alteration is associated with chlorite and sulphides. The alteration assemblage in RS 32 is:- zoisite + sericite + chlorite + calcite. In RS 43, the alteration assemblage is : chlorite + calcite + potash feldspar.

The modal compositions of the rock specimens are plotted on the QAPF diagram (Streckeisen, 1976, Figure 3.1). Specimens RS 32 and RS 59, from drill core in Area 4, plot in the field of quartz diorite (tonalite), whose volcanic equivalent is quartz andesite. RS 32 and RS 59 are therefore, meta-quartz-andesites. Specimens RS 15 (from Area 4), RS 43 and RS 81 (from Ngundu Block) plot in the fields of diorite and monzodiorite (Figure 3.1), whose volcanic equivalents are andesites. The compositions of these meta-andesites and meta-quartz andesites are similar to that of enderbites. The andesitic rocks and enderbites can be differentiated using textural characteristics such as grain size and intensity of the regional foliation. Andesitic rocks are fine-grained and intensely sheared, whereas enderbites are coarse-grained and relatively massive.

#### Meta-rhyolite

Meta-rhyolite (specimens RS 42 and RS 80) was mapped in the greenstone belt on Ngundu Block. The tuff is buff coloured, laminated and brecciated, with abundant disseminated sulphides (pyrite). The mineral assemblage is:- microperthite + microcline + quartz + plagioclase + sericite + biotite. The potash feldspars are the most abundant minerals (approximately 60% of rock). Quartz constitutes approximately 30% of the rock. Plagioclase makes up approximately 9% of the rock. Microperthite forms abundant flattened and slightly rotated porphyroblasts. The porphyroblasts are being altered to sericite and are cut by late-stage quartz veins. The microperthite also occurs in the groundmass. Microcline is less abundant than microperthite, and occurs in the groundmass. Primary quartz is fine-grained and occurs in the groundmass, where small grains surround potash feldspar porphyroblasts. Secondary quartz occurs in veins that crosscut potash feldspar porphyroblasts and primary quartz. The secondary quartz grains

are serrated, elongate and form ribbons. The characteristics of these quartz grains are typical of dynamic re-crystallization accompanying deformation (Shelley, 1993). The secondary quartz also occurs in pressure shadows of the porphyroblasts. A few grains of plagioclase feldspar occur in the groundmass. Biotite, sericite and sphene are accessory minerals. Biotite is a late-phase mineral commonly occurring at contacts of secondary ribbon quartz and late-stage cross-cutting quartz veins. Sericite is associated with the late-stage cross-cutting quartz veins. In RS 80, disseminated euhedral sulphide (pyrite) grains occur in ribbon quartz veins. A gossan is developed above the meta-rhyolite on Ngundu Block. The fresh meta-rhyolite and gossan were sampled and assayed for gold and various base metals. The results indicated low levels of gold (up to 800 ppb) and elevated values of manganese (up to 4575 ppm).

The modal compositions of the two specimens are plotted on the QAPF diagram (Figure 3.2). Both specimens plot in the field of syenogranite, whose volcanic equivalent is rhyolite.

#### Meta-Sediments

(a) Garnet-biotite gneiss (Meta-greywacke)

The garnet-biotite gneiss was mapped on surface and logged in drill core in Area 4. The garnet-biotite gneiss (meta-greywacke) is interbedded with meta-volcanic rocks of the Area 4 "greenstone" belt. The rock is represented by specimens RS 31, RS 57, RS 61 and RS 90. The rock is grey, intensely sheared, banded and rich in quartz, biotite and garnet.

The dark bands are characterized by biotite, garnet, sulphides (pyrite), plagioclase (porphyroblasts and in groundmass), microcline, microperthite, quartz (in groundmass), orthopyroxene and sphene. The biotite flakes are abundant and are being replaced by chlorite. Garnet forms ubiquitous porphyroblasts with inclusions of quartz. The abundance of the garnet is indicative of high aluminium content of the rock. The plagioclase is being altered to sericite. Microperthite and microcline also occur in the groundmass and as porphyroblasts. Very few grains of orthopyroxene were observed.

The leucocratic bands are composed of plagioclase (in groundmass and as porphyroblasts), quartz (in groundmass), microperthite porphyroblasts, microcline, garnet porphyroblasts, sericite, apatite, and lesser amounts of biotite, sphene, amphibole, zircon, chlorite, calcite and sulphide (pyrite). Garnet is also abundant in the leucocratic bands. Quartz is the most abundant mineral in the leucocratic bands. The quartz grains

are elongate and have a preferred orientation parallel to the foliation. The quartz appears to have undergone dynamic re-crystallization as the grains are tightly packed and have serrated edges. The grains form a pseudo-mylonitic texture.

Late-stage quartz veining is common in both dark and leucocratic bands. Ribbon quartz occurs in the veins. In RS 57, the quartz veins have chloritized contacts, depicting retrograde alteration during late low-temperature veining. RS 31, with sparse sulphide mineralization, has an alteration assemblage of chlorite + biotite + calcite. Orthopyroxene, which is present in small amounts, is being altered to biotite.

The chemical composition of the garnet-biotite gneiss is plotted on Figure 3.13, which is a diagram for classifying terrigenous sandstones (Rollinson, 1993). The composition is plotted using  $\log (\text{Na}_2\text{O}/\text{K}_2\text{O})$  against  $\log (\text{SiO}_2/\text{Al}_2\text{O}_3)$ . The garnet-biotite gneiss plots in the field of greywacke.

(b) Meta-quartzite

Meta-quartzites were mapped in the metamorphosed greenstone belts on Area 4, Ngundu Block and Zvamapere Block. On Area 4, the quartzite is iron-stained and on Zvamapere and Ngundu blocks, gossans are developed on it. The meta-quartzites are represented by specimens RS 75 and RS 84.

The rocks are composed almost entirely of re-crystallized quartz. Most of the quartz grains are small, tightly packed and have serrated edges. Some of the grains are large and made up of several elongated sub-grains that are parallel to the foliation. A few intensely weathered and iron-stained porphyroblasts of microperthite are also present. Sparse disseminated sulphides and iron hydroxides also occur. On Zvamapere Block, several rock grab samples were collected from the meta-quartzite and gossan, and assayed for gold and base metals. The results indicated low levels of gold (up to 60 ppb) and elevated values of manganese (up to 927 ppm) and copper (up to 875 ppm). XRF analysis of a gossan sample (RS 75) from Zvamapere Block yielded the following elevated values:-

78.71% Fe<sub>2</sub>O<sub>3</sub>, 103.50 ppm Zn, 142.50 ppm Ni, 221.50 ppm Cu, 253.10 ppm Cr and 150.90 ppm V.

(c) Calc-silicate rocks

Calc-silicate rocks were mapped on Zvamapere, Ngundu and Area 4 "greenstone" belts. The calc-silicate rocks occur as two types, (a) a white, medium-grained gneiss with

sugary texture, and (b) a greenish–grey gneiss with alternating mafic and felsic bands. Type (a) is represented by specimens RS 5, RS 41 and RS 74, from Zvamapere Block. Type (b) is represented by specimens RS 1 and RS 2 from Ngundu Block, and RS 46 and RS 47 from Area 4.

Type (a) is composed of plagioclase, clinopyroxene, quartz, apatite and sphene. The mineral grains have a preferred orientation parallel to the foliation. In RS 41 and RS 74, plagioclase is the most abundant mineral, and is being altered to sericite. Clinopyroxene (diopside) is also abundant. Quartz is a late-phase mineral that cuts plagioclase and diopside. The quartz occurs in late-stage veins that also contain fine-grained plagioclase. Specimen RS 5 is a quartz vein in a calc-silicate rock. The quartz vein itself comprises ~75% quartz, ~10% orthopyroxene, ~1% plagioclase and ~14% sulphides. The transition zone between the quartz and the wall-rock (calc-silicate rock) is composed of ~40% quartz, ~20% orthopyroxene, ~20% clinopyroxene, ~1% plagioclase and ~19% sulphides. Specimen RS 74 also has sparsely disseminated, anhedral to subhedral sulphides (pyrite, pyrrhotite and chalcopyrite). In specimens RS 41 and RS 74, zoisite occurs as a late-phase mineral replacing diopside. In specimen RS 74, abundant crystals of vesuvianite (idocrase) occur as a late-phase mineral that cuts plagioclase, diopside and quartz.

Type (b) comprises diopside, plagioclase, quartz, sphene, hornblende, sulphides, biotite and garnet. In specimens RS 1 and RS 2 (from Ngundu Block), the dark bands are composed of abundant diopside, disseminated sulphides (~7%), biotite and hornblende, and lesser amounts of plagioclase and quartz. The leucocratic bands contain abundant plagioclase and quartz, and lesser amounts of diopside, sulphides (2%), biotite and hornblende. Brown hornblende (accessory) appears to be replacing diopside. The quartz is a late-phase mineral that cuts diopside and plagioclase in the groundmass. The quartz also occurs in late-stage veins. The sulphides (pyrite, pyrrhotite, chalcopyrite and sphalerite) are late-phase minerals that cut diopside, plagioclase and quartz. In RS 1, diopside cuts plagioclase. In RS 46 and RS 47, the dark bands comprise abundant diopside, sulphides and sphene, garnet porphyroblasts and lesser amounts of quartz. The quartz grains cut diopside. The sulphides are late-phase, and in RS 47, they constitute approximately 10% of the rock. The leucocratic bands are extremely sheared and siliceous, consisting of quartz, garnet porphyroblasts and lesser amounts of sulphides. The quartz grains are aligned parallel to the foliation. The garnet is a late-phase mineral that cuts diopside.

Calc-silicate rocks have been defined as meta-sediments that are rich in Ca- or Ca-Mg silicates (such as zoisite, grossular, amphibole or diopside), but which contain little or no carbonate (Yardley, 1989).

(d) Banded chert and tuff

Banded chert and tuff was mapped in Area 4 "greenstone" belt. One of the exposures is a long narrow outcrop along the northern contact of the "greenstone" belt. The banded chert and tuff (specimens RS 16 and RS 17) is sheared, fine-grained, grey, siliceous and laminated. The rock comprises alternating leucocratic and dark bands.

The dark bands are composed of orthopyroxene, clinopyroxene, disseminated to semi-massive sulphides, hornblende, garnet and lesser amounts of fine-grained quartz. The sulphides (pyrite, chalcopyrite, chalcocite and sphalerite) are elongate and aligned parallel to the foliation or lamination. Hornblende is replacing pyroxenes. The leucocratic bands comprise mainly fine-grained quartz and a few pyroxene porphyroblasts. The quartz grains are tightly packed and have serrated boundaries. This texture is typical of dynamic re-crystallization. The pyroxene porphyroblasts have lensoid shapes that are typical of mylonites. The porphyroblasts, which are surrounded by rims of very fine-grained quartz, have  $\sigma$  tails depicting sinistral movement.

The XRF analysis on RS 17 also yielded values of 1.7% sulphur, 240 ppm zinc and 271 ppm chromium.

**3.3** Chamo-enderbites (Plutonic Assemblage)

The chamo-enderbites are intrusive into the metamorphosed greenstone belts (supracrustal assemblage). Within the chamo-enderbites, rocks of the supracrustal assemblage occur as xenoliths of various sizes. The xenoliths are subangular bodies that commonly have an internal deformation fabric that is cut by the contacts with chamo-enderbites. The contacts of the chamo-enderbites with the xenoliths are irregular and clearly magmatic.

Charnockites and enderbites are the dominant rock types in the study area (Tokwe EPO). These orthopyroxene-bearing rocks have various compositions, which include gabbro, quartz diorite, tonalite, granodiorite and granite, with the last three dominating. Since they are hypersthene-bearing, these felsic to intermediate rocks are in granulite-facies of metamorphism. Odell (1975) defined the chamo-enderbites of the NMZ as hypersthene-

bearing, oversaturated, leucocratic to mesocratic rocks, which occur in zones of granulite metamorphism. If potash feldspar is the dominant feldspar, the rock is a charnockite (*sensu stricto*). The rock is an enderbite when plagioclase is the dominant feldspar. Shelley (1993) defined a charnockite as a plutonic or metamorphic rock, possibly meta-igneous, which contains orthopyroxene (or fayalite plus quartz) and has the composition of granite. An enderbite is a charnockitic rock with the composition of tonalite.

In the NMZ, contacts between enderbites and charnockites are magmatic, with the latter being mostly intrusive into the former (Berger *et al.*, 1995). The charno-enderbite intrusions have been dated at between 2.72 and 2.62 Ga (Kamber and Biino, 1995). The charno-enderbites have a pervasive ENE-trending foliation, produced by SSE-NNW compression (Stage 3) that occurred after their intrusion. The charno-enderbites are silicified by late-stage quartz veining along the fabric. Narrow shear zones along the foliation became conduits for fluid movement through the rocks, resulting in ribbon quartz veining. The ribbon quartz texture comprises elongate, tightly packed quartz grains with serrated edges. This texture is typical of dynamic re-crystallization of quartz and is common in the charno-enderbites, K-feldspar granites and some supracrustal lithologies.

In the study area, three types of charno-enderbites were mapped. These are enderbite, charnockite and magnetite-charnockite. Charnockite is more abundant than enderbite. Magnetite-charnockite is the least abundant.

#### Charnockites

The charnockites (specimens RS 3, RS 6, RS 34, RS 69, RS 78, RS 85, RS 87, RS 91, RS 91, RS 92 and RS 96) are grey to buff coloured, medium- to coarse-grained, and generally have a penetrative ENE-trending foliation. The typical mineral assemblage is:- quartz + potash feldspar + plagioclase + orthopyroxene + biotite + magnetite ± zircon ± sphene ± apatite. Quartz is usually the most abundant mineral. The quartz is bimodal and occurs in two phases, (a) early-phase, in the groundmass and interstitial, wrapping around larger feldspar grains, and (b) late-phase, in late veins cutting the feldspars, orthopyroxene and early quartz. The late-phase quartz forms large, elongate grains that have serrated edges. This ribbon quartz texture is typical of dynamic re-crystallization due to deformation.

The alkali feldspar occurs as microperthite and/or microcline. These feldspars form porphyroblasts and also occur in the groundmass. In RS 87, RS 92 and RS 96, some alkali feldspar grains have graphic intergrowth with quartz. Plagioclase feldspar occurs

mostly in the groundmass, but also forms a few porphyroblasts. The plagioclase has polysynthetic twinning or occurs in antiperthite. In RS 85 and RS 87, some of the plagioclase is not twinned. Myrmekitic intergrowth of plagioclase and quartz is common. Some of the plagioclase is being altered to sericite. In RS 78, sericite is replacing potash feldspars and plagioclase. Orthopyroxene (hypersthene) is less abundant than quartz and feldspars. Biotite or chlorite is replacing some of the hypersthene. In RS 6, the hypersthene crystals appear in bands along the foliation planes, where it is closely associated with biotite and magnetite.

Biotite, magnetite, zircon, apatite, chlorite and sphene are accessory minerals. RS 92 also has monazite, which has high interference colours, and unlike zircon, it is not zoned. Magnetite is a late mineral that is associated with and overprints hypersthene and biotite. In RS 96, a green spinel (hercynite) and magnetite, overprint biotite. In RS 85 and RS 91, garnet occurs as a late phase mineral. In RS 85, garnet porphyroblasts are slightly symplectic around magnetite and in RS 91, the porphyroblasts overprint late-phase quartz. Specimen RS 32 is of sulphide-bearing core from drill hole C2D4. The specimen has typical sulphide mineralization and alteration for Area 2s. The sulphides are late-phase, very sparse and closely associated with altered hypersthene, biotite and quartz veining. The potash feldspars are being altered to sericite and calcite. A green spinel (hercynite or gahnite) is also present. The alteration assemblage includes:- potassium (sericite) + biotite + quartz (+ calcite).

The modal compositions of the charnockites are plotted on a QAPF diagram (Figure 3.3). The majority of the specimens (RS 3, RS 6, RS 69, RS 78, RS 85, RS 91, and RS 96) plot in the granite field, making them charnockites *sensu stricto*. Specimen RS 34 is an alkali-feldspar charnockite that plots in the alkali granite field. Specimen RS 87, which plots in the granodiorite field, is an opdalite (Shelley, 1993). Specimen RS 93, which is a garnet-biotite-feldspathic gneiss that resembles charnockite, but lacks orthopyroxene, plots amongst the charnockites. It is possible that the specimen was collected where a charnockite locally lacked orthopyroxene.

#### Magnetite-charnockite

A large body of magnetite-charnockite was mapped in the eastern part of the study area. On the aeromagnetic map, the magnetite-charnockite appears as a positive, high-amplitude magnetic anomaly. The eastern extent of the magnetite-charnockite body is beyond the boundary of the study area. Specimens RS 44, RS 67 and RS 68 were obtained from the magnetite-charnockite. The rock is pale pink to buff coloured, medium-

to coarse-grained and strongly sheared. In hand specimen, the minerals that can be identified are:- quartz + potash feldspar + plagioclase + magnetite + biotite ± garnet.

In thin section, the mineral assemblage observed in the rock comprises quartz + microperthite + microcline + plagioclase + magnetite ± hercynite or gahnite + hypersthene + biotite ± garnet ± zircon ± apatite. The quartz occurs in two phases, (a) early-phase in the groundmass, and small interstitial grains surrounding feldspar porphyroblasts, and (b) late-phase, dynamic re-crystallized quartz in late-stage veins. The late-phase elongate quartz grains have serrated margins and form ribbons. Microperthite and microcline are the potash feldspars, which are more abundant than plagioclase. The potash feldspars form lensoid porphyroblasts and also occur in the groundmass. Some of the potash feldspars have graphic intergrowth with quartz. Plagioclase occurs mostly in the groundmass, where in places, it has myrmekitic intergrowth with quartz. Some of the plagioclase is being altered to sericite. Hypersthene occurs as few grains, which are being replaced by biotite and chlorite in places. Magnetite is common throughout the rock and is commonly associated with biotite. In RS 68, a green spinel (hercynite or gahnite) is associated with the magnetite.

Biotite, chlorite, garnet, zircon, apatite, sphene and calcite are accessory minerals. In RS 68, garnet porphyroblasts are associated with late-phase quartz veins and are cut by the quartz grains. The zircons are small and zoned. Calcite is an alteration mineral associated with sericite.

The magnetite–charnockite is believed to have been derived from an **I-type** granitoid, which is rich in magnetite, biotite and hornblende (Shelley, 1993).

The modal compositions of the three specimens are plotted on a QAPF diagram (Figure 3.4). All of the specimens plot in the granite field, which makes them charnockites since they contain orthopyroxene.

#### Enderbites

Enderbites occur throughout the study area. They commonly form long elongate outcrops conformable with the regional fabric. In the northern part of the area, long narrow enderbites are tightly infolded with charnockites. On the aeromagnetic map, the enderbites appear as positive, high-amplitude magnetic anomalies. Specimens RS 11, RS 12, RS 79, RS 86, RS 88 and RS 89 were obtained from the enderbites. The

enderbites are grey, dark green to pale brown, massive, coarse- and even- grained. They are characterized by bluish quartz, honey-brown feldspars and a greasy appearance.

In thin section, the enderbites have a mineral assemblage comprising:- plagioclase + quartz + hypersthene  $\pm$  clinopyroxene  $\pm$  potash feldspar + magnetite + biotite  $\pm$  hornblende + apatite  $\pm$  ilmenite  $\pm$  zircon  $\pm$  sphene. Plagioclase is the most abundant mineral and the dominant feldspar. The plagioclase has polysynthetic twinning and sometimes occurs as micro-antiperthite. In RS 86, some of the plagioclase is not twinned. In RS 12 and RS 79, the plagioclase has, in places, myrmekitic intergrowth with quartz. Quartz occurs in two phases, (a) in the groundmass and interstices, surrounding feldspar grains, and (b) as ribbon quartz in late-stage veins. Hypersthene is more abundant in the enderbites than in charnockites. Hornblende and biotite are replacing the orthopyroxene. Clinopyroxene is less abundant than hypersthene, and is also being altered to hornblende and biotite. Biotite is a late-phase mineral that is also replacing hornblende (RS 86). Magnetite is a late phase mineral and is sparsely disseminated throughout the rock, where it is commonly associated with hypersthene and biotite. In RS 86, ilmenite is an accessory mineral forming small grains associated with hornblende. Other accessory minerals are apatite, zoned zircon and sphene. In RS 79, calcite is associated with biotite alteration.

Figure 3.5 shows the plots for modal compositions of the specimens. The majority of the specimens, except RS 89, plot in the diorite field. RS 89 plots in the quartz diorite or tonalite field. All the specimens are enderbites, since they have orthopyroxene.

#### **3.4 Leuco-mylonites and proto-mylonites**

Leuco-mylonites and proto-mylonites occur in shear zones, where the charno-enderbites have been deformed. The majority of the shear zones in the study area are parallel to the regional ENE-trending foliation. A few shear zones follow the NNE trend (S2), the E-W trend (S3) and the WNW trend (S4). Shelley (1993) defines a mylonite as a dynamically metamorphosed rock exhibiting a foliation of mylonitic origin, and a protomylonite as a mylonitic rock containing > 90% of pre-mylonitic material. The process of dynamic re-crystallization also plays an important role in producing some of the very fine-grained material that typifies mylonites. Elongate grains, sub-grain structures and serrated grain boundaries generally characterize dynamic re-crystallization. Shear sense indicators include S-C planes (especially in mylonites), porphyroblast fracture patterns, rolling structures ( $\delta$ -type porphyroblasts),  $\sigma$ -type porphyroblasts, asymmetrical pressure shadows and deformed vein systems. The mylonites typically have well-developed

lineations, which are usually absent in proto-mylonites. The mylonite zones are flanked by proto-mylonite zones.

#### Leuco-mylonites

In the study area, the most prominent mylonite zone is the Mauch Shear Zone, which follows the ENE-trend and extends for several hundreds of kilometres NE and SW of the area. The shear zone attains a maximum width of approximately 1 km, and has a persistent lineation plunging at ~ 80° towards the SW (~ 250°). Another mylonite occurs in a shear zone (S2 trend) that splays off from the Mauch Shear, on Area 4. At the NE corner of the study area, a mylonite zone occurs in an EW shear zone. In places, the Tokwe River follows a system of en-echelon WNW-trending shears with mylonite.

The leuco-mylonites are represented by specimens RS 9, RS 14, RS 45, RS 55 and RS 62. The lithology is buff to pale pink, fine-grained and has a strong foliation and quartz lineation. Potash feldspar and garnet form porphyroblasts that show rotation. In the Mauch Shear Zone, the majority of the rolling structures indicate a sinistral sense of vorticity. Other kinematic indicators are asymmetric folded mafic xenoliths.

In thin section, the typical mineral assemblage includes:- quartz + potash feldspar + plagioclase ± garnet (almandine) ± biotite ± chlorite ± sericite.

Quartz is the most abundant mineral and occurs in the groundmass and as ribbons. Quartz ribbons wrap around potash feldspar porphyroblasts and sometimes cut across them. The potash feldspar (perthite and microcline) occurs in the groundmass and also forms porphyroblasts. In RS 9 and RS14 (from the Mauch Shear Zone), some of the porphyroblasts are  $\delta$ -type rolling structures. Plagioclase feldspar is less abundant than potash feldspar, and occurs in the groundmass. In RS 9, plagioclase occurs in bands of pervasive alteration. These bands, which are remnants of the original rock, also have microcline, perthite, garnet, biotite and chlorite that wrap around garnet porphyroblasts. The original rock was granitic. Quartz ribbons cut the bands of alteration. In the zones of re-crystallization, garnet porphyroblasts cut the quartz ribbons. In RS 45, RS 55 and RS 62 (from the mineralized shear zone in Area 4), additional minerals, such as hypersthene, sulphides (pyrite, pyrrhotite and chalcopyrite), sphene and apatite, are present. In RS 45, the sulphides are more concentrated in the pressure shadows of microperthite porphyroblasts, which occur in strings along the foliation. Biotite and sericite are also abundant in the pressure shadows. In the groundmass, the sulphides are elongate and have a preferred orientation parallel the foliation. In RS 55, the garnet porphyroblasts are flattened and being altered to chlorite. The sulphides are late-phase and cut potash

feldspar and the late-phase ribbon quartz. The biotite is a late-phase mineral that cross-cuts ribbon quartz. The apatite is fairly abundant and has hexagonal basal sections. In RS 62, most of the microperthite porphyroblasts have been altered to sericite. The plagioclase feldspar has abundant zoisite inclusions. The plagioclase is also being altered to sericite. The alteration of plagioclase to zoisite is termed saussuritization (Shelley, 1993), which is commonly accompanied by sericite. Zoisite and sericite are late stage minerals that overprint the ribbon quartz. Late stage-veins, with sericite and zoisite, cut across the foliation. Sparsely disseminated, euhedral to subhedral sulphides are also present. Other accessory minerals are sphene, chlorite and zircon.

The proto-mylonites occur in shear zones of less intense deformation than mylonite zones, and in the flanks of mylonite zones. They are pale pink to buff coloured, medium grained and have a strong foliation. Specimens RS 21 and RS 73 (from the southern boundary of the area) represent the proto-mylonites. The general mineral assemblage includes:- potash feldspar + quartz + garnet + biotite  $\pm$  magnetite  $\pm$  sericite. The quartz occurs as early-phase in the groundmass and as late-phase ribbons. The potash feldspars (microperthite and microcline) occur in the groundmass and also form porphyroblasts. In RS 73, some of the potash feldspars are being altered to sericite. Biotite, garnet, magnetite, and a green spinel (hercynite) are accessory minerals in RS21. In RS73, the accessory minerals are garnet, sericite and monazite.

### **3.5 Migmatites and Leucogneiss (Leucosome)**

The migmatites are high-grade, pervasively heterogeneous rocks that are metamorphic, and partly igneous-like in appearance (Shelley, 1993). The igneous-like part is most commonly granitic (leucosome) and the metamorphic part is generally a biotite schist or gneiss (melanosome). In the Northern Marginal Zone, migmatization was coeval with the SSE-NNW compression that produced a penetrative weak- to medium-strength foliation (Kamber and Biino, 1995). The migmatization occurred during a high temperature, tectono-metamorphic event (Stage 3). Two migmatite types have been recognized in the field; (a) has a hololeucocratic leucosome with typical charnockite appearance, is coarse-grained and was produced from a charnockite, and (b) is white, granitic in composition and garnet  $\pm$  magnetite bearing. The leucosome mineralogy of the first type comprises perthitic potash feldspar (up to 50% plagioclase exsolution), quartz and minor plagioclase and magnetite. The leucosome of the second type has additional minerals such as garnet, green spinel and very fine crystalline sillimanite. The presence of garnet, sillimanite and green spinel in the second type of leucosome indicates aluminium excess

during migmatisation. Columnar sillimanite is a prograde phase, which only survived when rimmed by plagioclase and potash feldspars (Kamber and Biino, 1995).

The migmatites normally concentrated more strain than the surrounding lithologies and are found where deformation was strongest. In the study area, the migmatites are located close to the Mauch Shear Zone and its splay shears, and are in contact with metabasalts. Across the Tokwe River, the largest migmatite body strikes parallel to the splay shear from the Mauch Shear Zone. In the riverbed, the migmatite is stromatic and is composed of alternating narrow layers of melanosomes and leucosomes. Specimen RS 7 was collected from this stromatic migmatite. Towards the NE, the migmatite becomes agmatitic, with the melanosomes getting wider and broken up into discrete fragments. The melanosome fragments are flattened and attain sizes of up to 90 cm in length and 15 cm in width. The melanosomes, which are amphibolitic, have inclusions of quartz or epidote. Some of the melanosomes have pinch and swell structures with quartz-filled pressure shadows. Sparsely disseminated sulphides (pyrite) are common in the melanosomes. The melanosomes are set in a matrix of granitic material (leucosome) and pegmatites. The granitic leucosome has a foliation (regional) that truncates the melanosomes in places. Adjacent to the migmatite is a ridge of white leucogneiss, which is believed to be a leucosome or a melt from the migmatite. The white leucogneiss has a few ptygmatically folded mafic restites. This leucogneiss is similar to the second type of leucosome described above. Specimen RS 70 was obtained from this leucogneiss.

Other migmatites are developed locally from chamo-enderbites. In Area 2s, the K-feldspar granite, which has typical charnockite appearance, is believed to be a partial melt of the charnockite. The K-feldspar granite is similar to the first type of leucosome mentioned above.

In thin section, the stromatic migmatite (RS 7) is composed of alternating melanosome and leucosome bands. The melanosome bands contain abundant orthopyroxene, clinopyroxene, magnetite (~ 5%), and less quartz and plagioclase. Some of the pyroxene grains are being replaced by hornblende. The leucosomes have abundant quartz and plagioclase, and lesser amounts of magnetite, orthopyroxene and clinopyroxene. The plagioclase is being altered to sericite. The stromatic migmatite has experienced granulite-facies metamorphism, since it contains orthopyroxene.

The white leucosome is represented by specimens RS 70 (from outcrop mentioned above) and RS 36 (from core, drill hole C2D5). The mineral assemblage is:- quartz +

microperthite + microcline ± plagioclase + garnet ± biotite ± sericite. Zircon and apatite are accessory minerals. Quartz, which is the most abundant mineral, occurs in two phases, (a) early-phase, in the groundmass as small interstitial grains surrounding feldspars, and (b) late-phase ribbon quartz in discontinuous veins. Microperthite and microcline form porphyroblasts and also occur in the groundmass. Some of the potash feldspar is being altered to sericite. Plagioclase seems to be absent in RS 36, but a few grains were observed in RS 70. The plagioclase and antiperthite are intensely altered to sericite. Garnet porphyroblasts are common in both specimens, and in RS 70, some of them are flattened and aligned parallel to the foliation. Very sparsely disseminated sulphides (pyrite, pyrrhotite and chalcopyrite) are present in RS 36.

### **3.6 Potash-feldspar Granite**

The large K-feldspar granite body in Area 2s is believed to be a partial melt, produced by migmatization of the charno-enderbites. It is thought to be a hololeucocratic leucosome with a typical charnockite appearance. The K-feldspar granite is in contact with the Mauch Shear Zone. East-west shears that cross-cut the Mauch Shear Zone, also pass through the granite. The granite hosts the majority of the gold-bearing quartz veins in Area 2s. The K-feldspar granite is grey to pale pink, medium- to coarse-grained and sheared. Orthopyroxene is absent in the K-feldspar granite.

Specimens RS 25, RS 35, RS 37, RS 38, RS 39, RS 50, RS 51, RS 52, and RS 94 were obtained from the K-feldspar granite. The general mineral assemblage is:- potash feldspar + quartz ± plagioclase + biotite ± garnet + sericite + chlorite ± calcite ± magnetite ± sillimanite. Potash feldspar (microperthite and microcline) is the most abundant mineral forming porphyroblasts and also occurring in the groundmass. Graphic intergrowth between potash feldspars and quartz is common. Some of the potash feldspar grains are being altered to sericite. The quartz occurs in two phases, (a) fine-grained quartz in the groundmass, surrounding feldspar porphyroblasts, and (b) late-phase, coarse-grained stockwork of ribbon quartz. The late-phase quartz veining also has sericite, disseminated sulphides and calcite (e.g. in RS 50). Most of the specimens have small amounts of plagioclase ± antiperthite. In RS 25, some of the plagioclase grains have myrmekitic intergrowth with quartz. In most specimens, some of the plagioclase is being altered to sericite. Biotite is a late-phase mineral that overgrows quartz and feldspars. In RS 51, some of the biotite flakes have pleochroic haloes surrounding zircon inclusions. In RS 93 green chlorite is replacing some of the biotite. Garnet porphyroblasts are late-phase, as they cut quartz, feldspars and the late-phase ribbon quartz. Sparse, disseminated sulphides are closely associated with biotite and chlorite near quartz veins. A small

amount of calcite is associated with chlorite. In RS 37, RS 51 and RS 93, rutile needles occur in chlorite. Alteration of biotite produced chlorite and rutile. In RS 52, sillimanite occurs with the sulphides. The sillimanite, which commonly surrounds and cross-cuts sulphide grains, is colourless and forms prismatic crystals with square basal sections. Magnetite, zircon, sphene and apatite are the other accessory minerals.

Potassium alteration, which is typical of the granite, occurred prior to silica alteration. The ribbon quartz veining (silica alteration) resembles a stockwork, which cuts the potash feldspars. Small quartz grains, forming rims around larger grains, are part of the silica alteration process. The sequence of potash feldspar and silica growth seems to have occurred in three stages, (a) graphic intergrowth of K-feldspar and quartz (earliest phase), (b) fine-grained quartz in the groundmass and K-feldspar porphyroblasts, and (c) coarse quartz veins (ribbon quartz). In (b), the rims of small quartz grains could be due to fluid movement around grain boundaries during high temperature deformation. Small grains of potash feldspar also accompany the small quartz grains. Shearing and fluid movement gave rise to the ribbon quartz veins in (c). Other alteration minerals occur associated with the sulphide mineralization. The typical alteration assemblage for the Area 2s anomaly is:- potash feldspar + sericite + quartz + biotite + chlorite ± calcite ± sillimanite ± rutile.

The modal compositions of the K-feldspar granites are plotted on the QAPF diagram (Figure 3.6). Specimens RS 38, RS 39, RS50, RS51 and RS 94 plot in the alkali granite field. Specimens RS 25, RS 35, RS 37 and RS 93 plot in the syenogranite field. Specimen RS 51 plots in the monzogranite field.

### **3.7 Quartz Veins, Feldspar Porphyry and Pegmatite**

Quartz veins and pegmatites are common throughout the study area. The feldspar porphyry was mapped in the mineralized shear zone in Area 4. The quartz veins, feldspar porphyry and pegmatite veins are intrusive into the metamorphosed greenstone belts and charno-enderbites. Specimens were collected where the quartz veins and feldspar porphyries are mineralized. The pegmatites are coarse- to very coarse-grained and generally not mineralized. The pegmatites do not have the penetrative regional foliation and are therefore, post-deformational.

The quartz veins are represented by specimens RS 4, RS 33, RS 40, RS 48, RS 49, RS 53, RS 54, RS 64 and RS 65. Specimens RS 40, RS 53 and RS 54 are from core of drill hole C2D20 in Area 2s. In handspecimen, the quartz has very sparse specks of free gold.

In thin section, RS 40 and RS 53 are composed of approximately 98 % ribbon quartz. In RS 40, the accessory minerals are muscovite (sericite), chlorite and calcite. Calcite is associated with muscovite. In RS 53, the accessory minerals are muscovite (sericite), garnet, chlorite, calcite, microperthite, plagioclase and gold. Muscovite (sericite) flakes are aligned parallel the foliation. Garnet is being altered to chlorite, sericite and calcite. Plagioclase and microperthite are being altered to muscovite. The opaques (gold) are very sparse and fine-grained. The alteration assemblage in both specimens is:- muscovite (sericite) + chlorite + calcite.

In RS 54, the veins are aplitic, comprising quartz and microcline. The veins contain ribbon quartz, microcline, sericite and calcite. The wall-rock is composed of microperthite, microcline, quartz, garnet, plagioclase, chlorite, amphibole, muscovite (sericite), calcite, sillimanite and gold. Microperthite forms porphyroblasts that have graphic intergrowth with quartz. Garnet is being altered to chlorite. Muscovite (sericite), calcite and chlorite occur in late-stage veins that cut across the foliation. Gold specks are very fine-grained and associated with amphiboles and chlorite. Prismatic sillimanite appears to be with the late-stage veins.

Specimens RS 33, RS 48, RS 64 and RS 65 are from Area 4. The quartz veins are composed of late-phase ribbon quartz. Specimens RS 33, RS 64 and RS 65 were obtained from core of drill hole C4D14 (in Area 4), which intersected chalcopyrite, chalcocite, pyrite, pyrrhotite and molybdenite mineralization. The wall rock comprises:- quartz + plagioclase ± antiperthite ± amphibole ± gahnite ± biotite ± garnet + chlorite + zoisite + calcite ± tourmaline ± monazite + sulphides. The plagioclase has, in places, myrmekitic intergrowth with quartz. The plagioclase is intensely saussuritized to sericite and zoisite. Chlorite is replacing garnet. Disseminated to semi-massive sulphides are late-phase minerals. The sulphides occur in both the quartz veins and the wall-rocks. The biotite is late-stage as it cross-cuts the sulphides, quartz and plagioclase. A small amount of calcite is associated with the chlorite alteration. Abundant apatite and tourmaline are associated with the biotite. In RS 64, the amphibole, biotite, apatite, garnet and tourmaline are most abundant in the contact zone between the quartz vein and the tonalitic host rock. In RS 65, a pseudo-isotropic spinel, with a deep green colour and high relief, occurs in large amounts, interstitial to plagioclase grains. The spinel is either hercynite or gahnite. Sulphides cut the spinel grains. Chlorite also occurs in late-stage veins that cut the ribbon quartz veining and sulphides. Monazite occurs as an accessory mineral in RS 65. The alteration assemblage on the "Copper Shear" of Area 4 seems to be:- sericite + zoisite + biotite + chlorite + calcite ± apatite + garnet ± amphibole ±

tourmaline. The Cu–Mo mineralization on the “Copper Shear” occurs in quartz veins and the wall rocks. Specimen RS 48 was obtained from a quartz vein in garnet–biotite gneiss (meta–greywacke). The vein is composed of ribbon quartz. Microperthite and microcline porphyroblasts are lensoid and aligned parallel to the foliation. The pressure shadows of the porphyroblasts contain fine-grained quartz. Biotite schistosity wraps around the porphyroblasts and cuts the quartz in the pressure shadows. Potash feldspars also occur in the groundmass. Plagioclase and antiperthite occur in the groundmass and as porphyroblasts. The potash and plagioclase feldspars are being altered to sericite. Garnet porphyroblasts, with biotite inclusions, cut quartz grains and feldspars. Opaque grains (sulphides and/or magnetite) are accessory.

Specimen RS 4 was obtained from a quartz vein within calc-silicate rocks in Zvamapere Block. Ribbon quartz comprises > 80% of the rock. The other minerals are hypersthene, plagioclase and sulphides (pyrite, chalcopyrite, covellite and sphalerite). The sulphides are subhedral and disseminated to semi–massive. Grab samples, obtained from the quartz vein and assayed for gold and base metals, yielded up to 80 ppb Au, 595 ppm Cu and 478 ppm Mn.

Specimen RS 49 was obtained from a quartz vein in the Cu–Mo Anomaly west of Area 4. In handspecimen the quartz has azurite–stained chalcopyrite, pyrite and molybdenite. In thin section, the rock comprises quartz, potash feldspar, garnet, plagioclase, sericite, sulphides and tourmaline. Quartz occurs as ribbons, with inclusions of garnet. Garnet porphyroblasts occur in bands and are being altered to chlorite. Ribbon quartz cuts garnet, indicating that the latter is older than the former. Microcline porphyroblasts are being altered to muscovite (sericite). Plagioclase is present in small quantities. Tourmaline forms small crystals. Sulphides occur in small quantities and are aligned parallel to the foliation. Grab samples were collected from the quartz vein and assayed for Au, Cu and Bi. The peak values were 1.8 g/t Au, 803 ppm Cu and 783 ppm Bi.

Feldspar porphyry occurs as dykes hosting mineralization in the “Gold Shear” of Area 4. The lithology is represented by specimen RS 27, which was collected from core of drill hole C4D3. The rock has a bimodal (phenocrystic) texture comprising (a) phenocrysts of microperthite (with graphic intergrowth); (b) groundmass of quartz, microcline, microperthite, plagioclase, biotite, chlorite, sericite, sphene and sulphides; and (c) ribbon quartz veining, cross-cutting (a) and (b). Some of the potash feldspar is being altered to sericite. Disseminated sulphides (pyrrhotite, pyrite, chalcopyrite, chalcocite and sphalerite) are most abundant in the ribbon quartz, where they have a preferred



orientation parallel to the foliation. Chloritic alteration is typical of the sulphide mineralization in the "Gold Shear" in Area 4. Biotite and sphene are accessory minerals. Feldspar porphyry dykes in Area 4 slightly postdate peak metamorphism in the NMZ, but are synchronous with ductile deformation. The feldspar porphyries are sheared and contain ribbon quartz veining, but lack granulite-facies minerals such as orthopyroxene.

### **3.8 Picritic rocks, Olivine Pyroxenite and Dolerite**

Picritic rocks, olivine pyroxenite and dolerite are intrusive rocks that are post-metamorphism. These rocks have igneous textures and intrude mainly late NNE and ESE fractures. They also intrude the regional ENE-trending fractures. The ultramafic intrusives are more common in the central and eastern parts of the study area. Dolerite dykes are common throughout the area.

Picritic rocks outcrop west of Area 4, and were also intersected in drill holes C4D6-D9 within the Area 4 "greenstone" belt. The lithology is represented by specimens RS 58 and RS 60. The picritic rock is composed of olivine + clinopyroxene ± orthopyroxene + plagioclase + biotite + magnetite + serpentine. The olivine forms discrete cumulate grains and is being altered to serpentine and magnetite along cracks. In RS 58, some olivine crystals are enclosed in larger poikilitic clinopyroxene grains, forming a poikilitic texture. Plagioclase forms a few laths, which in RS 60, form a sub-ophitic texture with clinopyroxene. Biotite is an accessory mineral. The rock consists of >90% ferromagnesian minerals and <10% plagioclase. This composition indicates that it is a picritic rock.

Olivine Pyroxenite is represented by specimens RS 13 and RS 19. The rock is composed of clinopyroxene + orthopyroxene + olivine + plagioclase ± biotite ± magnetite ± serpentine. Orthopyroxene forms phenocrysts that have an ophitic texture with plagioclase laths. Late-phase plagioclase is slightly deformed (bent). The rock has an igneous texture and is post-metamorphic.

Specimens RS 20 and RS 71 were obtained from dolerite dykes. The specimens are composed of clinopyroxene (augite) + plagioclase + magnetite + biotite ± hornblende ± chlorite ± apatite ± quartz. The augite and plagioclase laths form ophitic to sub-ophitic textures, which are igneous textures (Shelly, 1993). Some of the augite is being altered to hornblende and chlorite. The plagioclase is being replaced by sericite. Apatite occurs with chlorite and sericite alteration. Biotite and magnetite are accessory minerals. In RS 71, quartz forms few small interstitial grains, hence the rock is a quartz dolerite.

### 3.9 Geochemistry (XRF Analyses)

Fifteen rock specimens of ~ 2 kg were collected from the various lithologies in the study area. Fresh specimens were collected from outcrops and drill core. Table 3.8 shows the specimen numbers, lithology and symbols used on diagrams. Each specimen was crushed using a jaw-crusher to < 0.5 cm<sup>3</sup>. Splits of 200g were further pulverized to < 60 µm using a ball mill (30 minutes). For the XRF analysis of major elements, 0.75 g of rock powder was fused (1150°C, 30 minutes) with 4.5 g of lithium metaborate or tetraborate to a homogeneous glass disc. For the XRF analysis of trace elements, pressed powder pellets with 8 g of rock powder and 1.6 g of wax (Hoechst ceridust) were used.

The XRF analyses were conducted at the Geology Department, Rhodes University, using a Philips PW 1404/10 spectrometer with a Sc-anode X-ray tube. Major elements were measured at 50 KV and 50 Ma, and trace elements at 80 KV and 35 Ma. The method was calibrated with international standard reference materials. For the major elements, correction for residual matrix effects was based on theoretical inter-element influence coefficients ( $\alpha$ -coefficient). Results were recalculated to oxide weight percentages. Trace element corrections for inter-element effects were based on the Compton-scattered Rh-K $\alpha$  anode emission line and analyte lines were corrected for background and spectral overlap. Results were recalculated in ppm weights. The analytical results are tabulated on Table 3.7.

#### Major Elements

Major elements data were used for rock classification and construction of variation diagrams. Variation diagrams display the data as bivariate or trivariate plots on an x-y graph or on a triangular graph respectively. The variation diagrams show the interrelationships between elements.

The major element concentrations (wt. %) were plotted against the silica content (wt. %) on Harker variation diagrams. Figures 3.9 shows variations in "plutonic" and meta-basaltic rocks. The sampled "plutonic" rocks are charnockite, enderbite, potash feldspar granite, feldspar porphyry and leucogneiss. The meta-basaltic rocks are amphibolite and mafic granulite.

On the Harker diagrams, major element oxides TiO<sub>2</sub>, Al<sub>2</sub>O<sub>3</sub>, Fe<sub>2</sub>O<sub>3</sub>, MnO, MgO, CaO and P<sub>2</sub>O<sub>5</sub>, all show strong negative correlation with SiO<sub>2</sub>. The more differentiated rocks (charnockites, potassic granites, feldspar porphyry and leucogneiss (leucosome)) show

increasing  $K_2O$  with increasing  $SiO_2$ . In the less differentiated rocks (meta-basalts and enderbite)  $K_2O$  does not have positive correlation with increasing silica. These trends demonstrate the control of titanite, ilmenite or magnetite, plagioclase, apatite and a mafic mineral (probably hornblende) in the fractionation process (Jelsma, 1993).  $Na_2O$  shows only a slight increase with increasing  $SiO_2$ . The felsic lithologies have more  $Na_2O$  and  $SiO_2$  than the mafic rocks.

Figure 3.10 is a trivariate diagram of  $K_2O$ ,  $Na_2O$  and  $CaO$ , on which the "plutonic" and meta-basaltic rocks are plotted. The trend for the less evolved lithologies (basaltic granulite, basaltic amphibolite and enderbite) is characterized by an increase in  $CaO$ , whereas the more differentiated rocks show a general increase in  $K_2O$  and  $Na_2O$ .

The "plutonic" rocks are plotted on a TAS (total alkalis vs. silica) diagram, Figure 3.11. The charnockites and feldspar porphyry plot in the field of granite. This indicates that the charnockites are granites, which contain hypersthene. The leucogneiss (leucosome) plots in the field of alkali granite. Potassic granites plot in both fields of granite and alkali granite. The enderbite plots in the field of diorite. The more differentiated lithologies, which have more  $K_2O$ , plot in the field of alkali granite.

The basaltic amphibolite and silicified basaltic granulite are plotted on a TAS diagram for volcanic rocks (Figure 3.12). The basaltic amphibolite plots in the field of basalt. Due to shearing and late-phase silica addition (ribbon quartz), the silicified basaltic granulite has the composition of an intermediate rock, and plots in the field of andesite.

The garnet–biotite gneiss (meta–greywacke) is plotted on Figure 3.13, which is a diagram for classifying terrigenous sandstones using  $\log (Na_2O/K_2O)$  versus  $\log (SiO_2/Al_2O_3)$ . The rock plots in the field of greywacke. The greywacke produced abundant garnets during high-grade metamorphism in the Northern Marginal Zone.

### Trace Elements

Trace element data were used as an indicator of petrological processes. Trace element studies are more capable of discriminating between petrological processes than are the major elements (Rollinson, 1993). The trace elements are commonly studied in three groups, which are (a) rare earth elements (REE), (b) transition metals and (c) platinum group elements (PGE). In this study, only the first two groups were analysed. The REE are the most useful and have important implications in igneous, sedimentary and metamorphic petrology. In this study only three REE (La, Ce and Nd) analyses were

conducted. The analyses also included Rb, Sr, Y, Zr, Nb, Ba and Th, which are other important trace elements in geochemistry.

Trace element data for metamorphosed igneous rocks were normalized to chondrite. Chondritic meteorites are used as standards, since they are thought to be unfractionated. Trace element data for meta-sediments were normalized to NASC (North America Shale Composite). Normalized REE data were presented as "spider diagrams" (Rollinson, 1993) of concentration against atomic number.

#### *Felsic and Intermediate "Plutonic" Rocks*

Figure 3.14 is a "spider diagram" of trace elements Rb, Sr, Y, Zr, Nb, Ba, La, Ce, Nd and Th, for the felsic "plutonic" rocks (charnockite, potassic granite, feldspar-porphyry and leucogneiss). The felsic "plutonic" rocks are enriched in these trace elements, but have higher Rb, Ba and Th, and lower concentrations of Sr, Y, Nb and Nd.

The normalized transition metal (Sc, V, Cr, Co, Ni, Cu and Zn) concentrations for felsic "plutonic" rocks, are plotted on a "spider diagram", Figure 3.15. All the felsic "plutonic" rocks are depleted in transition metals, with a strong negative Ni anomaly. There are elevated values of Sc, V, Cu and Zn. The feldspar-porphyry has a slight enrichment of Sc.

Figure 3.16 is a Rb – (Y + Nb) geotectonic discrimination diagram for granites (Rollinson, 1993). Rocks of the "Plutonic Assemblage" plot in the field of Volcanic Arc Granites. This trend is similar to that of granitoids in the Mutare area and the Wedza Granitoid Suite of the Zimbabwe Craton, which were studied by Jelsma (1993) and Chenjerai (1996) respectively. Also, on Figure 3.17, which is a Nb – Y geotectonic discrimination diagram for granites (Rollinson, 1993), the rocks of the "Plutonic Assemblage" plot in the field of Volcanic Arc Granites (+ syn-collisional granites).

#### *Mafic Meta-volcanic and Intermediate Rocks*

Figure 3.18 is a "spider diagram" for trace elements in the less evolved mafic and intermediate rocks (basaltic amphibolite, silicified basaltic granulite and enderbite). These rocks are enriched in the trace elements, with higher Rb and Ba, and lower concentrations of Y, Zr, Nb and Nd.

Figure 3.19 is a "spider diagram" of normalized transition metal concentrations in the mafic and intermediate rocks. The rocks are enriched in Sc and V, and depleted in Cr, Co, Ni, Cu and Zn. They have a strong negative Ni anomaly.

Figure 3.20 is a  $TiO_2-Zr / (P_2O_5 \times 10\ 000)$  discrimination diagram for basalts (Rollinson, 1993). The basaltic amphibolite (RS 8) plots in the field of tholeiitic basalt. Figure 3.21 is a  $MnO-TiO_2-P_2O_5$  geotectonic discrimination diagram for basalts and basaltic andesites (Rollinson, 1993). The basaltic amphibolite, silicified basaltic granulite and enderbite, all plot in the field of Island Arc Tholeiite. This trend is similar to that for tholeiitic basalts on the Zimbabwe Craton, which were studied by Jelsma (1993) and Chenjerai (1996).

#### *Meta-sediments*

The trace element data for meta-sediments (banded chert and tuff, garnet-biotite gneiss and calc-silicate rock) are plotted on a "spider diagram", Figure 3.22. Available data indicate that the banded chert is depleted in Sr, Zr, Ba, La, Ce and Nd, with peak values in La and Ce. The garnet-biotite gneiss is enriched in Sr, Y, Ba, La and Th, but depleted in Zr and Nb. The peak values are in Y and La. The calc-silicate rocks have high Y, Zr, Nb, La and Ce, and low concentrations of Rb, Sr and Ba. The peak is in Y and lowest concentration is in Sr.

Trace elements (REE) in a metamorphosed clastic sediment reflect the chemistry of its source (Rollinson, 1993). The provenance of the meta-greywacke (garnet-biotite gneiss) appears to be the meta-basalts and meta-andesites in the "greenstone" belts. REE in chemical meta-sediments (calc-silicate rocks and banded chert) most likely reflect the composition of the seawater from which they were precipitated.

The available data for transition metal concentrations in meta-sediments are plotted on a "spider diagram", Figure 3.23. The garnet-biotite gneiss is enriched in Sc, V, Cr, Co and Ni. The calc-silicate rocks are enriched in Cr and Ni. The banded chert is enriched in Cr, but depleted in Sc, Co and Ni.

#### *"Plutonic", Mafic Meta-volcanic Rocks and Meta-sediments*

The degree of fractionation of a REE pattern may be expressed by the concentration of a light REE (La or Ce) ratioed to the concentration of a heavy REE (Yb or Y) (Rollinson, 1993). The ratio  $(La/Y)_N$  or  $(Ce/Y)_N$  is plotted against  $Y_N$ , and is a measure of the degree of REE fractionation with changing REE content. Figures 3.24 and 3.25 show such ratios. Both plots show a decrease in REE fractionation with increasing heavy REE content.

REE fractionation was highest in the magnetite–chamockites, some potassic granites and enderbite, and lowest in the calc-silicate rocks, garnet-biotite gneiss and basaltic amphibolite and silicified basaltic granulite. The rocks of the “Plutonic Assemblage” have high REE fractionation. The plots also indicate the basaltic amphibolite and basaltic granulite as possible sources of the meta-sediments.

### 3.10 Metamorphism

The rocks in the study area and the Northern Marginal Zone (NMZ), have been metamorphosed to granulite-facies. The granulites are characterized by the presence of hypersthene. Kamber & Biino (1995) have identified 4 metamorphic stages, 2 major plutonic episodes and at least 3 deformation events, which occurred during the evolution of the NMZ. These stages have also been discussed in Chapter 2. Mafic granulites, which are the oldest rocks, record all the 4 stages of metamorphic mineral growth. The first two stages predate deposition of sediments and the intrusion of chamockites and enderbites between 2.72 and 2.62 Ga (Kamber & Biino, 1995). All Archaean rocks in the NMZ were subjected to granulite-facies metamorphism and varying degrees of retrogression. Prograde heating occurred in the sillimanite stability field. The calculated peak metamorphic conditions vary along the NMZ from  $5 \pm 1$  kbar,  $825 \pm 50^\circ\text{C}$  in the west to  $8.4 \pm 1$  kbar,  $850 \pm 50^\circ\text{C}$  in the east, indicating differential uplift (Rollinson & Blenkinsop, 1995). The thermal peak was followed by an increase in pressure to a maximum of 8.5 kbar. The retrogression is associated with late deformation, and the P-T conditions are poorly constrained at c. 4 kbar,  $600^\circ\text{C}$ . The NMZ granulites were finally exhumed in a separate event, along upper greenschist-facies thrusts, at 2.0 Ga (Kamber & Biino, 1995).

The 4 metamorphic mineral blastesis events, identified by Kamber & Biino (1995), can be used as relative time markers representing the 4 metamorphic stages. Stages 1 and 2 were recorded in lithologies of the metamorphosed greenstone belts. The basaltic granulites (e.g. RS 10, RS 22, RS 72, RS 76, RS 77 and RS 82) have the general assemblage :-

orthopyroxene + clinopyroxene + plagioclase  $\pm$  hornblende  $\pm$  biotite  $\pm$  magnetite  $\pm$  ilmenite. Garnet is absent in the meta-basites at stage 1. The orthopyroxene was produced during prograde granulite-facies metamorphism (Stage 1). Alternating orthopyroxene-rich and clinopyroxene-rich layers show compositional banding, produced by the high-grade Stage 1 event. In charno-enderbites, xenoliths of meta-basites and meta-sediments sometimes show a pre-intrusive compositional banding of pyroxene, hornblende and plagioclase. Plagioclase shows albite and pericline twins of

tectonic origin. The twins are closely spaced, curved, discontinuous and tend to taper at the crystal edge. The orthopyroxene and clinopyroxene show wavy extinction.

The parasitic hornblende, which is replacing the orthopyroxene and clinopyroxene, is indicative of retrograde metamorphism (Stage 2). Hornblende, at Stage 2, commonly contains acicular ilmenite exsolution along cleavage planes. In the basaltic amphibolites (e.g. RS 8), the pyroxenes are almost completely replaced by hornblende which constitutes approximately 80% of the rock. Post-peak cooling and hydration is indicated by the growth of hornblende + magnetite + ilmenite, at the expense of orthopyroxene and clinopyroxene. The hornblende is characterized by a deep green, pale bluish pleochroism.

Stage 3 was a high-temperature tectono-metamorphic event. The most common mineral transformation was the symplectic intergrowth of orthopyroxene + plagioclase + clinopyroxene replacing hornblende. Grain boundary migration can be proved by relict magnetite + ilmenite layers, included in the orthopyroxene or symplectite, still defining the old hornblende crystal shape (Kamber & Biino, 1995). Dynamic re-crystallization of orthopyroxene and clinopyroxene was confined to small Stage 3 shear zones. The basaltic granulites were sheared and silicified by ribbon quartz to produce the silicified basaltic granulite (e.g. RS 23, RS 30 and RS 83). Chamo-enderbites intruded the NMZ between 2.72 and 2.62 Ga. The chamo-enderbites have magmatic orthopyroxene and minor clinopyroxene. The chamo-enderbites underwent variable degrees of deformation and re-crystallization during Stage 3.

The SSE-NNW compression, which produced the penetrative foliation, was coeval with incipient to total migmatization. Migmatites concentrated more strain than the surrounding lithologies and occur where deformation was strongest. Two types of migmatite have been identified in the field, (a) has hololeucocratic leucosomes with typical charnockite appearance (similar to the K-feldspar granite), is coarse-grained and was produced from a charnockite, and (b) white, granitic in composition and garnet-magnetite bearing (e.g. RS 70). Sillimanite was observed in K-feldspar granite (RS 52) and an aplitic vein (RS 54) in K-feldspar granite. Where migmatization was pervasive, restites with unusual mineralogy (orthopyroxene + sillimanite + garnet + spinel + quartz) occur as metre-size lenses or in narrow bands (Kamber & Biino, 1995). Chamo-enderbites which escaped migmatization recorded a weak to medium foliation developed during NNW-SSE compression. The feldspars have a honey-brown and greasy appearance. Potash feldspar has distinct, very fine-scale cross-hatch twinning (microperthite), or is

occasionally untwinned. Some sodic feldspars are also untwinned and contain antiperthitic patches of untwinned potash feldspar. Such minerals and their textures are characteristic of intermediate pressure, orthopyroxene–plagioclase granulite sub-facies (Odell, 1975). In proto–mylonites, quartz is found in almost monomineralic ribbons, in which feldspar grains are rotated. Bulbous quartz + plagioclase myrmekites are re-crystallized during the high temperature deformation. Orthopyroxene grains show internal deformation (wavy extinction), but are re-crystallized only marginally.

Stage 4 is the hydration event of the granulite assemblages. It is a retrograde upper greenschist facies metamorphic event that occurred at ~1.9 Ga (Kamber & Biino, 1995). A new generation of hornblende developed, replacing orthopyroxene and clinopyroxene of Stage 3. The hornblende has no inclusions. Small flakes of red biotite are restricted to zones of intense hydration. The red biotite has not been found in other stages, implying K–metasomatism during Stage 4 hydration. The retrograde metamorphism only occurred where H<sub>2</sub>O-rich fluids were available, mainly in decimetre to metre wide, reverse shear zones. In charno–enderbites, greenschist assemblages are developed in shear zones that are parallel or sub-parallel to the Stage 3 foliation. The assemblage comprises epidote, green hornblende, spinel, albite, quartz and biotite. Usually, retrogression is only partially developed, such that orthopyroxene and clinopyroxene are marginally replaced by biotite and hornblende.

### 3.11 Structural Geology

In the study area, structural deformation produced a regional ENE-trending foliation and two major phases of folding. The rocks have a pervasive, weak to medium regional foliation, which is penetrative in the NMZ (*sensu stricto*). The foliation is developed in the greater part of the area, except in some bodies of enderbite and charnockite, which are massive and only foliated near their edges. The regional foliation was produced by the main NNW–SSE compression, during the Stage 3 high-temperature, tectono–metamorphic event (Kamber & Biino, 1995). The lineations plunge steeply and rare shear sense indicators show a reverse character. In the greater part of the study area, the foliation generally dips steeply to the south–east. However, in the south–eastern corner of the area, there are alternating zones with SE- and NW–dip directions, suggesting horizontal folding in that domain (stereonet (d), Figure 3.0). The horizontal antiforms and synforms in the SE corner of the E.P.O. were formed during the first phase of folding. In the northern part of the area, bands of enderbite are folded into what appear to be mainly reclined isoclinal folds (stereonet (c), Figure 3.0). These isoclinal folds were formed during the second phase of folding. The regional ENE trend is, in this study, regarded as

the first-order fabric and designated "S1". The strike of the foliation varies from 060° to 070°. Away from the fold structures, dip angles vary from 60° to 85° SE. On fold structures, dip angles can be as gentle as 25°.

A prominent structural feature in the study area, is the Mauch Shear Zone, which extends from the SW to the NE corner of the area. On the aeromagnetic map, the Mauch Shear Zone and other shear zones, have low to very low magnetic signatures. The Mauch Shear Zone generally follows the regional S1 trend, and extends for hundreds of kilometres NE and SW of the area. South of Renco Mine, it is known as the Mtirikwi Shear Zone. The Mauch Shear Zone is a first-order, transcrustal-scale shear zone. The mylonite zone, which is mainly sheared charnockite, attains a maximum horizontal width of 1 km. A medium-grained proto-mylonite zone flanks the fine-grained mylonite zone. Dips in the shear zone are generally steep (70° - 85°) to the SE, but in the middle of the mylonite zone, some dips are steep NW. The leuco-mylonite has potash feldspar and garnet porphyroblasts that are  $\delta$ -type rolling structures. The majority of the rolling structures indicate sinistral horizontal sense of movement. Other kinematic indicators, such as folded mafic xenoliths, also suggest sinistral movement. The shear zone has a quartz lineation that has persistent steep plunges of 70° to 85° SW (stereonet (i), Figure 3.0). The plunge suggests that the movement can be resolved into vertical and horizontal components. The bulk of the movement was due to the vertical component. Since the shear zone generally dips steeply to the SE, and the horizontal sense of movement is sinistral, the vertical sense of movement was reverse. The steeply plunging lineation could also have been produced by reactivation after the initial sinistral movement. The shear zones were reactivated during the 2.0 Ga. retrograde tectono-metamorphic event (Kamber & Biino, 1995). This event was associated with the final, low-temperature thrusting of the NMZ onto the Zimbabwe Craton.

The deformation that produced the Mauch Shear Zone and other smaller shear zones parallel to the regional trend, is believed to be coeval with the NNW–SSE compression, which produced the regional foliation. These shear zones and the foliation, have the same strike and dip directions. Rollinson & Blenkinsop (1995) state that these structures are compatible with a bulk strain consisting of NNW–SSE horizontal shortening and vertical extension. These structures are a result of a single progressive deformation.

Towards the eastern boundary of the area, the Mauch Shear Zone has a splay shear that follows the 040° trend and dips SE or NW at angles between 50° and 80° (stereonet (a), Figure 3.0). The 040° trend is a second-order structure designated S2, which is

characterized by shear zones with sinistral movement. The sense of movement is indicated by S–C planes and  $\delta$ -type rolling structures. A metamorphosed greenstone belt is located in the acute angle ( $20^\circ$ ) between the Mauch Shear Zone and the splay shear. The “greenstone belt” hosts the Area 4 gold and Cu–Mo mineralization. A third-order shear zone trending on  $060^\circ$  hosts the Cu–Mo mineralization. Gold mineralization occurs in a fourth-order shear zone trending on  $055^\circ$ . Convergence of the first- and second-order shear zones, both with sinistral movement, resulted in dilation or deformation in the  $20^\circ$ -acute angle. Such deformation zones are favourable sites for gold mineralization (Hodgson 1989).

In the SW corner of the area, The Mauch Shear Zone has flexure caused by the intersection of an E-W trending shear zone. The E-W shear zone is a third-order structure (S3), which is typified by dextral movement. A potassic granite with quartz veins that host gold mineralization occurs in Area 2s immediately south of the flexure. Several E-W shears are present in the granite. Stereonet (f), Figure 3.0, shows the major structural trends and lineations in Area 2s. Quartz lineations plunge steeply to the west ( $75^\circ$ - $87^\circ$ → $270^\circ$ ). Interference of the sinistral first-order and dextral second-order shear zones resulted dilation as a consequence of bulk, inhomogeneous shortening (Hodgson, 1989). The dilation zone is a favourable site for mesothermal gold mineralization. The structural data for the Mauch Shear Zone, the splay shear and the E-W flexure, are plotted on stereonet (i), Figure 3.0.

The shear structures in the study area can be categorized into four major structural patterns. The first-order pattern, S1, is the regional fabric mentioned above. The azimuth of this pattern varies from  $060^\circ$  to  $070^\circ$ . Shear zones along the S1 are sinistral. The second-order pattern, S2, cross-cuts the S1, and also has sinistral shears. The azimuth of the S2 trend varies from  $035^\circ$  to  $045^\circ$ . The third-order pattern, S3, cross-cuts the S1 and S2, and has dextral shears. In the NE corner of the area, E-W foliations and a fairly wide S3 shear zone occur (stereonet (b), Figure 3.0). Lengths of the S3 structures are not well developed on surface, probably because they rake steeply (at the nearby Renco Mine, they rake steeply to the east). The strike of the S3 pattern varies from  $085^\circ$  to  $095^\circ$ . The fourth-order pattern, S4, cross-cuts S1 to S3, and has dextral shears. The strike of the S4 pattern varies from  $125^\circ$  to  $150^\circ$ .

Bands of metamorphosed greenstone belts, meta-basites and enderbite, depict the folding in the area. South of the Mauch Shear Zone, some of the proto-mylonites are infolded with the mafic bands. At least two major phases of folding occurred within the

study area. The first phase formed horizontal synforms and antiforms, which were refolded during the second phase. The second phase produced folds that vary from gentle to open to tight isoclinal. The Zvampere fold structure, which is a refolded synform (Figure 3.0), shows both phases of folding. Axes of the second-phase fold structures generally plunge gently to the north-east. The axis of the Tokwane fold structure plunges at approximately  $16^\circ$  towards  $040^\circ$  (stereonet (e), Figure 3.0). In the Zvampere fold structure, the axis plunges at  $10^\circ$  towards  $070^\circ$  (stereonet (g), Figure 3.0). The axis of the Ngundu fold structure plunges at approximately  $32^\circ$  towards  $084^\circ$  (stereonet (h), Figure 3.0). The folding is believed to have occurred during Stage 3 deformation, when there was NNW–SSE horizontal shortening and vertical extension (Rollinson & Blenkinsop, 1995).

## CHAPTER 4

### GEOPHYSICAL SURVEYS

#### 4.1 INTRODUCTION

Airborne geophysical surveys were carried out over the study area (Tokwe EPO 847), during the early stages of exploration activities. The surveys were conducted by a contractor, Geodass (Pty) Limited. The contractor was commissioned to undertake the acquisition, processing and initial interpretation of rotary wing-borne high-resolution magnetic and radiometric data. The surveys were conducted during the dry winter month of July, in 1994.

#### MAGNETIC METHOD

The magnetic method was used to measure the local lithospheric magnetic fields, which are produced by variations in the intensity of magnetization in rock formations. Magnetization of rocks is partly due to induction by the magnetizing force associated with the earth's field and partly to their permanent (remanent) magnetization (Parasnis, 1979). The induced intensity depends upon the magnetic susceptibility as well as the magnetizing force, and the intensity upon the geological history of the rock. The susceptibility of rocks is almost entirely controlled by the amount, grain size and distribution of ferrimagnetic minerals in them. High magnetization of rocks is due to ferrimagnetic minerals, which may be divided into two geochemical groups: (a) magnetite ( $\text{Fe}_3\text{O}_4$ ), titanomagnetite ( $\text{FeO}(\text{Fe}, \text{Ti})_2\text{O}_3$ ) and ilmenite ( $\text{FeTiO}_3$ ), and (b) the iron-sulphur group, of which pyrrhotite ( $\text{Fe}_7\text{S}_8$ ) is the most important. The susceptibility of rocks with fine-grained magnetic minerals is less than for rocks containing an equivalent concentration of coarse-grained minerals. The susceptibility of a rock is approximately linearly proportional to the volume percentage of the ferrimagnetic mineral present (Comer, 1994).

The form of a magnetic anomaly resembles a sine curve and is due to the interaction between the field lines associated with the dipolar field of a body and the earth's field. Upward intensity vectors are additive and give rise to the positive amplitude of the anomaly. Downward intensity vectors are subtractive and result in the negative amplitude of the anomaly. The location of the body on the earth controls the inclination of the inducing field. Other factors that control the form of the anomaly include strike direction, dip and geometry of the body, as well as remanent magnetization.

Magnetic anomalies comprising the lithospheric field provide valuable information, such as:

- (a) *magnetic susceptibilities* of magnetic minerals, which cause the anomaly amplitudes to vary as result of lithological changes, enabling mapping of the geology,
- (b) the *dipolar nature* of magnetic anomalies (positive and negative components) is related to the direction of magnetization in, as well as the attitude of, the causative rock formation. Analysis of anomaly form and study of the causative rocks provides information on (i) structure, (ii) amplitude, which together with structure, indicate the geometry of the body, and (iii) paleomagnetism,
- (c) the *wavelength* of the anomaly indicates the depth and geometry of a causative body, and
- (d) the *patterns or fabric* of magnetic anomalies as seen on contour maps and images indicate the disposition of the causative bodies, and enable the mapping of sub-outcrop geology and structural detail (Corner, 1994).

Some of the uses of the magnetic method are:

- (a) *geological mapping* – the direct location of specific rock types or mineral deposits either by virtue of their magnetic or non-magnetic responses, and
- (b) *identification of structures* – strike, dip, geometry, depth of burial, faults, shear zones, folds and lineaments (Corner, 1994).

In this study, the magnetic method was used to map the regional geology and to identify major structures in the E.P.O. area. The most obvious control on the distribution of mesothermal gold deposits is structure. Gold deposits are usually located in or adjacent to high-strain zones within or close to magnetic greenstone successions (Smith *et al.*, 1997). The main objective was to apply geological concepts for targeting structural settings favourable for gold mineralization.

Favourable structural settings include first-order transcrustal shear zones or faults and deformation zones (second- or lower-order structures). With respect to the first-order shear zones/faults, the structurally anomalous segments or deformation zones include (a) splays from the shear zone/fault, (b) pronounced inflections in the shear zone/fault, (c) intersections with other shear zones/faults, (d) imbricate splays at shear zone terminations, (e) *en echelon* segmentation and duplexes, and (f) folding within or adjacent to the shear zone (Campbell and Pitfield, 1994).

Other second-order targets are in specific lithologies and lithological contrasts in or adjacent to the first-order shear zones (Campbell and Pitfield, 1994). Some of these include:

- (a) If in a granitoid gneiss, proximity of the shear zone to the margin of a greenstone belt,
- (b) Proximity of the shear zone to the margin of a granitoid pluton within a greenstone belt,
- (c) Alternating felsic and greenstone lithologies and their contacts in particular, and
- (d) Evidence of alteration related to shear zones.

Targets with respect to folding include:

- (a) fold noses and associated axial shearing,
- (b) limb shearing and fold asymmetry,
- (c) associations of fold axes with syn-volcanic felsic intrusions,
- (d) folding of interbedded felsics, greenstones, or BIF, and
- (e) fold axial traces parallel to the nearby granitoid margins.

### RADIOMETRIC METHOD

The radiometric method is based on the detection and measurement of natural radioactivity, particularly gamma radiation, which comes from three naturally occurring radioactive elements (isotopes), namely potassium, uranium and thorium. Calibration procedures enable gamma-ray detectors to measure the concentrations of the three elements in the soil and rock in the field. The amounts of potassium, uranium and thorium present are usually proportional to the numbers of gamma rays detected (Richards, 1979). Gamma rays are a type of electromagnetic radiation and are commonly used in radiometric prospecting because of their great penetrative power. The energy of the gamma ray is characteristic of the isotope from which it originated. Measurements of the energies of the gamma rays emitted from a sample thus provide a method of identifying the isotopes present in the sample. This principle makes it possible to distinguish between potassium, uranium and thorium.

The energy of gamma radiation is measured in electron volts (eV). Prospecting instruments count the number of gamma rays detected over a pre-selected time interval and express this in counts per unit time, often counts per second (cps). Calibration is used to establish the proportionality between the instrument reading and the amount of K, U or Th present. It is conventional to express the uranium content as parts per million (ppm) or kilograms per tonne (kg/t) of uranium oxide (Richards, 1979). 1% = 10 kg/t and 1 kg/t = 1000 ppm.

The K channel monitors the 1.46 MeV gamma-rays emitted by  $^{40}\text{K}$ . Since  $^{40}\text{K}$  occurs as a fixed proportion of K in the natural environment, the gamma-ray flux from  $^{40}\text{K}$  can be used

to estimate the total amount of K present (Gunn *et al.*, 1997). Uranium occurs naturally as radioisotopes  $^{238}\text{U}$  and  $^{235}\text{U}$ , whilst thorium occurs as  $^{232}\text{Th}$ . Neither U nor Th emit gamma-rays, but gamma-ray emissions from their radioactive daughter products are used to estimate their concentrations. Gamma-ray emissions from  $^{214}\text{Bi}$  and  $^{208}\text{Tl}$  are used to estimate the concentration of U and Th respectively. Estimates of U and Th are usually reported as "equivalent uranium" and "equivalent thorium" (Gunn *et al.*, 1997).

In airborne surveys, the intensity of the radiation from the radioactive source decreases rapidly with the height of the observation point above the earth's surface (Parasnis, 1979). The effect is due, in part, to geometrical divergence and, in part, to absorption and scattering in the air. Spectrometers or scintillometers of the highest sensitivity are used in airborne work, and the flight heights are kept low (50–100 m). Very large crystal volumes are used in the sensor. Air attenuation limits the height to a maximum of ~150 m (Richards, 1979). The lower the terrain clearance, the greater the sensitivity of the system, but the narrower the field of view. Calibration and processing procedures have to be carried out to convert the airborne measurements to ground concentrations of potassium, uranium and thorium (Grasty *et al.*, 1997). On account of the shallow depths (generally 1 m or less) sensed by radioactivity, the method is often described as a technique for mapping soils, except where barren rock is exposed (Parasnis, 1979). However, the radiometric character of the parent rock is preserved in the overlying *in situ* soil (Gunn *et al.*, 1997; Richards, 1979; Parasnis, 1979). Therefore, it is possible to map lithologies and lithological contacts by airborne radioactivity measurements. Also, high-grade temperature and pressure metamorphism does not markedly affect the radiometric properties of rocks (Gunn *et al.*, 1997). Radiometric data are a useful guide to geological mapping in an area where metamorphic processes have obliterated the visual identification of lithologies.

Radiometric methods are able to detect directly, the presence of potassium, uranium and thorium, and can therefore be used to prospect for or to map the distribution of the three elements. The radiometric methods are also used in geological mapping (Richards, 1979; Parasnis, 1979; Grasty *et al.*, 1997; Gunn *et al.*, 1997; Jayawardhana and Sheard, 1997). Relative concentrations of K, U and Th tend to be fairly constant for a particular lithology in a particular area. It is therefore possible to distinguish certain lithologies on the basis of their radiometric responses. However, some rock types, such as granite, typically exhibit local variations in radioelement content. The method can also be used to map radioelement distribution within a particular lithology (Richards, 1979).

In this study, the radiometric method was used mainly to map potassium alteration associated with mineralization. Alteration associated with mineralization produces potassium anomalies that can be distinguished from normal lithologic potassium variation by characteristic low Th/K ratios (Shives *et al.*, 1997). The low Th/K ratios provide powerful guides to mineralization. Use of the radiometric method to determine concentrations of elemental potassium, regardless of the associated potassium mineral species, enables alteration mapping in a wide range of geological settings. In the granite-greenstone terrains of the cratons, potassium alteration in the form of sericite is proximal in many gold and VMS base metal deposits. K-feldspar alteration is usually a distal, regional alteration product at these deposits. The radiometric method was also used to map lithological contacts in some areas of the E.P.O.

#### **4.2. AIRBORNE SURVEYS**

The surveys were conducted using sensors suspended from a helicopter. Magnetic and radiometric sensors were used simultaneously, in order to achieve maximum cost-effectiveness. Traverses were flown across the generally NE-trending lithologies and fabric. A flight line trend of 135° (NW-SE) was used, taking 045° as the main strike direction (Tinnion, 1995). Flight line direction was taken perpendicular to geological strike in order that coverage of all horizons in a sequence was obtained. The traverse line spacing was 250 m. Diurnal drift (magnetic) was monitored by flying tie-lines, and minimizing the mismatches at the intersections of flight lines and tie-lines. Ground base-station magnetometers were used for the measurement of diurnal drift during the high-resolution surveys. The tie-line trend was 045°, orthogonal to the traverse line azimuth. The spacing of the tie-lines was 1250 m, giving a ratio of 5:1 with the traverse line spacing. The minimum traverse line length was 3000 m and the total traverse length was 2076 km. Sensor terrain clearances were approximately 50 m for magnetics and 80 m for radiometrics. For a terrain clearance of 80m (radiometric sensor), the effective instantaneous field of view was a ground circle of approximately 120m radius. Horizontal sample intervals were  $\leq 6$  metres for magnetic data and  $\leq 60$  metres for radiometric data.

A Scintrex H8 Caesium vapour magnetometer and a gamma ray spectrometer (Exploranium GR-820-3) are the instruments that were used. Thallium activated GPX NaI radiometric crystals were utilized in the sensor of the spectrometer. The radiometric crystal volumes were (a) 256 cubic inch (UP) and (b) 1024 cubic inch (DOWN). Flight path navigation and tracking was done using a Garmin GPS. Radar (Sperry 200) and barometric (AIR 3B) altimeters were utilized for the digital terrain model. The sensitivities

of the instruments were (a) 0.005 nT for the magnetometer, (b) ~1 metre for radar altimeter, and (c) ~1 metre for the barometric altimeter.

### 4.3 AEROMAGNETIC DATA

#### DATA PROCESSING

Preprocessing software was used to perform the following:

- (a) editing of magnetic data and removal of culturally induced spikes,
- (b) removal of observed diurnal magnetic variations from survey data,
- (c) optimization of the diurnal fit and *flight line levelling* – to reduce to a minimum, any differences between the field values at the points where flight lines intersect with tie-lines. These differences may arise from navigation errors, differences in height and heading errors,
- (d) *block levelling* – to reduce intensities to a common *epoch*, any mismatches between adjacent data sets. The mismatches may be due to secular variations of the earth's field or to changes in nominal survey height,
- (e) *noise editing* – a quality control measure to remove noise, such as a spike, a step, hash and drift,
- (f) *gridding* – of magnetic data employing a line gridding algorithm at 1:4 of line spacing cell size (Tinnion, 1995). A high data density exists along flight- and tie-lines with relatively very low density between the flight lines. The effect is that gridding algorithms are pushed to their limits to extrapolate as many points as possible between lines. The number that can be extrapolated is dependent on the flight line spacing and the wavelength of the recorded anomalies.

Total magnetic field data were further manipulated and image processed on an IBM PC compatible 486/50 M/Hz microcomputer using software from RTI-CAD Geopak programs and Geosoft Inc. of Toronto, Canada.

#### PRESENTATION

Total magnetic field data were presented mainly as images. Images are the most powerful for pattern recognition and transformations. The data were transformed to the Fourier domain and the following filter operations were applied: (a) X, Y and Z derivatives, (b) Upward continuation, (c) Reduction to the pole, and (d) Vertical integration.

Total magnetic field data were also presented as vertical gradient profiles along the flight lines. Profiles were useful for inspecting data quality, particularly at the time of surveying. The profiles are also valuable for interpreting geological sections.

Processed total magnetic field data were plotted on maps using the Universal Transverse Mercator (UTM) projection, zone 36, and a datum of Arc 1950.

### INTERPRETATION

In this study, only *qualitative interpretation* was carried out. The basis of qualitative interpretation is that the magnetic map or profile reflects the variation in magnetic mineral content of the underlying rocks (Corner, 1994). For a rock type or structural feature to be detectable, it must be associated with a change in bulk susceptibility or remanent magnetization. Qualitative interpretation entails the mapping or estimation of geological contacts, structural trends, shapes and areas of common signature. The interpretation was correlated with geological and structural data for Tokwe E.P.O., shown on Figure 3.0.

Figure 4.1 is a magnetic map of the study area. Total magnetic field data are presented as an image. The magnetic field intensity ranged from 29 880 to 30 496 nT. Lithological contacts are indicated by variations of anomaly amplitude as a function of changes in magnetic susceptibilities. Due to high magnetic mineral content, the mafic granulites, silicified mafic granulites, amphibolites, meta-andesites, migmatites, lherzolite, enderbites, magnetite-charnockite, dolerites and olivine-pyroxenite dykes appear as positive, short wavelength, high-amplitude magnetic zones (>30 200 nT). The magnetite-charnockite was distinguished from the other charnockites by its positive, high-amplitude magnetic signature. Metamorphosed greenstone belts, which are composed of mainly mafic granulites, silicified mafic granulites, amphibolites and meta-andesites, appear as zones of positive, high-amplitude magnetic signatures. The "greenstone belts" are Zvamapere, Ngundu, Area 1s and Area 4. Magnetic susceptibilities, measured by the author on outcrops of some of the lithologies, are shown on Table 4a. The measured magnetic susceptibility values were compared with expected ranges of values given by Berkman, 1976. In the rocks of positive, high amplitude magnetic response, the average magnetic susceptibilities ( $\times 10^6$  cgs units) ranged from 14.52 in the magnetite-charnockite to 694.07 in the basaltic granulite. The peak magnetic susceptibility was 1950, in basaltic granulite.

Banded chert + tuff, which is a meta-sediment in the Area 4 "greenstone belt", has a mean susceptibility of 2.54. The meta-sediment has fine-grained disseminated magnetite. Another meta-sediment in the "greenstone belt", the garnet-biotite gneiss, has a low, negative magnetic susceptibility of -0.26.

**Table 4a:** Magnetic Susceptibilities of some of the lithologies.

Lithology	Measured Magnetic Susceptibility – Max. ( $\times 10^6$ cgs units)	Measured Magnetic Susceptibility – Mean ( $\times 10^6$ cgs units)	Expected Magnetic Susceptibility ( $\times 10^6$ cgs units)
Basaltic granulite	1950	694.07	50 - 5800
Silicified basaltic granulite	88.1	71.35	
Basaltic amphibolite	95.4	84.7	30 - 110
Picritic rock	43.3	38.05	
Migmatite	67.3	53.93	10 - 1200
Enderbite	68.6	47.26	
Dolerite	78.2	59.04	30 - 4900
Magnetite-charnockite	23.8	14.52	
Banded chert and tuff	3.62	2.54	<10
Garnet-biotite gneiss	-0.10	-0.26	
Charnockite	7.62	5.20	<10 - 170
Proto-mylonite	0.86	-0.19	
Leuco-mylonite	-0.10	-0.75	

The charnockite, which contains varying amounts of disseminated magnetite, appears as low-amplitude zones with positive to negative magnetic response (30 140 - 30 200 nT). The average magnetic susceptibility measured in the charnockite is  $5.20 \times 10^6$  cgs units.

Proto-mylonites and leuco-mylonites show negative magnetic response. The magnetic field intensity is less than 30 140 nT. Mylonites in the major shear zones have the strongest negative magnetic anomalies (< 30 090 nT). The measured mean magnetic susceptibilities ( $\times 10^6$  cgs units) for proto-mylonites and mylonites are -0.19 and -0.75 respectively. The very low, negative magnetic susceptibilities are due to the alteration of magnetic minerals. The Mauch Shear Zone is the most prominent shear zone in the

study area. The shear zone, which follows the regional 060° trend, is located several hundreds of kilometres northeast and southwest of the E.P.O. Within the study area, the shear zone has a north-north-east (040°) trending splay shear. The shear zone is in contact with the Zvmapere "greenstone belt" in the southwest and the Area 4 "greenstone belt" in the northeast. In the north, a zone of low to negative magnetic response occurs on proto-mylonite and charnockite.

The metamorphic terrain displays a strong regional, semi-linear magnetic fabric controlled by structural deformation. The magnetic fabric is defined by high-frequency anomalies due to mafic granulites, ultramafic rocks and dolerites. The magnetic fabric follows a pronounced east-north-east (060°) regional trend, designated S1. Some of this fabric follows a north-north-east (040°) trend, designated S2. An east-west trending (S3) magnetic fabric is less common. Displacements on the magnetic fabrics mark southeast (S4) trending faults and shears.

The magnetic map also shows the major fold structures in the study area. Some of the mafic granulites, enderbites, greenstone belts and proto-mylonites are folded. The Zvmapere "greenstone belt" and Shehudo enderbite bodies show tight folding. Proto-mylonites and mafic granulites in the Area 1s "greenstone belt" show gentle, open folding.

#### EXPLORATION TARGET SYNTHESIS

Exploration targets were selected using shear zones and "greenstone belts" indicated by magnetic data. In the Archaean cratons of Zimbabwe, Australia and Canada, structure is the most important control on mesothermal gold mineralization (Campbell and Pitfield, 1994; Groves *et al.*, 1989; Hodgson, 1989). The spatial distribution of gold deposits is controlled by second-order kilometre-scale faults/shears linked to first-order, deep-seated crustal-scale shear zones. Transcrustal shear zones provide the first-order control on gold mineralization. Second- and higher-order faults/shears form deformation zones, which are favourable structural settings for gold mineralization. These geological concepts were applied to the magnetic map, to synthesize targets for gold exploration.

In the study area, the Mauch Shear Zone is a regional transcrustal, first-order structure. Second- or lower-order shear zones, on or close to the Mauch Shear Zone, are likely to form deformation or dilation zones. Such dilation zones should be within "greenstone belts" or in granitoids close to "greenstone belts" in contact with the first-order shear zone (Campbell and Pitfield, 1994). Greenstone belts are believed to be the source of some of

the gold. In the folded "greenstone belts", axial shearing, limb shearing and fold noses are favourable sites for mineralization. The selected target areas are shown on Figure 4.1.

#### Target A

The structural setting on Target A comprises the first-order, sinistral, transcrustal Mauch Shear Zone and its sinistral, second-order splay. The shear zones trend on 060° and 040° respectively. In the 20° acute angle between the two shear zones, there is a "greenstone belt". The "greenstone belt" is in contact with both shear zones.

In the acute angle, dilation is likely to occur due to convergence of the two sinistral shear zones. The deformation zone is favourable for the development of higher-order shear zones with gold mineralization. The ore fluids and gold can be mantle-derived and/or produced by metamorphic devolatilization of the "greenstone belt".

#### Target B

In Target B, the first-order, transcrustal Mauch Shear Zone appears to have a flexure or an offset on the magnetic map. On the ground, the flexure or offset is due to an intersection with a dextral, east-west (085° - 090°) shear zone. A folded "greenstone belt" (Zvamapere) is close to the intersection of the two shear zones. The nose and northern limb of the fold are in contact with the Mauch Shear Zone.

The intersection of the sinistral Mauch shear Zone and a dextral east-west shear zone could have resulted in dilation due to bulk, inhomogeneous shortening (Hodgson, 1989). Lower-order shears with gold mineralization may have developed in the deformation zone. Ore fluids and gold can be produced by mantle degassing or metamorphic devolatilization of the "greenstone belt".

### 4.4 RADIOMETRIC DATA

#### DATA PROCESSING

- (a) **Dead Time Correction:** during the time that the spectrometer is processing a pulse, it is unable to detect any other pulses that arrive at the detector. The instrument dead time, which is normally <5µs/count, is quoted by the manufacturer. The dead time correction was carried out using a formula in the pre-processing software.
  
- (b) **Background determination:** two types of background radiation were determined and subtracted from the radiometric data:

(i) absolute background, which is the countrate measured in the absence of radiation from the ground. The countrate is a result of the radioactivity of the aircraft and its equipment, high-energy cosmic ray particles that interact with the air, the aircraft and the detector, airborne dust, and radon decay products in the atmosphere. The absolute background was determined over a large body of water, as water itself is non-radioactive and since 1.5 m of water can effectively shield the instrument from any ground radiation;

(ii) relative (or "geological") background, to establish the normal amount of radioactivity for a rock type in order that anomalous amounts can be recognized. The normal radiation level was measured at some arbitrary base in the survey area. All measurements were made relative to the base value and survey measurements corrected to the relative background gave the contrast in composition between the field point and the base station.

The background values were later converted to equivalent concentrations using calibration constants.

(c) **Compton stripping:** a channel interaction correction (stripping) for (i) Compton scatter of gamma rays, and (ii) for overlapping energy peaks. Pad calibration was carried out to determine stripping ratios. The stripping ratios are similar to calibration constants for 3-channel airborne spectrometers except that they are not expressed in cps per unit concentration, but cps per unit count due to a particular element. After stripping, the recorded countrates are such that a thorium anomaly is characterized by a response above background in the thorium channel only.

(d) **Levelling:** to reduce to a minimum, any differences between the countrates at the point where flight lines and tie-lines intersect. The differences can be due to navigation errors, differences in height and heading errors.

(e) **Height correction:** The height attenuation coefficient for each channel and the sensitivity coefficients were calculated for the nominal survey altitude of the helicopter system. The measurements were achieved by hovering at different heights over a fixed location where the airborne system was viewing a limited small sampling area on the ground. The selected small sampling area had uniform radioelement concentrations.

- (f) **Conversion of spectrometer readings to equivalent ground concentrations:** counts corrected for (a)-(e) above were converted to equivalent ground concentrations using calibration graphs or constants. Conversions were carried out using pre-processing software on a digital computer. The equivalent ground concentrations were expressed as K (%), U (ppm) and Th (ppm).
- (g) **Gridding:** the radiometric data were further manipulated and image processed on an IBM PC compatible 486/50 M/Hz microcomputer using software from RTI-CAD Geopak programs and Geosoft Inc. of Toronto, Canada. The final maps were produced in UTM projection, zone 36, using Arc 1950 map datum.

### PRESENTATION

The radiometric data, which can be regarded as geochemical data, were presented on maps as colour images. The colour images were for (a) potassium data, (b) thorium data, and (c) uranium data.

The radiometric data were also presented as ratio maps, which are a popular aid to interpretation. Ratios of radiometric data were calculated as their results are less affected by source geometry and surface variability than are the individual element data (Tinnion, 1995). Taking ratios of countrates above background enables change from three independent variables (K, Th, and U) to two dependent variables (the ratios). The (Th/K) ratio is calculated as:  $Th/U \times U/K = Th/K$ . In this study, only the Th/K ratio was used.

### INTERPRETATION

The low effective penetration ( $\leq 100$  cm) of the radiometric method implies that the instrument can detect only the surface radiometric character of the earth (mainly weathered material). However, the weathered surface material commonly retains the radiometric character of the parent material underneath (Richards, 1979). A continuous cover of more than 100 cm-thick transported, non-local material effectively masks the radioactivity arising from underlying rocks. Gamma-ray spectrometric response of unweathered, exposed bedrock reflects the constituent concentrations of K, Th and U in the parent rock.

Potassium is a common element comprising about 2% of the earth's crust (Gunn *et al.*, 1997). The main potassium response arises from potassic feldspars and micas. The percentage of K is generally high in acid felsic rocks and low in mafic rocks. Potassium does not occur in all mafic rocks. Uranium has an average concentration of 2.5 ppm in

the earth's crust (Gunn *et al.*, 1997). It occurs as U oxide and silicate minerals, such as zircon. Uranium minerals tend to be present in pegmatites, syenites, carbonatites, granites and some shales. Th is a minor constituent of the earth's crust with a concentration of approximately 9 ppm (Gunn *et al.*, 1997). Thorium occurs in allanite, monazite, xenotime and zircon, and as trace elements in other rock-forming minerals. The U and Th concentrations in igneous rocks generally increase as the K and silica content of the rocks increase (Gunn *et al.*, 1997).

Basic and ultrabasic rocks such as basalts, gabbros and serpentinites, have very low radioelement concentrations and give very low radiometric responses (Richards, 1979). Intermediate rocks (andesites and diorites) and acid-intermediate tuffs and agglomerates, contain small but appreciable radioelement concentrations. The intermediate and acid rocks are regarded as possible source rocks for the uranium found as secondary deposits in sedimentary rocks. Acid rocks such as granites, syenites, alkali rocks and pegmatites commonly give high responses from all three radioelements.

Sedimentary rocks normally have quite low radioelement concentrations and low, but often recognizable radiometric responses (Richards, 1979). Exceptions include dark shales, which are frequently enriched in U, and immature feldspathic sandstones, which usually give a K anomaly. Immature sediments such as arkoses, greywackes and shales have radioelement concentrations similar to those of their source rocks (Gunn *et al.*, 1997). Uranium is more mobile under low temperature oxidizing conditions than potassium or thorium. Mature sediments such as quartzites tend to have elevated Th compositions. Limestones may be relatively enriched in uranium.

Metamorphic rocks give variable responses depending particularly on the original composition of the rock before metamorphism.

#### Statistics of Radiometric Data

The statistical analyses of the individual element and ratio data are listed on Table 4b.

**Table 4b.** Statistics of radiometric data.

ELEMENT	MIN.	MAX.	MEAN	Std. Dev.
Potassium	0	4.6	1.7	0.7 %
Thorium	1.3	154.8	24.7	10.9 ppm
Uranium	0	11.9	2.8	1.1 ppm
Th/K	1.2	394	18.5	10.1 ( $\times 10^{-4}$ )

### Potassium Data

The potassium data are plotted on Figure 4.2. The K values range from 0 to 4.6% converted and estimated ground concentrations. The mean and standard deviation values are 1.7% and 0.7% respectively. Using the *mean + 2 standard deviations* formula for threshold estimation (Sinclair, 1991), the upper limit of the background values is 3.1%.

Anomalous concentrations of potassium occur on K-feldspar granite and some of the charnockites, leuco-mylonites and proto-mylonites. The largest zone of anomalous potassium concentrations occurs in the southwest part of the E.P.O. Mafic granulites, silicified mafic granulites, meta-andesites, ultramafic dykes, dolerite dykes and enderbites have low concentrations (<1.2 %) of potassium. The Ngundu, Zvamapere, Area 1s and Area 4 "greenstone belts" appear as zones of low K concentrations. The potassium map (Figure 4.2) also shows the Ngundu "greenstone belt" fold structure and open folds on and south of Area 1s "greenstone belt". The southeast-trending Tokwe Fault/Shear and other fractures can also be inferred on the map.

### *Target synthesis*

Target areas A and B (Figure 4.2) are located on zones of high K and low Th concentrations (also see Figure 4.5). These areas of very low Th/K ratios are zones of potassium alteration. Potassium alteration associated with mineralization can be distinguished from normal lithologic potassium variation by characteristic low Th/K ratios (Shives *et al.*, 1997). As thorium does not accompany potassium enrichment during hydrothermal processes, Th/K ratios provide excellent identification of potassium anomalies associated with alteration. The minimum Th/K ratio value is  $1.2 \times 10^{-4}$ . Generally, a strong potassium alteration anomaly is characterized by Th/K ratio values of less than  $2.5 \times 10^{-4}$  (Shives *et al.*, 1997). Unaltered lithologies typically reflect the normal ratio of crustal abundance of K and Th, of approximately  $5 \times 10^{-4}$ .

### Thorium Data

The thorium data are plotted on Figure 4.3. Thorium values range from 1.3 to 154.8 ppm equivalent ground concentrations. The mean and standard deviations are 24.7 and 10.9 ppm respectively. A threshold value of 46.5 ppm is estimated. Anomalous concentrations Th concentrations occur in some parts of the felsic and intermediate rocks, such as charnockite, magnetite-charnockite, proto-mylonite and enderbite. Some of the mafic rocks and "greenstone belts" such as Ngundu have low Th concentrations (<22 ppm). The Th map shows the Ngundu "greenstone belt" fold structure and the gentle, open

folds of rocks in the southern part of the E.P.O. The map also shows the southeast-trending Tokwe Fault/Shear and other fractures.

#### *Target Synthesis*

Areas with low Th and high K concentrations are of interest as they are zones of potassium alteration associated with mineralization (Shives *et al.*, 1997). Zones and "bull's eyes" associated with very low Th/K ratios ( $<2.5 \times 10^{-4}$ ) are shown on Figure 4.5. Exploration targets A and B (Figure 4.3) were selected on the basis of having very low Th/K ratios.

#### Uranium Data

The uranium data are plotted on Figure 4.4. The values range from 0 to 11.9 ppm equivalent ground concentration. The mean and standard deviation were 2.8 and 1.1 ppm respectively. A threshold value of 5.0 ppm is estimated.

The majority of anomalous values occur on proto-mylonites. Some parts of charnockites and migmatites also have anomalous values. The map shows open folding of the proto-mylonites in the southern part of the E.P.O. The mafic granulites, meta-andesites, enderbites and dolerite dykes generally have low uranium concentrations ( $<2.7$  ppm).

### **4.5 CONCLUSIONS**

The magnetic method was successful in delineating major shear zones, which appear as zones of strong, negative magnetic response. The method mapped the transcrustal, first-order, sinistral Mauch Shear Zone, its sinistral splay shear zone and an intersecting dextral shear zone. Exploration targets A and B (see Figure 4.6) were selected where the Mauch Shear Zone interferes with the splay and the dextral shear zone respectively. In Area A, the convergence of the splay and the transcrustal shear zone is likely to have resulted in dilation in the  $20^\circ$  acute angle between the two shears. In Area B, the intersection of the Mauch Shear Zone and an east-west shear zone is also likely to have resulted in dilation as a consequence of bulk, inhomogeneous shortening (Hodgson, 1989). The dilation or deformation zones are structural settings favourable for gold mineralization.

The magnetic method also delineated metamorphosed greenstone belts, which are some of the positive, high amplitude anomalies. The "greenstone belts" are some of the possible sources of metamorphic ore fluids and gold that become available to the first-order shear zone in contact with them (Campbell and Pitfield, 1994; Groves *et al.*, 1989).

Due to its transcrustal nature, the Mauch Shear Zone is deep seated and provides a first-order control on magmatic and metamorphic ore fluids. In Area A, a "greenstone belt" is situated in the deformation zone, and is in contact with both the Mauch Shear Zone and the splay shear (see Figure 4.6). In Area B, a folded "greenstone belt" is in contact with the Mauch Shear Zone, and the intersection of the east-west shear zone is close to the fold nose.

The radiometric data were used to map areas with potassium alteration (see Figure 4.6). Alteration associated with mineralization produces potassium anomalies that can be distinguished from normal lithologic potassium variation by characteristic low Th/K ratios (Shives *et al.*, 1997). The low Th/K ratios are typically  $<2.5 \times 10^{-4}$ , with a minimum of  $1.2 \times 10^{-4}$ . On Figure 4.6, zones and "bull's eyes" of the low Th/K ratios also plot in target areas A and B. The K alteration compliments geological and magnetic data, which mapped the structural settings and "greenstone belts" in the target areas. The K data also mapped "greenstone belts" as some of the zones with low K concentration ( $<1.2\%$ ).

Further investigations for gold mineralization were recommended in Targets A and B. Drainage and soil sampling methods were used in the follow-up work.

## CHAPTER 5

### DRAINAGE GEOCHEMISTRY

#### 5.1 INTRODUCTION

Drainage sampling was conducted during the early stages of the exploration program in Tokwe E.P.O. The sampling was carried out in three sequential phases, which were (a) orientation sampling, (b) first-pass sampling, and (c) second-pass sampling. Stream sediment samples were collected from selected trap sites in the streams and rivers.

The aim of the drainage sampling exercise was to investigate for gold mineralization upstream of the stream sediment sample positions. A stream sediment sample represents a composite of the geology and mineralisation of the catchment upstream of the sample site. Drainage geochemistry is a potentially valuable technique for low cost reconnaissance of large areas for gold mineralization. In all the three phases, drainage samples were sieved and analyzed for gold using the fire assay + AAS method (Appendix B). During orientation survey, samples were sieved to four size fractions, which are  $-425+180\mu$ ,  $-180+125\mu$ ,  $-125+75\mu$ , and  $-75\mu$ . First-pass and second-pass samples were sieved to  $-75\mu$ .

Also, during the first-pass sampling-phase only, the coarser size fraction ( $-2000+425\mu$ ) was used to investigate for kimberlite or diamond indicator minerals. Pyrope garnet, microilmelite, diopside, chrome diopside, chrome spinel, phlogopite, forsterite olivine, enstatite/bronzite, potassic richterite, magnesio katophorite, priderite and diamond, are the indicator minerals (Muggeridge, 1985). During the period that gold exploration was in progress in Tokwe E.P.O., several other mining companies were involved in diamond exploration throughout Zimbabwe, hence it was decided to investigate if the Tokwe area had any kimberlites or other host rocks for diamonds.

The terrain in Tokwe E.P.O. area is generally hilly and well drained by streams and rivers. The topography is well dissected with a good drainage network. Topography influences the quality of the stream sediments by increasing concentration levels and variability in a rugged as compared to subdued terrain (Mazzucchelli, 1987). In a rugged topography, the trap site efficiency is increased due to local variations in the streambed. The drainage sampling method was found to be suitable for the exploration program due to the rugged nature and good drainage characteristics of the topography.

## **5.2 ORIENTATION DRAINAGE SAMPLING**

Orientation drainage sampling was the first phase of stream sediment sampling. The objectives of the orientation sampling were to examine the nature of trap sites and their gravels, and to determine the most suitable sample size fraction (mesh size) to be used in the drainage sampling of the entire E.P.O. area. In the study, four different screen aperture sizes were used for sieving the orientation drainage samples. The aperture sizes used were 425 $\mu$ , 180 $\mu$ , 125 $\mu$  and 75 $\mu$ . These aperture sizes were chosen because Rio Tinto Zimbabwe had used them successfully in other orientation surveys in various regions of the country. Sieving through these screen sizes produces –425+180 $\mu$ , -180+125 $\mu$ , -125+75 $\mu$ , and –75 $\mu$  size fractions.

The orientation sampling was carried out in Area 4 in the E.P.O. (see Figure 5.6). The area was selected for the orientation drainage sampling because it is located in a structural setting favourable for mesothermal gold mineralization (Target A, Chapter 4). The area lies in an acute angle (20°) between the sinistral Mauch Shear Zone trending on 060° and a sinistral splay shear zone trending on 040°. Convergence of the two shear zones is likely to have resulted in dilation or deformation, which is conducive to mineralization. The target area, which is in a “greenstone belt”, was regarded to be the most prospective to host gold mineralization in Tokwe E.P.O. The structural aspects are discussed in Chapter 3 and Chapter 4.

### **Drainage Sampling**

Orientation drainage samples were obtained from eight separate sites (CD4/1-8) within an area of approximately 3 km<sup>2</sup>. Sample locations are shown on Figure 5.1. The position of each sample site was determined accurately with the use of a GPS instrument set to Arc 1950 Map Datum. Universal Transverse Mercator (UTM) coordinates were used for plotting on topographic maps and for Auto CAD draughting.

At each sampling site, the sample was obtained from a trap site in the stream or river. According to Muggeridge (1995), a trap site is where as much heavy mineral material as possible has accumulated. Heavy minerals are generally classified as those with specific gravities greater than those of quartz and feldspar. The heavy minerals concentrate where gravels have been deposited on the streambeds, particularly where the gravels are trapped amongst large boulders and bedrock projections, or in depressions or cavities such as potholes and crevices. Rapids, pegmatites and dykes across the streams and rivers, also form trap sites. Gold, with a specific gravity of 15.0–19.3 (Berkman, 1976), is a heavy mineral that can be accumulated at a trap site. Other heavy

minerals, such as magnetite, pyrope garnet, picroilmenite, chrome diopside, diopside, forsteritic olivine and diamond, which are indicator minerals for kimberlite, can also accumulate at a trap site. These heavy minerals have specific gravities  $>2.95$ .

At the trap site, stream sediment material was excavated on the main channel of the stream or river. The main channel is the deepest part of the river and may have increased heavy mineral concentration potential due to its constricted width (Muggeridge, 1986). Heavier minerals are relatively prominent in the deeper parts of the riverbed, owing to natural jiggling and sagging processes operating in the lower precincts of the river flow regime. The sampling site was therefore, located on the main channel, which is the most active flow channel and the most conducive to heavy mineral concentration.

At the sampling location, the excavation was carried out either upstream or downstream of the obstacle forming the trap site. The stream sediment was excavated to reach the bedrock. Major heavy mineral sorting and concentration processes occur on the riverbed rather than higher up in the flow (Muggeridge, 1986). The gravel immediately overlying the bedrock was sampled. A shovel, domestic "dustpans", small garden shovels and brushes, were used to "sweep clean" the bedrock base to recover the fine particles lodged in small cracks and hollows.

Characteristics of the sampled gravel varied from one trap site to another. A gravel bed, which is clast-supported, poorly sorted and tightly packed, was considered to have the best potential for concentrating heavy minerals. Muggeridge (1986) emphasized that these characteristics are essential for a gravel to concentrate heavy minerals. Such a framework of coarser, light pebbles or boulders provides an environment conducive to interstice entrapment of heavy minerals. This concept is also mentioned by Minter and Toens (1970), who carried out flume experiments using gravels similar to those of the gold-bearing bankets of the Witwatersrand System. Minter and Toens (1970) mention that the size distribution of the particles comprising these conglomerates is bimodal and that the detrital heavy minerals are hydraulically equivalent in size to the sand-sized mode.

The high density of pebble packing in these conglomerates indicates that they were open-work gravels that were subsequently filled with sand and heavy minerals. The conglomerates, which contain detrital gold in the matrix, are supposed to have entrapped the gold particles mechanically. The heavy minerals are in hydraulic equilibrium with the finer-grained mode (matrix) which is presumed to have settled into the pebble-supported

conglomerates. Auriferous sand thus entrapped in the interstices of a gravel bed, is preserved against removal by water, provided that the water velocity is insufficient to move the pebbles.

The flume experiments indicated that gravel beds thinner than one and a half pebble diameters, accumulated fine-grained sediment much more slowly than thicker gravel beds. During the experiments, there was a conspicuous drop in trapping efficiency when small pebbles were used, because the matrix clogged the interstices as it was too coarse in relation to the pore spaces, which are controlled by pebble size. Another observation from the experiments was that the gravel layers are normally filled by matrix from the base upwards. The proportion of pebbles to the finer fraction should be high (clast supported) for the gravel bed to be a potential trap for heavy minerals. In the Kimberley Reef conglomerate it was demonstrated by point counting, that there is very little gold if the pebbles are less than 45% of the conglomerate.

During the sampling, the quality of trap sites was classified into standard categories. Figure 5.2 (adapted from Muggerridge, 1986) shows how the trap sites are divided into 5 classes, ranging from a top rating *good* (class 5), to the lowest rating *poor* (class 1). A good site has tightly packed and poorly sorted gravel with boulders. The gravel is trapped against a rock bar, or in a pothole, depression or crevice in bedrock in the main river channel. Sites that occur in exposed bedrock environments, but fall somewhat short of one or two of the criteria listed above, may be classified as *moderate to good* (class 4). A *moderate* (class 3) site may have slightly loose to tight packing, with gravel trapped amongst boulders, or a shallow type of bedrock trap. If the trap itself is good, but the material is sorted to some extent, or lacks boulder size material, then this rating may also be appropriate. It is not necessary for the bedrock to be present in this category.

The sites described by classes 3 to 5 all contain clast-supported material. Sites in the lower classes 1 and 2 contain matrix-supported material. A *poor to moderate* (class 2) site has very little gravel present and may occur where a thin veneer of small pebbles lies loosely on the surface. A *poor* site (class 1) may have a fine gravel (small pebbles and granules) deposit in an unconfined setting and the chance of having entrapped heavy minerals is very low. The 8 sites sampled in the orientation survey were rated from class 3 to class 4.

The sampling was conducted soon after the rainy season, when the trap sites were exposed and there was adequate water for sieving. The sampled gravels were wet

sieved to -2000 $\mu$  size fraction. After sampling and sieving at each site, all the tools were cleaned thoroughly before sampling the next site, to avoid contamination. After screening to -2000 $\mu$  size fraction, the mass of each sample was at least 40 kg. Muggeridge (1995) states that the recommended stream sediment sample size is > 40 kg, after screening around 1000 - 2000 $\mu$  to remove coarser material unlikely to contain heavy minerals.

### **Sample Preparation**

Each of the eight orientation stream sediment samples (-2000 $\mu$  size fraction) was sieved to -425 $\mu$  size fraction to further remove coarse material. The size fraction between 425 $\mu$  and 2000 $\mu$  was not used in this orientation survey, but was used on first-pass samples to investigate for kimberlite indicator minerals. The -425 $\mu$  size fraction was subsequently sieved to -180 $\mu$ , -125 $\mu$  and -75 $\mu$ . The sieves and their respective trays were cleaned thoroughly after sieving every sample, to avoid contamination of the next sample to be screened. Ultimately, each of the eight orientation samples had four resultant samples representing the four size fractions (-425+180 $\mu$ , -180+125 $\mu$ , -125+75 $\mu$  and -75 $\mu$ ) as shown on Figure 5.1. The mass of each sub-sample was >100g. Each of the four sub-samples, from the original orientation samples, was allocated a unique assay number. At the laboratory, 50g were split from every sub-sample, for assay. The 32 sub-samples were analyzed for gold using the fire assay + AAS method (Appendix B).

The assay values were expected to indicate the best or the most suitable size fraction to be used during the subsequent drainage sampling of the entire E.P.O. area. The most suitable size fraction would be the one that consistently yields the highest gold values.

### **Assay Results, Discussions, Conclusions and Recommendations**

Fire assay gold values for the 32 sub-samples, are tabulated on Figure 5.1 and shown as bar graphs on Figure 5.3. The lowest recorded value was 10 ppb Au, and the peak value was 230 ppb Au. Gold concentration at site CD4/5 was very low, as all the 4 sub-samples (all the size fractions) from it assayed 20 ppb Au.

The peak value of 230 ppb Au was in the -75 $\mu$  size fraction of sample CD4/2. From the same sample (CD4/ 2), the -125+75 $\mu$  size fraction assayed 70 ppb Au, the -180+125 $\mu$  size fraction assayed 40 ppb Au, and the -425+180 $\mu$  size fraction assayed 20 ppb Au. These assay values for the 4 sub-samples of CD4/2, tend to suggest that the detected gold concentration increases with decreasing aperture size (size fraction). A similar trend of gold concentration is shown by the sub-samples of sample CD4/7, where the highest value of 90 ppb Au was detected in the -75 $\mu$  size fraction. Also in sample CD4/1, the

highest gold value was in the  $-75\mu$  size fraction. Therefore, in three (37.5%) of the eight sampled sites, the  $-75\mu$  size fraction yielded the highest gold concentration, as well as the overall peak value of 230 ppb Au considering all the eight samples.

In three samples, CD4/3, CD4/6 and CD4/8, the highest gold concentrations were detected in the  $-125+75\mu$  size fractions. The highest gold value in these samples was 110 ppb Au, in the  $-125+75\mu$  size fraction from sample CD4/6. This highest value for the  $-125+75\mu$  size fraction is far less (less than half) than the peak value of 230 ppb Au detected in the  $-75\mu$  size fraction. Three (37.5%) of the eight orientation samples, had their peak values in the  $-125+75\mu$  size fraction. This proportion is same as for the samples with their highest value in the  $-75\mu$  size fraction. Since the  $-75\mu$  size fraction yielded the peak gold value, it is a better size fraction than the  $-125+75\mu$  fraction. The  $-75\mu$  and  $-125+75\mu$  size fractions, which were the two smallest size fractions, together yielded the elevated and better gold concentrations. These sub-samples that yielded elevated gold values, were from six (75%) of the eight original orientation samples. The total gold content, detected in each size fraction of the eight samples together, was also expressed as a percentage of the total gold content in the 32 sub-samples and plotted as a pie chart (Figure 5.4 and as bar graphs (Figure 5.5). Both illustrations show that the  $-75\mu$  size fraction yielded the highest gold concentration (37.2 % of the total gold content), followed by the  $-125+75\mu$  fraction (29.6 %).

It was recommended that the  $-75\mu$  size fraction should be used in the subsequent first-pass, reconnaissance drainage sampling in the entire E.P.O. area. The  $-75\mu$  size fraction was found to be the best, since it yielded the peak value of 230 ppb Au and the highest percentage of the total gold content.

Mazzucchelli, (1987) recommends the use of the finest practicable size fraction (usually the -200# or  $-75\mu$ m fraction) in stream sediment surveys for gold. The nugget effect is substantially reduced, by excluding coarse gold particles, from the sample taken for analysis. The fine gold retained has the potential to recognize anomalies missed by earlier prospectors who panned and recovered only coarse gold ( $>50\mu$ m). The  $-75\mu$  size fraction has favourable costs for both field and laboratory work.

One of the eight orientation samples, CD4/4, had its highest gold value (80 ppb Au) detected in the  $-425+180\mu$  size fraction. The second highest gold value (70 ppb Au) was detected in the  $-75\mu$  size fraction. This is just one sample representing 12.5% of the eight original samples.

### 5.3 **FIRST-PASS DRAINAGE SAMPLING**

First-pass, reconnaissance drainage sampling was carried out in the entire area of Tokwe E.P.O. The total number of samples collected was 121. The sample sites were spaced at an average density of 1 site per 4 km<sup>2</sup>. This density was chosen because it had successfully located anomalies in previous reconnaissance drainage sampling surveys in other regions of the country. Levinson (1974) states that stream sediments collected at a density of 1 sample per 1-5 square miles are the mostly used geochemical reconnaissance technique, where the objective is to locate specific areas of interest. Rose *et al.* (1979) recommend that, for reconnaissance drainage sampling, the spacing should be 1 or 2 samples collected per 10 km<sup>2</sup>. Figure 5.6 shows the sample positions.

The main objective of the first-pass drainage sampling exercise was to investigate for gold mineralization in the areas upstream of the sample sites.

#### **Drainage Sampling**

Drainage sampling was carried out in the manner described under section 5.1 above. Sampling was conducted in trap sites at selected positions on the streams and rivers. The sample sites were on streams or rivers draining from within the Tokwe E.P.O. area. Large rivers such as the Tokwe River, draining from outside the area, were not sampled, but their tributaries draining from within the area were sampled. Sample sites were located upstream and close to a confluence of streams. The first-pass sampling was conducted in the dry season, soon after the rainy season, when the trap sites were exposed and there was enough water for wet sieving.

The sampling was carried out on the main, active channel of the stream or river, as discussed under section 5.1. Where possible, the stream sediment was excavated down to reach the bedrock. The gravel bed, immediately overlying the bedrock, was sampled. The sample material was sought from good gravels. Good gravels were those that were poorly sorted, clast supported and tightly packed. The quality of the trap sites was rated using the system described under section 5.1. Most of the 121 trap sites were in classes 3 (*moderate*) to 5 (*good*). At each sampling site, the sampled gravel was wet sieved to <math>-2000\mu</math> size fraction. The minimum mass of the screened sample was 40 kg.

### **Sample Preparation**

The first-pass drainage samples (-2000 $\mu$  size fraction) were dry screened, using the 425 $\mu$  sieves, to produce two sub - samples, (a) - 2000+425 $\mu$  size fraction, and (b) -425 $\mu$  size fraction. The -2000+425 $\mu$  sub-sample was used to investigate for kimberlite and diamond indicator minerals. The -425 $\mu$  sub-sample was further screened and used for gold assays. The minimum grain size of 425 $\mu$  for the coarser sub-sample, was above the minimum practical cut-off grain size of 300 $\mu$ . The cut-off grain size of 300 $\mu$  is recommended in Muggeridge (1995).

The -2000+425 $\mu$  sub-samples were mechanically jigged to isolate and concentrate heavy minerals. The heavy mineral concentrates produced by jigging were concentrated further by immersion in tetrabromoethane (TBE) with a specific gravity of 2.95. The heavy minerals, with specific gravities >2.95, sank into the TBE, and were collected for mineralogical studies. The heavy mineral grains were passed through an electromagnetic separator, to remove magnetite grains. The remaining heavy minerals were observed microscopically for kimberlite or diamond indicator minerals. None of the 121 drainage samples had the kimberlite or diamond indicator minerals. However, coarse gold grains were observed in some of the samples from Areas 2s, 1s and 6, which also had geochemical drainage anomalies.

The -425 $\mu$  sub-samples were screened further to -75 $\mu$  size fraction. The -75 $\mu$  size fraction sub-samples were used for gold analysis using the fire assay + AAS method (Appendix B). From each sub-sample, 50g was split and used for the assay.

### **Assay Results, Discussions and Recommendations**

Assay values are plotted as proportional symbols on Figure 5.6. The lowest recorded value was 2 ppb Au and the peak value was 1214 ppb Au detected in a sample from Area 4B.

Figure 5.7 is a histogram of the gold values, which shows a log-normal distribution with, leptokurtic strong positive skewness and a mode (76.86% of values) in the 0-9 ppb Au class. The background population has a peak value in the 20-29 ppb Au class. There are no values in the 30-39 ppb Au class. Values of 40 ppb Au and above, form several, discontinuous and smaller populations that are anomalous. Figure 5.8 is a log-probability plot of the gold values, which indicates a threshold value of 75 ppb Au.

Gold concentrations between 40 and 75 ppb, occur in Zvamapere and Area 1s "greenstone belts" only. Values above the 75 ppb Au threshold indicated by the log-probability plot, define several drainage anomalies in the E.P.O. area (see Figure 5.6). A strong drainage anomaly, with a peak of 1214 ppb Au, lies in Area 4 and 4B in the central part of the E.P.O. area. Another strong anomaly, with a peak of 741 ppb Au, lies in Area 2s towards the south-western boundary of the E.P.O. area. Area 1s has a fairly significant anomaly with a peak value of 217 ppb Au. Area 6 has a small drainage anomaly with a peak value of 207 ppb Au.

A decision was made to carry out follow-up (second-pass) drainage sampling on areas 2s, 4 + 4B, 1s and 6. Second-pass drainage sampling was not planned for Zvamapere Area, because the anomaly was believed to be due to a well exposed gossan on a "greenstone belt" in that area. The second-pass sampling was planned to check the reproducibility of the original anomalies and to locate the approximate positions of the source mineralization.

#### **5.4 SECOND-PASS DRAINAGE SAMPLING**

Second-pass drainage sampling was carried out on areas 2s, 1s, 4 + 4B and 6. The exercise was conducted as a follow-up on the drainage anomalies indicated by first-pass sampling. The river courses and their tributaries, upstream of first-pass anomaly sites, were sampled. Most or all of the tributaries were sampled, depending on the presence of trap sites. The sample density was very high, depending on the network of streams and their tributaries. The high sampling density was necessary to maximize the length of the anomalous dispersion train and to facilitate for a regular concentration gradient with distance from the source mineralization. During the second-pass sampling, the total number of samples collected was 221.

The objectives of the second-pass drainage sampling were to check the reproducibility of the first-pass anomalies, and to locate the approximate positions of the source mineralisations. The follow-up drainage sampling was expected to reveal vectors towards mineralization.

##### **Drainage Sampling**

Drainage sampling was conducted in trap sites as described under section 5.1. In the selected areas, the quality of trap sites varied from class 1 (*poor*) to class 5 (*good*), since almost all the streams and tributaries were sampled. However, the majority of the trap

sites were in the range of class 3 (*moderate*) to class 4 (*moderate to good*). The sample positions and numbers are shown on Figure 5.9.

The sampled stream bed gravels were wet sieved to  $-2000\mu$  size fraction. The minimum mass of each sample after screening was 40 kg.

### **Sample Preparation and Processing**

All the 221 second-pass drainage samples ( $-2000\mu$  size fraction) were panned to concentrate heavy minerals, including gold. Since the panning method requires a substantial amount of skill, a well-trained and experienced crew conducted the exercise. In panning, heavy mineral concentration of the sample is achieved by manual swirling or rotating or rocking action on the pan to get the lighter material into suspension, and the heavier grains remaining at the base of the pan. The top layer of light material is periodically scooped off, and the process repeated until a concentrate is obtained.

Second-pass drainage samples were panned to enhance (a) the chances of finding anomalies, and (b) the magnitudes of the anomalies. The preparation of the heavy mineral concentrates (HMC) was intended to concentrate the most important component of the sample, by removal of the barren lighter fractions, which largely comprise quartz, clays or common rock-forming silicates. Panning eliminates dilution of samples and brings the gold concentrations of weakly anomalous samples within the capabilities of conventional analysis. The mass of each HMC sample varied between 200g and 600g. The concentrate samples were visually examined and assayed in the laboratory. Assay results were expressed as gold content of the concentrate.

After panning, the HMC samples were visually examined for coarse gold grains. Subsequently, the HMC samples were crushed and pulverized to  $-75\mu$  size fraction and homogenized in the laboratory. The pulverized HMC samples were analyzed for gold, using the 50g fire assay + AAS method (Appendix B).

### **Results, Discussions, Conclusions and Recommendations**

Visual examination was carried out on all the HMC samples during the panning exercise in the field. Hand lenses and a binocular microscope were used to examine the heavy mineral concentrates. The HMC contained minerals such as gold, magnetite and brown garnet. Coarse gold grains were recovered and observed in heavy mineral concentrates from Area 2s, 1s and 6 (see Figure 5.10). Coarse gold grains were not characteristic of concentrates from Area 4 (except for one sample). The highest concentration of coarse

gold grains was observed in samples from Area 2s. In Area 1s and 6, fewer coarse gold grains were observed in the concentrates.

Approximately 50 gold grains, from Area 2s, were observed in detail under a binocular microscope. The sizes of the grains ranged from 0.15 mm to 0.80 mm. The grain shapes were very variable, with many grains sub-spherical, but others distinctly elongate. Many of the grains were well rounded with smooth surfaces (Plate 5a), but others were more irregular with rougher surfaces (Plate 5b). These variations occurred across the size range. The variations in roundness and smoothness imply that the rougher grains had shorter transport distances, probably not exceeding 2 km from their source(s). The more rounded and smoother grains had greater transport distances, probably up to 5 km from their source(s).

Gold assay values for the 221 pulverized HMC samples were plotted on Figure 5.10 as proportional symbols and on a histogram (Figure 5.11). The lowest recorded value is 40 ppb Au. The peak value is 80 000 ppb Au, in a sample from Area 4C (the only sample with coarse gold in Area 4). On the histogram, the mode of the values is in the 0–49 ppb Au class. The histogram shows several overlapping populations up to a concentration of 650 ppb Au. There is a gap between 650 and 800 ppb Au. Several populations occur between 800 ppb and 80 000 ppb Au. The threshold value for the panned concentrates is approximately 650 ppb Au. Figure 5.12 is a log-probability plot of the gold assay values, which shows a threshold of 650 ppb Au.

Drainage HMC samples from Area 2s were characterized by the presence of coarse gold grains and high gold concentrations. In Area 2s, the peak gold value was 54 000 ppb. Each of the four river systems draining the area, had several samples with concentrations in excess of the 650 ppb Au threshold value (see Figure 5.10). The river system draining towards the ENE direction had the greatest occurrence of coarse gold, and longest dispersion train (~3km) of anomalous values, with several values in excess of 10 000 ppb Au. The two rivers draining southwards also had several high gold values in excess of 10 000 ppb, but had fewer coarse gold occurrences. The river draining towards the SW had only one sample with coarse gold. That sample had a gold concentration of 45 000 ppb. The high gold concentrations in all of the four river systems, reproduced the drainage anomaly indicated by the three anomalous first-pass samples in Area 2s. The source(s) of the geochemical anomalies and gold nuggets, lie upstream or in the watershed, of the rivers and tributaries with the anomalies and nuggets. Repeat gold assays on some of the HMC samples from Area 2s, indicated poor reproducibility, due to the nugget effect.

Repeat analyses for eight samples are shown on Table 5.13. Each of these samples was assayed twice, and the two gold values for each sample had very wide ranges of magnitude, sometimes with a standard deviation greater than the mean value.

**Table 5.13**

Poor reproducibility of gold values (ppb) in HMC samples from Area 2s

<u>Sample No.</u>	<u>Au 1</u>	<u>Au 2</u>	<u>Total</u>	<u>Mean</u>	<u>Std. Dev., s</u>
CD2/ 589	720	1280	2000	1000	395.98
CD2/ 598	360	42000	42360	21180	29443.93
CD2/ 599	2000	12500	14500	7250	7424.62
CD2/ 614	3600	13600	17200	8600	7071.07
CD2/ 609	10000	45000	55000	27500	24748.74
CD2/ 620	3200	11000	14200	7100	5515.43
CD2/ 622	3200	24000	27200	13600	14707.82
CD2/ 624	1250	10500	11750	5875	6540.74

A decision was made to conduct follow-up work in the Area 2s drainage anomalies, using the soil sampling method. Soil sampling was planned to cover the common watershed of the four river systems and the areas upstream of anomalous sample sites on tributaries. The soil sampling was expected to indicate the positions of the anomaly sources.

In Area 4, gold values for the HMC samples indicated the presence of three clusters of geochemical drainage anomalies (see Figure 5.10). In Area 4B, the anomaly was defined by two anomalous samples, with values of 800 ppb and 1520 ppb Au. Anomaly 4B reproduced the first-pass sampling anomaly, but at 2.5 km upstream of the original position. The central cluster of Area 4 was a more consistent drainage anomaly, with gold values of higher magnitude. This anomaly reproduced the original, first-pass anomaly. The anomalous values form a 2km long dispersion train, with several values in excess of 1 000 ppb Au. The peak value in the central cluster was 36 000 ppb Au. In the NE part of Area 4, gold values above background defined Area 4C, which appears to have two divergent dispersion trains of anomalous values, each being approximately 2 km long. Anomaly 4C had several gold values in excess of 1000 ppb and the peak value was 80 000 ppb. The sample with the peak value, was the only HMC sample, where coarse gold

was observed in the whole of Area 4. Generally, coarse gold is not characteristic of the Area 4 HMC drainage samples. The three clusters of anomalous gold values (4B, 4, and 4C) tend to lie in a linear zone, trending towards the location of Renco Gold Mine. The strike between Area 4C and Renco Mine (~10.5 km), which has not been sampled, may host more of such anomalies. A decision was made to do follow-up work, on the drainage anomalies of Area 4, using the soil sampling method. In current work, follow-up work was planned on anomalies 4 and 4B only. The soil sampling was expected to locate the approximate positions of the anomaly source mineralisation. Second-pass drainage sampling on Area 4C was only done much later in the exploration program. Follow-up work on Area 4C will be carried out by the exploration department at Renco Mine.

In Area 1s, gold values and coarse gold occurrences in HMC samples indicated drainage anomalies, particularly in the central and eastern parts of the area. In the central stream draining southwards, anomalous values with a peak of 18 000 ppb Au, indicate a 2.5 km long dispersion train. In the western part of the area, a stream draining towards the SE, had a weak dispersion train with a peak value of 5000 ppb Au. The original first-pass drainage anomalies were reproduced in Area 1s. Repeat analyses on some of the HMC samples in Area 1s, had poor reproducibility due to the nugget effect. The poor reproducibility is similar to that in HMC samples from Area 2s. It was recommended that follow-up work be carried out, on the drainage anomalies of Area 1s, using the soil sampling method.

In Area 6, anomalous gold values and coarse gold occurrences in HMC samples indicated an anomaly along the Matedzi River and its western tributaries. The peak value of the anomaly was 12 000 ppb Au. The original first-pass drainage anomaly was reproduced. Some of the repeat analyses on HMC samples also had poor reproducibility due to the nugget effect. Soil sampling was also recommended as a follow-up on the drainage anomaly, particularly on the western side of the Matedzi River.

## CHAPTER 6

### SOIL GEOCHEMISTRY

#### 6.1 INTRODUCTION

Soil sampling was carried out as a follow-up on drainage gold anomalies indicated in Chapter 5. The aim of the soil sampling surveys was to locate, as closely as possible, the sources of the drainage anomalies. Soil sampling is generally employed in follow-up surveys where a drainage basin reconnaissance survey has isolated an anomaly, or narrowed an anomaly down to a watershed (Levinson, 1974). Soils are weathering products that remain in situ on top of weathering parent rocks. Where the bedrock is mineralized, some kind of chemical pattern almost always can be found in the residual soil that results from the weathering of that rock (Rose *et al.*, 1979). Residual soil surveys are particularly applicable in areas of deep residual cover and sparse outcrops.

Soil sampling was conducted in Area 4, Area 2s, Area 1s and Area 6. An orientation soil sampling study was carried out to obtain information for use in optimum routine surveys in the EPO.

#### 6.2 ORIENTATION SOIL SAMPLING

Orientation soil sampling was conducted in Area 2s. The area was selected for the exercise because:

- (a) it is in a structural setting favourable for mesothermal gold mineralization (Target B, Chapter 4), and
- (b) it had the most consistent, high drainage gold anomalies with coarse gold, discussed in Chapter 5.

The orientation study was conducted in an area that had not been disturbed by human activity, so that a natural geochemical pattern could be observed. The survey comprised a number of experiments aimed at determining the existence and characteristics of anomalies associated with the type of mineralization being sought. The objectives of the orientation soil sampling were to determine (a) the best sampling medium, (b) the soil horizon from which samples should be taken, (c) the size fraction to be analyzed in routine surveys, and (d) the upper limit of the background values.

Different soil horizons yield different amounts of trace elements, hence it is essential that the type of soil collected be consistent (Levinson, 1974). In order to realize the greatest potential from routine soil sampling surveys, it is essential to sample the particular soil horizon that yields the most significant anomaly. The concentrations of trace elements also vary with the size fractions of the soil to be analyzed.

Although orientation soil sampling studies are normally conducted before the actual detailed exploration begins (Rattigan, 1965; Levinson, 1974; and Rose *et al.*, 1979), this orientation survey was carried out at the middle of the exploration program, when some of the target areas had been sampled.

### **Method**

In the orientation survey, a traverse was conducted across an area with quartz veins hosted in proto-mylonite. The traverse was 45 m west of Line 9800 E of Grid 2s, from 7975 N to 8150 N (see Figure 6.1). Eight pits, spaced at 25 m, were excavated down to hard rock. Most of the pits reached the saprolite (C-horizon) or the parent rock (D-horizon). One of the pits (8100 N) only reached a hard quartz stoneline, which lies on top of the C-horizon in some of the pits.

### Soil Profiles

The vertical soil profiles were studied in each of the pits. The A-horizon was divided into A<sub>1</sub> and A<sub>2</sub> sub-horizons (see Figures 6.2 - 6.9). The A<sub>1</sub> sub-horizon comprises dark, sandy soil with organic debris (humus). The A<sub>2</sub> sub-horizon is a leached, light-coloured sandy soil. The A<sub>1</sub> sub-horizon is a zone of maximum eluviation, which is depleted in trace elements that have been leached by organic acids from A<sub>1</sub> sub-horizon.

The B-horizon is present in some pit profiles and missing in others, where it has been eroded. Where it is present (pits 8025 N, 8100 N, 8125 N and 8150 N), the B-horizon is brownish sandy soil, sometimes with dark brown pisoliths of up to 1 cm diameter. The B-horizon is richer in clay minerals and iron than the A-horizon. Accumulation (illuviation) of material, by deposition or precipitation from percolating water, occurs in the B-horizon. Some of the leached material from the A<sub>2</sub>-horizon is deposited in the B-horizon.

The C-horizon is present in most of profiles, but missing in others such as in pit 8075 N, where it has been eroded. The C-horizon comprises soil in its upper part and saprolite with relict bedrock structures towards the bottom.

In the some of the profiles, a quartz stoneline lies on top of the C-horizon. The stoneline (H-horizon) comprises angular, tightly packed, and maroon-stained quartz pebbles, which vary in size from 0.5 cm to 40 cm across. The thickness of the stoneline is not uniform, as it becomes thinner in some pit sections (e.g. Figure 6.9) and missing in others. The maximum thickness intersected in the pits was 32 cm. Since the quartz pebbles are

angular, they were not transported for long distances, but were derived from local quartz veins.

### Sampling

Channel samples were obtained from all the soil profile horizons and sub-horizons. The entire thickness of each horizon or sub-horizon was sampled. Each sample was sieved into four size fractions using screens of 425 $\mu$ m, 180 $\mu$ m, 125 $\mu$ m and 75 $\mu$ m apertures. The size fractions of the sieved samples were (a) –425+180  $\mu$ m, (b) –180+125 $\mu$ m, (c) –125+75  $\mu$ m, and (d) –75 $\mu$ m. These size fractions were selected because Rio Tinto Zimbabwe (Pvt.) Ltd. had previously used them in similar orientation surveys in other regions. Each of the sieved sub-samples was allocated a unique sample number to be used during assaying. To avoid contamination of samples during sieving, the screens were thoroughly cleaned after sieving each sub-sample. The minimum mass of each sub-sample was 200g.

At the laboratory, the 200g sub-samples were homogenized and 50g was split from each sample. The 50g soil samples were assayed for gold using the fire assay + AAS method (Appendix B).

The entire thickness of each stoneline horizon was also sampled. The quartz stoneline samples were crushed, pulverized to –75 $\mu$  and assayed for gold using the fire assay + AAS method (Appendix B).

### **Assay Results and discussions**

Assay values are plotted on Figures 6.2–6.9 and tabulated on Tables 6.10 and 6.11. The highest C-horizon assay values (up to 810 ppb Au) occurred in pits 8000 N and 8025 N (figures 6.3 and 6.4), implying that these pits are closest to the source of one of the gold anomalies in the area. The lowest C-horizon gold values (up to 60 ppb) occurred in pits 7975 N and 8050 N, suggesting that these pits are further away from the source of the anomaly. The chemistry of the C-horizon usually resembles that of the parent rock. Since C-horizon is normally under thick soil cover, it may only be chosen for routine sampling surveys if the A- and B- horizons are missing, or if the anomalous values are only expected to be in it.

Assay values for pits 7975 N and 8050 N, which are further away from the source of the anomaly, provide an indicator of the background values in barren areas. The average value for the A<sub>1</sub>- and A<sub>2</sub>- horizons in the two pits is 62 ppb Au. The peak value in the C-

horizon is 60 ppb Au. These A- and C-horizon values suggest that the background values have an upper limit of approximately 60 ppb Au.

Assay results indicate that the peak gold values occur in the quartz stoneline (H-horizon). Where it was sampled in pits 8050 N, 8100 N, 8125 N and 8150 N, stoneline yielded gold values of 2930 ppb, 9490 ppb, 4780 ppb and 230 ppb respectively. In the soil horizons (A<sub>1</sub>, A<sub>2</sub> and B) above the stoneline, the peak gold values (up to 530 ppb) were far much less than those in the stoneline. The results indicate that the quartz stoneline is the best sampling medium. However, in these pits spaced at 25m across strike, the stoneline is missing in some of the profiles. Where present, the stoneline occurs at various depths to a maximum of 175 cm. Since the stoneline occurs under thick soil cover, it is not practically suitable for routine soil sampling programs in the study area.

Assay values of the A<sub>1</sub>, A<sub>2</sub> and B soil horizons indicate that the B-horizon generally yields the highest gold concentrations. On Table 6.10, the combined total gold values for each of the horizons (where the B-horizon is present) are shown. The B-horizon yielded 1570 ppb Au, which is 44.92% of the grand total for these soil horizons from the selected pits. The A<sub>1</sub>- and A<sub>2</sub>- horizons yielded 1010 ppb Au (28.90%) and 915 ppb Au (26.18%) respectively. The total values for each soil horizon clearly indicate that the A<sub>2</sub> horizon is a zone of eluviation and that the B-horizon is one of illuviation. On Figure 6.12, which shows bar graphs of total gold values for each horizon against soil horizon, the B-horizon yielded the highest concentration of gold.

The B-horizon has significant concentrations of clay minerals, which have negative charges at the edges of their platy structures. Clay minerals adsorb metals (or cations) such as gold and iron oxides. Iron oxides contribute a significant role in the fixation of the gold. Gold complexes are readily broken by reducing agents such as ferrous iron (Smith, 1987). Oxidation of iron is an important reaction in the weathered zone and gold is often intimately associated with iron oxides. In routine soil sampling programs for gold exploration, it is best to sample the iron-rich B-horizon. It is essential that fine-grained clay or silty-clay be sampled, rather than sands, which have little adsorptive capacity for metals (Levinson, 1974).

Assay values for the four soil sample size fractions are shown on Table 6.11. Total values for each size fraction indicate that the -180+125 $\mu$  size fraction yielded the highest concentration of gold. The -180+125 $\mu$  size fraction yielded 2115 ppb Au, which is 31.17% of the grand total. The -75 $\mu$  size fraction yielded the second highest

concentration of gold (1730 ppb) which is 25.50% of the grand total. The  $-425+180\mu$ , and the  $-125+75\mu$  size fractions yielded 1540 ppb Au (22.70%) and 1400 ppb Au (20.63%) respectively. On Figure 6.13, which shows bar graphs of total gold concentration against size fraction, the  $-180+125\mu$  size fraction yielded the highest concentration.

### **Conclusions**

Assay values indicate that the quartz stoneline is the best sampling medium, since it gave the highest gold values of up to 9490 ppb Au. However, since the stoneline occurs at various depths to a maximum of 175 cm, it was not practically suitable as a sampling medium for routine surveys in the study area. The stoneline is not always present, and is unique to Area 2s. Other selected targets for soil sampling surveys do not have the stoneline. For these reasons, the stoneline was not used as the sampling medium for routine soil surveys in the study area. A compromise was made to use a method that would save time, be cost effective and yield the soil anomalies. It is preferable to avoid the costly crushing procedure in sample preparation. Samples of iron-rich soil fractions are preferred. It was decided to use the B-horizon as the sampling medium for routine soil surveys.

The B-horizon is common in all the selected targets for soil sampling surveys. Out of all soil horizons overlying the stoneline, the B-horizon yielded the highest gold concentrations.

The  $-180+125\mu$  size fraction ( $-80+120$  mesh) yielded the highest concentration of gold. This mesh size was the most suitable for soil sampling in the study area and was used in routine surveys.

Gold assay values for the A- and C- horizons in pits far away from the source of the anomaly, suggest that the upper limit of the background values is approximately 60 ppb Au.

## **6.3 GRID SOIL SAMPLING SURVEYS**

### **Sample Grid Patterns**

Soil sampling surveys were conducted in grids laid out in Area 4, Area 2s, Area 1s and Area 6. Sampling grids were planned to have maximum coverage of the drainage anomaly basins and their watersheds. The grids were initially laid out using a tape and compass survey, but a theodolite was used if subsequent drilling had to be conducted. Rectangular grids were used for the soil sampling.

In each area, a baseline was surveyed along an azimuth parallel to the dominant fabric or structural trend. Traverse lines were surveyed perpendicular to the baseline, and their lengths were planned to cover the entire widths of the drainage anomalies. The traverse line spacing and sample spacing were selected so that they would cross the strike of a mineralized zone and outline it. In the initial reconnaissance grids, a traverse line spacing of 400 m was used. Where subsequent follow-up surveys were carried out, the traverse line spacing was reduced to 200 m, and further to 100 m. Soil sampling was carried out in several stages using finer and finer grids, to define the source of an anomaly as closely as possible. Rose, *et al.* (1979) recommend that the traverse line interval should be less than one-third of the minimum economic strike length.

Sample spacing was 25 m along the traverse lines. This spacing of sample points along the traverse lines, conformed to the recommendations by Levinson (1974) and Rose, *et al.* (1979), which state that at least two sample points on each line should fall within the soil anomaly. It was expected that the type of gold mineralization would be in narrow vein systems in long shear zones (~2 km long, ~75m wide). On steep gradients, slope correction was done using grid spacing and elevation conversion tables (Berkman, 1976), to maintain a horizontal sample spacing of 25 m. The sample points were labeled using Cartesian grid co-ordinates in metres, with the baseline having a northing of zero, and traverse line numbers increasing eastwards.

Universal Transverse Mercator (UTM) co-ordinates for the grids were obtained using a GPS instrument. The instrument was tuned to Arc 1950 Map Datum, which gives more accurate co-ordinates. Co-ordinates were obtained for both ends of the baseline and each traverse line.

### **Soil Sampling and Preparation**

At each sample point, a pit was excavated using a pick and shovel, to reach the B-horizon. The pits were dug on undisturbed soil, far from termite mounds or streams and rivers. The B-horizon material was sampled and sieved to  $-180+125\mu$  ( $-80+120$  mesh) size fraction. Wet or damp samples were dried before sieving. The average weight of a sieved sample was 200g. Each sieved sample was allocated a unique sample number to be used for assaying. The sample number, sample position number, soil colour and soil type, were recorded on standard soil sample-collection forms. Prior to sieving, the types of soil were described as loam, sandy, sandy-loam or clay. Additional notes were also

made where the sampled material had quartz pebbles, or where sample pits were close to quartz veins.

Non-contaminating sieves, made of stainless steel or nylon, were used. After sampling and sieving at a sample point, the pick, shovel, drying pad and sieve were thoroughly cleaned, to avoid contamination of the next sample.

Duplicate samples and several check standards were inserted in every batch of soil samples. Within every 20 samples in a batch, a check standard or a duplicate sample was inserted, and allocated a sample number in sequence with the soil samples. The value of each check standard was an average of analyses carried out by a significant number of independent laboratories. Each check standard had values for various elements such as Au, Cu, Pb, Zn, As and Ag. One of the check standards was a blank made of crushed, barren silica.

### **Sample Analysis**

At the laboratory, the samples were assayed for gold and copper. Copper was also selected for analysis because at Renco Mine east of the study area, copper is associated with gold mineralization. The 200g samples were dried, homogenized and split to remove 50g. The 50g sample was used in the analysis and the remainder was retained for repeat analysis, if required. Gold assays were carried out using the fire assay + AAS method (Appendix B). Copper assays were conducted using Aqua regia digestion + ICP-MS method (Appendix C).

When analytical results were received, accuracy of the assay procedure was measured by plotting assay values of control standards on control charts. The assay values of the control standards were compared with the expected values, using a menu in the Chembase Software, which plots the values against the certified mean  $\pm 2$  standard deviations (SD). If the assay values of the control standards fell within the range of the mean  $\pm 2SD$ , then the results of the batch were accepted. If the values fell outside the range, the results were rejected, and the laboratory was asked to repeat the analysis of the batch. To assess the precision of the assay procedure, values of duplicate samples were plotted on scatter plots. Scatter plots are an effective means of assessing the repeatability or scatter of duplicate assay data. The two sets of data are plotted against each other on an X-Y chart. From the origin, a 45° line drawn onto the graph assists in assessing the data and helps to highlight any "deviations" from the 45° line. If there is a wide range of concentrations to be viewed, the data can be plotted onto a log-log plot.

### **Preparation of Geochemical Maps**

The preparation of geochemical maps was carried out with the use of a computer. Assay data, co-ordinates and sample positions were captured into the Excel and Chembase Programs. Using the UTM co-ordinates at the ends of a traverse line, the programs calculate the co-ordinates of the rest of the sample points on the line. Assay values of control standards and duplicate samples were removed from the Excel spreadsheet, which was then imported into Geosoft Program.

Data were processed and gridded using the Geosoft or Chembase program. Gold and copper values were plotted as (a) profile curves (b) ranges of concentration, or (c) proportional symbols. Intervals for proportional symbols and contours were selected as factorial multiples of the threshold value, such that for a threshold of 60 ppb and a factor of 2, the intervals would be 60 ppb, 120 ppb, 240 ppb, 480 ppb, and so on (Rose *et al.*, 1979). The ranges of concentration were also presented as colour images.

### **Interpretation of Data**

Interpretation of geochemical soil data involved (a) estimation of background and threshold values, (b) distinguishing between significant and non-significant anomalies, (c) distinguishing between lateral and superjacent anomalies, and (d) appraising the significance of anomalies in terms of possible ore, with a view to selecting those that merit further investigation.

Geological mapping was conducted in the soil sampling grids. Interpretation of the geochemical soil data was carried out in conjunction with the geology. The geological mapping is described in Chapter 7.

#### **(a) Estimation of Background and Threshold Values**

Estimations of threshold values were carried out using frequency distribution histograms and log-probability plots. According to Sinclair (1991), the histograms are used in experiential methods and model-based subjective approaches to threshold selection. Experiential methods depend on the experience of explorationists and include techniques of visual evaluation of histograms. In model-based subjective approaches, background and anomalous samples are represented by different probability density functions (i.e. different histograms), each of which can be represented by a normal density function. Model-based subjective approaches also apply some type of formal statistical model, that the threshold of a data set is the mean plus two standard deviations.

Log-probability plots are utilized in the model-based objective techniques method (Sinclair, 1991), in which the thresholds are defined by the data themselves rather than by an arbitrary decision of the explorationist. This method depends on a general conceptual geochemical model, which recognizes that a background population in a homogeneous geological environment, has a characteristic probability density function that results from the summation of processes that have produced the background substrate. In this study, the log-probability plots were done and interpreted in the manner described by Levinson *et al.* (1987) and Sinclair (1991).

(b) Recognition of Non-significant Anomalies

Principal anomalies that are not related to mineral deposits include those resulting from (i) barren rock types characterized by a relatively high background metal content; (ii) human contamination; and (iii) sampling and analytical errors (Rose *et al.*, 1979).

Anomalies resulting from the weathering of high background rocks may be suspected wherever the patterns coincide with all or part of a mapped rock unit, or cover very large areas compared with the expected size of an ore deposit. Anomalous patterns caused by contamination are those related to agriculture, roads, railways or old mine workings and dumps. False anomalies related to sampling commonly reflect unnoticed variations in (i) the nature of the sample material, particularly with regard to content of clays or hydrous Fe-Mn-oxides, (ii) the depth of the different soil horizons in relation to sampling depth, (iii) the nature of the vegetation and its influence on the accumulation of biogenic metal in the soil, and (iv) local drainage conditions. False anomalies due to analytical errors are readily spotted and can be corrected by repeat analyses. Erratic high values are suspect, as are patterns that are related to batches of samples.

(c) Distinguishing Between Lateral and Superjacent Anomalies

Errors may occur in interpreting geochemical data due to the assumption that the source of metal lies immediately beneath the soil anomaly. The soil anomaly would have been assumed to be superjacent, when in reality it was a lateral anomaly developed by horizontal movement of ground water or the soil.

Two major types of superjacent dispersion are the relic patterns in residual soils due to simple weathering in place, and hydromorphic or biogenic patterns in transported cover resulting from the upward movement of metal-rich solutions. Residual patterns are syngenetic, and may be recognized by the presence of diagnostic primary minerals. The

superjacent patterns of hydromorphic or biogenic origin have a predominance of more mobile metals. A soil anomaly whose shape and trend shows little or no correlation with the topography, but consistent with a probable geological trend, is more likely to be a superjacent anomaly. Lateral patterns are nearly always hydromorphic in origin and show a close relationship with local topography.

(d) Appraisal of Anomalies

The main considerations in assessing the possible significance of geochemical anomalies include (i) magnitude of the values, usually expressed as the contrast between the peak values and background, (ii) size and shape of the anomalous area, (iii) geologic setting, and (iv) extent to which the local environment may have influenced the metal content and pattern of the anomaly (Rose *et al.*, 1979).

In residual soils, all whose dimensions are consistent with the possibility of a sizeable deposit should be listed for further investigation. Priorities generally depend on the favourability of the geological setting. Shallow overburden and restricted mobility may lead to local enhancement of metal values and to the development of a relatively strong anomaly from a low-grade bedrock source. A local variation in the environment, such as a deeper overburden or more intensive leaching, can result in relatively feeble values that are actually related to a high-grade source.

## 6.4 GRID 4

### **Soil Sampling**

In Grid 4, soil sampling was carried out as a follow-up on drainage anomalies in Area 4 and 4B (Chapter 5). The reconnaissance grid was 10.2 km long and 2.2 to 3.6 km wide (see Figure 6.14). The azimuth of the baseline was 040°. This trend was selected because it is parallel to a second-order shear zone, which is a splay from the first-order Mauch Shear Zone that trends on a regional fabric of 060°. In the reconnaissance grid, the initial traverse line spacing was 400m. The sample points were at 25-m intervals along the traverse lines. Soil samples were obtained from the B-horizon, sieved to -180+125 $\mu$  size fraction and assayed for gold and copper.

Assay results of the reconnaissance samples indicated scattered anomalous values (>60 ppb Au) between (a) Line 10000 E and Line 14400 E, and (b) Line 14800 E and Line 20200 E. The traverse line spacing in these two areas was reduced to 200m during second-pass soil sampling. Assay results of the second-pass samples indicated the possibility of more consistent anomalies between Line 15000 E and

17400 E. The traverse line spacing between these two lines was reduced to 100 m during third-pass soil sampling. The total number of samples collected in all the three phases was 4745.

### **Gold Values**

The lowest recorded value is 20 ppb Au and the peak value is 900 ppb Au. Figure 6.17 is a frequency distribution histogram of the gold values. The histogram shows a leptokurtic log-normal distribution with positive skewness. There is an overlap between the background and anomalous values in the 61-80 ppb class, suggesting that the threshold value is within that class. A better estimation of the threshold value is shown on the log-probability plot (Figure 6.18). Each population, which has a log-normal distribution, plots as a straight line. The threshold value is the upper limit of Population 1 (background values), and marks the lower limit of Population 2 (anomalous values). The threshold value is 60 ppb Au.

Anomalous gold values define two significant soil anomalies (a) from Line 16100 E to Line 17400 E, and (b) from Line 15000 E to Line 15200 E. The former and the latter were named the East Anomaly and West Anomaly respectively. The two anomalies, which appear to be on the same linear feature, are separated by a gap of 900 m.

The East Anomaly attains a persistent strike length of 1300 m and a maximum width of 200 m. The large width is likely to be due to lateral dispersion caused by the movement of soil and ground water down the gradient. Within this strike length, the peak gold value in the soil was 800 ppb. The overall peak value of 900 ppb Au for the entire grid, is an isolated point anomaly on Line 17800 E further to the east. The East Anomaly, which trends on 055°, is situated on a shear zone that appears to be a splay from another shear trending on 060°. Anomalous copper values in both the east and west anomalies occur on the 060° shear zone. The 055°-shear zone has been named the "Au Shear", whereas the 060°-shear zone was named the "Cu Shear" (see Figure 6.15). The shear zones have mylonite and intrusions of feldspar porphyry dykes.

The West Anomaly, with a peak value of 640 ppb Au, attains a strike length of 200 m and a maximum width of 50 m. The anomaly trends on 060° and is coincident with the copper anomaly.

A weak anomaly occurs north of the West Anomaly, from Line 15300 E to 15600 E. This anomaly, which has a peak value of 120 ppb Au, occurs on a quartz vein flanked by an

olivine pyroxenite dyke and a dolerite sill. Such weak and small, together with single point Au anomalies located in several parts of the grid, were not selected for follow-up work in this study.

### **Copper Values**

The lowest recorded value is 0.51 ppm Cu and the peak value is 446 ppm Cu. Figure 6.19 is a frequency distribution histogram of the copper values. The histogram shows a leptokurtic, log-normal distribution with positive skewness, and a mode in the 20-39 ppm class. The histogram suggests that the threshold value is in the 100-149 ppm class, whose midpoint is 125 ppm Cu. The log-probability plot (Figure 6.20) suggests the existence of two threshold values of 40 ppm Cu and 125 ppm Cu. The threshold value of 40 ppm Cu could be for soils derived from felsic rocks (population 1), and the 125 ppm Cu threshold may be for soils on mafic rocks only (population 2), which have relatively high background metal content. Population 3 is anomalous. The threshold value of 125 ppm Cu was used in the interpretation of data.

Background values less than 40 ppm Cu are generally for soils derived from felsic rocks (such as charnockites and leuco-mylonites). Soils derived from mafic granulites (such as basaltic granulite), and mafic/ultramafic intrusives (such as dolerite and olivine pyroxenite), generally have background values between 40 and 125 ppm Cu.

Within the East Anomaly and West Anomaly, copper values above threshold define patchy, discontinuous anomalies (see Figure 6.16). In the East Anomaly, two copper anomalies, trending on 060°, occur between (a) Line 17000 E and Line 17100 E, in the south, and (b) Line 16700 E to Line 16800 E, in the north. The south anomaly is on the "Cu Shear" (see Figure 6.15), as is the peak value of 446 ppm Cu, which is a single point anomaly. The north anomaly is associated with a shear zone at the contact of silicified mafic granulite and garnet- biotite gneiss. In the West Anomaly, a copper anomaly is defined by only two consecutive samples on Line 15100 E. This anomaly, which is on the "Cu shear", is concurrent with the gold anomaly.

In the north-eastern part of the grid, an anomaly (up to 249 ppm Cu) stretches from Line 18600 E to 19800 E, a strike length of 1200 m. However, this copper anomaly does not have the support of anomalous gold values, and no further work was carried out on it. In the south-eastern area of the grid, an anomaly (up to 370 ppm Cu) extends from Line 18600 E to 19000 E. This copper anomaly also lacks the support of anomalous gold values. Several single point copper anomalies occur in other areas of the grid.

## **Conclusions**

In Grid 4, soil geochemistry delineated two significant gold anomalies, the East Anomaly and West Anomaly. The East Anomaly, with a strike length of 1300 m and peak value of 800 ppb Au, was the first priority for follow-up work. In the East Anomaly, anomalous gold values follow a trend of 055°, whereas anomalous copper values (up to 446 ppm) occur on a trend of 060°. The West Anomaly had a strike length of 200 m, a peak value of 640 ppb Au, and concurrent copper support, with values up to 221 ppm Cu. The West Anomaly was the second priority for follow-up work. The soil gold anomalies reproduced the drainage gold anomalies indicated in Chapter 5.

It was decided to carry out further investigations on the East and West anomalies, using the method of trenching.

## **6.5 GRID 2s**

### **Soil Sampling**

In Grid 2s, soil sampling was carried out as a follow-up on drainage anomalies in the northern and southern parts of Area 2s. The reconnaissance soil sampling grid was 4.0 km long and 2.7 km wide. The azimuth of the baseline was 065°, parallel to the dominant penetrative foliation, which is also the regional fabric. The baseline had a northing of 10000 N, and traverse lines were numbered from 8600 E to 12600 E. Tie-lines with a northings of 7500 N and 9300 N were surveyed in the grid. In the reconnaissance grid, the traverse lines had a spacing of 400 m. Soil sample points were spaced at 25-m intervals along the traverse lines. Soil samples were collected from the B-horizon and sieved to  $-180+125\mu$  size fraction.

The reconnaissance soil samples were assayed for gold and copper. Assays results of the reconnaissance samples indicated anomalous gold values ( $>60$  ppb Au) from Line 9400 E to Line 12600 E.

Between Line 9400 E and 12600 E, the traverse line spacing was reduced to 200 m during in-fill second-pass soil sampling (see Figures 6.21 and 6.22). Gold assay results of the second-pass samples indicated persistent anomalies from Line 9800 E and 12000 E. The total number of samples collected on Grid 2s was 1572.

### **Gold Values**

The lowest recorded value is 20 ppb Au and the peak value is 980 ppb Au. Figure 6.23 is a frequency distribution histogram of the gold values. The histogram shows a log-normal distribution with positive skewness and an overlap of two populations in the 61-80 ppb Au class, suggesting a threshold value of 60-70 ppb Au. Figure 6.24 is a log-probability plot of the gold values, which indicates a threshold value of 60 ppb Au. The background values are shown as population 1 and the anomalous values as populations 2 to 4. The majority of anomalous gold values have magnitudes that are greater than those for Grid 4.

Anomalous gold values define two sinusoidal anomalies from Line 9800 E to Line 12000 E. The two anomalies anastomose at the north-eastern and south-western corners of the grid (see Figure 6.22). The strike length for each anomaly is approximately 2.2 km. The sinusoidal shape of the two anomalies could be due to an intersection of east-west shears and north-north-east (030°- 040°) shears. Where the two anomalies anastomose in the south-western corner, a wide (800 m) soil anomaly occurs on Line 10000 E. However, after trenching, the large width was found to be due to a thick transported quartz stoneline. Widths of the anomalies are not uniform, but vary from 25 m to 350 m. In the anomalies, the majority of quartz veins follow the regional trend of 065°, but others follow the east-west trend and the north-north-east trend. The quartz veins are discontinuous along strike.

### **Copper Values**

Copper values are generally very low and range from <1 to 80 ppm, with the majority being <10 ppm. The copper values in Grid 2s are very low because the local lithologies are felsic (such as charnockite, leuco-mylonite, leucogneiss and K-feldspar granite).

The copper values are not as high as those of Grid 4, where the threshold value was 125 ppm Cu. The anomalous gold values in Grid 2s do not have copper support. No geochemical map was produced for copper in Grid 2s.

### **Conclusions**

Anomalous gold values in Grid 2s indicated two anastomosing sinusoidal anomalies, each with a strike length of 2.2 km. The anomalies are associated with discontinuous quartz veins. In Grid 2s, the anomalous gold values are higher in magnitude, as compared to the anomalous values in Grid 4. Anomalous gold values in Grid 2s do not

have copper support. The soil gold anomalies reproduced the drainage anomalies indicated in Chapter 5.

A decision was made to carry out follow-up work in the soil gold anomalies, using the method of trenching.

## 6.6 **GRID 1s**

### **Soil Sampling**

Soil sampling in Grid 1s was carried out as a follow-up on drainage gold anomalies discussed in Chapter 5. The reconnaissance grid was 4.4 km long and between 1.1 and 2.1 km wide (see Figure 6.25). The baseline had an azimuth of  $062^\circ$ , parallel to the dominant regional foliation in the area. Soil sample points were at 25-m intervals along the traverse lines, which were 400 m apart. Soil samples were collected from the B-horizon, sieved to  $-180+125\mu$  size fraction and assayed for gold and copper. The total number of samples collected was 860.

### **Gold Values**

The lowest recorded value is 20 ppb Au and the peak value is 220 ppb Au. Figure 6.27 is a frequency distribution histogram of the gold values. The histogram shows a log-normal distribution with positive skewness and suggests a threshold of 60 ppb for the gold values. Figure 6.28 is a log-probability plot of the gold values, which indicates a threshold value of 60 ppb Au. Population 1 represents the background values, and populations 2 and 3 represent the anomalous values.

Gold values above threshold define patchy or continuous anomalies with short strike lengths. The peak value of 220 ppb Au occurs in an anomaly at the north-eastern part of the grid, from Line 11600 E to Line 12000 E (see Figure 6.25). The anomaly is 400 m long and east-west trending. Another 400-m long anomaly occurs in the central part of the grid, from Line 10000 E to Line 10400 E. This anomaly has a peak value of 80 ppb Au. These anomalies are associated with discontinuous quartz veins in silicified basaltic granulite. Several isolated anomalies occur in various parts of the grid. When compared to the anomalies in grids 2s and 4, the Grid 1s anomalies are smaller and weaker, giving them a lower priority ranking for follow-up work. In this study, in-fill second-pass soil sampling was not carried out in Grid 1s.

### **Copper Values**

The lowest recorded value is 1 ppm Cu and the peak value is 224 ppm Cu. Figure 6.29 is a frequency distribution histogram of the copper values with a mode in the 40-59 ppm class. The histogram shows three populations with log-normal distributions, most probably related to different rock types in the grid. These distributions suggest threshold values at 40 ppm Cu and 80 ppm Cu. The threshold value of 40 ppm Cu relates to soils derived from felsic rocks (such as charnockites), whereas the threshold of 80 ppm Cu relates to soils on lithologies of intermediate or mafic compositions (such as silicified basaltic granulite, meta-andesite or basaltic granulite). Figure 6.30 is a log-probability plot of the copper values, on which four populations are shown with upper limits at 50, 80 and 125 ppm Cu for the first three. Background values are in population 1, which comprises soils derived from the felsic rocks, with a threshold of 50 ppm Cu. Populations 2 and 3 are likely to be due to granulites of intermediate to mafic composition. Anomalous values on the mafic granulites have a lower limit at 125 ppm Cu. A threshold value of 125 ppm Cu was used. This threshold value is the same as the one for Grid 4, which has similar rock types.

Anomalous values indicate single point anomalies or anomalies with short strike lengths (see Figure 6.26). The peak value of 224 ppm Cu is a single point anomaly, which is coincident with the gold anomaly between Line 10000 E and 10400 E. A narrow east-west trending anomaly, extends for 400 m, from Line 10800 E to Line 11200E. This anomaly is not associated with a gold anomaly. On lines 11600 E and 12000 E are isolated copper anomalies, which do not concur with any gold anomaly.

### **Conclusions**

Anomalous gold values indicated two anomalies with short strike lengths and several single point anomalies. Those anomalies intersected by at least two traverse lines only had strike lengths that were not much greater than 400 m. The peak gold value of 220 ppb was far less than the peak values of Grid 2s (980 ppb) and Grid 4 (900 ppb). Copper anomalies were also patchy or had short strike lengths. The peak copper value (224 ppm) is a single point anomaly concurrent with one of the gold anomalies, but the other isolated anomalies are not related to the gold anomalies.

The soil gold anomalies reproduced the drainage anomalies indicated in Chapter 5. However, the gold anomalies of Grid 1s had low priority ratings due to their small size and relatively lower concentrations of gold. In this study, follow-up work was not recommended in Grid 1s.

## **6.7- GRID 6**

### **Soil Sampling**

In Grid 6, soil sampling was carried out as a follow-up on drainage anomalies in Area 6. The reconnaissance grid was 2 km long and 800m wide, with a baseline azimuth of 050°, which is parallel to the dominant foliation in the area. Sample points were spaced at 25-m intervals along the traverse lines, which were 400 m apart. Soil samples were collected from the B-horizon, sieved to  $-180+125\mu$  size fraction and assayed for gold and copper. The total number of samples collected was 198.

### **Gold Values**

The lowest recorded value is 20 ppb Au and the peak value is 80 ppb Au. The majority of the samples had values of 20 ppb Au, with only 34 having values between 40 and 80 ppb Au. When compared to the peak values of Grid 2s (980 ppb Au) and Grid 4 (900 ppb Au), the Grid 6 peak value of 80 ppb Au is very low. Using a cut-off value of 60 ppb Au for Grid 2s and Grid 4, the values between 60 and 80 ppb Au on Grid 6 are isolated and do not indicate any anomalous zones. Follow-up work was not recommended in Grid 6.

### **Copper Values**

The lowest recorded value is 7 ppm Cu and peak value is 171 ppm Cu. Using a cut-off value of 125 ppm Cu for Grid 2s and Grid 4, values greater than 125 ppm Cu in Grid 6 occur in two samples only. The values  $>125$  ppm Cu do not indicate an anomaly and are not associated with the elevated gold values.

### **Conclusions**

In Grid 6, the gold values greater than 60 ppb Au are isolated and do not indicate continuous anomalous zones. When compared to the peak values of Grid 2s and Grid 4, the Grid 6 peak value of 80 ppb Au is very low. For these reasons, second-pass soil sampling was not recommended on Grid 6.

## CHAPTER 7

### GRID MAPPING, ROCK SAMPLING AND TRENCHING

#### 7.1 INTRODUCTION

##### **Geological Mapping**

Geological mapping was carried out concurrently with soil sampling in Grid 4 and Grid 2s. The mapping was conducted in more detail on the soil sampling grids, than on a regional scale. The detailed geological maps were used for interpretation of soil geochemical data and other data sets (such as geochemical and geophysical data). The mapping entailed lithology, structure and streams. Additional features plotted on the maps included man made infrastructure such as roads, powerlines, dams, etc. Streams and general topography were useful in the interpretation of lateral dispersion of soil anomalies. Geological maps were also utilized for planning and conducting rock sampling surveys on the grids. Another objective of grid geological mapping was to study structural controls of mineralization. The mineralization in Grid 4 and Grid 2s was compared with similar well-documented deposits.

##### **Rock Sampling**

Rock sampling was carried out on quartz veins, feldspar porphyry veins, and sulphide-bearing mylonites and banded cherts. Iron-stained host rocks close to quartz veins were also sampled. Grab, chip or channel samples were obtained from exposures and sub-outcrops. Where the rock was fine-grained and relatively homogeneous, a single grab sample was obtained. If the rock was fine- to coarse-grained with erratic distribution of minerals or quartz stringers, channel or chip samples were taken along several traverses at a sampling site. Different types of sampling methods are used because of the uneven distribution patterns of elements and minerals throughout the rock mass, the uneven occurrence of some minerals in segregations or fracture fillings, and variations of texture in some rock types (Levinson, 1974). Rock samples are representative only of the material actually collected. Each method was selected to obtain a representative sample of the lithology and possible mineralization.

At each sampling site, UTM Co-ordinates were obtained using a GPS instrument. Each sample was allocated a unique number to be used for assaying. The sample positions were marked on the geological map, and captured into Excel, Geosoft and Chembase databases. The sampled rocks were described on sample-collection forms. The descriptions included characteristics such as lithology, colour, iron staining, grain size,

shearing and visible mineralization (sulphides and/or gold, and their distributions). Duplicate samples, particularly of sulphide-bearing rocks, were inserted in every batch. One duplicate sample was inserted within every 20 samples in a batch. The mass of each rock sample was influenced by grain size. Fine-grained (0-1mm), medium-grained (1-10 mm) and coarse-grained (1-3 cm) weighed 500g, 1000g and 2000g respectively.

At the laboratory, the samples were crushed and pulverized to  $-75\mu$  fraction. The pulverized sample was homogenized before splitting out 50g for gold analysis by fire assay and AAS, and 2 x 2g for copper and bismuth analyses by aqua regia digestion and ICP-MS. The remainder was retained for repeat analyses, if required. Bismuth analyses were carried out on rock samples from Grid 4 only, where the geology is similar to that at Renco Mine. Bismuth occurs with the gold mineralization at Renco Mine. The fire assay and aqua regia digestion methods are described in Appendix B and Appendix C respectively.

When assay results were received, the values of duplicate samples were plotted on control charts to monitor the repeatability or precision of the assays and the assay process. Control charts (scatter plots) were plotted manually or using the Chembase Program. If the assay data were not acceptable, the laboratory was instructed to repeat the analyses. Scatter plots are an effective means of visually assessing the repeatability or scatter of duplicate assay data. On the scatter plot, the two sets of data are plotted against each other on an X-Y chart. From the origin, a  $45^\circ$  line drawn onto the graph usually assists in assessing the data and helps to indicate any "deviations" from the  $45^\circ$  line. Where there is a wide range of concentrations to be viewed, the data can be plotted onto a log-log plot.

Gold and copper data were plotted on log-probability graphs to determine their threshold values or their natural cut-off values. Separate plots were made for gold data from (a) mineralized quartz veins in felsic granulites, and (b) feldspar porphyry dykes/veins in silicified mafic granulite. Assay data for quartz veins in mafic granulites (in Grid 4) were used for Cu plots. The threshold values of the gold data were used to plot frequency-distribution histograms. On the histograms, the class intervals were selected as factorial multiples (factor of 2) of the background value, according to Rose *et al.* (1979).

Gold assay values were plotted as proportional symbols on the geological plan. The copper and bismuth values were elevated, but not of economic grades. The correlation between gold, copper and bismuth values was calculated using Spearman Rank

Correlation Coefficients. The Spearman rank coefficient of correlation ( $r_s$ ), in which data are measured on a ranking scale, is applicable to major or trace element data (Rollinson, 1993). The Spearman rank coefficient of correlation is a non-parametric statistic, which can be used for all geochemical data, whether normally or log-normally distributed (Levinson *et al.*, 1987). The Spearman rank correlation coefficient is calculated as:  $r_s = 1 - [6\sum d^2 / (n^3 - n)]$ , where  $d$  is the difference in ranking between the  $x$ -values and  $y$ -values, and  $n$  is the number of pairs. If the rank orders are the same, then  $d = 0$  and  $r_s = +1.0$ . If the rank orders are the reverse of each other, then  $r_s = -1.0$ . The Spearman rank correlation coefficients were calculated in the manner described by Levinson *et al.* (1987).

### **Trenching**

Trenching was carried out in Grid 4 and Grid 2s. The exercise was a follow-up on the soil gold anomalies indicated on these grids. Trenches were sited in anomalous areas with poor exposure. The objective of the trenching was to locate gold anomalies in the C-zone or parent rock. The trenching was carried out to expose the near-surface expression of the mineralized zones giving rise to the gold anomalies.

Trenches were excavated parallel to the traverse lines, but were sited away from arable land, road tracks, etc. Where possible, the trenches were planned to traverse the entire widths of the soil anomalies. On average, the trenches were spaced at 100 m in Grid 4 and at 200 m in Grid 2s.

The trenches were dug using a mechanical excavator or picks and shovels. The excavation was done to reach the lower part of the C-zone or the parent rock. In some localities where the trenches were deeper than 1½ m, the walls of the trenches were terraced to avoid collapse. Cleaning-up of the floors and walls of the trenches was carried out to enable logging and sampling.

The geology of the C-zone or parent rock was mapped. The logging entailed host lithology, quartz and/or feldspar porphyry dykes/veins, visible mineralization and structure. The geology was recorded on log sheets and plotted on trench plans, which were initially on a scale of 1:500, and later on 1:5000 or 1:4000. Channel or panel samples were collected from the C-zone or parent rock. In Grid 4, channel samples were obtained from the trench walls, using a chisel and hammer, to avoid contamination that can occur at the trench floor. In Grid 2s, where there is sparsely disseminated coarse gold, panel samples were obtained from the trench walls or thoroughly cleaned floors.

Where the samples were obtained from the floor, the sampled surface was cleaned using a hard broom and water, prior to the sampling. Panel sampling was selected to produce a larger, more representative sample, which would counter the nugget effect.

Channel or panel samples were collected at 1-metre lengths along the trench, except at geological contacts, where samples were collected over shorter lengths to reach the contacts. Quartz and feldspar porphyry dykes/veins or host rocks with visible mineralization were also sampled separately. The average masses of the channel and panel samples were 2kg and 5kg respectively. Samples were allocated unique sample numbers to be used for assaying. Sample numbers were plotted on the log sheets and trench plans, and captured into the Chembase database. A duplicate sample was inserted in every 20 samples in a batch.

At the laboratory, samples were crushed, pulverized to  $-75\mu$ , homogenized and split for analysis. The samples were assayed for gold and copper, but those from Grid 4 were also assayed for bismuth. Copper and bismuth assays were conducted using the aqua regia + ICP-MS method (Appendix C). Gold assays were conducted using the fire assay + AAS method (Appendix B).

When assay results were received from the laboratory, quality control of the assay procedure, was carried out by plotting control charts, as described in "Rock Sampling" above. Assay values were plotted on histograms and log-probability plots. Assay values were also plotted on the 1:500 trench plans, and as proportional symbols on 1:4000 or 1:5000 plans.

## **7.2** **GRID 4**

### **Geology**

The geology of Grid 4 is shown on Figure 7.1. The lithologies comprise mafic granulites (basaltic- and silicified basaltic-), picritic rocks, basaltic amphibolite, meta-andesite, garnet-biotite gneiss, ferruginous meta-quartzite, calc-silicate rocks, banded chert and tuff, enderbite, charnockite, proto-mylonite, mylonite, migmatite, quartz veins, feldspar porphyry dykes/veins, pegmatites, olivine pyroxenite, dolerite and ferricrete. These rock types are described in Chapter 3. The grid is located on a "greenstone belt" sequence comprising (a) mafic meta-volcanic rocks (mafic granulites and amphibolites), (b) intermediate meta-volcanic rocks (meta-andesite), and (c) meta-sediments (garnet-biotite gneiss, meta-quartzite, calc-silicate rocks and banded chert). Younger charno-enderbites and their sheared varieties (proto-mylonites and mylonites) flank the "greenstone belt".

Pegmatites and quartz veins intruded the "greenstone belt" and the charno-enderbites. Feldspar porphyry dykes/veins intruded a shear zone within, but close to the northern contact of the silicified basaltic granulite. Picritic rocks, olivine pyroxenite and dolerite, which all contain igneous textures, are post-metamorphism.

There are two major structural trends in the grid, which are (a) 060° in the south and (b) 040° in the north. In the south, the proto-mylonite and mylonite, which are part of the Mauch Shear Zone, follow the regional 060° trend ( $S_1$ ). Quartz veins in the south are parallel to the  $S_1$  trend. In the north, the proto-mylonite and mylonite, which form a splay shear zone from the Mauch Shear, follow the 040° trend. The splay shear zone, which dips at 55° to the southeast, is a second-order structure ( $S_2$ ) in the region. Quartz veins in the north are parallel to the  $S_2$  trend. The feldspar porphyry dykes/veins are in a shear zone generally trending on 055° and dipping steeply to the southeast at 70°. This sinistral shear zone is within the silicified basaltic granulite, but nearer to the northern contact. The 055° and 060° trends have been named the "Au Shear" and "Cu Shear" respectively (in Chapter 6). Towards the southeastern end of the grid, there is interdigitation of the silicified basaltic granulite and mylonite. In all the lithologies, foliations dip southeast at 55° - 80°. Quartz lineations plunge towards south-south-west at 55° - 75°.

Disseminated sulphide mineralization was observed in feldspar porphyry dykes/veins and adjacent mylonite, banded chert, calc silicate rocks, some quartz veins in the south, and in various parts of the meta-andesite. The sulphides in the feldspar porphyry dykes/veins are pyrrhotite, chalcopyrite, subhedral pyrite, chalcocite and sphalerite (specimen RS 27). In the mylonite adjacent to the feldspar porphyry dykes/veins, ore minerals are pyrite, chalcopyrite, magnetite and bismuth (specimen RS 45). Ore minerals in banded chert are mostly chalcopyrite, with chalcocite, pyrite, magnetite and sphalerite (specimens RS 16 and RS 17). In calc-silicate rocks, ore minerals are fine-grained pyrite, chalcopyrite, pyrrhotite and magnetite (specimen RS 46). In the south, ore minerals in quartz veins of the "Cu Shear" are mainly chalcopyrite, pyrite, magnetite, bismuth and molybdenite. The meta-andesite contains occasional sparse pyrite and magnetite.

### **Rock Sampling**

Rock samples were collected from exposures and sub-outcrops of quartz veins, feldspar porphyry dykes/veins and adjacent mylonite, banded chert, calc-silicate rocks and some of the wall-rocks to the veins. The number of samples collected was 348. Samples were assayed for gold, copper, and bismuth.

### Feldspar porphyry dykes/veins

Figure 7.2 is a log-probability plot of gold values of 39 samples of feldspar porphyry dykes/veins. The lowest recorded value is 20 ppb Au and the peak value is 9800 ppb Au. The plot shows a natural threshold value of 1750 ppb Au (1.75 g/t Au). The actual economic cut-off grade depends on several factors such as metal price, recovery, mining method, production costs, etc. Gold values were also plotted on a histogram (Figure 7.3). On the histogram, values above the threshold are shown as a separate population. Gold values were plotted as proportional symbols on the geology plan (Figure 7.1). Anomalous gold values reproduced the East and West anomalies indicated by soil geochemistry in Chapter 6.

In the feldspar porphyry dykes/veins, the minimum value for copper is 5 ppm and the peak value was 571 ppm. The peak value is not high enough to reach economic grade. Similarly, bismuth has a minimum value of <1 ppm and a peak value of only 57 ppm.

In the feldspar porphyry dykes/veins, the correlation between Au and Cu, Au and Bi, and Cu and Bi, is shown as Spearman Rank Correlation Coefficients on Figure 7.1. Gold shows a weak correlation with copper (+0.4076) and no correlation with bismuth (-0.0010). Copper and bismuth show a fairly strong correlation (+0.6708).

### Quartz Veins in Charnockite

Figure 7.4 is a log-probability plot of 107 samples of quartz veins in charnockite, in the southeast part of the grid. The minimum gold value is 20 ppb and the peak value is 2400 ppb. The log-probability plot indicates a threshold value of 600 ppb Au. Figure 7.5 is a histogram of the gold values. On the histogram, anomalous gold values are shown as a separate population. The anomalous gold values occur over a strike length of 200 m (Figure 7.1, Line 19400 E to Line 19600 E).

Copper values range from 4 to 489 ppm. The peak value is not sufficiently high to be of economic grade. The quartz veins in charnockite were not assayed for bismuth.

The correlation between gold and copper is shown on the Spearman Rank Correlation matrix on Figure 7.1. The correlation coefficient of +0.1879 implies that there is very weak correlation between gold and copper in the quartz veins hosted in charnockite.

### Quartz Veins in "Cu Shear" and Mafic Granulites

Figure 7.6 is a log-probability plot of copper values of 44 samples collected from quartz veins in the "Cu Shear" and mafic granulites. The values range from 3 to 571 ppm Cu. The plot indicates a threshold value of 100 ppm Cu. Anomalous values, with a peak of 571 ppm Cu, are not high enough to be of economic grade.

### **Trenching**

Trenches were excavated along thirteen traverse lines across the soil anomalies in the East and West anomalies. Figure 7.7 shows the locations of the trenches. The thickest soil cover was down to a depth of 3 m. Unlike the soil profile in Grid 2s, the soil cover in Grid 4 did not have a quartz stoneline. Trenches exposed several pegmatites, a series of parallel feldspar porphyry dykes/veins (up to a maximum of 7) in mylonite, and the host silicified basaltic granulite. Feldspar porphyry dykes/veins had maximum horizontal widths of up to 2½ m. The foliation in mylonite and host rock, and feldspar porphyry dykes/veins, all dip 75° southeast. The feldspar porphyry dykes/veins had intense maroon staining due to weathered sulphides. In the West Anomaly, some of the dykes/veins contain fresh, disseminated, pyrite, chalcopyrite and pyrrhotite. The mineralized shear zone has maximum horizontal width of 25 m.

One-metre channel samples were collected from the C-zone or parent rock on the walls of the trenches. Separate samples were obtained across the widths of feldspar porphyry dykes/veins and sulphide-bearing mylonite. Duplicate samples were collected from some of the sulphide-bearing veins and mylonite. The total number of samples collected was 999. The samples were assayed for gold, copper and bismuth.

### Gold Values

The assay results indicate that gold mineralization occurs mainly in the feldspar porphyry dykes/veins. Occasionally, the adjacent and intervening host mylonite is also mineralized. The gold values range from 20 to 70460 ppb. The peak value is 70 g/t Au x 0.2 m or 35 g/t Au when sampled over 1 metre.

Figure 7.8 is a log-probability plot of the gold values in the feldspar porphyry dykes/veins and the host mylonite. The plot indicates a threshold value of 4200 ppb Au (4.2 g/t Au). The histogram (Figure 7.9) shows the background values (0-4200 ppb) and the anomalous values (>4200 ppb). The threshold value of 4.2 g/t Au could be higher than the economic cut-off grade, which depends on factors such as the mining method and the metal price. Gold values are plotted as proportional symbols on Figure 7.7. Gold values

above 1 g/t occur over a strike length of 300 metres in the West Anomaly and 600 metres in the East Anomaly. In the East Anomaly, the trenches did not traverse the entire length of the soil anomaly, hence the trench anomaly is still open towards the east.

#### Copper Values

In the feldspar porphyry dykes/veins, quartz veins and the host mylonite, copper values range from 9 to 1978 ppm. The peak value of 1978 ppm (0.2 % Cu) is not sufficiently high to attain economic grade. Figure 7.10 is a log-probability plot of the copper values, which indicates a threshold value of 200 ppm Cu. The histogram of the data (Figure 7.11) shows a log-normal distribution, with the background values in the 0-200 ppm class and the anomalous values above 200 ppm. Copper values are plotted as proportional symbols on Figure 7.7. The West Anomaly has the peak value and the majority of the copper values above 500 ppm. In the East Anomaly, only one value was above 500 ppm Cu.

#### Bismuth Values

The bismuth values range from 11 to 53 ppm. The peak value of 53 ppm Bi is not high enough to be of economic significance.

#### Correlation

Spearman rank correlation coefficients between (i) Au and Cu, (ii) Au and Bi, and (iii) Cu and Bi, were calculated and plotted as matrices on Figure 7.7. In the East Anomaly, there is weak correlation between (i) gold and copper (+0.2970), and (ii) gold and Bismuth (+0.2121). There is no correlation (-0.1636) between copper and bismuth. In the West Anomaly, there is a fairly strong correlation (+0.5636) between gold and copper. The "Au Shear" and the "Cu Shear" are concurrent in the West Anomaly, but bifurcate towards the east.

#### **Structural Controls on Gold Mineralization**

In Grid 4, the mineralization is located where a first-order shear zone converges with a second-order shear zone (see Figure 7.12). The first-order ( $S_1$ ) structure is the Mauch Shear Zone, which stretches for several hundreds of kilometres along strike. In the study area, the Mauch Shear Zone attains a maximum horizontal width of 1 kilometre. The first-order shear zone follows the 060° regional trend ( $S_1$ ) and dips steeply (70°- 85°) to the southeast. The second-order ( $S_2$ ) shear zone is a splay from the Mauch Shear Zone. The splay shear zone, which is 7 km long and 200 m wide, trends on 040° and dips 55°

southeast. Mineralized zones are situated in the acute angle ( $20^\circ$ ) between the two shear zones.

The Mauch Shear Zone, which is a major structural "break" in the NMZ of the Limpopo Belt, is similar to the major shear zones and faults that control gold mineralization in (a) the Zimbabwe Craton (Campbell and Pitfield, 1994), (b) the Yilgarn Block, Australia (Groves *et al.*, 1989), and (c) the Canadian Shield (Hodgson, 1989; Robert, 1990). In these cratons, gold mineralization invariably is associated with second- and lower-order shear zones/faults, which in many cases, are splays of the first-order shear zones/faults (Hodgson, 1989). The major structures and their associated splays form corridors of anastomosing shear zones and faults, commonly referred to as deformation or tectonic zones. All the giant deposits occur in deformation zones within a few kilometres, mostly <5 km, of the first-order shear zones/faults.

The shorter (relative to the "break") shear zones/faults within the deformation zones are the structures that commonly host, or are closely related to the gold mineralization (Hodgson, 1989). Shear zones that have a closer spatial correlation with gold deposits tend to be shorter and narrower than the first-order shear zones (Poulsen and Robert, 1989). Second-order shears, typically 5 to 10 km long and less than 100 m wide, occur both parallel and oblique to the first-order shears. The second-order shears are rarely gold-rich, but commonly form an important structural element at deposit scale. Third-order shear zones, up to 1 km long and a few tens of metres wide, typically intersect with second-order shears to form networks. The third-order shears are important at the scale of an orebody and segments of them commonly constitute orebodies. Vein-type mineralization most commonly occurs in brittle and brittle-ductile shear zones, and less commonly in extension veins in the walls of shear zones or between shear zones in a shear zone system (Hodgson, 1989).

In the study area, the convergence of the splay shear zone and the Mauch Shear Zone, both with sinistral movement, resulted in dilation in the acute angle ( $20^\circ$ ) between them. In the acute angle, extensional forces resulted in the dilation. Dilatancy, which results in the development of vein mineralization, is caused by tectonic forces, and is an integral part of the bulk strain of mineralized areas (Hodgson, 1989). The mineralization appears to have been formed by fluids of deep crustal origin, which escaped up the major ( $S_1$ ) shear zone, and deposited gold in structurally-induced dilation zones. The main ore control at the deposit scale is dilatent zones formed by the interference of intersecting shear zones. Vein emplacement is not just a result of pre-existing weak zones being

pumped open by excess fluid pressure. However, fluid pressure in gold vein-forming environments must be high, and be close to, or for short periods of time exceed, lithostatic pressure (Hodgson, 1989).

In Grid 4, the gold mineralization occurs in feldspar porphyry veins/dykes and the host mylonite, which are in a narrow fourth-order shear zone trending on 055°. This shear zone appears to be a splay from another narrow third-order shear zone, which trends on 060° and hosts Cu-Mo mineralization. The mineralization in Grid 4 is an association of gold-only veins with porphyry copper-type, Cu-Mo mineralization. This association is similar to that in the Hollinger-McIntyre deposit in the Timmins area, Abitibi belt, Canada, and the Boddington deposit, Yilgarn Block, Australia (Hodgson, 1989). In the Boddington deposit, the hypogene gold mineralization is dominantly associated with chalcopyrite, pyrrhotite and pyrite, which occur with other ore mineral phases such as molybdenite, arsenopyrite, scheelite, bismuth and galena. In the Hollinger-McIntyre deposit, the composition of the ore is mainly Au, Ag and W, with less amounts of Cu, Mo, Bi, Zn, Te and B (Robert and Poulsen, 1997). However, whilst the Grid 4 deposit in the study area is granulite facies, the Hollinger-McIntyre and Boddington deposits are in greenschist facies. In many other deposits, porphyry-type mineralization may be present, but is unrecognized, or is at depth in the system, because felsic intrusions are very common in mesothermal gold deposits (63 % of the giant deposits in volcanic rock dominated belts).

In the study area, Cu-Mo-Au mineralization occurs in the West Anomaly, where the "Au Shear" and the "Cu Shear" are concurrent. In the East Anomaly, there are gold-only veins on the "Au Shear", which is a splay from the "Cu Shear" with the Cu-Mo veins. The porphyry-type Cu-Mo-Au mineralization could be of a different age to the gold-only veins. The former could be syn-intrusive and overprinted by much later gold-only veins, in similarity to Perron Mine in the Val d'Or area, Quebec (Hodgson, 1989). In the southern Abitibi and Yilgarn Blocks, the felsic intrusions hosting porphyry-style mineralization are at least 15 m.y., and probably 50-100 m.y. older than the associated gold veins, and gold is synchronous with younger penetrative structural fabrics.

The Grid 4 deposit can also be compared with the Renco Mine deposit, which is 12 km to the northeast, and also within the northern marginal zone of the Limpopo Belt. Renco Mine is described in Chapter 2.

### 7.3 GRID 2s

#### Geology

The geology of Grid 2s is shown on Figure 7.13. The lithologies are predominantly felsic and comprise charnockite, leuco-mylonite, proto-mylonite, leucogneiss (leucosome), K-feldspar granite, quartz veins, pegmatites and minor mafic granulite xenoliths. These rock types are described in Chapter 3. The charnockite was sheared to proto-mylonite and more intensively to leuco-mylonite. The leucogneiss (leucosome) and K-feldspar granite are believed to be products of migmatization of pre-existing charno-enderbites. The quartz veins and pegmatites are intrusive into the main rock types mentioned above.

The area has a well-developed intersection of two main structural trends, which are 065° and 085°. The 065° trend is the regional ( $S_1$ ) penetrative foliation. The sinistral Mauch Shear Zone, in the northern part of Grid 2s, follows the 065° trend. In the Mauch Shear Zone, the dips are predominantly steep (75°) to the southeast, and quartz (elongation) lineations plunge steeply (70°- 85°) to the southwest. Since the elongation lineation is plunging, the movement in the shear zone had a vertical component and a horizontal component. The sinistral horizontal sense of movement implies that the vertical movement was reverse.

The 085° trend truncates the regional 065° fabric. Proto-mylonites and mylonites in shear zones, which cross-cut the Mauch Shear Zone in the northeast and southwest parts of the grid, represent this east-west trend. The east-west trend, which also truncates the 040° fabric, has been designated as the  $S_3$  trend. In the southern part of the grid, the east-west shear zone dips south at 75°. The east-west-shear zone in the north has dips varying from 75° south, to vertical and to 84° north. Both east-west shear zones have dextral horizontal sense of movement and quartz lineations plunging steeply (75°- 87°) to the west.

The north-north-east (030°-040°) trend is not well developed in Grid 2s. A prominent joint and a few minor sinistral shears represent this  $S_2$  trend.

Visible mineralization occurs in the form of fine-grained, disseminated gold nuggets in some of the quartz veins (see Figure 7.13). Sparse, disseminated pyrite and chalcopyrite also occur in the quartz veins and the immediate host rocks. The quartz veins are discontinuous along strike and have widths that vary from narrow stringers to one metre. The majority of the quartz veins follow the 065° trend, but a few are aligned along the 085° and 040° trends. Some of the outcrops of mylonite and proto-mylonite are maroon-

stained due to weathering of sulphides. In these host rocks, the pyrite and chalcopyrite grains are closely associated with sparse biotite and chlorite clusters.

### **Rock Sampling**

Rock samples were obtained from exposures and sub-outcrops of quartz veins and some of the immediate host rocks. Chip and channel samples were collected, since (a) some of the quartz veining occurs as stringers and (b) some of the mineralization occurs as randomly distributed gold nuggets. The samples, which numbered 94, were assayed for gold and copper.

### Gold Values

Assay results indicate that gold mineralization occurs in the quartz veins and stringer zones. Gold values range from 20 to 27000 ppb. Figure 7.14 is a log-probability plot of the gold values. The plot indicates a threshold value of 2250 ppb Au (2.25 g/t Au). Figure 7.15 is a frequency distribution histogram of the gold values. The histogram shows the background values in the 0-2250 ppb class, and the anomalous values above the threshold.

Gold values are plotted as proportional symbols on Figure 7.13. Values above 1 g/t Au occur within the envelope of the soil anomalies. Gold values between 5 and 27 g/t are located in three parts of the grid, which are (a) southwest, (b) north central, and (c) northeast. In the southwest, the mineralized quartz veins are situated at the intersection of an east-west shear zone and a north-north-east fabric (030°-040°) sub-parallel to the prominent joint in the area. The mineralization in the north-central area is located at the intersection of the Mauch Shear Zone and an east-west shear zone. The peak value of 27 g/t Au occurs in the north-central area. In the northeast, the mineralized quartz veins are in third-order shears that are parallel to the Mauch Shear Zone and cross-cutting the east-west shear zone. Gold mineralization in Grid 2s is thus, structurally controlled. Mineralized areas (a)-(c) are all within 700 m of the Mauch Shear Zone.

### Copper values

Copper values are generally very low and range from 7 to 265 ppm. The majority of the values are below 30 ppm Cu. Although disseminated chalcopyrite is present, its concentration is too sparse to yield significant copper mineralization.

### Correlation

The Spearman rank correlation coefficient, between the gold and copper values, is shown as a correlation matrix on Figure 7.13. The coefficient of correlation is -0.2592. There is no correlation between gold and copper.

### **Trenching**

Trenches were excavated along 10 traverse lines across the two soil anomalies. Some of the trenches were offset from the traverse lines to avoid arable land, infrastructure, etc. The northern soil anomaly was not trenched on traverse lines 10400 E–10800 E. Positions of the trenches are shown on Figure 7.16. Trenches were excavated to the C-zone or parent rock. Soil cover is thickest in the southern part of the grid where it attains a maximum thickness of 3 metres. Within the soil profile, a quartz stoneline occurs above the C-zone. The stoneline attains a maximum thickness of 1 metre. This stoneline is described under "Orientation Soil Sampling" in Chapter 6. Rock samples of the stoneline assayed gold values of up to 9.5 g/t. The stoneline is thus, an ore resource.

Trenches exposed quartz veins in leuco-mylonite, proto-mylonite, leucogneiss and K-feldspar granite. Quartz veining occurs in the form of stringers and veins with widths of up to 1 metre. The majority of the veins have a strike direction of 065°, but a few have the 085° and 040° strike directions. The quartz veins dip steeply (65°-85°) to the southeast and south. Some of the quartz veins contain fine-grained, sparsely disseminated gold nuggets. In some localities, the wall-rocks contain sparse, disseminated pyrite and chalcopyrite.

Panel samples, which were taken at 1-metre lengths along the trenches, were obtained from the C-zone or parent rock on the walls and floors of the trenches. Separate samples were obtained from quartz veins and host rocks with visible mineralization. Duplicate samples were collected from some of the quartz veins and host rocks. The number of samples collected was 2714. The samples were assayed for gold and copper. On each sample, two repeat analyses were carried out to check the reproducibility of the values.

### Gold Values

Repeat assays of the large panel trench samples gave good reproducibility of the gold values. The reproducibility of the gold values in the trench samples was better than that in the drainage samples from the same area. Gold values ranged from 5 ppb to 174720 ppb (174.72 g/t). Figure 7.17 is a log-probability plot of the gold values. The plot indicates a threshold value of 7500 ppb Au (7.5 g/t Au). Figure 7.18 is a frequency distribution

histogram of the gold values. The histogram shows the background values in the 0-7500 ppb class and the anomalous values above the threshold. The threshold value of 7.5 g/t Au could be too high, as the actual cut-off grade is determined by other factors such as metal price, mining method, etc. Gold mineralization is mainly in the quartz veins and stringers, but also occasionally occurs in the wall rocks in some localities.

Gold values above 1 g/t Au are plotted as proportional symbols on Figure 7.16. In the southwest part of the grid, the mineralization occurs within a 100-metre wide envelope trending north-northeast, sub-parallel to the prominent joint in the area. Although the broad mineralized zone trends on 030°, the majority of quartz veins trend on 065° within the zone. The strike length of this trench anomaly is 600 metres. In the northeast area of the grid, the mineralization between trenches 11000 E and 11325 E, is also in a north-north-east trending zone. Between these two trenches, the indicated strike length of the trench anomaly is 400 metres. However, the strike between trenches 11325 E and 11800 E was not adequately trenched. In that strike, rock sampling indicated mineralization trending on 065°, which was not trenched. The soil anomaly in that strike appears to have been removed by a northerly draining stream, resulting in the trenching program missing that target. In the north-central area, the anomalies indicated by soil and rock sampling were not adequately trenched, but were later investigated by diamond drilling.

#### Copper Values

The copper values are generally low and range from <1 ppm to 209 ppm in the felsic rocks, but a mafic granulite xenolith assayed 908 ppm. The majority of the copper values are less than 40 ppm. Elevated values such as 140, 209 and 908 ppm Cu are not spatially related and do not define an anomaly.

#### Correlation

The Spearman rank correlation coefficient, between the gold and copper values, is shown as a correlation matrix on Figure 7.16. The coefficient of correlation is -0.3212. There is no correlation between gold and copper.

#### **Structural Controls on Gold Mineralization**

In Grid 2s, the mineralized zones are located where two parallel east-west shear zones intersect the Mauch Shear Zone (see Figure 7.19). The sinistral Mauch Shear Zone is the main, first-order shear zone, and has been described above, in "Structural Controls in Grid 4". The dextral east-west shear zones are second-order shears. The intersection of two shear zone systems with different senses of movement, resulted in dilation as a

consequence of bulk, inhomogeneous shortening (Hodgson, 1989). Inhomogeneous shortening is achieved by successive, alternating increments of movement on the two sets of intersecting shears. The mechanism leads to the development of a crack-seal ribbon vein in which each ribbon is slickensided before being incorporated into the vein. The movement occurs on both of the two shear systems, with movement on one of the shears consisting only of simple shear, and on the other shear, of alternating increments of simple shear parallel to, and dilation sub-normal to, the shear fracture (see Figure 7.20). This mechanism results in the common occurrence of mineralization in only one set of an intersecting shear system, and produces shear veins that have ribbon, laminated textures and slickensides.

In Grid 2s, the majority of the mineralized quartz veins are in third-order shears, which trend on 065°, parallel to the first-order shear zone. These third-order shears commonly cross-cut the second-order east-west shears. According to the mechanism mentioned above, movement on the east-west shear (northern shear) comprised only simple shear, but on the Mauch Shear Zone, movement comprised alternating increments of simple shear parallel to, and dilation sub-normal to, the shear fracture. A few other mineralized quartz veins trend on 040°, which is a weakly developed fourth-order, sinistral shear system in the grid. In the southwest part of the grid, a few east-west trending quartz veins are mineralized.

Gold mineralization in Grid 2s is similar to the Westonia (formerly Edna May) and Griffin's Find deposits in the Yilgarn Block, Western Australia. The Westonia deposit is hosted in a late Archaean (2.7 Ga) granodiorite (Edna May Gneiss). The mineralization is controlled by a broad ductile shear zone (100°/45° N), with "hook-shaped" brittle quartz veins (Cassidy, 1990). The ore-related fabrics are laminated quartz veins and pervasive foliation in granitoid. The mineralization occurs in (a) major vein lodes (100°/45° N), (b) closure of "hook-shaped" veins (plunges 45° NW), and (c) foliation-parallel veinlets (100°/45° N). Pyrrhotite, pyrite, molybdenite, scheelite and galena are the major opaque minerals. The accessory opaque minerals are chalcopyrite, arsenopyrite, sphalerite, hessite, wolframite, magnetite, and native bismuth and gold. Gold is sited in sulphides (pyrite and pyrrhotite), quartz veins and silicate minerals (feldspar, and possibly amphibole and diopside). Alteration minerals are quartz + K-feldspar ± diopside ± hornblende ± biotite ± muscovite. The ore metal association is Au-Ag-Pb-Cu ± W ± Mo ± Bi. From the fluid inclusion data, the P-T conditions were >370° C, 3±1 kbar. The calculated T, P conditions (thermodynamic data) were 570±50° C, 2±1.5 kbar. The mineralization, which is post-granitoid and marginally post-peak metamorphism, was

dated at  $2636 \pm 28$  Ma (Pb model age). The metamorphic grade of Westonia deposit is mid-upper amphibolite facies (3-5 kbar,  $665 \pm 30^\circ$  C).

The Griffin's Find deposit is hosted in an Archaean granulite (plagioclase-quartz-biotite-garnet-orthopyroxene), believed to have a sedimentary precursor (Fare and McNaughton, 1990). The metamorphic grade is lower-granulite facies ( $6 \pm 1$  kbar,  $700$ - $750^\circ$  C). The lode is a north-plunging sigmoid located on the fold axis of a large basinal structure, within an inferred ductile shear zone ( $>1$  km wide) parallel to the fold axis. The NW-SE striking ductile shear zone, which is an inferred axial planar, is the controlling structure. The ore-zone comprises intensely quartz-diopside veined rocks with relatively massive quartz-diopside  $\pm$  garnet alteration. The quartz-diopside veins are laminated and parallel to the foliation. Pyrrhotite, arsenopyrite and loellingite are the major opaque minerals, and graphite is accessory mineral. The gold is non-refractory, almost exclusively occurring as free gold within composite arsenopyrite/loellingite grains. No gold is associated with pyrrhotite or silicates. The ore metal association is Au-Ag-As. Calculated T, P conditions (thermodynamic data), indicates that the ore fluid was synchronous with peak metamorphism at  $\sim 700^\circ$  C,  $\sim 6$  kbar. The Pb-Pb isochron age of the mineralization is  $2635.6 \pm 3.2$  Ma.

#### 7.4 **CONCLUSIONS**

Assay results of rock and trench samples reproduced the gold anomalies indicated by soil geochemistry in Grid 4 and Grid 2s. Geological mapping in the grids was useful in the interpretation of soil, trench and rock geochemical data. In the two grids, the mineralization indicated by trench and rock sampling had a strong ore possibility and a fairly large potential to merit further investigation by drilling.

Gold mineralization is structurally controlled in Grid 4 and Grid 2s, and can be hosted by any rock type. In Grid 2s, the mineralization occurs in quartz veins and stringers hosted by proto-mylonite or K-feldspar granite. The Grid 2s mineralization comprises fine-grained free gold in quartz veins, and very sparsely disseminated pyrite and chalcopyrite, associated with few mafic grains in the host rocks. The felsic host rocks had insufficient iron to react with sulphur in the fluids, therefore few sulphides were formed, and free gold was deposited in quartz veins. In Grid 4, the gold mineralization is in (a) feldspar porphyry veins/dykes and some parts of the host mylonite, in silicified mafic granulite and (b) quartz veins in charnockite. In type (a) mineralization, the ore minerals comprise pyrrhotite, pyrite, chalcopyrite, molybdenite  $\pm$  sphalerite  $\pm$  bismuth, and traces of gold. In

the silicified mafic granulite, the iron reacted with sulphur in the fluids, to precipitate sulphides with the gold.

In Grid 4, where the gold occurs with copper and molybdenum, the mineralization is porphyry-type. Cu-Mo mineralization occurs in earlier veins, whereas Au is in later veins. At the nearby Renco Mine, Cu-Mo mineralization also occurs with gold, and could be hosted in veins that are locally termed "pegmatoids", which are very similar to feldspar porphyry.

In both Grid 4 and Grid 2s, gold mineralization is spatially associated with the regional, first-order Mauch Shear Zone. In Grid 4, the mineralization occurs 300 metres north of the Mauch Shear Zone, and is located in a dilation zone formed by the convergence of a second-order splay shear zone and the first-order shear zone. Cu-Mo quartz veins and feldspar porphyry dykes/veins occur in a third-order shear, which is parallel to the first-order shear zone. Au feldspar porphyry veins/dykes occur in a fourth-order shear, which is a splay from the Cu-Mo shear. In Grid 2s, mineralization is in and within 700 metres of the Mauch Shear Zone. Gold mineralization is in quartz veins/stringers in dilation zones formed as a result of bulk inhomogeneous shortening at the intersection of the dextral, second-order shear zones and the sinistral, first-order Mauch Shear Zone. Gold mineralization is predominantly in third-order shears, which are parallel to the first-order shear zone. In both Grids, the mineralization was formed by fluids that escaped up the major first-order shear zone, and deposited gold in structurally-induced dilation zones.

Renco Mine, which is 12 km northeast of Grid 4, is located between the Mauch (Mtirikwi) Shear Zone in the south and the North Limpopo Thrust Zone (NLTZ) in the north. On surface, the distance between the two shear zones is 8 km. Gold mineralization is in mylonitic lateral, frontal and Riedel shears, which are consistent with thrust geometry. The thrusting at Renco is associated with the thrusting on the NLTZ (Kisters *et al.*, 1998), and the lateral ramp represents a second-order splay from the Mauch Shear Zone or NLTZ thrust system. This could imply that the Mauch Shear Zone, which has vertical reverse sense of movement, is part of the NLTZ system. On the Tokwe River section beyond 1½ km north of the Mauch Shear Zone, foliation dips are gentle, ranging from 27° to 35° to the southeast. These gentle dips could be indicative of the thrusting on the NLTZ. The structural setting of the gold prospects/deposits (Grid 4, Grid 2s and Renco) in the Northern Marginal Zone, is similar to that for the Southern Marginal Zone (SMZ) deposits, e.g. Franke Mine. The SMZ deposits are spatially and temporally related to the Hout River Shear Zone and the thrusting of the SMZ onto the Kaapvaal craton.

The mineralization at Renco and SMZ deposits is associated with retrogression (mid-amphibolite facies) in granulite facies rocks. At Renco, the mineralization occurred at temperatures approximately 600° C, and has been dated at 2553-2532 Ma. At Franke Mine, the mineralization occurred at T, P conditions of 600-620° C, 6 kbar.

The reefs at Renco, Grid 4 and Grid 2s are mesothermal deposits, which formed at temperatures above 300° C and pressures > 800 bars. The most significant characteristic of these mesothermal deposits is the tectonic structural control by the Mauch Shear Zone and the NLTZ, and deposition of gold in structurally-induced, second-order and lower-order shears in dilation and thrust zones. The mineralization, which is post-peak metamorphism, occurs over several kilometres and is in the form of disseminated to massive ore. Ribbon to massive quartz veins, feldspar porphyry and mylonite, typically host the ore. The occurrence of pyrrhotite, sphalerite and native gold as some of the ore minerals, is also characteristic of mesothermal deposits.

## CHAPTER 8

### DIAMOND DRILLING

#### **8.1** INTRODUCTION

Diamond drilling was carried out in Grid 4 and Grid 2s. The drilling was conducted as a follow-up on trench and rock anomalies indicated on the grids. During the course of the study, the diamond drilling program was the final stage of mineral appraisal. The drilling was conducted on a reconnaissance basis only, aimed to intersect the mineralization in fresh rock at a vertical depth of 50 metres. Further follow-up drilling was to be carried out by Renco Mine.

Drilling is the cheapest method of testing a mineral deposit at depth, and is a method that is used on prospects that offer both a strong ore possibility and a large potential (Elliston, 1965). A cored diamond drill hole provides a small continuous sample along its path, from which mineral composition, metallurgical properties and some structural information may be obtained by inspection and analysis (Hughes, 1965). Inspection of the core provides direct information about the sequence of rock types, ore minerals, textures and the alteration present in the ore zone, and some cases, the structure and attitude of the rocks may be deduced (Lissiman, 1965). The task of diamond drilling is to obtain intersections that show the presence or absence of economic grade and width of a deposit. Alteration (hypogene) is due to reactions caused by the ascending hydrothermal mineralizing fluid permeating parts of the wall-rocks (Evans, 1993). Since they are formed in response to various pressure, temperature and compositional changes, different wall-rock alteration mineral assemblages can be compared with metamorphic facies. The wall-rock alteration can be used as an exploration tool in other areas of the same geological environment.

The objectives of the reconnaissance drilling program were to (a) test the anomalies indicated by trenching and rock sampling, (b) study the prospect geology, mineralization and alteration, (c) obtain samples for assay, (d) determine the grades of the intersections, (e) determine the thickness of the reefs, (f) estimate ore resources, and (g) determine the depth of the weathered zone.

#### **8.2** METHOD

##### **Planning of Drill Holes**

The planning of drill holes was carried out using geological information and geochemical data from trenching and rock sampling. The exercise was done on cross-sections, where drill holes were planned to intersect the projected mineralized zones at vertical depths of

50 metres below surface. Each hole was planned to do a specific task. According to Hughes (1965), some of the aspects that were considered in planning the holes were: (a) the task that the hole should accomplish, (b) the nature of the target to be tested, and (c) the expected course of the hole. These factors were also coupled with hole diameter, estimate of time and cost of drilling. The attitude of the targeted mineralized zones determined the course of the planned drill holes. Since the mineralized zones are steeply dipping ( $70^{\circ}$ - $75^{\circ}$ ), inclined holes were planned. Inclined holes give an opportunity to core across the mineralized zone, and give information on thickness, grade and dip. Inclinations of the holes were in the range of  $50^{\circ}$  to  $70^{\circ}$ . With inclinations  $< 50^{\circ}$ , it is difficult to gain vertical depth, as the holes tend to flatten (Elliston, 1965). Holes collared at inclinations  $>75^{\circ}$  have little directional stability. The holes were planned to intersect the mineralized zones perpendicular to strike, and to traverse the entire widths of the mineralization. Another factor that was considered in planning the drilling was depth of the hole, or cost of the work in relation to the potential of the deposit to be tested. Drilling costs rise steeply with increasing depth.

Collars of the planned holes were plotted on trench plans and surface geological maps. On the ground, the collars and drill hole azimuths were surveyed and pegged using a theodolite. A GPS instrument was used to obtain the drill hole collar coordinates.

### **Drilling**

The holes were drilled to produce large diameter, HQ (63.5 mm) core. The advantages of larger diameter diamond drilling are (a) deviation resistance, (b) improved core recovery, (c) longer runs of core, and (d) large sample size (Hughes, 1965). Large diameter core is stronger and does not break up readily, giving longer runs. The HQ diameter core provides an adequate sample. The core recovered enables (i) detailed logging and sampling of the ore zone, and (ii) determination of geomechanical properties (Barnes, 1987).

On selected traverse lines of Grid 4, one hole was drilled per section. Each hole was drilled to intersect the veins hosting the ore and the entire width of the mineralized zone. The planned drill hole depth was adjusted until the hole reached the footwall of the mineralized zone. On Grid 2s, where some of the drilling was carried in areas that could not be trenched, the holes were drilled in a fencing pattern, guided by the width of the soil anomaly. Since most of the holes were not very deep, drill hole deflection surveys were not conducted during the course of this study.

### **Core Logging**

Core recovery measurements were conducted prior to the actual logging of the drill core. Between depth markers, the length of recovered core was measured and expressed as a percentage of the drilled length. The whole length of the core was marked at one-metre lengths. The lithologies were logged along the entire drill hole length. The logging entailed identification of rock types, quartz veins/stringers, feldspar porphyry veins/dykes, textures, ore minerals and alteration minerals, and measurement of structures. Visible sulphide mineralization, which was predominantly disseminated, was categorized as sparse (< 5%), moderate (5-20%) and abundant (20-50%). Some intersections on Grid 4 had semi-massive (50-70%) and massive (> 70%) sulphide. In the core from Grid 4, the common sulphides were pyrrhotite, chalcopyrite and pyrite. Sparse disseminated pyrite and chalcopyrite were observed on Grid 2s core. Fine-grained, sparsely disseminated free gold was also observed in core from Grid 2s. The geology and mineralization was plotted on log sheets and drill hole sections.

Geotechnical core logging was conducted before the drill core was split. The logging comprised geomechanical properties such as weathering, hardness, joint sets and their spacing, joint surfaces and filling material, faults, shear zones, and the overall ground condition. Heavily weathered rock and overburden were classified as bad ground, whereas hard, fresh rock with few fractures was designated as good ground. Geomechanical properties were recorded on the log sheets.

### **Drill Core Sampling and Preparation**

A diamond saw was used to half-split the entire length of core from each drill hole. One half of the split core was used in the initial sampling. Within the same lithology, the core was sampled at one-metre lengths. At contacts of contrasting lithologies or different concentrations of sulphide mineralization, the core was sampled to the contact. The other half of the split core was retained for petrological examination, ore microscopy and re-assay, if necessary. Core samples were allocated unique numbers to be used during assaying. Sample lengths and sample numbers were recorded on the log sheets and in Chembase database.

Core samples were crushed, pulverized to  $-75\mu$  and homogenized. Each sample was split into 3 x 200g for assay at three different laboratories. The remainder of the samples was retained for repeat analysis, if necessary. A duplicate sample was inserted within every 20 samples in a batch. A check standard sample or a blank sample was also inserted within every 25 samples in a batch.

## **Assays**

The samples were assayed at Eiffel Flats (Kadoma, Zimbabwe), GA Goldlabs (Pretoria, South Africa) and Omac (Ireland). The 50g Fire Assay + AAS method (Appendix B) was used for the gold assays. Copper and molybdenum assays were carried out using the aqua regia + ICP-MS method (Appendix C). Samples from some of the early drill holes were also assayed for arsenic using the aqua regia + ICP-MS method.

When analytical results were received, the assay values of duplicate samples, check standards and blank samples were used to check the precision and accuracy of the assay procedure, as described in Chapters 6 and 7. Comparisons were also made of the assay values given by the three laboratories. The assay values given by the three laboratories indicated the same mineralized intersections, with grades within the same ranges of magnitude.

## **Ore Resource Estimation**

The assay values were plotted on drill hole sections. On each section, correlation was made between the geology and mineralized zones of the drill hole and the trench. Where the holes were drilled in a fencing pattern, correlation was made from one drill hole to another. The correlation delineated the mineralized zones on the sections. In plan, the mineralized zones were correlated from one section to another.

Ore resource estimation was conducted to a vertical depth of 50 m below surface. Weighted average grades and true thickness of ore zones were calculated and used in the ore resource estimation. To estimate specific gravity, samples of ore were weighed in air and in water. The specific gravity was calculated as weight in air divided by apparent loss of weight in water. The volume of a mineralized zone was calculated to vertical depth of 50m, using the strike length, true thickness and inclined depth. Tonnage was calculated as a product of volume and specific gravity.

## **Petrography and Ore Microscopy**

On selected depths of the drill holes, the core was quarter-split and sampled for the preparations of thin sections and polished sections. Petrographic studies were carried out to determine the minerals, lithologies and the alteration present. Ore microscopy entailed the study of the various opaque minerals present, their textures, abundance and distribution.

## **GRID 4**

Figure 7.7 shows positions of the holes drilled on Grid 4. Fifteen inclined holes were drilled along an azimuth of 330°, approximately perpendicular to the 060° trend of the anomalies. Drill holes were numbered C4D1 and C4D3-16. The total drilled metreage was 2496 m, with an average core recovery of 95%. Core logging was conducted and the geology was plotted on 1:500 cross-sections. In general, the drill holes intersected, from south to north, (a) silicified basaltic granulite, (b) picritic rocks, (c) mylonite in shear zones within the silicified basaltic granulite, (d) feldspar porphyry veins/dykes, pegmatites and quartz veins in mylonite zones, (e) meta-andesite, and (f) garnet-biotite gneiss. Drill core was split and sampled. The samples, which numbered 2298, were assayed for gold and copper. Some of the samples, from holes drilled on the "Cu Shear", were also assayed for molybdenum. Assay results were captured into the Chembase database and plotted on drill hole sections. Mineralized drill hole intersections are shown on Table 8.12.

### **East Anomaly**

Some of the holes drilled on the East Anomaly are C4D3, C4D5, C4D12, C4D13 and C4D14. These holes provide typical cross-sections of the "Au Shear" and "Cu Shear" anomalies.

### **C4D3**

Figure 8.1 is a drill hole section for C4D3, which was drilled on the "Au Shear" to investigate the trench anomaly indicated on Traverse Line 16 400 E. The hole intersected mylonite, silicified basaltic granulite, basaltic granulite, feldspar porphyry veins/dykes and pegmatites. The vertical depth of the weathered zone was 24 m. The highest concentration of disseminated sulphide mineralization occurs in the feldspar porphyry veins/dykes, which form the mineralized zone. The hanging wall mylonites and mafic granulites occasionally host sparse, disseminated pyrite.

The gold mineralization occurs in a 10 m-wide feldspar porphyry within a mylonite zone and sheared silicified basaltic granulite. The feldspar porphyry is intruded by younger pegmatites. The feldspar porphyry intersected in the drill hole correlates with the mineralized porphyry veins/dykes exposed in the trench above. The mineralized zone dips 70° to the southeast, parallel to the foliation. Gold mineralization is associated mainly with pyrrhotite. Pyrite and chalcopyrite are also present. Higher sulphide concentrations occur in minor shears within the feldspar porphyry. As a result of varying sulphide concentrations, there are several zones grading above 1 g/t Au (up to 6 g/t Au), separated by zones of lower gold values. A single mineralized zone had a maximum thickness of 1.16 m. The peak copper value in this intersection was 851 ppm. In the other

holes drilled on the "Au Shear", the peak copper value was 1955 ppm (in C4D4). The molybdenum concentrations were very low, attaining a peak value of 15 ppm (in C4D3). In the other holes drilled on the "Au Shear", the peak Mo value was 155 ppm (in C4D4). The correlation between Au and Cu, Au and Mo, and Cu and Mo, is shown as Spearman rank correlation coefficients on Figure 8.1. Au has a fairly good correlation (+0.5515) with Cu, and a negative (-0.6970) or no correlation with Mo. Cu has a very weak correlation (+0.0182) with Mo.

Specimen RS 27 represents a sheared, mineralized feldspar porphyry intersected by C4D3. The rock has a bimodal texture of microperthite porphyroblasts and groundmass. The groundmass is composed of fine-grained quartz, microcline, microperthite, plagioclase feldspar, sericite, biotite, chlorite and sulphides. Late-stage ribbon quartz forms veins. The specimen has abundant (~30%) disseminated sulphides, which are mainly pyrrhotite and subhedral to euhedral pyrite, with subordinate chalcopyrite and chalcocite. The other opaque minerals are sphalerite and magnetite. In general, the sulphides are more abundant in ribbon quartz-rich bands, which are aligned parallel to sub-parallel to the foliation. Chlorite is closely associated with the sulphide mineralization. Chlorite alteration is typical of this mineralization.

Specimen RS 23 is a silicified basaltic granulite intersected by C4D3 in the hanging wall of the mineralized zone. The early-phase minerals are plagioclase feldspar, orthopyroxene and clinopyroxene. Late-stage ribbon quartz forms veins that are parallel to the foliation. Some of the plagioclase feldspar is being replaced by sericite. Hornblende and biotite are replacing the orthopyroxene. Magnetite is an accessory mineral, which occurs with the hornblende and biotite schistosity. Apatite is another accessory mineral in the rock. Late-stage calcite veins cross-cut the foliation.

#### C4D5

Hole C4D5 (Figure 8.2) was drilled on the "Au Shear" to investigate the trench anomalies indicated on Traverse Line 16 700 E (see Figure 7.7). The drill hole intersected leucomylonite, silicified basaltic granulite, basaltic granulite, basaltic amphibolite and garnet-biotite gneiss. The vertical depth of the weathered zone was 12 metres. Feldspar porphyry dykes/veins, which typically intrude the main shear zone and host the majority of the sulphides, were not intersected in this drill hole. The mineralized zone is in the main shear zone, where several, narrow zones of disseminated sulphides (< 5-50%) occur in schistose basaltic granulite and mylonite. The intersected true thickness of the mineralized zone is 13 metres. The schistosity is due to intense biotite alteration. A 5 cm-

wide semi-massive sulphide vein, comprising mainly pyrrhotite, occurs in the mineralized main shear zone. Pyrite, chalcopyrite and magnetite are the other ore minerals present in the mineralized zone.

Gold mineralization (>1 g/t Au) occurs in several, narrow schistose zones, which vary in intersected width from 0.50 to 1.95 metres. The peak value was 5 g/t Au (with 3355 ppm Cu) x 0.90 m. A semi-massive sulphide vein occurs in the mineralized shear with the peak value. Gold mineralization occurs where pyrrhotite is the dominant sulphide. This zone with the peak gold value correlates with the peak trench value of 10 g/t Au. On this section, the dip of the mineralized zone is 65° to the southeast. Sparse, disseminated pyrite (< 5%) and occasional molybdenite occur in the footwall and hanging wall lithologies.

Specimen RS 28 represents typical abundant (~ 40%) disseminated sulphide mineralization in a micaceous basaltic granulite from the shear zone. Sulphide mineralization is associated with late-phase quartz veining that cross-cuts early-phase plagioclase feldspar, orthopyroxene and clinopyroxene. In places, orthopyroxene reaction rims form between quartz glomero-porphyroblasts and the surrounding semi-massive sulphides. Biotite, which is the most abundant mineral, forms a schistose fabric that wraps around the early-phase minerals. Intense biotite alteration is characteristic of the mineralized zone. Sulphides cross-cut biotite. In polished section, the opaque minerals are subhedral pyrrhotite (po), pyrite (py), chalcopyrite (cpy), subhedral to euhedral magnetite, bismuth and a few, fine-grained gold grains. The order of abundance of the main sulphides is  $po > py > cpy$ . Magnetite is commonly associated with pyrrhotite.

Specimen RS 29 represents semi-massive sulphide mineralization in the micaceous basaltic granulite. Plagioclase feldspar, orthopyroxene and clinopyroxene are the early-phase minerals, which are crosscut by late-phase quartz veins, biotite and ore minerals. Quartz, which is cross-cut by biotite and opaque minerals, forms glomero-porphyroblasts in places. Red biotite, forms a schistose fabric that wraps around feldspar and quartz porphyroblasts. Excessive biotite alteration characterizes the mineralization. Semi-massive sulphides occur in the interstices of early-phase minerals and in veinlets. The sulphides also cross-cut the quartz veinlets. In polished section, the opaque minerals are pyrrhotite, euhedral pyrite, magnetite, chalcopyrite, sphalerite and bismuth. Pyrrhotite is the most abundant sulphide, followed by pyrite and chalcopyrite. Some of the pyrite grains have inclusions of the host mafic schist. In places, the rims of the chalcopyrite grains show alteration to covellite. A few grains of gold are associated with the sulphides.

Specimen RS 55 represents a leuco-mylonite in the immediate hanging wall to the mineralized zone. The early-phase minerals are microperthite, quartz, microcline, plagioclase feldspar and orthopyroxene. The rock has a stockwork, pseudo-mylonitic texture, with microperthite porphyroblasts having a lensoid shape. Late-stage quartz forms veins that are parallel or sub-parallel to the strong fabric. Garnet, which occurs as flattened porphyroblasts, is also a late-stage mineral. Late-stage, red biotite flakes are aligned parallel the fabric. In places, the microperthite is being altered to sericite. Orthopyroxene and garnet are being altered to chlorite. Abundant apatite is associated with the other alteration minerals. Ore minerals cross-cut the early-phase minerals and late-stage quartz veining. Sphene occurs as an accessory mineral.

Specimen RS 56 represents a pyroxene-rich basaltic granulite, which has undergone some amphibole alteration in the footwall to the mineralized zone. The early-phase minerals comprising orthopyroxene and clinopyroxene, are zoned into discrete bands that are parallel to the foliation. Plagioclase feldspar is another early-phase mineral. Quartz occurs as a late-stage mineral that forms veins. Late-stage hornblende also forms bands parallel to the foliation. Biotite is a late-stage mineral that occurs as abundant flakes parallel to the foliation. Ore minerals are late-stage and cross-cut the hornblende and biotite. The amphibole is a product of retrograde alteration of the pyroxenes. Tourmaline and apatite occur with the biotite. In places, the pyroxenes are being altered to chlorite. Ilmenite occurs with hornblende, indicating lower-amphibolite facies (Eilu *et al.*, 1997). Sphene is an accessory mineral.

Specimen RS 57 is a garnet-biotite gneiss in the footwall of the mineralized zone. The rock is strongly sheared and has alternating leucocratic and dark bands. Dark bands comprise plagioclase feldspar, quartz, garnet, biotite, pyrite and sphene. The feldspar is being altered to sericite. Biotite is late-stage and cross-cuts the feldspar, quartz and garnet. The biotite is ubiquitous and is being altered to chlorite. In addition to the above, the leucocratic bands contain an ortho-amphibole, microperthite and apatite. Leucocratic bands contain less biotite and pyrite. Garnet is skeletal and has quartz inclusions. In places, the amphibole is undergoing alteration to chlorite. In both bands, there is late-stage quartz veining with chloritized biotite at contacts. This is indicative of retrograde alteration and low temperature quartz veining.

#### C4D12

Hole C4D12 (Figure 8.3) was drilled on the "Au Shear" to test the soil anomalies indicated on traverse lines 16 800 E and 16900 E. The drill hole intersected silicified basaltic granulite, leuco-mylonite, meta-andesite, garnet-biotite gneiss, feldspar porphyry veins/dykes and pegmatites. The meta-andesite and the garnet-biotite gneiss contain calcite, biotite and chlorite as joint-filling material. Calcite also forms veinlets in the rocks. Biotite, chloritic and carbonate alteration is common in both rock types. The garnet-biotite gneiss has abundant brown garnets. The vertical depth of weathering is 22 metres.

Scattered, sparse (< 5%) pyrite mineralization was observed in all the lithologies, except pegmatites. A few narrow zones with abundant (>20%) disseminated pyrite, pyrrhotite and chalcopyrite, occur in the main feldspar-porphyry and in the meta-andesite below the garnet-biotite gneiss. There is no gold mineralization associated with these zones of elevated sulphide concentration. The peak value was 1.6 g/t Au x 1m, situated in a leuco-mylonite. Assay results indicate that east of Line 16 800 E, the gold mineralization becomes weaker. The gold mineralization was intersected over a strike length of 600 m, from Lines 16200 E to 16800 E. In the next exploration phase, further drilling is recommended, to investigate the down-dip continuity of this mineralization.

Specimen RS 63 was collected close to a contact between the garnet-biotite gneiss and the meta-andesite. Both rock types have a strong foliation, and late-phase ribbon quartz veining, calcite + chlorite veining, biotite and opaque minerals. Biotite cross-cuts the ribbon quartz veining. The garnet-biotite gneiss has more late-phase garnets, biotite, quartz veining and calcite + chlorite veining.

#### C4D13

Hole C4D13 (Figure 8.4) was drilled on both the "Au Shear" and the "Cu Shear". The hole was drilled to test the soil anomalies indicated on traverse lines 16 500 E and 16 600 E (see Figure 7.7). The hole intersected leuco-mylonite, silicified basaltic granulite, meta-andesite and pegmatites. The vertical depth of the zone of weathering was 40 metres.

Disseminated (< 5% to 30%) sulphide mineralization occurs in some parts of all the intersected lithologies. Pyrite is the dominant sulphide, but on the "Cu Shear" and "Au Shear", chalcopyrite and pyrrhotite are also present. Mineralization in the "Cu Shear", which had a peak of 1309 ppm Cu x 0.60m, was intersected over a width of 1.70 metres. In the "Cu Shear", the peak gold value was only 138 ppb. In the hanging wall to the "Cu Shear", the alteration minerals are calcite, chlorite and epidote. Mineralization in the "Au

"Shear" occurs in two zones, (a) an upper reef and (b) a lower reef. Reef (a) has an intersected width of 1.60 metres in basaltic granulite and within it is a peak value of (1.5 g/t Au, 788 ppm Cu) x 0.4m. Reef (b) has an intersected width of 2.0 metres in meta-andesite and within it is a peak value of (10 g/t Au, 402 ppm Cu) x 1m. The "Au Shear" is close to the contact of the silicified basaltic granulite and the meta-andesite.

Specimen RS 32 represents zone (b) in the "Au Shear". The early-phase minerals are orthopyroxene, plagioclase feldspar and fine-grained quartz. Late-stage quartz forms veins that cross-cut the early-phase minerals. Disseminated ore minerals are more abundant in the quartz veins than in the host meta-andesite. Biotite occurs as a late-stage mineral cross-cutting the early-phase minerals. The pyroxene and feldspar are intensively altered to chlorite, and sericite + zoisite, respectively. Calcite occurs in veins that cross-cut the early-phase minerals and the late-stage quartz veins. The specimen indicates retrograde alteration in the mineralization on Grid 4. In the polished section, the ore minerals are, in order of decreasing abundance, pyrrhotite, magnetite, chalcopyrite, euhedral pyrite and bismuth.

#### C4D14

Figure 8.5 is a drill hole section for C4D14, which provides a typical section across the "Cu Shear". The hole was drilled to investigate the soil anomaly indicated on Traverse Line 17 000 E. The hole intersected leuco-mylonite, silicified basaltic granulite, quartz veins and pegmatites. The vertical depth of weathering was 40 metres. Sulphide mineralization is mainly associated with the quartz veins, but also occurs in the intervening mylonites and mafic granulites. The concentration of the disseminated sulphides ranges from sparse (< 5%) to abundant (~30%). The sulphide mineralization comprises chalcopyrite, pyrite, pyrrhotite and molybdenite. Chalcopyrite is the most abundant sulphide.

Assay results indicate weak gold mineralization, with only one sample assaying above 1 g/t Au, i.e., (1.05 g/t Au, 417 ppm Cu, 168 ppm Mo) x 1m. This mineralized intersection is in sulphide-bearing mafic granulite. The peak copper value was 904 ppm x 1 m, associated with a mafic granulite schist close to a quartz vein. Copper values are elevated where the concentration of chalcopyrite ranges between 15 and 30%. The peak Mo value, which occurred in a quartz vein, was 633 ppm x 1m. The correlation between Au and Cu, Au and Mo, and Cu and Mo, is shown as Spearman rank correlation coefficients on Figure 8.4. Gold has a fairly good correlation (+0.5879) with copper, and

negative (-0.0061) or no correlation with molybdenum. Copper has negative (-0.5394) or no correlation with molybdenum.

Specimen RS 64 represents a quartz vein and wall-rock in the mineralized zone, with weak gold (0.6 g/t) and copper (479 ppm) mineralization, and the peak molybdenum value (633 ppm). The wall-rock is a tonalitic gneiss, which shows intense alteration of plagioclase feldspar to sericite. The thin section also shows garnet being altered to chlorite. Carbonate (calcite) alteration is associated with the chloritic alteration. Ore minerals are associated with the alteration zones. The quartz vein is late-phase and is parallel to the foliation. Abundant biotite, apatite, amphibole, garnet and chlorite alteration occurs between the host tonalitic gneiss and the quartz vein. Apatite and tourmaline are associated with biotite. Spinel is an accessory mineral in this zone. Ore minerals are late-stage and cross-cut the biotite. The biotite + sericite + amphibole + apatite + garnet + chlorite + calcite retrograde alteration is typical for the mineralization in the "Cu Shear". In the polished section, the ore minerals are chalcopyrite, pyrrhotite, pyrite, magnetite, chalcocite and molybdenite. Chalcopyrite is the dominant sulphide.

Specimen RS 65 represents a sulphide-bearing quartz vein with a xenolith of a mafic rock. The quartz vein has inclusions of microperthite and plagioclase feldspar, which are intensively altered to muscovite (sericite) and epidote. Sparse, anhedral to subhedral ore minerals are present in the quartz vein. In the xenolith, plagioclase feldspar is intensively altered to muscovite and epidote. A green spinel (hercynite or gahnite) occurs in the interstices of the saussuritized plagioclase. Other alteration minerals present are chlorite, biotite, apatite, monazite and calcite. Monazite is common at the contact of the quartz vein and the xenolith. Abundant ore minerals are associated with late-stage biotite. Ore minerals also cross-cut the green spinel. In the polished section, the ore minerals are chalcopyrite, pyrite, magnetite, bismuth and molybdenite.

Specimen RS 33 represents a quartz vein in a mafic granulite. Early-phase plagioclase feldspar and orthopyroxene are almost completely altered to sericite and zoisite respectively. Chlorite is also replacing garnet. Quartz is late-phase and forms the veins. The opaque minerals occur with the quartz, feldspar and biotite. The biotite is late-phase and cross-cuts early-phase minerals and ore minerals. Zoisite and a small amount of calcite occur close to the quartz vein and ore minerals. The alteration assemblage comprises chlorite + sericite + zoisite + calcite. The polished section shows that the ore minerals are subhedral to euhedral chalcopyrite and euhedral pyrite.

### **West Anomaly**

C4D6, C4D7 and C4D9 are some of the holes drilled on the West anomaly, where the "Au Shear" and the "Cu Shear" are concurrent. The holes were drilled to investigate trench anomalies on traverse lines 15100E, 15200 E and 15000 E respectively (see Figure 7.7).

### **C4D6**

Figure 8.6 is a drill hole section for C4D6, which was drilled under the peak (35 g/t Au, 0.2% Cu x 1m) of the trench anomalies of Grid 4. The hole intersected silicified basaltic granulite, a picritic rock, leuco-mylonite, feldspar porphyry veins/dykes, pegmatite and dolerite dykes. The vertical depth of weathering was 37 metres.

Semi-massive (~60%) sulphide mineralization occurs in two of the feldspar porphyry veins/dykes. Disseminated (< 5% to 20%) sulphide mineralization is also present in the hanging wall mylonite and the footwall mafic granulite. Disseminated sulphides (pyrite and pyrrhotite) occur along foliation planes. Intersected widths of the semi-massive sulphide zones were (a) 0.53 m and (b) 1.95 m. The zones assayed 40 g/t Au, 0.27% Cu, <1 ppm As; and up to 21 g/t Au, 0.22% Cu, <1 ppm As, respectively. The semi-massive sulphides, comprising pyrrhotite, chalcopyrite and pyrite, occur as blebs in sheared grey quartz within the feldspar-porphyry. Magnetite also occurs with the sulphide mineralization. The entire mineralized zone, with a true thickness of 3 metres, is situated within a shear zone in the mafic granulite. Leuco-mylonite is part of the shear system. Correlation between the mineralized intersection in the drill hole and the peak of the trench anomaly, indicates that the reef dips 72° southeast. Within the shear zone, the foliation planes and joint surfaces have chlorite and calcite. Calcite veining is present in the immediate hanging wall of the mineralized zone.

Specimen RS 30 represents silicified basaltic granulite between feldspar porphyry veins/dykes in the mineralized zone. The rock contains semi-massive sulphides and was obtained from the immediate hanging wall to zone (a) above. In thin section, the early-phase ortho-pyroxene and plagioclase feldspar are being altered to biotite and sericite, respectively. Late-phase, fine-grained quartz occurs as veins that cross-cut early-phase minerals. Sulphides form semi-massive aggregates that cross-cut the pyroxene and feldspar. Sulphide mineralization occurs in the quartz veins and wall-rock. Late-phase biotite, which cuts the sulphides, forms a schistose fabric that wraps around the early-phase minerals. Chlorite, Fe-rich carbonate (ankerite), biotite, serpentine, hornblende

and colourless amphiboles are secondary alteration minerals, which are associated with the ore.

Specimen RS 45 is a mineralized leuco-mylonite from the trench above hole C4D6. The rock is strongly sheared and comprises ribbon quartz veining, microperthite porphyroblasts, sulphides, and accessory amounts of biotite, plagioclase feldspar and sphene. Microperthite porphyroblasts are stretched and lensoid, and seem to be a result of K-feldspar alteration where they are replacing sericite. The majority of the sulphides occur in pressure shadows either side of microperthite porphyroblasts, indicating a strong structural control on the mineralization. Some of the biotite occurs with the microperthite and sulphides in the pressure shadows. Quartz veining, which comprises quartz and biotite, cross-cuts the microperthite porphyroblasts. Some of the sulphides are in late-stage quartz veins. The rock has K-feldspar and biotite alteration. In polished section, the ore minerals are pyrite, chalcocopyrite, pyrrhotite, magnetite and bismuth.

#### C4D7

Figure 8.7 is a drill hole section for C4D7. The hole intersected a picritic rock, dolerite, leuco-mylonite, feldspar porphyry veins/dykes, and silicified basaltic granulite. The sequence of the lithologies is similar to that for C4D6. The vertical depth of the weathering was 34 metres. The mineralized zone is in two feldspar porphyry veins/dykes, which have narrow zones (up to 0.25m) of semi-massive sulphides. Pyrite, pyrrhotite and chalcocopyrite constitute the semi-massive sulphides. The peak values in the semi-massive sulphides were 3.6 g/t Au x 0.50m, and 780 ppm Cu x 0.20m. Correlation between the mineralized zone in the drill hole and that in the trench, indicates that the zone dips southeast at 70°. The entire mineralized zone has a true thickness of 5 metres. Disseminated (< 5% to 50%) sulphides (mostly pyrite) occur in the hanging wall mylonite and footwall mafic granulite. Other disseminated sulphides are pyrrhotite and chalcocopyrite. Gold values in the disseminated sulphide zones are less than 0.5 g/t, since the amount of pyrrhotite is not high enough. Calcite veining is common in the feldspar porphyry. In the footwall mafic granulite, the alteration minerals are biotite, calcite and chlorite.

#### C4D9

Figure 8.8 is the drill hole section for C4D9. The hole intersected a picritic rock, dolerite, leuco-mylonite, silicified basaltic granulite, meta-andesite and garnet-biotite gneiss. The vertical depth of the weathered zone was 32 metres. Zones of disseminated (< 5% to 50%) sulphide mineralization (mostly pyrite) occur in the mylonite, mafic granulite, meta-

andesite and garnet-biotite gneiss. Pyrrhotite and chalcopyrite are also present in lesser amounts. A 45 cm-wide semi-massive sulphide zone occurs near the lower contact of the meta-andesite. The semi-massive sulphide zone contains pyrrhotite, pyrite and chalcopyrite. However, all the samples from the entire length of the hole, assayed less than 0.55 g/t Au. All the copper values were less than 350 ppm. The mineralization (up to 1.6 g/t Au) indicated in the trench was not reproduced in the drill hole. The feldspar porphyry veins/dykes, intersected in C4D6 and C4D7, were not present in C4D9. Similarly, drill hole C4D8, east of C4D7, did not intersect the feldspar porphyry. Therefore, in the West Anomaly, the indicated length of the reef is approximately 250 metres. Further drilling is recommended, to investigate the down-dip continuity of the mineralization.

Chlorite is the most abundant alteration mineral along the entire length of the hole. A 5 metre-wide zone of chloritic meta-andesite occurs near the sheared upper contact of the lithology. In shear zones at or close to contacts of lithologies, the alteration minerals are calcite and chlorite. In the mafic granulite, biotite is also a common alteration mineral. Garnet is ubiquitous in the garnet-biotite gneiss.

Specimen RS 59 is a meta-andesite near the upper contact of the lithology. The early-phase minerals comprise orthopyroxene, clinopyroxene, plagioclase feldspar and quartz. The pyroxenes occur in alternating zones of compositional banding. Quartz occurs as late-stage veining. Biotite is late-stage and occurs with the quartz veining. Sulphides are mostly associated with the biotite and pyroxenes. Apatite and sphene are accessory minerals.

Specimens RS 31 and RS 61 represent garnet-biotite gneiss. They are similar to RS 57, which is a garnet-biotite gneiss from C4D5. However, RS 31 and RS 61 contain more quartz, microcline, microperthite and calcite alteration. In the dark bands, biotite is late-stage and cross-cuts garnet porphyroblasts, feldspars and sulphides. In the leucocratic bands, some of the plagioclase feldspar is being altered to sericite. The leucocratic bands contain more garnet and chlorite.

Specimen RS 62 represents a leuco-mylonite near the top of the hole. The early-phase minerals comprise microperthite porphyroblasts, microcline, quartz, plagioclase feldspar and a few grains of orthopyroxene. Sphene and zircon are accessory minerals. Late-stage ribbon quartz veining cross-cuts the early-phase minerals. Microperthite is being altered to sericite, and is in places, cross-cut by veins with sericite. Plagioclase feldspar

has undergone saussuritization to zoisite and sericite. Chlorite is the other alteration mineral.

### **Mineralized Zones and Ore Resource Estimation**

Mineralized drill hole intersections and ore resource estimations are listed in Table 8.12. A specific gravity of 2.9 t/m<sup>3</sup> was used in tonnage estimation. In the East Orebody, gold values above 1 g/t indicate ore zones that can be up to 3 in number, as in C4D4. The ore zones commonly occur in feldspar-porphyry dykes and the immediate sheared wall rocks. The orebody has a strike length of 1000 metres (16150E- 17150E), a dip of 70° SE and an average aggregate true thickness of 2.11 metres. In the orebody, the tonnage down to 50 m below surface, is estimated to be 325 531 t, with a weighted average grade of 2.98 g/t Au. Within the orebody, the main reef with the peak gold values (up to 10 g/t) attains a strike length of 700 metres (16150E-16850E) and an average true thickness of 1.03 metres. The main reef has an estimated tonnage of 111 236 t and a weighted average grade of 5.62 g/t Au.

In the West Orebody, the gold mineralization occurs in one zone, which is hosted in a feldspar-porphyry dyke and the immediate wall rocks. The ore zone, which at dips 70° SE, attains a strike length of 200 metres (15050E-15250E) and an average true thickness of 1.15 metres. The estimated tonnage (to 50 m below surface) and weighted average grade are 35 484 t and 12.3 g/t Au, respectively.

In all, the Grid 4 Deposit has a total strike length of 1200 metres and an average true thickness of 1.63 metres. Ore resource estimation to a depth of 50 metres below surface, indicate a tonnage of 361 015 t with a weighted average grade of 6.27 g/t Au. A few drill holes, which intersected the reefs at lower elevations (such as at -150 m in C4D13), indicate down-dip continuity of the gold mineralization. It is recommended that more holes be drilled to intersect the reefs at various elevations to enable estimation of proven ore reserves. Some of the proposed drill holes are shown on the drill hole sections. Considering the total strike length and average true thickness, the Grid 4 Deposit has the potential for a medium-scale gold mine.

### **Wall-rock Alteration**

In Grid 4, the envelope of the alteration halo is narrow, generally not exceeding 200 metres in horizontal width. In drill hole sections, the envelope is marked by the first appearance of pyrite. In the East Anomaly, the horizontal width of the alteration zone varies from 35 to 145 metres in the hanging wall, and from 40 to 50 metres in the

footwall. In the West Anomaly, the horizontal width varies from 12 to 42 metres in the hanging wall, and from 10 to 55 metres in the footwall. The alteration assemblages are shown on Appendix D.

In all the lithologies in the alteration zone, the most abundant alteration minerals are biotite (biotitic alteration), ribbon quartz (silicification), pyrite (sulphidation) and chlorite (chloritic alteration). Orthopyroxene (hypersthene) is present in the majority of the lithologies, which include mafic granulites, meta-andesite, charnockite and leuco-mylonite. Although it is undergoing alteration to amphiboles, biotite or chlorite, the orthopyroxene indicates lower-granulite facies (Eilu *et al.*, 1999). Biotite and ribbon quartz occur throughout the alteration zone, and become more intense in the mineralized shear zones. The biotite is normally among the earliest hydrothermal events in the formation of a porphyry mineral deposit and may precede or accompany the main-stage alteration and mineralization (Thompson and Thompson, 1996). The presence of hydrothermal biotite denotes prograde lower- to upper-amphibolite facies. Chlorite is more common in the mineralized feldspar porphyry, leuco-mylonite and quartz veins, and also in the wall-rock meta-andesite and garnet-biotite gneiss. Chlorite, which denotes upper-greenschist to lower-amphibolite facies (Eilu *et al.*, 1997), indicates retrograde overprinting alteration of hydrothermal biotite (Thompson and Thompson, 1996).

Other minerals fairly common in the alteration halo are sericite, magnetite, pyrrhotite, calcite, apatite and garnet. The least abundant alteration minerals are hornblende, tremolite-actinolite, tourmaline, zoisite, serpentine, microperthite, ilmenite, ankerite, monazite and hercynite/gahnite.

#### Distal Alteration Zone

All the rock types in the distal alteration zone contain ribbon quartz and biotite as the main alteration minerals. The mafic granulites (RS 23 and RS56) contain hornblende, sericite, magnetite, calcite, apatite, chlorite, tourmaline, pyrite, ilmenite and serpentine, as additional alteration minerals. In the meta-andesite (RS 59), the other alteration minerals are apatite, pyrite and pyrrhotite. The leuco-mylonite (RS 55, RS 62) contains chlorite, sericite, zoisite, apatite and pyrite, as the additional alteration minerals. In the garnet-biotite gneiss, (RS 57, RS 61 and RS 63), the additional alteration minerals are chlorite, tremolite-actinolite, sericite, garnet, apatite, pyrite, pyrrhotite and calcite.

Apatite is a common secondary mineral in high-temperature hydrothermal alteration zones (Thompson and Thompson, 1996). Tourmaline occurs in quartz vein envelopes in

the "Cu Shear", and is associated with biotite in the "Au Shear". The presence of orthopyroxene in meta-andesite, garnet-biotite gneiss, leuco-mylonite and mafic granulite indicates prograde lower-granulite facies. Retrograde minerals are common in the distal alteration zone. Chlorite, sericite and zoisite are retrograde minerals formed by the partial replacement of pyroxenes, amphiboles and feldspars. The chlorite is also replacing garnet. The occurrence of pyrite together with pyrrhotite, indicates lower-amphibolite facies (Eilu *et al.*, 1999). At upper-amphibolite to lower-granulite facies, only pyrrhotite would be present. The presence of calcite in the distal zone also indicates lower-amphibolite facies.

#### Proximal Alteration Zone

The proximal alteration zone is within the envelope of the mineralized zones. In the "Au Shear", the zone is in the mineralized feldspar porphyry veins/dykes, micaceous mafic granulite and leuco-mylonite. In the "Cu Shear", the zone is in the mineralized quartz veins. Ribbon quartz and biotite alteration is dominant in all the lithologies in the proximal zone. In the proximal zone, the silicic and biotite alteration is more intense than in the distal zone. The leuco-mylonite and mafic granulites contain orthopyroxene, which indicates prograde lower-granulite facies.

In the "Au Shear", the additional alteration minerals in the feldspar-porphyry (RS 27) are chlorite, sericite, magnetite, pyrite and pyrrhotite. In drill hole C4D7, the feldspar porphyry also contains carbonate (calcite) alteration. The leuco-mylonite (RS 45) contains potassium feldspar (microperthite), magnetite, pyrite and pyrrhotite. In the micaceous mafic granulites (RS 28, RS29 and RS 30), the additional alteration minerals are calcite, ankerite, chlorite, hornblende, tremolite-actinolite, sericite, magnetite, pyrite and pyrrhotite. A few free gold grains and bismuth occur with the semi-massive sulphides. The meta-andesite contains chlorite, sericite, zoisite, calcite, magnetite and pyrite.

K-feldspar and intense biotite alteration is early and occurs in the high temperature, cores of porphyry deposits (Thompson and Thompson, 1996). Biotite is typically more abundant in the mafic to dioritic host rocks and the K-feldspar is predominantly in the felsic host rocks. Biotite alteration may be earlier or coeval with the mineralization. The concentration of sulphides increases gradually towards the gold bearing shears and veins/dykes, and is highest in the economic ore. The amount of pyrrhotite is greater than that of pyrite. Pyrrhotite and pyrite are partially replacing magnetite. In the vein envelopes, Fe-Mg carbonate (ankerite) is proximal and calcite is more distal. Retrograde alteration is indicated by the presence of chlorite, sericite and zoisite. The presence of

native bismuth, which is a low-temperature ore mineral, may reflect subsolidus reactions between the originally high-temperature minerals under retrograde conditions (Eilu *et al.*, 1999). The presence of a significant amount of pyrite also indicates post-peak, lower-amphibolite metamorphic conditions.

In the "Cu Shear", the proximal zone comprising quartz veins and immediate wall-rocks (RS 64, RS 65 and RS 33), contains ribbon quartz, biotite, chlorite, tremolite-actinolite, sericite, tourmaline, garnet, magnetite, calcite, apatite, monazite, zoisite, pyrite and pyrrhotite.

The presence of orthopyroxene, in the host charnockite and mafic granulite, indicates prograde lower-granulite facies conditions. The apatite is a common secondary mineral in high-temperature hydrothermal alteration zones (Thompson and Thompson, 1996). Monazite is another phosphate mineral associated with the apatite. Chlorite, sericite, tremolite-actinolite and zoisite, indicate retrograde conditions. The presence of bismuth, which is a low-temperature ore mineral, also indicates retrograde conditions. The occurrence of both pyrrhotite and pyrite, in the proximal zone, indicates lower-amphibolite facies conditions (Eilu *et al.*, 1999). Tourmaline, which occurs in the quartz vein envelopes and with the biotite alteration, is typical of the Cu-Mo deposits (Thompson and Thompson, 1996), such as the "Cu Shear".

#### **8.4 GRID 2s**

Figure 7.16 shows collar positions of holes drilled in Grid 2s. The holes were drilled on a fencing pattern (a) on traverse lines 10000 E and 10800 E, and (b) on longitudinal section 8025 N, between lines 9800 E and 10200 E. On each of these traverse lines, five holes were drilled with inclinations of  $-60^\circ$  towards  $335^\circ$ . Each hole was drilled to an average depth of 100 metres. However, on Traverse Line 10000 E, hole C2D6 drilled to a depth of 227.20 metres. In the longitudinal section 8025 N, two holes inclined at  $-50^\circ$  towards  $245^\circ$ , were drilled to a depth of 350 metres each. In all, twelve holes were drilled on Grid 2s. The total drilled metrage was 1853.66 m, with an average core recovery of 96%. At the end of the duration of this study, some of the targets had not yet been investigated by drilling. In the next phase of exploration, further drilling needs to be carried out to investigate the other targets.

Core logging was carried out and the geology was plotted on 1:500 sections. The intersected lithologies include charnockite, leuco-mylonite, K-feldspar granite, pegmatites and quartz veins/stringers. Drill core was split and 1945 samples were collected. The

samples were assayed for gold and copper. Samples from some of the early holes were also assayed for arsenic. Assay values were captured into the Chembase database and plotted on the drill hole sections. Correlation of lithologies and mineralized zones was carried out from one drill hole to the next. Mineralized drill hole intersections are shown on Table 8.13.

### **Cross-Section 10800 E**

Figure 8.9 is a section for drill holes C2D1 to C2D5 on Traverse Line 10800 E. The holes were drilled to investigate a 200 metre-wide soil gold anomaly. The peak of the soil anomaly was 560 ppb Au. The holes intersected charnockite in the south and a wide K-feldspar granite in the north. Holes C2D2 and C2D3 intersected a wide (up to 8m thick) quartz vein. North of the quartz vein, the holes intersected numerous quartz veinlets and stringers in K-feldspar granite. The drill holes also intersected a dolerite dyke, leucogneisses in charnockite, and pegmatites in K-feldspar granite. The vertical depth of the weathered zone varied from 7m in the south to 14m in the north.

Zones of very sparse to sparse (< 5%), disseminated sulphide mineralization were intersected in all of the holes. A few isolated zones contain moderately (5-20%) disseminated sulphides. The sulphides are predominantly pyrite and pyrrhotite. Chalcopyrite is less common, having been observed mainly in charnockite. Sulphides occur as clusters associated with the few mafic grains (such as chlorite) that are present. The clusters are spatially aligned along foliation planes. The K-feldspar granite has abundant quartz stringers. Some of the quartz stringers have fine-grained free gold. A number of mineralized zones occur close to the south contact of K-feldspar granite. The mineralized zones are parallel to the foliation and dip southeast at 75°.

The widest mineralized zone, **A**, was intersected by drill hole C2D4. The zone has a weighted average grade of 0.92 g/t Au x 26 m. The true thickness of the mineralized is 19 metres. Several individual values within this zone, are between 1.0 g/t and the peak of 6.6 g/t Au. In this zone, the majority of the values of the values are greater than 0.50 g/t Au. Zone **A** is in a sheared K-feldspar granite and charnockite, which both have quartz stringers. In Zone **A**, the charnockite hosts the highest values. C2D4 and C2D5 intersected Zone **B**, which has a true thickness of 4.5 metres. The peak value in Zone **B** is 4.5 g/t Au x 1m. A narrow mineralized zone in C2D5, between zones **A** and **B**, assayed up to 27 g/t Au x 0.45 m, which is the peak value on Section 10800 E. The narrow zone is in a K-feldspar granite with more intense shearing. Several other narrow mineralized zones occur in the K-feldspar granite. In all the drill holes, the copper values were very

low (<300 ppm). The correlation between the Au and Cu values is shown as a matrix on Figure 8.9. There is negative (-0.5273) or no correlation between gold and copper. The majority of the arsenic values are <1 ppm, even within the zones of gold mineralization. The peak arsenic value was 29 ppm. There is no correlation between Au and As, or Cu and As. During the next phase of exploration, further drilling is recommended, to investigate zones **A** and **B** plus the intervening width, both along strike and down-dip.

The main mineralized zones, which are south of the wide quartz vein, occur in a 78 metre-wide zone of minor calcite veining and joint-filling. The secondary carbonatization occurs mostly as joint-filling material than as veins. Where present, the calcite veinlets are in narrow zones with true widths of up to 1.9 metres. The zone of carbonatization is also characterized by chlorite and biotite alteration. Chlorite is the dominant alteration mineral in the zone and the hanging wall charnockite. North of Zone **A**, the wide quartz vein and the numerous quartz veinlets/stringers do not contain gold mineralization, except for one narrow zone in C2D2. These quartz veins and stringers are a result of silicic alteration, which is also associated with barren pyritic alteration.

Specimen RS 34 is a charnockite from the K-feldspar granite in mineralized Zone **A**. Early-phase minerals are quartz, microcline, orthopyroxene and minor plagioclase feldspar. Potash feldspar also occurs as microperthite porphyroblasts, which are being altered to sericite. Muscovite occurs as a secondary alteration mineral. Calcite is with the sericite alteration. Late-stage ribbon quartz veining is parallel to the foliation. The orthopyroxene is being altered to biotite, which crosscuts the feldspars. Some of the biotite is being altered to chlorite. Very sparse, disseminated sulphides are closely associated with altered orthopyroxene, biotite and ribbon quartz veining. A green spinel (hercynite or gahnite) is also present. The rock is a K-feldspar Charnockite with K-feldspar + biotite + sericite (muscovite) + calcite + quartz alteration. In polished section, the ore minerals are subhedral pyrite, pyrrhotite, chalcopyrite, magnetite and minor sphalerite. Pyrite is the most abundant ore mineral.

Specimen RS 50 is a quartz vein in K-feldspar granite of mineralized Zone **A**. The host K-feldspar granite comprises microperthite porphyroblasts, fine-grained quartz, microcline, plagioclase feldspar, biotite, chlorite, garnet and accessory sphene. The microperthite is being altered to sericite. Calcite is associated with the sericite alteration. Quartz veining is a late-phase, coarse-grained stockwork. The silicic alteration post-dates the K-feldspar alteration in the host rock. Sericite, calcite and ore minerals also occur with the quartz veining. Ore minerals are commonly associated with biotite and chloritic bands in the

foliation. There are fewer opaque minerals in the felsic groundmass. The rock has typical Grid 2s deposit alteration, which comprises K-feldspar + quartz + sericite + calcite + chlorite.

Specimen RS 37 is a K-feldspar granite from mineralized Zone **B**. The early-phase minerals are fine-grained quartz, microcline and plagioclase feldspar. Microperthite occurs as porphyroblasts. Potash feldspar is more abundant than plagioclase. Some of the plagioclase is being altered to sericite. Ribbon quartz forms late-stage veins. Biotite occurs as an accessory, late-stage mineral that cross-cuts the early-phase minerals. Other minerals present are garnet, chlorite, zircon and rutile. Rutile needles are associated with chlorite, which is replacing garnet. Late-stage euhedral sulphides are closely associated with chlorite and biotite. In polished section, the ore minerals are fine-grained, sparse, disseminated pyrite, chalcopyrite and magnetite. Pyrite is the more abundant sulphide. A few gold grains, which are fine-grained, are associated with pyrite.

Specimen RS 38 is a K-feldspar granite in the immediate footwall to mineralized Zone **B**. Early-phase minerals are fine-grained microcline, quartz, plagioclase and antiperthite. Microperthite occurs as porphyroblasts. Coarse-grained quartz forms late-stage veins. Biotite is a late-stage mineral that crosscuts the early-stage minerals. Chlorite is replacing biotite. Sparse disseminated ore minerals are mainly associated with the quartz veining.

Specimen RS 39 is a K-feldspar granite in the narrow, mineralized high-grade (27 g/t Au x 0.45m) zone between zones **A** and **B**. The early-phase minerals are microcline and fine-grained quartz. Microperthite occurs mainly as porphyroblasts. Late-stage ribbon quartz forms veins and stringers parallel to the foliation. Potash feldspars are being replaced by sericite. Late-stage biotite cross-cuts early-phase feldspars and quartz. Chlorite and calcite alteration is also present. Ore minerals are concentrated in zones with abundant biotite and chlorite, adjacent to quartz veining. In polished section, the ore minerals are pyrite, pyrrhotite, chalcopyrite and magnetite. A few, fine-grained gold grains are associated with the quartz veining.

Specimen RS 51 is a pegmatitic vein adjacent to RS 39. The main constituent minerals are microperthite, fine-grained quartz, ribbon quartz, microcline and plagioclase. The rock is pegmatitic due to graphic intergrowth between microperthite porphyroblasts and quartz. Ribbon quartz forms late-stage veins that cut early-phase fine-grained feldspars and quartz. Sericite is replacing some of the microperthite. Late-stage biotite occurs in bands, which are parallel or sub-parallel to the foliation and cross-cut the early-phase

minerals. Some of the biotite is undergoing alteration to chlorite + rutile. Calcite alteration is also present. A few garnet porphyroblasts occur in the pegmatitic vein. Opaque minerals are closely associated with biotite and chlorite. In polished section, the ore minerals are pyrrhotite, pyrite, chalcopyrite and fine-grained free gold.

Specimen RS 35 is a K-feldspar granite at the upper contact of the lithology. The early-phase minerals are microcline, fine-grained quartz and minor plagioclase feldspar. Microperthite is the other K-feldspar present. Late-stage ribbon quartz forms veins parallel to the foliation. Biotite, garnet, chlorite and sulphides are late-stage accessory minerals. Sphene also occurs as accessory mineral. The sulphides are pyrite, pyrrhotite and chalcopyrite.

Specimen RS 36 is a leucogneiss (leucosome) within the K-feldspar granite intersected by C2D5. The minerals are microperthite porphyroblasts, microcline, fine-grained quartz, late-stage coarse-grained quartz, garnet porphyroblasts and sparsely disseminated sulphides. Ribbon quartz forms discontinuous veins. Some of the K-feldspar is undergoing alteration to sericite. The sulphides are pyrite, pyrrhotite and chalcopyrite.

Specimen RS 52 is a K-feldspar granite in the hanging wall of the mineralized zones. The early-phase minerals are microcline, plagioclase feldspar, and fine-grained quartz. Perthite, microperthite and antiperthite porphyroblasts are also present. The microcline has graphic intergrowth with quartz. Late-stage ribbon quartz forms veins parallel to the foliation. The quartz veining indicates intensive silicic alteration. The potash and plagioclase feldspars are undergoing alteration to sericite + calcite. Chlorite is another alteration mineral. Late-stage biotite and sulphides form in bands that crosscut the early-phase minerals and the quartz veining. The sulphides are pyrite, pyrrhotite and chalcopyrite. Sphene occurs as an accessory mineral. Sillimanite occurs as prismatic crystals and commonly surrounds the ore minerals.

#### **Cross-Section 10 000 E**

Figure 8.10 is a section for holes C2D6 to C2D10 drilled on Traverse Line 10000 E. The holes were drilled to investigate the trench anomalies indicated on the traverse line. The peak of the trench anomalies was 14 g/t Au. Charnockite, K-feldspar granite, pegmatites and quartz veins are the lithologies intersected by the holes. The vertical depth of the weathered zone varied from 5 to 29 metres. Depths of the overburden also varied from 1.5 to 12 metres.

The holes intersected several, scattered zones of very sparse (< 5%) to abundant (20%) disseminated sulphides. Pyrite is the most common sulphide present. Pyrrhotite and chalcopyrite are the other sulphides present. The sulphides are closely associated with clusters of biotite and chlorite, which are aligned along foliation planes. Numerous quartz veinlets/stringers in K-feldspar granite, were intersected by hole C2D6. Some of the stringer zones contain consistent widths of disseminated sulphides, which however, lack gold mineralization. The majority of the mineralized zones occur in the charnockite.

Drill hole C2D10 intersected the widest zone of gold mineralization. The 8 metre-wide zone, which is at the interface of weathered and fresh rock, has a peak value of (2.98 g/t Au, 9 ppm Cu) x 0.81m. Within the zone, the other values are above 0.3 g/t Au x 1m. In fresh rock, the peak gold value for core samples was 4.7 g/t Au x 1m. There appears to be some surface enrichment of gold concentration as the trench values had much higher magnitudes (up to 14 g/t Au x 1m). Between C2D6 and C2D8, where the overburden is thick, the trench anomalies do not quite coincide with the projected drill hole intersections. This suggests some lateral movement of the soil and overburden.

Correlation of the mineralized zones from one hole to the next, e.g. C2D8 to C2D9, indicates that the zones dip 75° southeast, parallel to the foliation. Copper values are very low and generally less than 50 ppm. In similarity to Section 10800 E, there is no correlation between the gold and copper values. In the next exploration phase, further drilling is warranted to investigate the strike and down-dip extents of the mineralized zones. The azimuths of the holes should be perpendicular to the strike indicated by the trench anomalies.

The alteration observed on drill core includes K-feldspar, quartz, biotite, calcite, chlorite, pyrite, pyrrhotite and garnet. Calcite alteration is secondary, occurring mainly as joint-filling material, but also occasionally as veining. Biotite and chloritic alteration is more common in charnockite, whereas K-feldspar alteration is more developed in K-feldspar granite.

#### **Longitudinal Section 8025 N**

Figure 8.11 is a longitudinal section with drill holes C2D19 and C2D20. The holes were drilled on a local grid northing of 8025 N, between traverse lines 9800 E and 10200 E (see Figure 7.16). The two holes were drilled to investigate a wide (up to 800 m wide) soil gold anomaly between traverse lines 9800 E and 10200 E. Lithologies intersected are charnockite, K-feldspar granite, ultramafic intrusives, pegmatites and quartz veins. Most of the quartz veins occur in K-feldspar granite intersected by drill hole C2D20. Some of

the quartz veins contain sparse, fine-grained disseminated free gold. The vertical depth of the weathered zone is 11 metres.

Both drill holes intersected scattered zones of sparse (<5%) disseminated sulphides. Drill hole C2D20 intersected more sulphide zones than C2D19. The sulphides are pyrite and pyrrhotite, with the former being the dominant type. Sulphides occur as clusters associated with chlorite and biotite. In C2D19, the gold values were low and less than 0.75 g/t Au. Gold mineralization was intersected in C2D20 only, where the peak value was 16.6 g/t Au x 1.24m. Gold mineralization does not seem to be associated with the sulphides, but occurs in some of the quartz veins and quartz stringer zones. Several zones with gold mineralization occur between inclined depths of 70 and 165 metres. Individual mineralized zones are narrow and have apparent widths ranging from 0.5 to 1.5 metres, as the drill hole intersected zones at an oblique angle. The gold mineralization is spiky and separated by low-grade zones. Copper values are very low and generally less than 50 ppm, except in the ultramafic intrusive, where values are up to 252 ppm. The sample with the peak gold value (16.6 g/t Au) only assayed 16 ppm Cu. In similarity to Section 10800 E, there is no correlation between the gold and copper values. Alteration minerals observed on drill core include K-feldspar, biotite, chlorite, calcite, quartz, pyrite, pyrrhotite, garnet and epidote. The K-feldspar granite has intense potash feldspar alteration and secondary calcite veining. During the next exploration phase, drilling is recommended to investigate the strike and down-dip extents of the mineralized zones. The azimuths of the holes should be perpendicular to the strike indicated by trench anomalies.

Specimen RS 40 is a mineralized quartz vein that assayed 16.6 g/t Au. Quartz constitutes approximately 99% of the rock. The quartz grains are elongate and parallel to the foliation. Muscovite, calcite and chlorite are accessory, alteration minerals. Calcite occurs together with the muscovite. In polished section, fine-grained gold forms sparse clusters.

Specimen RS 53 is another mineralized quartz vein that assayed 2.0 g/t Au. Quartz forms approximately 97% of the rock. The other minerals present are muscovite, chlorite, calcite, microperthite, plagioclase feldspar, garnet and a few gold grains. The muscovite and calcite occur together in zones that are parallel to the foliation. Chlorite, muscovite and calcite are replacing the garnet. Muscovite is also replacing the feldspars. In places, the calcite is replacing muscovite. Calcite also forms late-stage veins that cross-cut the quartz grains and foliation.

Specimen RS 54 is a mineralized aplitic vein that assayed 5.9 g/t Au x 1m. The vein is in K-feldspar granite and contains ribbon quartz, microcline, sericite and calcite. The wall-rock is composed of microperthite, microcline, quartz, garnet, plagioclase, chlorite, hornblende, muscovite (sericite), calcite and gold. Chlorite is replacing garnet. Chlorite, sericite and calcite are concentrated in late-stage veins that cross-cut the foliation. Sillimanite occurs in late-stage veins, and is closely associated with garnet.

### **Mineralized Zones and Ore Resource Estimation**

Mineralized drill hole intersections and ore resource estimations are listed in Table 8.13. A specific gravity of 2.8 t/m<sup>3</sup> was used in tonnage estimation. In the Grid 2s Deposit, gold values above 1 g/t Au indicate 3 orebodies, which are Southwest, North Central and Northeast (described in Chapter 7). Gold mineralization occurs mostly in quartz veins/veinlets and occasionally in the wall rocks comprising felsic mylonites and K-feldspar granite. In all of the orebodies, the majority of quartz veins dip at 75° SE. Quartz stoneline ore overlies these *in-situ* orebodies.

In the Southwest Orebody, the reefs attain a strike length of 700 metres and a combined average true thickness of 4.71 metres. Ore resource estimates to a depth of 50 metres below surface indicate a tonnage of 1 433 483 t with a weighted average grade of 4.18 g/t Au. The North Central Orebody comprises reefs that have a strike length of 660 metres and a combined average true thickness of 12.0 metres. The tonnage and grade estimates are 2 295 660 t and 1.47 g/t Au, respectively. Reefs of the Northeast Orebody attain a maximum strike length of 900 metres and a combined true thickness of 5.15 metres. The Northeast orebody has a tonnage of 2 378 008 t and a weighted average grade of 10.58 g/t Au, estimated down to a vertical depth of 50 metres below surface. The total ore resource of the Grid 2s Deposit is estimated to be 6 107 150 t grading at 4.20 g/t Au.

The quartz stoneline ore is more extensive on the Southwest Orebody, where it attains an average thickness of 1 metre and grade of 5 g/t Au. It is less extensive on the North Central and Northeast orebodies, where the average thickness is 0.75 metres. The total ore resource of the stoneline is estimated to be 1 069 466 t grading at 6.35 g/t Au.

The in-situ ore in the Grid 2s Deposit has a total strike length of 2260 metres and a combined average true thickness of 7.29 metres. Further drilling has to be conducted to intersect the orebodies, both laterally and down-dip, to facilitate the estimation of proven ore reserves. Considering the its total strike length, average true thickness and an

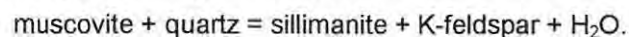
indicated tonnage of 6 107 150 t grading at 4.20 g/t Au, The Grid 2s has potential for a large-scale gold mine. The stoneline ore can be exploited initially, to generate capital for further drilling and evaluation.

### **Wall-rock Alteration**

In Grid 2s, the horizontal widths of the alteration haloes are  $\geq 260$  metres in Section 10800 E, and 295 metres in Section 10000E. Envelopes of the alteration haloes are marked by the first appearance of pyrite  $\pm$  pyrrhotite. In Section 10800 E, the horizontal widths of the alteration zone in the footwall and hanging wall are 160 and 50 metres, respectively. In Section 10000 E, where several sparse and narrow mineralized zones occur, the width of the alteration zone is 75 metres in the overall footwall. The alteration assemblages are shown on Appendix E.

The most abundant alteration minerals are ribbon quartz (silicification), microperthite (K-feldspar alteration), muscovite or sericite (potassic alteration), biotite (biotitic alteration) and chlorite (chloritic alteration). Within the alteration zone, the presence of orthopyroxene in the charnockite, indicates prograde lower-granulite facies (Eilu *et al.*, 1999). Lower-granulite facies mineral assemblages are characterized by the presence of hypersthene and K-feldspar. Potash feldspar is the most prominent alteration mineral on Grid 2s, and it is well developed in the K-feldspar granite. The K-feldspar is white or pink, and the latter is due to iron in the crystal structure or finely disseminated solid inclusions of iron oxide. K-feldspar alteration and biotite alteration normally form early in the hydrothermal history of a mineral deposit, and may either precede or accompany the main-stage alteration and mineralization (Thompson and Thompson, 1996). Early hydrothermal K-feldspar usually undergoes retrograde replacement by sericitic alteration. Chlorite is another retrograde phase replacing orthopyroxene, amphibole, biotite or garnet.

Alteration minerals that are fairly abundant include pyrite, pyrrhotite, calcite, garnet and fine-grained vein quartz. The least abundant alteration minerals are rutile, magnetite, hercynite/gahnite, and sillimanite. The presence of sillimanite, which is a polymorph of  $\text{Al}_2\text{SiO}_5$ , indicates high temperature conditions. Sillimanite of regional metamorphism is usually derived from the breakdown of muscovite and biotite in metapelites, or by the reaction between staurolite and quartz (Deer *et al.*, 1966). In the former (during migmatization) water is released from mica during the production of sillimanite and K-feldspar (Shelley, 1993), in a reaction such as:



Garnet, K-feldspar and water, are also produced by the reaction:

Biotite + 2 quartz +  $\text{Al}_2\text{SiO}_5$  = K-feldspar + garnet +  $\text{H}_2\text{O}$ .

#### Distal Zone

Within the distal zone of Section 10800 E, the alteration minerals in the K-feldspar granite (RS35, RS38, RS 52) are microperthite, vein quartz (fine-grained and ribbon), biotite, chlorite, muscovite (sericite), calcite, garnet, pyrite, pyrrhotite and sillimanite. In the leucogneiss (RS 36), the alteration minerals are microperthite, vein quartz (fine-grained, ribbon), muscovite (sericite), garnet, pyrite and pyrrhotite. K-feldspar is the major alteration mineral.

In mesothermal deposits, biotite forms at or immediately following peak metamorphic conditions (Thompson and Thompson, 1996). The presence of sillimanite and K-feldspar indicates high-temperature conditions. On the phase diagram of aluminium silicate polymorphs (Shelley, 1993), sillimanite is stable above 500°C. K-feldspar has undergone partial, retrograde replacement by muscovite or sericite (sericitic alteration). The sericite, which is coarse-grained, could have formed at temperatures between 250°C and 300°C (Thompson and Thompson, 1996). Another retrograde mineral is chlorite, which is replacing biotite and garnet. The occurrence of both pyrrhotite and pyrite indicates lower-amphibolite conditions (Eilu *et al.*, 1999).

#### Proximal Zone

In the proximal zone of Section 10800 E and Longitudinal Section 8025 N, the alteration minerals in both the K-feldspar granite (RS 37, RS 39) and the charnockite (RS 34), are microperthite, muscovite (sericite), vein quartz (fine-grained; ribbon), biotite, chlorite, calcite, magnetite, pyrrhotite and pyrite. In addition to above, the K-feldspar granite has rutile, garnet and gold, and the charnockite has hercynite/gahnite. K-feldspar is the major alteration mineral. Generally, the sulphides are sparsely disseminated. Pyrite constitutes a significant proportion of the total sulphide.

The presence of orthopyroxene in the mineralized charnockite indicates prograde lower-granulite facies conditions. K-feldspar alteration, which forms early in the hydrothermal history of a mineral deposit, has undergone partial retrograde replacement by muscovite (sericite). Chlorite is another retrograde mineral replacing biotite and garnet. Rutile, which occurs with the chlorite, is a hydrothermal alteration product of titanium-bearing minerals, such as biotite (Thompson and Thompson, 1996). Pyrrhotite and pyrite are partially

replacing magnetite. The occurrence of pyrite indicates retrograde, post-peak lower-amphibolite metamorphic conditions (Eilu *et al.*, 1999).

The proximal zone has three types of mineralized veins, which are quartz (RS 40, RS 50, RS 53), aplitic (RS 54) and pegmatitic (RS 51). In all of them, the alteration minerals are ribbon quartz, chlorite, microperthite, muscovite (sericite), calcite, garnet. In addition to the above, the aplitic vein contains sillimanite, which is associated with the garnet. Quartz and pegmatitic veins also contain biotite, pyrrhotite and pyrite. Aplitic and pegmatitic veins also contain fine-grained quartz veinlets. All the vein types have sparse, fine-grained gold. Calcite + sericite + chlorite alteration occurs in the envelopes of the veins, or in late-stage veinlets that cross-cut the main veins.

In the mineralized veins, the occurrence of sillimanite + K-feldspar, formed by the reaction between muscovite and quartz (Shelley, 1993), indicates high-temperature conditions, normally in excess of 500°C. K-feldspar and biotite have undergone partial, retrograde alteration to muscovite (sericite) and chlorite, respectively. Garnet is also partially replaced by chlorite. The presence of pyrite indicates post-peak, lower-amphibolite facies conditions.

## **8.5 MODELS FOR THE GOLD DEPOSITS**

The mesothermal gold deposits in the study area, which lies in the Northern Marginal Zone of the Limpopo Belt, can be compared to those in the granite-greenstone terrains of the Zimbabwe Craton, the Yilgarn Block of Australia and the Canadian Shield. As discussed in Chapter 3, the charno-enderbites and mafic granulites are high-grade metamorphic equivalents of the granites and greenstones of the Zimbabwe Craton. In the study area, the Grid 4 deposit is in a metamorphosed greenstone belt, and the Grid 2s deposit is in a K-feldspar granite. Both deposits are in prograde granulite and retrograde amphibolite-facies host rocks. In the granite-greenstone terrains, the majority of the gold deposits are in greenschist to amphibolite-facies host rocks.

### **Regional Setting of Mineralization**

#### *Major structures*

In the Yilgarn Block, the Canadian Shield and the Zimbabwe Craton, most of the giant mesothermal gold deposits occur adjacent to major (>100 km long) transcrustal, ductile to brittle-ductile shear zones (Groves *et al.*, 1989; Hodgson, 1989; Kerrich, 1989 a; Sibson *et al.*, 1988; Campbell and Pitfield, 1994). Due to their great lengths and steep dips, the shear zones are deep-seated. The transcrustal shear zones provide the first-

order control on gold mineralization, and act as the master plumbing system. The gold deposits occur in dilation sites within second-, third- or fourth-order brittle-ductile structures. In the study area, the transcrustal first-order structure is the Mauch Shear Zone, and the gold deposits are in third- and fourth-order shears within dilation zones.

#### *Associated magmatic activity*

Felsic intrusive rocks are commonly associated with gold deposits in the Yilgarn Block (Groves *et al.*, 1989), the Canadian Shield (Roberts, 1987) and the Zimbabwe Craton (Campbell and Pitfield, 1994). In the study area, porphyritic felsic intrusives occur in the Grid 4 deposit. In the Superior Province of Canada, more than 90% of the larger gold deposits (with production >1 million ounces) are hosted by, or are immediately adjacent to, felsic porphyries. Age dating indicates that approximately 15 m.y. elapsed between the end of volcanic activity and the emplacement of the porphyries (Roberts, 1987). Recent high precision dating suggests that the gold mineralization is considerably younger, perhaps 50-100 m.y. younger, than the porphyries (Hodgson *et al.*, 1992). This suggests that the spatial relationship of gold and felsic porphyries is structural. In the Yilgarn Block, deep mantle-sourced lamprophyres also occur with, or in close association with the gold mineralization and mantle-derived carbonation zones.

#### *Age of gold mineralization*

Gold mineralization is late in the evolution of the Yilgarn, Canadian and Zimbabwean greenstone belts (2.95 – 2.7 Ga). Some of the evidence for this includes (a) mineralized veins cross-cutting complexly deformed greenstone rocks, (b) mineralization is associated with major strike-slip, oblique-slip, and/or thrust faults that are late in greenstone evolutionary history, (c) mineralization is often associated with some of the latest movements on these faults, (d) where in contact, most mineralized structures cut granitoids, porphyries, or lamprophyres that intruded late in greenstone belt evolution, and (e) in many cases, wall-rock alteration is retrograde with respect to peak metamorphic conditions.

In the Yilgarn Block, the most likely age range for gold mineralization is 2.65 to 2.60 Ga (Groves *et al.*, 1989). The dates were determined using  $^{208}\text{Pb}$  vs  $^{204}\text{Pb}$  for pyrites and zircon dating on the felsic porphyries. In the Canadian Shield, the Archaean mesothermal gold mineralization has been dated at:

- (a) 2630-2600 Ma ( $^{40}\text{Ar}/^{39}\text{Ar}$  on green muscovite) for the main stage of vein formation and wallrock alteration, in the Timmins-Kirkland Area (Hodgson *et al.*, 1990);

(b)  $2682 \pm 2$  Ma on hydrothermal zircon, in Sigma-Lamaque quartz-carbonate veins (Robert & Poulsen, 1997); and

(c) 2720-2714 Ma in the Red Lake District (Robert & Poulsen, 1997).

At Renco Mine, which is 12 km northeast of the Grid 4 deposit in the study area, the age of gold mineralization is  $2532 \pm 35$  Ma (Kisters *et al.*, 1998). The age was determined using Pb-Pb dating on the high-grade metamorphic skarn-type alteration contained in the reefs. In the SMZ of the Limpopo Belt, Rb-Sr dating on wall-rock alteration at Franke, Klein Letaba and Birthday gold mines gave an age range of 2660-2427 Ma for the mineralization (Gan & van Reenen, 1995).

### **Genetic Models**

#### *Gold transport and deposition*

In the Australian and Canadian mesothermal gold deposits, fluid inclusions, stable isotope data, and thermodynamic calculations suggest that gold was normally transported as a reduced sulphur complex in moderate-density, relatively reduced, near-neutral H<sub>2</sub>O-CO<sub>2</sub> fluids of low salinity (Groves *et al.*, 1989; Roberts, 1987). The salinity of the fluids was <2 equivalent wt. % NaCl. Deposition of gold was normally at 250° to 350°C and 1 to 3 kbars. In a few deposits, the depositional temperatures were as high as 400°C (Kerrick, 1989). Pressures of 1 to 3 kbars correspond to depths of 4 to 11 km. The majority of these deposits are in greenschist-facies. In the mid- to upper-amphibolite facies Westonia deposit of the Yilgarn Block, P-T conditions were >370°C,  $3 \pm 1$  kbar (Ho *et al.*, 1990). The P-T conditions in the granulite facies Griffin's Find deposit, also in the Yilgarn Block, were ~700°C, ~6 kbar. In the Northern Marginal Zone of the Limpopo Belt (granulite facies), the fluid temperature of gold mineralization at Renco Mine, was ~600°C (Kisters *et al.*, 1998). At Franke Mine, in the Southern Marginal Zone of the Limpopo Belt, fluid P-T conditions were 650°C, 6 kbars (Gan & van Reenen, 1995). In the study area, the alteration assemblages in Grid 4 and Grid 2s deposits indicate prograde lower-granulite facies and retrograde lower-amphibolite facies. Figure 8.14 is a schematic crustal profile, at the time of gold mineralization, in late Archaean deposits over a wide range of facies extending from sub-greenschist to granulite.

A variety of depositional processes were involved in gold mineralization. Oxidation of the fluids (reduced sulphur-gold complexes) is an efficient mechanism for the precipitation of gold (Roberts, 1987). Gold may also be precipitated by changes in pH, a decrease in temperature, or through the destabilization of reduced sulphur by reaction with iron in the host rock to precipitate iron sulphide. Sulphidation of the host rocks, is one of the most important gold-depositing mechanisms.

### *Fluid infiltration*

Gold mineralization was related to enhanced fluid flux during deformation, as indicated by the structural control of mineralization, the zonal nature of associated wall-rock alteration around shear zones and fractures, and structural plus textural evidence (Groves *et al.*, 1989). In the granite-greenstone terrains, gold deposition was favoured at or below the amphibolite-greenschist metamorphic boundary, which corresponds to the ductile-brittle transition. Brittle and brittle-ductile deformation is characterized by fluctuating fluid pressures, multiple fracturing, and channeling of fluid along brittle-ductile fracture zones (dilation zones), which results in high fluid to rock ratios along channelways (Sibson *et al.*, 1988; Kerrich, 1989). These characteristics are ideal conditions for gold mineralization. On the regional scale, it is suggested that fluids were channeled along the transcrustal fault/shear zones and were focussed into the brittle-ductile structures by transient fluid flow. There would have been both temperature and pressure gradients between the hot, ductile, first-order faults and the cooler, brittle-ductile second-order structures in which there were fluctuating fluid pressures (Groves *et al.*, 1989). Fluid pressure fluctuations promote CO<sub>2</sub> + H<sub>2</sub>S immiscibility with attendant gold precipitation (Kerrich, 1989 b). In the lower-order splays, sulphidation reactions are promoted in Fe-rich lithologies. A decrease in pressure and temperature would have favoured gold deposition, although pressure differences provided the primary control on fluid flow. In the high-grade metamorphic terrains, such as the study area, the dilation zones are formed by ductile, second- to fourth-order shear zones.

### *Fluid and ore-component source*

In the gold deposits of the Canadian Shield and the Yilgarn Block, the proposed sources of hydrothermal fluids are (a) metamorphic fluids; (b) juvenile fluids formed by granulitization of the lower crust and/or degassing of the upper mantle; (c) magmatic hydrothermal fluids; and (d) re-circulated sea water (Roberts, 1987; Groves *et al.*, 1989).

The low chloride content and high carbonate content of the solutions make it very unlikely that the fluids are re-circulated sea water or connate water. Sea water, trapped in volcanic rocks or recharging into a thermal system, would quickly lose carbon dioxide by reactions with calcium-bearing clay minerals (Roberts, 1987). The salinity of the sea water would tend to increase as a result of water-rock reactions.

Compositions of fluids in metamorphic rocks are comparable in several respects with the ore-forming fluids (Roberts, 1987). Salinities of fluids from inclusions in metamorphic

rocks are generally low, and the CO<sub>2</sub> : H<sub>2</sub>O ratio increases from greenschist facies, where the fluids are H<sub>2</sub>O dominated, to the granulite facies, where they are almost pure CO<sub>2</sub>. Stable isotope studies of gold deposits indicate that fluids of metamorphic origin, focussed along structures of regional extent, are the most likely candidate for the ore-forming hydrothermal reservoirs involved in genesis of Au vein systems (Kerrick, 1989 b). The low salinity of the H<sub>2</sub>O-CO<sub>2</sub> fluids is most compatible with regional metamorphic fluids, although such fluids can also be derived from early separation of magmatic fluid (Groves *et al.*, 1989). In general, the introduction of gold post-dates regional metamorphism of the host rocks, and the postulated metamorphic fluids carrying Au appear to be related to motion on major thrusts or transpressional structures (Kerrick, 1989 b). Oxygen and hydrogen data cannot unequivocally discriminate between magmatic and metamorphic fluids. The CO<sub>2</sub>-rich magmatic hydrothermal fluids appear to be associated with molybdenum- and tungsten-bearing gold deposits (Roberts, 1987).

Fluids associated with granulitization are a potential source of hydrothermal fluids (Roberts, 1987). CO<sub>2</sub>-rich inclusions are ubiquitous in granulites over a wide range of rock compositions, suggesting an external source (juvenile fluids from the mantle) as a control to the fluid phase in these high-grade metamorphic rocks. Carbon isotope data are most compatible with dissolution of CO<sub>2</sub> from pre-existing mantle-derived carbonation zones, which are broadly coincident with the crustal-scale faults controlling gold mineralization (Groves *et al.*, 1989). However, the data cannot rule out a direct magmatic origin for the CO<sub>2</sub>. The CO<sub>2</sub> of juvenile fluids, based on the isotopic studies of carbonatites and diamonds, is interpreted to be of deep-seated origin (Roberts, 1987). However, the isotopic composition of granulite-associated fluids and the identification of the isotopic signature of the proposed juvenile fluid is not unequivocal.

There is no unique source rock for gold (Kerrick, 1989 b; Groves *et al.*, 1989). In the Yilgarn Block, Canadian Shield and the Zimbabwe Craton, the majority of the gold deposits occur in greenstone belts. In these terrains, the most obvious source of gold is the rocks of the greenstone belt (Roberts, 1987). In modern oceanic basalts, loosely attached, intra-crystalline gold and sulphur from magmatic sulphides are mobilized by the reaction of sea water with the still hot lava, from the crystalline interiors of pillows to the glassy rims. Similar processes operated in the Precambrian, and the gold leached from the volcanics was probably fixed in sulphide-bearing interflow sediments (Roberts, 1987). The remobilized gold would be readily accessible for later concentration into ore deposits.

Radiogenic compositions for some galenas and pyrites in the ore, appear to implicate an old crustal source for some of the Pb (Groves *et al.*, 1989). The old crustal source for the Pb, could be a sialic basement to at least part of the greenstone belts. The lead isotope data indicate that metamorphic devolatilization of greenstone belts was not the only source of ore fluid and ore components. Less radiogenic lead in ore-related sulphides could have been derived from the mantle, or from igneous rocks derived from the mantle at about the time of mineralization (Groves *et al.*, 1989).

Au-rich lamprophyres have temporal and spatial association with gold deposits (Kerrich, 1989 a). Both the lamprophyres and gold deposits are S, Au and CO<sub>2</sub>-rich. The  $\delta^{13}\text{C}$  of lamprophyre carbonate is similar to that of deposit carbonate. Lamprophyres form at the or near the core-lower mantle boundary, and the core is Au-rich. The lamprophyre magmas interact with the crust, and Au is released into the crustal metamorphic fluid system. Calc-alkaline lamprophyres are variably enriched in gold (up to 10<sup>2</sup> background values (1-2 ppb)). Their probable genetic connection to ubiquitous felsic porphyries, implicates large volumes of lamprophyric melts, and suggests their potential as a primary gold source for ore fluids (Groves *et al.*, 1989).

#### *Preferred genetic model*

Low-salinity H<sub>2</sub>O-CO<sub>2</sub> fluids were channeled up first-order, ductile transcrustal fault zones, in the granite-greenstone or high-grade metamorphic terrains, during the late stages of deformation and metamorphism. P-T gradients between lower-order splays and the regional ductile structures ensured transient, strongly focussed fluid flow into the former, where lower temperatures and fluid-wallrock reactions promoted gold deposition. Lithologies with high Fe / (Fe + Mg) ratios were particularly favourable host rocks, with sulphidation causing synchronous Fe sulphide and gold deposition. Low tensile strength lithologies underwent selective hydraulic fracturing, lithological contacts localized strain and fluid flow, and changes in pH and  $f_{\text{O}_2}$  induced gold deposition in a variety of host rocks (Groves *et al.*, 1989).

The association of crustal-scale faults or shear zones, mantle-derived carbonation, porphyries and/or lamprophyre intrusions, and gold deposits, suggests that gold mineralization was broadly related to a deep-seated tectonic-magmatic event (Groves *et al.*, 1989). The event involved melting of mantle to depths of some 150 km (lamprophyres), melting of the upper mantle or base of the crust (porphyries), melting of lower crust (granitoids), and mantle degassing (regional carbonation zones). Stable and radiogenic isotope data implicate a metamorphic and/or magmatic fluid that derived Pb

from from older sialic crust and greenstone belts, and C from pre-existing regional carbonation zones. It is very unlikely that felsic intrusions exposed at gold mineralization levels were the source of ore fluids, because they contain no definitive evidence for fluid saturation.

The ultimate source of gold is currently uncertain. Using the evidence for fluid focussing, the gold could have been derived from a large volume of rocks with background gold contents. The only realistic alternative is that the gold was liberated into the crustal fluids from gold-enriched lamprophyres during their ascent into, and contamination by, the continental crust (Groves *et al.*, 1989).

The preferred models, for the Grid 4 and Grid 2s deposits in the study area, are shown on Figures 8.15 and 8.16, respectively.

#### **Grid 4 Deposit – Preferred genetic model**

The proposed model for the Grid 4 deposit (Figure 8.15) is similar to the preferred model of Groves *et al.* (1989), discussed above. The first-order, transcrustal structure is the sinistral Mauch Shear Zone, trending on a regional fabric of 060° - 065°. The Mauch Shear Zone extends for several hundreds of kilometres and attains a maximum horizontal width of 1 km. A sinistral splay shear zone, trending on 040°, forms the second-order structure. Between these shear zones, the 20° acute angle is a deformation or dilation zone, caused by convergence of the two shear systems. A metamorphosed greenstone sequence is situated in the dilation zone. Third- and fourth-order splay shear zones occur in the dilation zone. Cu-Mo mineralization occurs on the third-order shear zone, which trends on 060°. Gold mineralization is on the fourth-order shear zone, which trends on 055°. The "Au Shear" is a splay from the third-order shear zone. Feldspar porphyry dykes and quartz veins host the Au-Cu-Mo mineralization. Gold mineralization is peripheral to the porphyry-type hydrothermal system centred on a Cu-Mo core of dykes and quartz veins. Bi, Zn and Fe are also associated with the mineralization.

H<sub>2</sub>O-CO<sub>2</sub> fluids were channeled up the Mauch Shear Zone, during the late stages of deformation and metamorphism, and focussed into the third- and fourth-order shears of the dilation zone. P-T gradients between the Mauch Shear Zone and the lower-order shears facilitated transient, strongly focussed fluid flow into the latter, where lower temperatures, changes in pH and *f*<sub>O<sub>2</sub></sub>, and fluid-wallrock reactions promoted gold deposition. The mafic granulites, which have high Fe / (Fe + Mg) ratios were favourable

host lithologies, where sulphidation resulted in simultaneous Fe sulphide and gold deposition.

The Au-Cu-Mo mineralization is associated with a crustal-scale shear zone, feldspar porphyry dyke intrusions and carbonation, suggesting that the mineralization was related to a deep-seated tectonic-magmatic event. The event entailed (a) melting of the lower mantle to produce lamprophyres, (b) differentiation of lamprophyric magmas, melting of the upper mantle or base of the crust, to produce feldspar porphyry and H<sub>2</sub>O-CO<sub>2</sub> - Au ± Pb fluids, (c) porphyry intrusions into shear zones, and (d) mantle degassing to produce carbonation zones. The fluids circulated in the plane of the Mauch Shear Zone and were transiently focussed into the higher-order shears. According to the preferred model of Groves *et al.* (1989), mentioned above, the fluids were metamorphic and/or magmatic, and derived C from pre-existing carbonation zones and Pb from older sialic crust or the greenstone belt.

The gold could have been released into crustal fluids from gold-enriched lamprophyres during their ascent into, and contamination by continental crust. The gold and ore-fluids could also have been derived from the metamorphic devolatilization of the greenstone belt where large volumes of the rocks have background gold values.

#### **Grid 2s Deposit – Preferred genetic model**

The proposed model for the Grid 2s deposit (Figure 8.16) is comparable to the preferred model of Groves *et al.* (1989), discussed above. The sinistral Mauch Shear Zone is the first-order, transcrustal structure, which trends on 065°. In the northern part of the deposit, a dextral east-west (085°-090°) shear zone forms the second-order structure. Another dextral, east-west shear zone marks the southern boundary of the deposit. As described in Chapter 7 and illustrated by Figure 7.20, the intersection of two shear zone systems with different senses of movement, resulted in dilation as a consequence of bulk, inhomogeneous shortening (Hodgson, 1989). Gold mineralization occurs mainly as fine-grained nuggets in quartz veins. The mineralization also occurs in pegmatitic and aplitic veins, and in the immediate wall-rocks to the veins. Very sparse, disseminated pyrrhotite, pyrite and chalcopyrite are associated with the mineralization. Mineralized veins occur mainly in third-order shears, which are parallel to the first-order Mauch Shear Zone. A few mineralized veins are parallel to the second-order east-west shear zones. The mineralized veins are hosted in K-feldspar granite and proto-mylonite (after charnockite). As described in Chapter 3, the K-feldspar granite is believed to be a product of migmatization of a pre-existing charno-enderbite. The granulite-facies charno-

enderbites were exhumed when the Northern Marginal Zone was thrust onto the Zimbabwe Craton, during the Limpopo orogeny (discussed in Chapter 2).

Low-salinity H<sub>2</sub>O-CO<sub>2</sub> fluids were channeled up the Mauch Shear Zone during the late stages of deformation and metamorphism. P-T gradients between the Mauch Shear Zone and the lower-order shear zones resulted in transient, strongly focussed fluid flow into the latter. In the second- and third-order shears, lower temperatures, changes in pH and *f*<sub>O<sub>2</sub></sub>, and fluid-wallrock reactions, induced gold deposition. Since the host lithologies are felsic, sulphidation was not well developed, and free gold was deposited.

Although the Grid 2s deposit is hosted in felsic rocks, a metamorphosed and folded greenstone belt occurs 1 km to the west. The northern limb of the fold is in contact with, and parallel to the Mauch Shear Zone. The association of the transcrustal Mauch Shear Zone, some carbonation, the greenstone belt and the gold deposit, suggests a metamorphic and mantle degassing model. Direct mantle degassing produced fluid and ore components (H<sub>2</sub>O-CO<sub>2</sub> ± Au), which experienced lower crustal contamination with Pb. The mantle fluids were channeled to the upper crust via lamprophyric melts. The fluid and ore components (H<sub>2</sub>O-CO<sub>2</sub> – Au) could also have formed by metamorphic devolatilization of the greenstone belt. The upper crustal metamorphic ore-fluids penetrated the lower-order shears in the K-feldspar granite and proto-mylonite, via convection in the Mauch Shear Zone.

## **CHAPTER 9**

### **SUMMARY AND CONCLUSIONS**

#### **9.1 Geology and metamorphism**

The Northern Marginal Zone (NMZ), of the Limpopo Belt, is composed of granulite-facies rocks of the "Supracrustal Assemblage" and the "Plutonic Assemblage". The "plutonic" rocks occupy approximately 90% of the NMZ area and "supracrustal" rocks constitute the remainder. The "Supracrustal Assemblage" (pre- 2.88 Ga) is composed of metamorphosed greenstone belt sequences, which include meta-basites, ultramafic rocks, acid to intermediate meta-volcanic rocks and meta-sediments. The "Plutonic Assemblage" (2.72-2.62 Ga) is composed of charnockites and enderbites. Crosscutting relationships indicate that the charno-enderbites are intrusive into the supracrustal rocks. The NMZ charnockites have compositions of granite, alkali granite and granodiorite. Enderbites have compositions of diorite, quartz diorite and tonalite. The charno-enderbites and meta-volcanic rocks are hypersthene-bearing. Results of litho-geochemical work conducted in this study and by previous writers (Odell, 1975; Rollinson & Lowry, 1992) indicate that the supracrustal rocks and charno-enderbites of the NMZ have similarities with the adjacent, greenschist- to amphibolite-facies greenstones and granitic rocks of the Zimbabwe Craton (ZC). The NMZ resembles the granite-greenstone terrain at granulite-facies.

Four stages of metamorphism have been identified in the NMZ (Kamber & Biino, 1995; Rollinson & Blenkinsop, 1995). Stage 1 was a high temperature event (c. 2.88 Ga) and Stage 2 was a retrograde event. The supracrustal rocks, prior to the intrusion of the charno-enderbites, experienced stages 1 and 2. Stage 3 was a high temperature (825°-850°C, 5-8.4 kbar), regional granulite-facies, tectono-metamorphic event, recorded by both charno-enderbites and supracrustal rocks. Stage 3 was associated with SSW-NNE compression, which produced the main foliation and shear zones, and resulted in the initial thrusting (c. 2.6 Ga) of the NMZ onto the ZC. The thrusting occurred at the North Limpopo (Umlali) Thrust Zone. Stage 4 (1.97 Ga) was a retrograde metamorphic event related to the final exhumation and thrusting of the NMZ onto the ZC.

The regional penetrative foliation, produced in Stage 3, is ENE-trending (060°-065°) and generally steep (70°-80°) southeasterly dipping. Within the study area, the Mauch Shear Zone is the most prominent shear zone, which is parallel to the regional penetrative foliation. In the NMZ, the Mauch Shear Zone is a first-order, transcrustal structure, which extends for several hundreds of kilometres along strike and attains a maximum horizontal

width of 1 kilometre. The shear zone dips steeply (70°- 85°) to the southeast. Due to its great length and steep dip, the shear zone is deep-seated. Rolling structures and fold asymmetry of mafic xenoliths indicate sinistral horizontal movement. The shear zone has a steeply plunging (70°- 85°→ 270°) quartz lineation. This lineation was probably produced by reactivation of the shear zone in Stage 4, during the final thrusting of the NMZ onto the ZC. In the vertical sense, the shear zone has reverse movement.

### **9.2 Structure**

In Area 4 of Tokwe E.P.O, the Mauch Shear Zone has a sinistral, second-order splay shear, which trends on 040° and dips southeast at 50°- 80°. Convergence of the two sinistral shear zones resulted in dilation or deformation in the 20° acute angle between them. Dilation zones are structural settings favourable for mesothermal gold mineralization (Groves *et al.*, 1989; Hodgson, 1989). A "greenstone belt" occurs in the acute angle. Feldspar porphyry dykes/veins and quartz veins are hosted in lower-order shear zones that are developed in the deformation zone. A third-order shear zone, trending on 060°, hosts Cu-Mo mineralization. Gold mineralization occurs in a fourth-order shear zone trending on 055°.

In Area 2s of Tokwe E.P.O., a dextral, second-order east-west trending (085°) shear zone crosscuts the Mauch Shear Zone. The intersection of the two shear zones occurs at the nose of a folded "greenstone belt" (Zvamapere). Interference of the two shear zones with opposing senses of movement, resulted in dilation/deformation as a consequence of bulk inhomogeneous shortening (Hodgson, 1989). The deformation zone occurs in K-feldspar granite and leucogneiss. Quartz veins are hosted in lower-order shear zones that are developed in the deformation zone. Gold mineralization occurs predominantly in third-order shear zones trending on 065°. A few quartz veins trending on 090° and 040° also contain gold mineralization.

### **9.3 Geophysical surveys**

Aeromagnetic data were successful in delineating mylonites and proto-mylonites, as zones of very low (<30 140 nT), negative magnetic anomalies. The magnetic data mapped the Mauch Shear Zone, the splay shear zone and a flexure/offset caused by the dextral east-west shear zone. This information, together with geological concepts discussed above, was used to synthesize targets (dilation zones) for gold exploration. Target A (Area 4) and Target B (Area 2s) were proposed for investigation. Magnetic data also mapped "greenstone belts" as zones of positive, high-amplitude magnetic anomalies. The "greenstone belts" associated with targets A and B were clearly

delineated. Major fold structures of "greenstone belts", enderbites and proto-mylonites were shown by magnetic data.

In future gold exploration programs in the region, the aeromagnetic method is recommended for mapping first-order shear zones and second-order shear zones that intersect it. Such intersections are likely to be dilation or deformation zones, which are structural settings favourable for mesothermal gold mineralization. The method also maps out "greenstone belts", which if in contact with the first-order shear zones, are some of the sources of the gold mineralization in the dilation zones. The sense of movement for each of the intersecting shear zones has to be determined on the ground, using kinematic indicators, to establish if dilatancy is likely to occur.

The limitation of the aeromagnetic method was that the "greenstone belts", dolerites, olivine pyroxenites, enderbites and magnetite charnockite all gave rise to positive, high-amplitude magnetic anomalies. Interpretation of the high-amplitude anomalies had to be conducted with the aid of a geological map, to separate the "greenstone belts" from the others.

Radiometric data were useful in mapping areas with K-alteration associated with mineralization. Such areas contain characteristic low Th/K ratios, which are less than  $2.5 \times 10^{-4}$  (Shives *et al.*, 1997). Since Th does not accompany K-enrichment during hydrothermal processes, Th/K ratios provide excellent identification of potassium anomalies associated with alteration. Areas of low Th/K ratios ( $1.2 - 2.5 \times 10^{-4}$ ) occur in Target A and Target B, and compliment the geological concepts and magnetic data, which indicated these targets as structural settings favourable for mesothermal gold mineralization.

In future gold exploration programs in the region, the use of Th/K ratios is strongly recommended as direct method of mapping K-alteration associated with gold mineralization. In this study, the individual K, Th and U data sets failed to map out the first-order shear zone (Mauch Shear Zone), structural settings favourable for gold mineralization or K-alteration associated with mineralization.

The Mauch Shear Zone is a first-order control on mesothermal gold mineralization in the study area. The mineralization occurs in dilation zones where the Mauch Shear Zone is in contact with a "greenstone belt". Some of the gold and ore fluids were probably derived by metamorphic devolatilization of the "greenstone belts" (Groves *et al.*, 1989). Ore fluids

and gold could also have been produced by mantle degassing and were liberated, via the Mauch Shear Zone, into crustal fluids. In Area 4, the gold and ore fluids are mainly magmatic, as the mineralization occurs in feldspar porphyry that intruded the lower-order shear zones. In Area 2s, the origin of the ore fluids and gold is metamorphic and mantle-derived. It is likely that, along the entire length of the Mauch Shear Zone in the region, there are more combinations of intersecting second-order structures and “greenstone belts”, which can host significant gold mineralization such as the Grid 2s and Grid 4 deposits. Investigations for such favourable settings should be conducted in future exploration programs.

#### **9.4 Drainage geochemistry**

Orientation stream sediment sampling conducted in Target A (Area 4) indicated the -75µm size fraction as the best for use in reconnaissance drainage surveys in the study area. In Target A, trap sites contained clast-supported, poorly sorted sediments with qualities ranging from *moderate* (class 3) to *good* (class 4). First-pass drainage sampling indicated anomalous gold values (>40 ppb) in Area 2s, Area 4, Area 1s and Area 6. In these areas, anomalous gold values (>650 ppb) in HMC samples of second-pass surveys reproduced the earlier anomalies. HMC samples from Area 2s, Area 1s and Area 6 contained gold grains.

Drainage geochemistry was successful in indicating the occurrence of gold mineralization in some parts of the E.P.O. The method succeeded as a follow-up on Targets A and B synthesized using geophysical methods mentioned above. Reconnaissance, first-pass drainage sampling in the entire E.P.O. succeeded in the reduction of the vast area to a few anomalies in Areas 1s, 2s, 4 and 6. Second-pass sampling resulted in the location of the watersheds or source areas of the drainage anomalies. The HMC samples enhanced the magnitudes of the anomalies and indicated the presence of coarse gold in Areas 1s, 2s and 6. However, un-panned second-pass samples could have been also assayed, to determine if they would have reproduced and defined the drainage anomalies as the HMC samples did.

In future gold exploration programs in the region, drainage sampling should be utilized to investigate for possible mineralization in various drainage watersheds and basins. The method is cheap and reduces large reconnaissance areas to a few anomalies for follow-up work.

#### **9.5 Soil geochemistry**

Orientation soil sampling conducted in Target B (Area 2s) indicated that a quartz stoneline, which assayed up to 9.5 g/t Au, is best sampling medium. However, the stoneline is not evenly distributed and occurs at various depths to a maximum of 1.75 metres. For these reasons, the stoneline was not practically suitable for routine soil sampling surveys in the study area. In the soil profile above or without the stoneline, the B-horizon contained the highest concentration of gold and was found to be the most suitable for soil sampling surveys. The -180+125 $\mu$  size fraction, which contained the highest concentration of gold, was found to be the most suitable for soil sampling surveys. Orientation soil sampling also indicated that the upper limit of background gold values is approximately 60 ppb.

The orientation soil geochemical survey was successful in confirming the presence of gold mineralization in Target B and indicating that, for routine surveys, the B-horizon and the -180+125 $\mu$  were the most suitable sampling medium and size fraction, respectively. The orientation survey also helped in the recognition of, in some parts of the target area, the quartz stoneline, which is an ore resource near surface. However, a separate orientation survey could have been conducted in Target A, where the soil profile does not have a stoneline.

Soil sampling surveys conducted in Grids 4, 2s, 1s and 6 indicated significant and consistent gold anomalies (>60 ppb) in Grid 2s and Grid 4. The threshold value was calculated using log-probability plots. In Grid 2s, two 2.2-km long "sinusoidal" gold anomalies, with a peak value of 980 ppb Au, were delineated. Two gold anomalies were indicated in Grid 4, where the peak value was 900 ppb. The East Anomaly attains a strike length of 1300 m and lies on a shear zone ("Au Shear"), which trends on 055°. The West Anomaly has a strike length of 200 m and trends on 060°. The two anomalies are separated by a gap of 900 m. Anomalous copper values (>125 ppm), with a peak of 446 ppm, lie on a shear zone ("Cu Shear"), which trends on 060° in Grid 4. In the West Anomaly, the gold and copper anomalies concur, but in the East Anomaly the "Au Shear" is a splay from the "Cu Shear".

In Grids 1s, 2s, 4 and 6, the soil geochemistry method succeeded in reproducing the gold anomalies indicated by the drainage geochemistry method. Grids 1s and 6, which had weaker and less consistent gold anomalies, were eliminated from further follow-up work. The method was successful in indicating residual soil anomalies in both Grid 2s and Grid 4, except for the southwest corner of the former, where a dispersed quartz stoneline gave

rise to a wide (800 m) anomaly on Line 10 000E. In the latter, the method led to the recognition of the "Au Shear" and "Cu Shear" trends.

In future gold exploration programs in the region, the soil geochemistry method should be utilized as it indicates the positions of the residual gold anomalies, except in places with transported soil. Orientation surveys should be conducted in each drainage anomaly, since the soil profiles vary from one area to another.

#### **9.6 Grid mapping and rock sampling**

Geological mapping and rock sampling in Grid 2s indicated that gold mineralization occurs mainly in quartz veins and stringers that are in third-order shear zones trending on 065°. A small number of mineralized quartz veins trend on 090° and 040°. The mineralization occurs in the form of fine-grained, sparsely disseminated free gold. Very few sulphides (pyrrhotite, pyrite and chalcopyrite) are associated with the gold mineralization. Assay data had a threshold of 2.25 g/t Au and a peak value of 27 g/t Au. Mineralized quartz veins occur within the envelopes of the two soil anomalies. In the quartz veins, copper values are very low (7-265 ppm) and the majority less than 30 ppm. The Spearman rank coefficient of correlation (-0.2592) shows that there is no correlation between values of gold and copper.

Detailed geological mapping in Grid 2s was successful as it led to the recognition of the major shear zones, which are the sinistral Mauch Shear Zone and a system of dextral east-west shear zones. The shear zones occur as leuco-mylonites and proto-mylonites, which have quartz lineations and rotated feldspar porphyroclasts. K-feldspar granite, charnockites and quartz veins were also mapped. The mapping exercise led to the observation of sparse, disseminated sulphides (pyrrhotite, pyrite and chalcopyrite) and free gold in quartz vein outcrops and sub-outcrops. The quartz veins and immediate host rocks were sampled and assayed. Rock assays >1 g/t Au all occurred within the envelopes of the soil anomalies. Rock sampling was successful in identifying quartz veins as the main host to the gold mineralization, and indicating the grades of mineralization.

In Grid 4, geological mapping and rock sampling indicated that gold mineralization occurs in feldspar porphyry dykes/veins and leuco-mylonite in the West Anomaly and "Au Shear" of the East Anomaly. Gold mineralization is associated with disseminated sulphides (pyrrhotite, pyrite and chalcopyrite) and occasionally with semi-massive sulphides. The gold values have a peak of 9.8 g/t and a threshold of 1.75 g/t. In the feldspar porphyry, the peak values for Cu and Bi are 571 ppm and 57 ppm respectively. Gold has a weak

correlation (+0.4076) with copper and no correlation (-0.0010) with bismuth. Copper and bismuth have a fairly strong correlation (+0.6708). In a charnockite east of the "greenstone belt", gold mineralization occurs in quartz veins over a strike length of 200 metres. The peak and threshold values are 2.4 g/t Au and 0.6 g/t Au respectively. The peak copper value is 489 ppm. There is weak correlation (+0.1879) between gold and copper.

In Grid 4, detailed geological mapping was successful in the identification of leucomylonites and proto-mylonites, which are in the sinistral Mauch Shear Zone and a sinistral splay shear zone. Meta-basalts, meta-andesites, feldspar porphyry veins/dykes and quartz veins are some of the other lithologies mapped. The exercise resulted in the observation of disseminated to semi-massive sulphide (pyrrhotite, pyrite, chalcopyrite and molybdenite) mineralization in the feldspar porphyry. Rock sampling on the feldspar porphyry and quartz veins succeeded in indicating that the former is the main host to the gold mineralization.

Detailed geological information, for both Grid 2s and Grid 4, was useful for the explanation and interpretation of other data sets, such as soil geochemistry and geophysics (aeromagnetic and radiometrics). The information helped in the location and identification of the hosts to the mineralization, which are sources of the drainage and soil anomalies. However, the geological mapping and rock sampling method is dependent on the availability of good outcrops. If there is thick soil cover, then the rocks are masked and not readily accessible for observation and sampling.

In future gold exploration programs in the region, detailed grid geological mapping and rock sampling are recommended. If there are good exposures, the lithologies and structures can be observed and mapped. In exploration targets with good outcrops, the quartz and feldspar porphyry veins can be sampled readily.

## **9.7 Trenching**

Trenching in Grid 2s exposed quartz veins and stringers in proto-mylonite, leucomylonite, leucogneiss and K-feldspar granite. Widths of the quartz veins are up to 1 metre. Most of the quartz veins trend on 065°, but others follow the 085° and 040° trends. The quartz veins dip steeply (65°-85°) to the southeast and south. Some of the quartz veins contain fine-grained, sparsely disseminated gold. In some places, wall rocks contain sparsely disseminated pyrite and chalcopyrite. In panel samples collected from the trenches, the peak and threshold gold values are 175 g/t and 7.5 g/t respectively. In

the SW part of the soil anomalies, the envelope of the trench anomaly is 700 m long, 100 m wide and trends on 030°. Within the envelope, the majority of quartz veins trend on 065°. In the NE part of the soil anomalies, the envelope of the trench anomaly is up to 900 m long, 100 m wide and trends on 030°. The strike of this anomaly is still open towards the east, as it was not adequately trenched. Copper values are generally <40 ppm, and attain a peak of 209 ppm in the felsic host rocks. There is no correlation between gold and copper values, as the coefficient of correlation is -0.3212.

In Grid 2s, panel sampling was successful in reducing the nugget effect of randomly distributed free gold in the quartz reefs. The panel samples gave good reproducibility of the gold assay values. Trench sampling was useful for indicating that the gold mineralization is not restricted to the quartz veins, but also occurs occasionally, in the immediate wall rocks. On Line 10 000E, trenching indicated that there is no bedrock mineralization below the dispersed quartz stoneline, which gave rise to a very wide (800m) soil anomaly. However, more trenches should have been excavated to test soil anomalies towards the NE end. In the SW soil anomaly, more trenches should have been excavated to enable correlation of the quartz reefs between traverse lines that are 200m apart. Trenching should also have been carried out along the major quartz veins, to establish their strike directions and extent in the SW anomaly. This would enable siting of drill holes perpendicular to the strike direction of the veins.

Trenching in Grid 4 exposed several (up to 7) parallel feldspar porphyry dykes/veins in the "Au Shear" and quartz veins in the "Cu Shear". Each of the dykes/veins may attain a maximum horizontal width of 2½ m. The dykes/veins dip at 75° to the southeast, and contain pyrrhotite, pyrite and chalcopyrite. Gold mineralization occurs mainly in the feldspar porphyry dykes/veins. Some of the adjacent and intervening host mylonite is also mineralized. The horizontal width of the entire shear zone is 25 m. The peak and threshold of the gold values are 70 g/t and 4.2 g/t respectively. In the West Anomaly, gold values >1 g/t occur over a strike length of 300 m. A strike length of 600 m is indicated for the East Anomaly, but it is still open towards the east. Copper values in the quartz veins, feldspar porphyry dykes/veins and mylonite have a peak of 1978 ppm and a threshold of 200 ppm. The magnitudes of copper values are greater in the West Anomaly than in the East Anomaly. Bismuth values have a peak of 53 ppm. In the East Anomaly, there is weak correlation between (a) Au and Cu (+0.2970), and (b) Au and Bi (+0.2121), but there is no correlation (-0.1636) between Cu and Bi. In the West Anomaly, where the "Au Shear" and "Cu Shear" are concurrent, there is a fairly strong correlation (+0.5636) between Au and Cu.

In Grid 4, trench sampling was successful in indicating that the gold mineralization is mainly in the feldspar porphyry veins/dykes, with the wall rocks occasionally containing ore. Trench sample assays confirmed the "Au Shear" and "Cu Shear" trends indicated by soil geochemistry. More trenches should have been excavated in the East Anomaly, to determine the eastern extent of the gold mineralization.

The trenching method was successful in exposing the *in-situ* mineralized zones near surface in both Grid 2s and Grid 4. In places where relatively fresh rocks were exposed, visible mineralization could be observed. Logging and sampling of trenches gave more information than rock sampling of outcrops and sub-outcrops. The method enabled measurement of strike and dip of the reefs, and determination of horizontal widths of the mineralized zones. This information was useful for siting diamond drill holes to intersect the mineralized zones at right angles to strike direction. The trenching method was not successful in a few areas of thick soil cover (>3m), which were commonly waterlogged and caving.

The trenching method is recommended for use in future gold exploration programs in the region. Trenching is useful for exposing the *in-situ* mineralized zones, which are the sources of drainage and soil anomalies. Information from trenching and sampling is useful for siting drill holes that will test the mineralization at depth.

## **.8 Diamond drilling**

Diamond drilling was a successful exploration method of testing mineralized zones at depth. In both Grid 2s and Grid 4, there was high recovery (95%) of the large diameter HQ core. Diamond drilling produced adequate core to enable geological and geomechanical logging, study of mineralization and alteration, and sampling. The method succeeded as a follow-up on the mineralized zones indicated by trenching, since it intersected the mineralization in fresh rock below the weathered zone. The fresh core provided better samples of ore and wall rocks for observation, study and assay. Drilling succeeded in indicating continuity of the ore zones, both laterally and down-dip to a vertical depth of 50 metres below surface. The method enabled the estimation of ore resources for the top 50-metre depth. In Section 10 000E (Figure 8.10) of Grid 2s, diamond drilling was helpful in indicating fresh, narrower and lower grade (up to 4 g/t Au) quartz reefs that are below a weathered zone with surface gold enrichment and a thick quartz stoneline ore (up to 14 g/t).

In the SW Anomaly of Grid 2s, diamond drilling was conducted without adequate trench information and reef strike directions. This resulted in the drill holes intersecting some of mineralized zones at oblique angles, and possibly missing other zones. The NE Anomaly, which has the greatest strike length and the highest gold values in trench and rock samples, was not drilled in this initial exploration phase. A few holes should have been drilled to investigate the mineralization at depth.

#### **9.8.1 Diamond drilling – Grid 2s**

In Grid 2s, diamond drilling intersected sulphide and gold mineralization in quartz, aplitic and pegmatitic veins, which are hosted in K-feldspar granite, proto-mylonite and charnockite. The mineralization occurs in the form of sparsely to moderately disseminated (up to 20%) pyrrhotite, pyrite, chalcopyrite and gold. Sulphide mineralization also occurs in some parts of the host rocks. In Section 10800E, drilling intersected two wide mineralized zones (North Central Orebody), which are parallel to the foliation and dipping at 75° to the southeast. Zone "A", which is in K-feldspar granite and charnockite, has a true thickness of 19 m, a peak value of 6.6 g/t Au and a weighted average grade of 0.92 g/t Au. Zone "B" has a true thickness of 4½ m and a peak value of 4.5 g/t Au. Between zones A and B, a narrow shear zone assayed 27 g/t Au x 0.45m. In the two zones, the copper values are <300 ppm, and there is negative (-0.5273) or no correlation between gold and copper values. The strike length of the two zones is open to the east and west. However, information available from trenching and rock sampling indicates a strike length of at least 660 metres.

In Section 10000E of Grid 2s, drilling intersected several isolated, narrow mineralized zones (Southwest Orebody) with a peak of 4.7 g/t Au x 1m. Copper values are <50 ppm, and there is no correlation between Au and Cu values. The mineralized zones, which dip at 75° to the southeast, have strike lengths that are open to the east and west, although data available from trenching indicate a minimum length of 700 metres. In Longitudinal Section 8025N, drilling intersected several, spiky mineralized zones with a peak value of 16.6 g/t Au x 1.24m. The copper values are <50 ppm, and there is no correlation between Au and Cu values.

#### **9.8.2 Ore resource estimation – Grid 2s**

Ore resource estimation conducted down to a vertical depth of 50 metres, indicates that the Grid 2s deposit has tonnage of 6 107 150 t grading 4.20 g/t Au. The deposit has 3 orebodies, which are Southwest, North Central and Northeast. The Southwest Orebody has an estimated resource of 1 433 483 tonnes grading 4.18 g/t Au, from reefs having a

strike length of 700 metres and a combined true thickness of 4.71 metres. In the North Central Orebody, the estimated resource is 2 295 660 tonnes grading 1.47 g/t Au, in ore zones of 660-m strike length and 12.0-m combined true thickness. The Northeast Orebody, with a strike length of 900 metres and combined true thickness of 5.15 metres, has an estimated resource of 2 378 008 tonnes grading 10.58 g/t Au. The 3 orebodies have a total strike length of 2260 metres and combined true thickness of 7.29 metres. Quartz stoneline ore, with average thickness ranging from 0.75 metres to 1 metre, overlies the 3 orebodies. The ore resource of the stoneline is estimated to be 1 069 466 t grading 6.35 g/t Au.

The Grid 2s Deposit has economic potential for a large-scale gold mine, considering the extensive total strike length, width, grade and bulk tonnage in the first 50 metres below surface. Further drilling is recommended, to intersect the orebodies laterally and down-dip. Most of the drilling should be conducted on the Northeast Orebody, which has the longest strike and highest grades. Further drilling will enable the estimation of proven ore reserves that are likely to turn the prospect into an economically viable gold mine. To generate some of the capital for further drilling and evaluation, the stoneline ore can be exploited initially.

### **9.8.3 Wall rock alteration – Grid 2s**

In the Grid 2s deposit, the mineralized zones have alteration haloes with horizontal widths of 260-300m, which are marked by the first appearance of pyrite ± pyrrhotite. K-feldspar and ribbon quartz are the most abundant alteration minerals. In the distal zone, the other alteration minerals are biotite, chlorite, muscovite (sericite), calcite, garnet, sillimanite, hercynite/gahnite, pyrite and pyrrhotite. The presence of sillimanite and K-feldspar alteration indicates high-temperature conditions (>500°C). K-feldspar has undergone partial, retrograde replacement by muscovite or sericite. Chlorite is a retrograde phase replacing biotite and garnet. The presence of both pyrrhotite and pyrite indicates lower-amphibolite facies conditions (Eilu *et al.*, 1999). In the proximal zone, the other alteration minerals are muscovite (sericite), biotite, chlorite, rutile, calcite, sillimanite, garnet, pyrrhotite and pyrite. The presence of orthopyroxene in mineralized charnockite indicates prograde lower-granulite facies conditions (Eilu *et al.*, 1999). Rutile, which occurs with chlorite, is a hydrothermal alteration product of titanium-bearing biotite (Thompson & Thompson, 1996), and indicates upper greenschist facies conditions (Eilu *et al.*, 1997). The occurrence of rutile and pyrite indicates retrograde, post-peak upper-greenschist to lower-amphibolite facies conditions.

#### **9.8.4 Diamond drilling – Grid 4**

In Grid 4, diamond drilling intersected sulphide mineralization in feldspar porphyry dykes/veins, mylonite and quartz veins, which are hosted in silicified basaltic granulite. Pyrrhotite, pyrite, chalcopyrite, chalcocite, covellite, sphalerite, bismuth, magnetite and gold are the ore minerals in the "Au Shear". The ore minerals are commonly sparse (<5%) to abundant (20-50%) disseminated, but are semi-massive (50-70%) in some narrow shear zones in mafic granulite. In the East Orebody, the mineralized zone (2.98 g/t Au), dips at 70° to the southeast and attains a strike length of 1000 metres and an average true thickness of 2.11 metres. The main reef in the mineralized zone, has an average true thickness of 1.03 m, a grade of 5.62 g/t Au, and stretches over a strike length of 700 m. The magnitudes of gold values increase with increasing amounts of pyrrhotite. In the "Au Shear", the peak values for copper and molybdenum are 1955 ppm and 15 ppm respectively. Au has a fairly good correlation (+0.5515) with Cu, and a negative (-0.6970) or no correlation with Mo. Cu has a very weak correlation (+0.0182) with Mo.

The West Orebody of Grid 4 dips at 70° southeast and attains a strike length of 200 metres and an average true thickness of 1.15 metres. The form of mineralization and ore minerals are similar to those of the "Au Shear" in the East Orebody mentioned above. Two semi-massive sulphide zones, with intersected widths of 0.53 m and 1.95 m, assayed up to 40 g/t Au and 0.27% Cu in drill hole C4D6.

In the "Cu Shear" of the East Anomaly" (Grid 4), disseminated (up to 30%) sulphide mineralization is mainly associated with quartz veins, but also occurs in the host mylonite and mafic granulite. The ore minerals are chalcopyrite, pyrite, pyrrhotite and molybdenite. The peak values are 1 g/t Au, 904 ppm Cu and 633 ppm Mo. Gold has a fairly good correlation (+0.5879) with copper, and negative (-0.0061) or no correlation with molybdenum. Copper has negative (-0.5394) or no correlation with molybdenum. The weakly mineralized zone is 4.6 metres wide and dips at 70° southeast.

#### **9.8.5 Ore resource estimation – Grid 4**

In the Grid 4 Deposit, ore resource estimation down to 50 metres below surface, indicates a total tonnage of 361 015 t grading 6.27 g/t Au. The East and West orebodies have a total strike length of 1200 metres and an average true thickness of 1.63 metres. The East Orebody has an estimated resource of 325 531 tonnes grading 2.98 g/t Au. The main reef has an estimated resource of 111 236 tonnes grading 5.62 g/t Au. In the West Orebody, the estimated resource is 35 484 tonnes grading 12.3 g/t Au. The Grid 4

Deposit has economic potential for a medium-scale gold mine, considering total strike length, width, grade and tonnage down to 50 metres below surface. A few drill holes intersected the orebodies at greater depth (such as –150 m in C4D13), indicating down-dip continuity of the mineralization. Further drilling is recommended, to intersect the ore zones at various depths to facilitate estimation of proven ore reserves, which are likely to turn the prospect into a viable mine.

#### **9.8.6 Wall rock alteration – Grid 4**

In the Grid 4 deposit, the horizontal width of the alteration halo, which is marked by the first appearance of pyrite, is less than 200m. The maximum widths are 55 m in the footwall and 145 m in the hanging wall. The most abundant alteration minerals are biotite, pyrite and ribbon quartz. In the distal zone, the other alteration minerals are hornblende, chlorite, sericite, calcite, apatite, tourmaline, zoisite, garnet, tremolite-actinolite, serpentine, ilmenite, magnetite and pyrrhotite. Orthopyroxene, which is present in leuco-mylonite, meta-andesite, charnockite and mafic granulite, indicates prograde lower-granulite facies (Eilu *et al.*, 1999). Apatite also indicates high-temperatures in the hydrothermal alteration zone (Thompson & Thompson, 1996). The orthopyroxene has undergone partial retrograde replacement by amphiboles, biotite or chlorite. Garnet has also undergone partial alteration to chlorite. Zoisite, sericite and calcite are retrograde minerals replacing feldspars. The retrograde alteration mineral assemblage, together with pyrite and pyrrhotite, indicate upper-greenschist to lower-amphibolite metamorphic conditions (Eilu *et al.*, 1999).

The proximal alteration zone in the Grid 4 deposit contains biotite, pyrite, ribbon quartz, chlorite, hornblende, tremolite-actinolite, sericite, microperthite, garnet, tourmaline, apatite, monazite, zoisite, ankerite, calcite, magnetite, bismuth, pyrite and pyrrhotite. The presence of orthopyroxene in leuco-mylonite and mafic granulite indicates prograde lower-granulite facies conditions. Apatite, monazite and K-feldspar indicate high temperatures in the hydrothermal alteration zone. The orthopyroxene has undergone partial retrograde replacement by amphiboles, biotite and chlorite. Sericite and zoisite are retrograde minerals replacing feldspars. Ankerite indicates proximity to the centre of the hydrothermal system. Bismuth, which is a low-temperature ore mineral, indicates retrograde conditions in originally high-temperature ore minerals. The retrograde alteration mineral assemblage, together with pyrite, indicates post-peak, upper-greenschist to lower-amphibolite facies (Eilu *et al.*, 1999).

### **9.9 Ore deposit model for the Northern Marginal Zone**

- 9.9.1 The Mauch Shear Zone and the North Limpopo (Umlali) Thrust Zone structurally control mineralization in the Grid 2s, Grid 4 and Renco gold deposits. The steeply dipping and transcrustal Mauch Shear Zone, is the first-order control of mantle-derived ore fluids. These gold deposits occur in structurally induced second- and lower-order shears in dilation and thrust zones. The mineralization (2.532 – 2.553 Ga at Renco), which is post-peak regional metamorphism, occurred under mid-amphibolite-facies conditions (Kisters *et al.*, 1998). The latest reverse movement along the North Limpopo Thrust Zone occurred at 1.9 Ga and is associated with retrograde, upper greenschist-facies metamorphism where H<sub>2</sub>O-rich fluids were available.
- 9.9.2 The three gold deposits are associated with rocks of mafic to intermediate composition, which are in contact with the first-order shear zone, on or near the intersection with the second-order shear zone. The mafic to intermediate rocks are sources of some of the gold, which is liberated by metamorphic devolatilization, into the mantle-derived H<sub>2</sub>O-CO<sub>2</sub> fluids.
- 9.9.3 There is similarity in gold and sulphide mineralization in the Grid 4 and Renco (discussed in Chapter 2) deposits, which are hosted in mafic granulites and enderbite respectively. In both deposits, mineralization occurs as disseminated to massive sulphides, with pyrrhotite as the dominant ore mineral. The other ore minerals are pyrite, chalcopyrite, sphalerite, molybdenite, magnetite, bismuth, gold and ilmenite. Widths of individual reefs vary from 0.5 to 2.5 metres. Several parallel reefs can occur within a broad shear zone. The feldspar porphyry, which hosts most of the mineralization in Grid 4, is similar to the "pegmatoid" reefs in the Renco deposit. Other reef types common to both deposits are mylonitic ore, breccia ore and massive ore.

Mineralization in the Grid 2s deposit, which occurs in leuco-mylonite and K-feldspar granite, comprises fine-grained, sparsely disseminated gold and sulphides, which include pyrrhotite, pyrite and chalcopyrite. Free gold occurs mainly in shear zone-hosted quartz veins and stringers, but it may also occur in wall rocks. Sparse sulphide mineralization is associated with the few mafic grains (biotite and chlorite) that are available. Sulphide mineralization is not well developed, since there was insufficient iron in the host rocks to react with the ore fluids. Due to differences in ore fluid focussing, low-grade (1 g/t Au) ore zones tend to be wider (up to 19m) than high-grade (up to 175 g/t Au) zones (<2m). The gold and sulphide mineralization in Grid 2s is most likely similar to that in the Harlequin and Bochum deposits of the Southern Marginal Zone (SMZ), mentioned by Gan & van

Reenen (1995). Harlequin and Bochum occur in quartz-feldspathic rocks within the granulite zone of the SMZ.

9.9.4 In similarity to the Renco deposit, the alteration mineral assemblages of the Grid 4 deposit can be classified into three facies, which are granulite, amphibolite and greenschist. The typical Grid 4 alteration assemblages are:

(a) *Granulite-facies mineral assemblages*

orthopyroxene + clinopyroxene + plagioclase + microperthite + microcline + quartz.

There is no significant mineralization associated with this assemblage.

(b) *Amphibolite-facies mineral assemblages*

hornblende + biotite + ribbon quartz + sericite + garnet + tourmaline + apatite + monazite + ankerite.

The gold and sulphide mineralization is associated with this alteration assemblage, indicating post-peak metamorphic conditions associated with rehydration. Within the mineralization, the presence of native bismuth, which is a low temperature ore mineral, also indicates retrograde conditions (Eilu *et al.*, 1999).

(c) *Greenschist-facies mineral assemblages*

calcite + chlorite + epidote + sericite + serpentine.

Late-stage calcite veins crosscut the foliation.

In the Grid 2s deposit, the alteration mineral assemblages can also be classified into 3 facies, which are:

(a) *Granulite-facies mineral assemblages*

K-feldspar (microperthite + microcline) + quartz + orthopyroxene ± plagioclase.

There is no significant mineralization associated with this assemblage.

(b) *Amphibolite-facies mineral assemblages*

ribbon quartz + sericite + muscovite + biotite + calcite + garnet + sillimanite.

The gold and sulphide mineralization is associated with this alteration mineral assemblage.

(c) *Greenschist-facies mineral assemblages*

chlorite + rutile + sericite + calcite.

Calcite and some of these greenschist-facies minerals also occur in late-stage veins that crosscut the foliation.

The characteristics stated in 9.9.1-9.9.4 above, are typical of the gold deposits in the Northern Marginal Zone of the Limpopo Belt, and describe an ore deposit model for the region. In future gold exploration programs in the region, these characteristics should be expected.



## **APPENDIX B**

### **FIRE ASSAY METHOD**

The Fire Assay method is a technique for determining the total precious metal content in a sample. The method is excellent for assaying samples containing gold and silver, and is the best for the determination of platinum group metals, since it ensures that all are isolated and included in the analysis (Levinson, 1974).

#### **SAMPLE PREPARATION**

##### **(a) *Rocks and drill core samples***

Reduction of rock fragments to powder involves crushing in a jaw crusher, followed by grinding in a ring mill, disc mill or ball mill. The sample is dried prior to crushing. A rock and drill core sample usually weighs between 3 and 5 kg. The jaw crusher, which can handle 50 kg/hr, reduces the sample to <2 mm. A 1 kg sub-sample of the <2 mm material is riffle-split and pulverized. The mills pulverize the sample material to <100  $\mu\text{m}$  (-75  $\mu\text{m}$  in this study). The capacities of the ring and ball mills are 4kg and 250 g respectively.

Fifty grams of the -75  $\mu\text{m}$  material is split out for gold analysis. If coarse (visible) gold is suspected, the entire sample is pulverized to -75  $\mu\text{m}$  and two 50g splits are taken for duplicate gold analysis. If samples are suspected to be highly-mineralized, a silica sand-cleaning step between samples is requested.

##### **(b) *Soil and stream sediment samples***

The soil and stream sediment samples are dried, manually disaggregated and screened for analysis. Disaggregation is achieved by light pounding in a porcelain mortar and pestle, to obtain natural grain size distribution. The soil and drainage samples are screened to -180  $\mu\text{m}$  and -75  $\mu\text{m}$  fractions respectively, as recommended by orientation surveys. These size fractions give good anomaly contrasts and are sufficiently abundant in soils and sediments to give enough samples for analysis. The fractions are sufficiently fine and additional size reduction by grinding is not required.

Stream sediment samples for gold analysis require special preparation due to the particulate nature of gold. The absolute value of the sediment is of no consequence, but finding gold that induces meaningful follow-up is the requirement. None of the gold grains should be missed due to sample preparation. Sieving reduces the sample

### *Fire assay method continued ----*

size and concentrates the gold. Where there is coarse gold, there is generally sufficient fine-grained gold to trigger follow-up work. The sample is dried and sieved to the fine fraction of  $-75\ \mu\text{m}$ . The whole of this final product is analyzed as several 50g sub-samples.

### GOLD ANALYSIS

The procedure involves heating the sample with a flux, which results in the separation of the precious metals that are then weighed. The 50g sample is mixed with a flux consisting of sodium carbonate, lead oxide (litharge), borax or sodium fluoride and charcoal, and heated to red hot in a clay crucible (Levinson, 1974). The precious metals alloy with lead, whereas the silica, alumina and other elements form a slag. The molten mass is poured into a steel mold, where the lead containing precious metals forms a "button" (pril) at the bottom of the mold. After cooling, the button is broken free of the slag.

The lead-precious metal button is placed on a cupel (a flat roasting dish) of magnesium oxide, and heated under oxidizing conditions. The lead is partly volatilized, oxidized and adsorbed by the cupel, leaving a bead of only precious metals. After cooling, the precious metals are weighed and converted back to a content of the original sample. Any one or all of the precious metals can be in the button. To determine the exact proportions of these elements, an Atomic Absorption Spectrometer is used. For gold analysis, the lower detection limits are normally 5 or 10 ppb.

Quality control is achieved by inserting check standards, blank and duplicate samples in a batch.

## APPENDIX C

### AQUA REGIA METHOD

Aqua Regia is a common acid digestion and hot extraction method for elements (such as Cu, As, Zn, Ni, Bi and Mo) that are concentrated in the sulphide and oxide phases. The method is usually used for sulphidic samples with >5 % sulphide.

#### SAMPLE PREPARATION

The sample preparation is similar to that for the Fire Assay Method (Appendix 2).

##### **(a) *Rock and drill core samples***

The entire sample is dried and Jaw-crushed to <2 mm. A sub-sample of 500g is riffle-split out and pulverized to <100 µm (-75 µm in this study). A 0.5g sample of the <75 µm is analyzed. A 1g sample can be used as it increases the detection limit and improves the precision. Some laboratories use lower weights such as 0.1g or 0.2g, but these potentially produce poor results.

##### **(b) *Soil and stream sediment samples***

The soil and drainage samples are dried, disaggregated and sieved to <180 µm and <75 µm respectively. A sample size of 0.5g is split out from the sieved sample, and used for a standard acid digest. A 1g sample is preferred.

#### AQUA REGIA DIGESTION AND EXTRACTION

Aqua regia is a mixture of 3 parts hydrochloric acid and 1 part nitric acid that react to produce nitrosyl chloride and chlorine, which are the active agents:



A sample is treated with aqua regia at 100°C or more for approximately an hour (Levinson, 1974). The action is vigorous at 90°C, and at 109°C aqua regia distills over. Aqua regia digests all the sulphides, oxides and noble metals (gold, silver and platinum), but only partially digests silicates, clays and resistant minerals. As a consequence, elements such as Al, Ba, Ti, Na and K are virtually never fully dissolved. On a practical basis, approximately 90% extraction is achieved on the sulphides, oxides and noble metals. The digestion is preferred for soil and drainage samples since trace metals are concentrated in the sulphide and oxide phase and contributions of metals from silicate phases is minimised. Individual element concentrations are detected by ICP-Mass spectrometer.

A detection limit of 0.1 ppm can be attained. Quality control is achieved by inserting check standards, blanks and duplicate samples.



APPENDIX E – GRID 2s – DRILL CORE MINERAL ASSEMBLAGES

DRILL HOLE No.	Specimen No.	ROCK NAME	ALTE'RATION MINERALS																												
			PHASE 1						ORE MINERALS					SILICATES						OXIDES		CARBONATE		SULPHIDES		Gold					
			Quartz	Microcline	Microperthite	Plagioclase	Antiperthite	Orthopyrox	Sphene	Zircon	Magnetite	Pyrrhotite	Pyrite	Chalcopyrite	Sphalerite	Gold	Graphitic	Fine-grained	Ribbon	Chlorite	Biotite	Muscovite / Sericite	Microperthite	Garnet	Sillimanite		Magnetite	Rutile	Hercynite / Gahnite	Calcite	Pyrrhotite
C2D4	RS 34	Charnockite	x	x	x	m		x			x	x	x	x			x	x	x	x	x			x		x		x	x		
C2D4	RS 50	Quartz Vein + K-feldspar Granite	x	x	x	m		x			x	x				x		x	x	x	x	x			x		x	x			
C2D5	RS 37	K-feldspar Granite	x	x	x	m			x	x		x	x	x			x	x	x	x	x	x			x	x				x	
C2D5	RS 38	K-feldspar Granite	x	x	x	m	m					x	x				x	x	x	x	x								x		
C2D5	RS 39	K-feldspar Granite	x	x	x					x		x	x	x			x	x	x	x	x				x			x	x		
C2D5	RS 51	Pegmatitic Vein	x	x	x	m				x		x	x	x			x	x	x	x	x	x			x			x	x		
C2D5	RS 35	K-feldspar Granite	x	x	x	m			x		x	x	x				x	x	x	x	x	x						x	x		
C2D5	RS 36	Leucogneiss	x	x	x						x	x	x				x	x			x	x	x					x	x		
C2D5	RS 52	K-feldspar Granite	x	x	x	m	m			x		x	x	x			x	x	x	x	x		x				x		x	x	
C2D20	RS 40	Quartz Vein												x			x		x											x	
C2D20	RS 53	Quartz Vein			x	m								x			x		x		x	x	x							x	
C2D20	RS 54	Aplitic Vein	x	x	x	m								x			x	x	x	x	x	x	x							x	

**KEY**  
"m" denotes minor proportion

## REFERENCES

- Amitage, M.G. 1993. The occurrence and distribution of gold in shear zones at Renco Mine, Zimbabwe. *Unpublished Ph D. Thesis, University of Bristol.*
- Barnes, J.F.H. 1987. Practical methods of drill hole sampling. In: Meaningful Sampling in Gold Exploration, *Australian Institute of Geoscientists, Bulletin No. 7*, p. 145-170.
- Barton, J.M. jr., Fripp, R.E.P. and Horrocks, P.C. 1983. Rb-Sr and U-Th-Pb isotopic studies of the Sand River gneisses, Central Zone, Limpopo Mobile Belt. In: van Biljon, W.J. and Legg, J.H. (eds). *The Limpopo mobile belt*. Geological Society of South Africa, Special Publications, **8**, p. 9-18.
- Berger, M. and Rollinson, H. 1997. Isotopic and geochemical evidence for crust-mantle interaction during late Archaean crustal growth. *Geochemica et. Acta*, Vol. **61**, No. 22, p. 4809- 4829.
- Berger, M., Kramers, J.D. and Nagler, T.F. 1995. Geochemistry and geochronology of charno-enderbites in the Northern Marginal Zone of the Limpopo Belt, Southern Africa, and genetic models. *Schweiz. Mineral. Petrogr. Mitt.* **75**, p. 17 - 42.
- Berkman, D.A. 1976. Field Geologists' Manual. *The Australasian Institute of Mining and Metallurgy, Monograph Series No. 9.*
- Blenkinsop, T.G. and Frei, R. 1996. Archaean and Proterozoic Mineralization and Tectonics at the Renco Mine (Northern Marginal Zone, Limpopo Belt, Zimbabwe). *Economic Geology*, Vol. **91**, pp. 1225-1238.
- Broderick, T.J. 1979. Explanation of the Geological map of the Country South of Nuanetsi, Nuanetsi and Beitbridge Districts. *Rhodesia Geological Survey, Short Report No. 46.*
- Campbell, S.D.G. and Pilfield, P.E. 1994. Structural Controls of Gold Mineralization in the Zimbabwe Craton-Exploration Guidelines. *Zimbabwe Geological Survey, Bulletin No. 101.*

Cassidy, K.F. 1990. Nature and Setting of Primary Gold Deposits – Westonia. In: Ho, S.E., Groves, D.I. & Bennett, J.M., (eds.), *Gold Deposits of the Archaean Yilgarn Block, Western Australia: Nature, Genesis and Exploration Guides*. The University of Western Australia, Publication No. 20, p. 177-179.

Chenjerai, K.G. 1996. The Mutare Greenstone Belt, Zimbabwe : Geology, Geochemistry and Gold Mineralisation. *Unpublished Ph D. Thesis. University of Gottingen, Germany.*

Corner, B. 1994. Gravity and Magnetic Potential Fields: Introductory Notes for Geologists. *Unpublished, RTZ Training Course.*

Coward, M.P., Graham, R.H., James, P.R. and Wakefield, J., 1973. A structural interpretation of the northern margin of the Limpopo orogenic belt, southern Africa. *Philosophical Transactions of the Royal Society of London, Series A 273*, p. 487– 492.

Coward, M.P., James, P.R. and Wright, L. 1976. Northern margin of the Limpopo mobile belt, southern Africa. *Geological Society of America Bulletin*, v. 87, p. 601–611.

De Wit, M.J., Roering, C., Hart, R.J., Armstrong, R.A., De Ronde, C.E.J., Green, R.W.E., Tredoux, M., Peberdy, E., and Hart, R.A., 1992. Formation of an Archaean continent. *Nature*, 357, p. 553–562.

Deer, F.R.S., Howie, R.A. and Zussman, J. 1966. An Introduction to the Rock-forming Minerals. *Longman Group Limited.*

Eilu, P.K., Mathison, C.I., Groves, D.I. and Allardyce, W.J. 1999. Atlas of Alteration Assemblages, Styles and Zoning in Orogenic Lode-Gold Deposits in a variety of Host Rock and Metamorphic Settings. *Geology and Geophysics Department (Centre for Strategic Mineral Deposits) & UWA Extension. The University of Western Australia, Publication 30*, 50 p.p.

Eilu, P.K., Mikucki, E.J. and Groves, D.I. 1997. Wallrock Alteration and Primary Geochemical Dispersion in Lode-Gold Exploration. *The Society for Geology Applied to Mineral Deposits, Short Course Series Vol. 1.*

Elliston, J. 1965. Exploratory Mineral Drilling. *In*: L.J. Lawrence (ed.), Exploration and Mining Geology, *Eighth Commonwealth Mining and Metallurgy Congress, Australia and New Zealand, Vol. 2*, p. 175-186.

Evans, A.M. 1993. Ore Geology and Industrial Minerals, An Introduction. *Blackwell Science Limited*.

Fare, R.J. and McNaughton, N.J. 1990. Nature and Setting of Primary Gold Deposits – Griffin's Find. *In*: Ho, S.E., Groves, D.I. & Bennett, J.M., Eds., *Gold Deposits of the Archaean Yilgarn Block, Western Australia: Nature, Genesis and Exploration Guides*. The University of Western Australia, Publication No. 20, p. 182-184.

Gan, S. and van Reenen, D.D. 1995. Geology of gold deposits in the Southern Marginal Zone of the Limpopo Belt and the adjacent Sutherland Greenstone Belt, South Africa – Franke Mine. *South African Journal of Geology*, 98(3), p.263-275.

Grasty, R.L., St. John Smith, B. and Minty, B.R.S. 1997. Developments in the Standardization and Analysis of Airborne Gamma-Ray Data; p.725-732, *Proceedings of Exploration 97:Fourth Decennial International Conference on Mineral Exploration*, edited by A.G. Gubins, GEO F/X, 1068p.

Groves, D.I. 1993. The crustal continuum model for late-Archaean lode-gold deposits of the Yilgarn Block, Western Australia. *Mineralium Deposita* 28, p. 366-374.

Groves, D.I., Barley, M.E. and Ho, S.E. 1989. Nature, Genesis and Tectonic Setting of Mesothermal Gold Mineralization in the Yilgarn Block, Western Australia. *In*: The Geology of Gold Deposits: The Perspective in 1988. R.R. Keays, W.R.H. Ramsay and D.I. Groves (eds.). *Economic Geology Monograph* 6, p.71-85.

Gunn, P.J., Minty, B.R.S. and Milligan, P.R. 1997. The Airborne Gamma-Ray Spectrometric Response over Arid Australian Terrains; p. 733-740, *Proceedings of Exploration 97:Fourth Decennial International Conference on Mineral Exploration*, edited by A.G. Gubins, GEO F/X, 1068p.

Hawkesworth, C.J., Moorbath, S., O'Nions, R.K. and Wilson, J.F., 1975. Age relationships between greenstone belts and "granites" in the Rhodesian Archaean craton. *Earth and Planetary Science Letters*, **25**, p. 251–262.

Ho, S.E., Groves, D.I. and Bennett, J.M. 1990. Gold deposits of the Archaean Yilgarn Block, Western Australia : Nature, Genesis and Exploration Guides. *The University of Western Australia, Publication No. 20*, p. 169-184.

Hodgson, C.J. 1989. Patterns of Mineralization. In: J.T. Bursnall (ed.), Mineralization and Shear Zones. *Geological Association of Canada, Short Course Notes, Volume 6*, p. 51-88.

Hodgson, C.J. 1989. The Structure of Shear-Related, Vein-Type Gold Deposits: A Review. *Ore Geology Reviews*, **4**, p. 231-273.

Hodgson, C.J., Hamilton, J.V. and Piroshco, D.W. 1990. Structural setting of gold deposits and the tectonic evolution of the Timmins-Kirkland Lake area, southwestern Abitibi greenstone belt. In: Gold and base metal mineralization in the Abitibi Subprovince, Canada, with emphasis on the Quebec segment; S.E. Ho, F. Robert and D.I. Groves (eds.), *Geology Department (Key Centre) and University Extension, The University of Western Australia*, p. 101-120.

Hodgson, C.J., Love, D.A. and Hamilton, J.V. 1992. Giant mesothermal gold deposits: Descriptive characteristics, genetic model and exploration area criteria. *Giant Ore Deposits workshop, Queen's University, Kingston, Ontario, Canada (unpublished)*.

Hughes, M.D. 1965. Geological Planning for Diamond Drilling. In: Lawrence, L.J. (ed.) *Exploration and Mining Geology, Eighth Commonwealth Mining and Metallurgy Congress, Australia and New Zealand, Vol. 2*, p. 167-174.

Jaeckel, P., Kroner, A., Kamo, S.L., Brandl, G. and Wendt, J.I. 1997. Late Archaean to early Proterozoic granitoid magmatism and high-grade metamorphism in the Central Limpopo belt, South Africa. *Journal of the Geological Society of London*, vol. **154**, p. 25–44.

James, P.R. 1975. A deformation study across the northern margin of the Limpopo Mobile Belt, Rhodesia. *Unpublished Ph D. Thesis. University of Leeds.*

Jayawardhana, P.M. and Sheard, S.N. 1997. The Use of Airborne Gamma-Ray Spectrometry by M.I.M. Exploration – A Case Study from Mount Isa Inlier, North-West Queensland, Australia; p. 765-774, *Proceedings of Exploration 97:Fourth Decennial International Conference on Mineral Exploration*, edited by A.G. Gubins, GEO F/X, 1068p.

Jelsma, H.A. 1993. Granites and greenstone in northern Zimbabwe: Tectono-thermal evolution and source regions. *Unpublished Ph D. Thesis. Vrije Universiteit Amsterdam, Netherlands.*

Kamber, B.S. and Biino, G.G. 1995. The evolution of high T – low P granulites in the Northern Marginal Zone *sensu stricto*, Limpopo Belt, Zimbabwe—the case for petrography. *Schweiz. Mineral. Petrogr. Mitt.* 75, p. 427 – 454.

Kerrich, R. 1989 (a). Geodynamic setting and hydraulic regimes: Shear-zone hosted mesothermal gold deposits. *In*: J.T. Bursnall (ed.), Mineralization and shear zones, *Geological Association of Canada, Short Course Notes, Volume 6*, p. 89-128.

Kerrich, R. 1989 (b). Geochemical evidence on the source of fluids and solutes for shear zone hosted mesothermal Au deposits. *In*: J.T. Bursnall (ed.), Mineralization and shear zones, *Geological Association of Canada, Short Course Notes, Volume 6*, p. 129-197.

Kisters, A.F.M., Kolb, J. and Meyer, F.M. 1998. Gold Mineralization in High-Grade Metamorphic Shear Zones of the Renco Mine, Southern Zimbabwe. *Economic Geology, Volume 93*, p. 587-601.

Levinson, A.A. 1974. Introduction to Exploration Geochemistry. *Applied Publishing Limited.*

Levinson, A.A., Bradshaw, P.M.D. and Thomson, I. 1987. Practical Problems in Exploration Geochemistry. *Applied Publishing Limited.*

Lissiman, J.C. 1965. A brief survey of exploration drilling. In: Lawrence, L.J. (ed.) *Exploration and Mining Geology, Eighth Commonwealth Mining and Metallurgy Congress, Australia and New Zealand, Vol. 2*, p. 162-166.

Mason, R. 1973. The Limpopo Belt–Southern Africa. *Philosophical Transactions of the Royal Society of London Series A* 273, p. 463–485.

Mazzucchelli, R. H., 1987. Gold in stream sediments: In Meaningful sampling in gold exploration. *Australian Institute of Geoscientists, Bulletin No. 7*, p. 85-100.

Mc Court, S. and Vearncombe, J.R. 1987. Shear zones bounding the Central Zone of the Limpopo Mobile Belt, southern Africa. *Journal of Structural Geology*, 9, p. 127–137.

Mc Court, S. and Vearncombe, J.R. 1992. Shear zones of the Limpopo and adjacent granitoid–greenstone terrains: implications for late Archaean collision tectonics in southern Africa. *Precambrian Research*, 55, p. 553–570.

Minter, W.E.L. and Toens, P.D., 1970. Experimental simulation of gold deposition in gravel beds. *Transactions of the Geological Society of S. Africa* 73, p. 89-99.

Mkweli, S., Kamber, B. and Berger, M. 1995. A westward continuation of the Zimbabwe craton–Northern Marginal Zone tectonic break and new age constraints on the timing of the thrusting. *Journal of the Geological Society of London*, 152, p. 77-83.

Moorbath, S., Wilson, J.F. and Coterill, P. 1976. Early Archaean age for the Sebakwian Group at Selukwe, Rhodesia. *Nature*, 264, p. 532–538.

Muggeridge, M.T., 1986. The efficiency of fluvial trap sites in concentrating kimberlitic indicator minerals: An experimental sampling survey. In: J. Ross (Editor), *Kimberlites and Related Rocks, Vol. 2. GSA Special Publication No. 14, Section 6* (edited by A.J.A. Janse), p. 1154 -1168.

Muggeridge, M.T., 1995. Pathfinder sampling techniques for locating primary sources of diamond: Recovery of indicator minerals, diamonds and geochemical signatures. *Journal of Geochemical Exploration* 53 (1995), p. 183-204.

Odell, J. 1975. Explanation of the Geological Map of the Country around Bangala Dam. *Rhodesia Geological Survey, Short Report No. 42.*

Parasnis, D.S. 1979. Principles of Applied Geophysics. *Chapman and Hall.*

Perring, C.S., Groves, D.I. and Ho, S.E. 1987. Constraints on the source of auriferous fluids for Archaean gold deposits. *In: S.E. Ho and D.I. Groves (eds.), Recent advances in understanding Precambrian gold deposits; Geology Department and Univ. Extension, University of Western Australia, Publication No. 11, p. 287-306.*

Poulsen, K.H and Robert, F. 1989. Shear zones and gold: practical examples from the southern Canadian Shield. *In: Bursnall, J.T.(ed.), Mineralization and Shear Zones. Geological Association of Canada, Short Course Notes, 6, p.239-266.*

Rattigan, J. 1965. The geochemical Prospecting Programme. *In: Lawrence, L.J. 1965. Exploration and Mining Geology, Eighth Commonwealth Mining and Metallurgy Congress, 2, Australasian Institute of Mining and Metallurgy.*

Retief, E.A., Compston, W., Armstrong, R.A. and Williams, I.S. 1990. Characteristics and preliminary U-Pb ages of zircons from Limpopo belt lithologies. *Extended abstracts, Limpopo Workshop, Rand Afrikaans University, Johannesburg, p. 95-99.*

Richards, D.J. 1979. Technical Manual on Radiometrics. *South African Geophysical Association, Geophysical Field Manual for Technicians No. 2.*

Ridley, J. 1992. On the origins and tectonic significance of the charnockite suite of the Archaean Limpopo Belt, Northern Marginal Zone, Zimbabwe. *Precambrian Research, 55, p. 407- 427.*

Robert, F. 1990. Structural Setting and Control of Gold-Quartz Veins of the Val d'Or Area, Southern Abitibi Subprovince. *In: Ho, S.E., Robert, F. and Groves, D.I. (eds.), Gold and base metal mineralization in the Abitibi Subprovince, with*

*emphasis on the Quebec segment*. Publication 24, Geology Department (Key Centre) and Extension, The University of Western Australia, p.167-210.

Robert, F. and Poulsen, K.H. 1997. World-class Archaean gold deposits in Canada: an overview. *Australian Journal of Earth Sciences*, 44, p. 329-351.

Roberts, R.G. 1987. Ore Deposit models # 11. Archaean lode-gold deposits: *Geoscience Canada, Volume 14*, p. 37-52.

Robertson, I.D.M. 1973. Potash granites of the southern edge of the Rhodesian craton and the northern granulite zone of the Limpopo Mobile belt. In: LISTER, L.A. (ed.) *Symposium on granites, gneisses and related rocks*. Geological Society of South Africa Special Publications, 3, p. 265–276.

Robertson, I.D.M. 1974. Explanation of the Geological Map of the Country South of Chibi. *Rhodesia Geological Survey Short Report No. 41*.

Roering, C., van Reenen, D.D., Smit, C.A., Barton, J.M. jr., De Beer, J.H., De Wit, M.J., Stettler, E.H., van Schalkwyk, J.F., Stevens, G. and Pretorius, S. 1992. Tectonic model for the evolution of the Limpopo Belt. *Precambrian Research*, 55, p. 539–552.

Rollinson, H.R. & Blenkinsop, T. 1995. The magmatic, metamorphic and tectonic evolution of the Northern Marginal Zone of the Limpopo Belt in Zimbabwe. *Journal of the Geological Society, London*, vol. 152, p. 65 – 75.

Rollinson, H.R. 1993. A Terrane interpretation of the Archaean Limpopo Belt. *Geological Magazine*, 130, p. 755–765.

Rollinson, H.R. 1993. Using Geochemical Data: Evaluation, Presentation, Interpretation. *Longman Scientific & Technical*.

Rollinson, H.R. and Blenkinsop, T.G. 1995. The magmatic, metamorphic and tectonic evolution of the Northern Marginal Zone of the Limpopo Belt in Zimbabwe. *Journal of the Geological Society of London*, vol. 152, p. 65–75.

Rollinson, H.R. and Lowry, D.L. 1992. Early basic magmatism in the evolution of the North marginal zone of the Archaean Limpopo belt. *Precambrian Research*, **55**, p. 33– 45.

Rose, A.W., Hawkes, H.E. and Webb, J.S. 1979. Geochemistry in Mineral Exploration. *Academic Press*.

Shelley, D. 1993. Igneous and metamorphic rocks under the microscope. *Chapman & Hall*.

Shives, R.B.K., Charbonneau, B.W. and Ford, K.L. 1997. The Detection of Potassic Alteration by Gamma-Ray Spectrometry—Recognition of Alteration Related to Mineralization; p. 741-752, *Proceedings of Exploration 97:Fourth Decennial International Conference on Mineral Exploration*, edited by A.G. Gubins, GEO F/X, 1068p.

Sibson, R.H., Robert, F. and Poulsen, K.H. 1988. High-angle reverse faults, fluid-pressure cycling, and mesothermal gold-quartz deposits. *Geology*, *Volume 16*, p. 551-555.

Sinclair, A.J. 1991. A fundamental approach to threshold estimation in exploration geochemistry: probability plots revisited. *In*: A.W. Ross and P.M. Taufen (eds.), *Geochemical Exploration 1989*, *J. Geochem. Explor.*, **41**; p. 1-22.

Smith, B.H. 1987. Dispersion of Gold in Soils. *In*: *Meaningful Sampling in Gold Exploration*, *Australasian Institute of Geoscientists, Bulletin No. 7*, 1987.

Smith, R.J., Dransfield, M.H. and Rajagopalan, S. 1997. Regional Geophysical Exploration in Arid Terrains; p. 821-828, *Proceedings of Exploration 97:Fourth Decennial International Conference on Mineral Exploration*, edited by A.G. Gubins, GEO F/X, 1068p.

Stagman, J.G. 1978. An Outline of the Geology of Rhodesia. *Rhodesia Geological Survey Bulletin No. 80*.

Stuart, G.W. and Zengeni, T.G. 1987. Seismic crustal structure of the Limpopo mobile belt, Zimbabwe. *Tectonophysics*, **144**, p. 323–335.

Thompson, A.J.B. and Thompson, J.F.H. 1996. Atlas of Alteration. A field and petrographic guide to hydrothermal alteration minerals. *Geological Association of Canada, Mineral Deposits Division*.

Tinnion, M.P. 1995. Geophysical Assessment of Tokwe (EPO 847). *Unpublished Report, Geodass (Pty.) Limited*.

Treloar, P.J., Coward, M.P. and Harris, N.B.W. 1992. Himalayan–Tibetan analogies for the evolution of the Zimbabwe craton and Limpopo Belt. *Precambrian Research*, 55, p. 571–587.

Van Reenen, D.D. 1986. Hydration of cordierite and hypersthene and a description of the retrograde ortho-amphibole isograd in the Limpopo Belt, South Africa. *Am. Mineral*, 71, p. 900–915.

Van Reenen, D.D., Roering, C., Smit, C.A., van Schalkwyk, J.F. and Barton, J.M. jr. 1988. Evolution of the northern high-grade margin of the Kaapvaal Craton, South Africa. *Journal of Geology*, 96, p. 549–560.

Watkeys, M.K. 1984. The Precambrian geology of the Limpopo belt north and west of Messina. *Unpublished Ph D. Thesis, University of Witwatersrand, Johannesburg*.

Watkeys, M.K., Light, M.P.R. and Broderick, T.J. 1983. A retrospective view of the Central Zone of the Limpopo Belt, Zimbabwe. In: van Biljon, W.J. and Legg, J.H. (eds) *The Limpopo mobile belt*. Geological Society of South Africa, Special Publications, 8, p. 65–80.

Yardley, B.W. 1989. An introduction to metamorphic petrology. *Longman Scientific & Technical*.

